NATURAL CONVECTION IN MAGNETIC NANOFLUIDS

Ph.D. THESIS

by

ADITYA KUMAR

DEPARTMENT OF MECHANICAL AND INDUSTRIAL ENGINEERING
INDIAN INSTITUTE OF TECHNOLOGY ROORKEE
ROORKEE-247667 (INDIA)
DECEMBER, 2020

NATURAL CONVECTION IN MAGNETIC NANOFLUIDS

A THESIS

Submitted in partial fulfilment of the

requirements for the award of the degree

of

DOCTOR OF PHILOSOPHY

in

MECHANICAL ENGINEERING

by

ADITYA KUMAR

DEPARTMENT OF MECHANICAL AND INDUSTRIAL ENGINEERING
INDIAN INSTITUTE OF TECHNOLOGY ROORKEE
ROORKEE-247667 (INDIA)
DECEMBER, 2020

INDIAN INSTITUTE OF TECHNOLOGY ROORKEE
ROORKEE, INDIA

CANDIDATE'S DECLARATION

I hereby certify that the work which is being presented in the thesis entitled "**NATURAL CONVECTION IN MAGNETIC NANOFLUIDS",** in partial fulfilment of the requirement for the award of the Degree of Doctor of Philosophy and submitted in the Department of Mechanical and Industrial Engineering of the Indian Institute of Technology Roorkee, Roorkee is an authentic record of my own work carried out during a period from July, 2015 to August, 2020 under the supervision of Dr. Sudhakar Subudhi, Associate Professor, Department of Mechanical and Industrial Engineering, Indian Institute of Technology Roorkee, Roorkee, India.

The matter presented in this thesis has not been submitted by me for the award of any other degree of this or any other Institute.

(Aditya Kumar)

This is to certify that the above statement made by the candidate is correct to the best of my knowledge.

(Sudhakar Subudhi)
Supervisor

The Ph.D. Viva-Voce Examination of Aditya Kumar, Research Scholar, has been held on **Dec 21, 2020**

M.V.Rane

Chairman, SRC   **Signature of External Examiner**

This is to certify that the student has made all the corrections in the thesis.

(Sudhakar Subudhi)   **Head of the Department**
Dated:

Abstract

In the forced convection heat transfer, the magnetic nanofluids have been proved efficient, theoretically and experimentally. But, a conflict exists between the theoretical and experimental studies on the natural convection heat transfer in magnetic nanofluids. The theoretical investigations evidenced an enhancement in the heat transfer capabilities of magnetic nanofluids in natural convection. In contrast, a deterioration was reported in the experimental findings, which are very few in number and based on the Rayleigh Bénard convection model. The above conflict between the theoretical and experimental studies on natural convection and to provide more information on the open cavity natural convection is the inspiration of the current study.

A cubic cavity, heated from the bottom and open from the top to a controlled environment, is filled by the water-based Fe_3O_4-water magnetic nanofluids. First, the analysis is done on the water as the working fluid to validate the test section as well as provide more information on the thermal boundary layer properties and temperature fluctuation in the open cavity, followed by the Fe_3O_4-water magnetic nanofluids of different particle concentrations. The particle concentrations of 0.01 and 0.1 vol.%, and the presence of externally applied magnetic field intensity from 0 to 730 Gauss are selected to investigate their effects on the heat transfer. In addition to the concentrations and magnetic field, the heat flux at the bottom plate is the other parameter, which is examined in the present study.

After the preparation of magnetic nanofluids by two-step methods, the thermophysical properties of the magnetic nanofluids are measured with different parameters. The viscosity, thermal conductivity and the density of magnetic nanofluids as a function of concentration, temperature and the magnetic field are measured precisely. These thermo-physical properties of magnetic nanofluids are used to calculate the non-dimensional parameters, such as Nusselt number, Rayleigh number, Prandtl number, and the thickness of the thermal boundary layer. Additionally, the statistical analysis, consisting of temperature histograms, probability density function, power spectral density is supervised on the experimental results to understand the responsible mechanisms behind the heat transfer in magnetic nanofluids.

Through the analysis of experimental values, various outcomes related to the alteration of heat transfer in the water and magnetic nanofluids are witnessed. The Prandtl number and Rayleigh number range reported in this work are $4 \leq Pr \leq 6$ and $10^5 \leq Ra \leq 10^9$, respectively. The validity criteria for Oberbeck-Boussinesq approximation is fulfilled for both water and magnetic nanofluids. For water, it has been confirmed that the existence of the different zones based on the temperature fluctuations in the vicinity of the thermal boundary layer in the turbulent thermal convection of the open cubic cavity. The heat transfer in the presence of nanoparticles in the base fluid has deteriorated. The heat transfer is increased with the Rayleigh number. At the low concentration of the magnetic nanofluid, the externally applied magnetic field has a negligible effect on the heat transfer. However, as the concentration is higher, the effect is significantly observed in the enhancement of heat transfer. The dependency of Nusselt number on the Rayleigh number and Prandtl number for the water in the open cavity is also formulated, which is a major contribution of the present study, as it is not reported in the literature. The above results are furthermore experienced by estimating the thermal boundary layer thickness and statistical analysis. A reduction in the boundary layer thickness is observed with the increment in the Rayleigh number. On the basis of the Rayleigh number, the difference between the transition regime and intensive turbulence is also explained using the probability density function of temperature fluctuation data. The various correlations are formulated by relating the different variables with the non-dimensional parameters and quantifying and validating the results of the present study.

Keywords: *Natural convection, Open cubic cavity, Magnetic nanofluids, Turbulent Convection, Magnetic field, Thermal conductivity, Nusselt number, Rayleigh number.*

Acknowledgments

This thesis represents not only my work at Microsoft word, it was a fulfilling endeavour with a very high learning curve at IIT Roorkee. My experience at the IIT Roorkee has been nothing short of amazing. This is hardly a place to put on record all the things that made this journey magnificent; nonetheless, I shall make an attempt to at least mention the name of remarkable individuals closely associated with it being so.

First and foremost, I owe my obligation and deliver my sincere gratitude to my supervisor **Prof Sudhakar Subudhi**, Department of Mechanical & Industrial Engineering, IIT Roorkee. I thank him for his time and consideration in providing plenty of insightful comments at each and every stage of my research work. I remember he used to say, "Be sincere and work hard, this is the most important time of your life" to encourage me to push myself beyond my capabilities. His painstaking efforts, suggestions for improvement, keen interest in the research work have an immense contribution.

My thesis committee guided me through all these years, I would like to deliver my gratitude to **Prof Ravi Kumar, Prof Manish Mishra** and **Prof Sumana Ghosh** for their timely encouragement and valuable, insightful comments and suggestions regarding the research work. I thank **Prof B K Gandhi**, Head of the Department and **Prof A K Sharma**, Chairman DRC and **Prof Navneet Arora**, former Chairman DRC for their support towards administrative clearances and timely encouragement.

A heartfelt thanks to my seniors **Dr Rajesh Choudhary** and **Dr Deepak Khurana,** for supporting & guiding me in the research work. Now, I want to deliver my thanks to my research group members **Dr Geleta Fekadu, Mr Shashikant Das, Mr Deepak Kumar, Ms Kalpna, Mr Sajesh M** for cooperation during research work and suggestions during our long discussions on various academic and non-academic topics. I am also thankful to **Mr Pawan Kumar, Mr Babloo Singh, Mr Raja Ram, Mr. Satya Veer Singh** and **Mr Inderpal Sharma,** who helped me in one way or another during the fabrication of experimental set-up.

I am incredibly thankful to many friends and groups that became a part of my life at IIT Roorkee, special thanks to **Mr Ankit Dev, Dr Shuvam Panwar, Mr Naveen Kumar,**

Table of Contents

List of Figures

XIII

List of Tables

Nomenclature

AR	aspect ratio		Nu	Nusselt number
A_c	cross sectional area of bottom plate		Pr	Prandtl number
A_s	surface area of solid particle		q	heat flux
BL	boundary layer		Q	heat transfer rate
C_p	specific heat		r	radius
D	diameter		R	resistance
DIW	de-ionized water		R_b	thermal boundary resistance
DW	distilled water		Ra	Rayleigh number
EDL	electrical double layer		S_T	Skewness
F_T	Flatness		T	Temperature
H	height		t_s	sonication time
I	current		u_T	total uncertainty
IEP	isoelectric point		V	voltage
k	thermal conductivity		V_p	Volume of particle
m	mass concentration		z	height from heating surface
N	no. of temperature values			

Greek symbols

α	thermal diffusivity		v	kinematic viscosity
β	thermal expansion coefficient		ρ	Density
δ_{th}	thickness of thermal boundary layer		Ψ	sphericity
Δ	gradient operator		σ	standard deviation
ϕ	particle concentration (vol.%)		$r.m.s.$	root mean square
λ	shear stress		$< >$	mean operator
μ	dynamic viscosity			

Subscripts

$avg.$	average		$MNfs$	Magnetic nanofluids
bf	base fluid		Max	Maximum
c	cold		np	nanoparticle
C	centre		nf	nanofluid
h	hot		p	particle

Chapter 1: Introduction

Index

कामस्तदग्रे समवर्तताधि मनसो रेतः प्रथमं यदासीत् ।
सतो बन्धुमसति निरविन्दन्हृदि प्रतीष्या कवयो मनीषा ॥

<div align="right">ऋग्वेद</div>

*In the beginning desire descended on it -that was the primal seed,
born of the mind. The sages who have searched their hearts with
wisdom know that which is, is kin to that which is not.*

<div align="right">*Rig Veda*</div>

1

Introduction

The phenomenon of heat transfer from one place to another by fluid motion is knowns as convection. It is ubiquitous in nature and technology and serving an essential and wide scope, for example, boiling of coffee, warming of the atmosphere, solar heaters, mixing of oceans and electronics assemblies. Broadly the convection can be categorised into forced & natural convection. Forced convection involves the motion of fluids molecules by means of external sources (pumps, blowers, fans). On the other hand, in natural convection, fluid motion arises from natural forces like gravity and buoyancy. Many of the literature comprising numerical and experimental work has been published on the natural convection heat transfer phenomena in water and other fluids. The cause behind the ubiquitous nature of natural convection heat transfer is the gravitational force, macroscopically similar everywhere. Rayleigh Bénard (R-B) convection (fluid enclosed between two plates, heated from below and cooled from above) is one of the best-studied classical paradigms to understand the multifaceted convection phenomenon. Whereas, the open cavity convection phenomena have a few take-overs and still some facts are unexplored by the researchers. However, the governing dimensionless numbers for convection and heat transport in the open cavity are the same as in R-B convection. In most of the cooling applications of natural convection, conventional fluids such as water, ethylene glycol, or oil are used as working fluids. However, during the last few decades, it was observed by the researchers that these conventional working fluids have low thermophysical properties, which limit the convection heat transfer rate. Hence, by improving the thermophysical properties of the working fluids, heat transfer can be increased.

1.1 Nanofluids

An overwhelming demand for high heat flow processes has embodied the new sophisticated technology in a sustainable manner. Nanofluids could be new dawn to the highly efficient heat flow technologies. Nanofluids is the colloidal suspension of solid

nanoparticles of higher thermal conductivity material into the conventional basic fluids. Perhaps, active methods like providing vibrations or rotations may enhance the heat transfer but these techniques have certain disadvantages. On the other hand, nanofluids as one of the passive methods increase the thermal properties of conventional base fluids. Enhanced thermal conductivity is the sole reason to make nanofluids. The idea of dispersion of solid particles was first proposed by Maxwell (1881), who perceived the enhancement in thermal conductivity. Thermal conductivity of any material is the measure of the ability of the material to conduct heat; higher thermal conductivity means high heat transfer and a lower value means less heat transfer. Table 1.1 summarizes the thermal conductivity of common materials used to make nanofluids. In the earlier decades of 20th century, Vand (1948) and Robinson (1949) reported the changes in the thermophysical properties after suspending the metallic and non-metallic solid particles into the conventional fluids. Later, Masuda et al. (1993) dispersed the ultrafine solid particles in the base fluid and witnessed the enhancement in thermal conductivity. However, the size of these solid particles was in the scale of micro or greater than the micro level which leads to sedimentation, abrasion and clogging in the flow of these fluids. S.U.S. Choi, a scientist from Argonne National Laboratory, USA, in 1995 suspended the nanosized solid particles into the base fluids to enhance the thermal conductivity of the conventional fluids and suggested the term nanofluids. Later on, several studies reported the enhancement in the thermal conductivity, which enhances the heat transfer due to nanoparticle addition in the conventional fluids in the various applications. A plethora of literature on nanofluids is reported in the various field of science and nature since 1995, the interest in the domain of nanofluids is increasing exponentially.

Table 1. 1 Thermal conductivities of common materials (nanoparticles and base fluids) used for nanofluids at room temperature, 300 K.

	Materials	Thermal Conductivity (W/mK)
	Silver	406
	Copper	385
Metals	Gold	314
	Aluminium	205
	Iron	79.5
	Aluminum Oxide	40
	Copper Oxide	32.9
Metals Oxide	Iron Oxide	10
	Titanium dioxide	8.3
	Silicon dioxide	1.5
Base Fluids	Water	0.615
(Conventional	Ethylene Glycol	0.252
Fluids)	Engine Oil	0.145
	Transformer oil	0.126

1.1.1 Magnetic Nanofluids

Magnetic nanofluids (MNFs), the colloidal suspension of ferromagnetic nanomaterial, have been taken into research fascinatingly. After contemplating its distinctive, interesting properties and unique eximious features, it offers numerous applications, not only in the heat transfer field but also immensely prevalent in medical, biological, aerospace, electronics and solar sciences. MNFs constitute a special class of nanofluids that exhibit both magnetic and fluid properties. MNFs are the suspension of ferromagnetic nanoparticles (Maghemite, Magnetite, Cobalt, Nickel etc.) into the nonmagnetic base fluids. Other than the enhancement in thermal conductivity, MNFs have one more exceptional feature that it has the magnetic properties as well i.e. a fluid with magnetic properties. It enables that MNFs can be controlled by applying the magnetic field. Such features of this kind of smart nanofluids make it eligible for a numerous plethora of fields.

1.2 Application Areas of Nanofluids

Nanofluids have many applications in the broad various areas of science & technology to improve the efficiency of the system. The common application areas of nanofluids are given as:

1.2.1 Applications in automotive

In any automobile, nanofluids are applicable as engine coolant, automatic transmission fluid, lubrication of gear etc. The use of nanofluids as an engine coolant is enhancing efficiency and reducing the size of the radiator (A. Kumar & Subudhi, 2019).

1.2.2 Applications in domestic refrigerator

Nano additive refrigerant in the refrigerator and air conditioning system are very effective and improve the performance of the system. $Al_2O_3/R134a$ and $TiO_2/R600a$ are examples of the nano-refrigerant used by the various researchers (Raghavalu and Rasu 2018; Borkar and Choudhary 2018).

1.2.3 Industrial cooling applications

Nanofluids are used in various industries to transport heat more effectively and efficiently. More than 3000 million kWh of energy can be saved per year from the electric power industry if nanofluids are used as working fluid (Saidur et al. 2011; Taylor et al. 2013).

1.2.4 Solar devices & thermal energy storage

Use of nanofluids in the thermal energy storages, solar collector, solar pond and photovoltaics enhances the efficiency of the system substantially (Khanafer & Vafai, 2018). The use of nanofluids enhances the efficiency of the thermal system around 10 % compared to the conventional fluid (Mahian et al., 2013).

1.2.5 Electronic applications

Cooling of high heat output electronic components like microprocessor by nanofluids shows a greater enhancement compared to the conventional way. For a particular type of nanofluid, the heat transfer coefficient is enhanced around 40 % compared to that of base fluid (Nguyen et al. 2007; Colangelo et al. 2017; Putra et al. 2011).

1.3 Application of Magnetic nanofluids

Magnetic nanofluids have many applications in various sectors such as medical, biological, electronic, optical and heat transfer applications. Magnetic nanofluids have various applications because their properties can be controlled by externally and their physical properties may change with the volume fraction of nanoparticles and with the

intensity of the magnetic field. Fortunately, some of the applications of natural convection heat transfer explore to the natural magnetic field e.g. geothermal energy extraction, the fusion reactors, metal casting, and crystal growths in liquids (Moreau, 2013).

Fumoto et al. (2007) produced an oval shape loop to develop a small heat transport device and the purpose of the study was to develop a device that could transport heat without any moving component. Nakatsuka et al. (2002) investigated the heat pipe and found an increment in heat transfer using magnetic fluid. Yamaguchi et al. (2004) studied both experimentally and numerically the design of direct heat to power energy conversion device using magnetic fluid. Li et al. (2008) and Lian et al. (2009) developed a miniature automatic energy transport device (AETD) by using temperature-sensitive fluid and a permanent magnet. The devices had no moving parts, so it was maintenance-free. It could be used for automatic cooling. The driving force for magnetic fluid has resulted from the synergic effect of the magnetic field and temperature gradient. The schematic diagram of the device is shown in Figure 1.1. The device contains two permanent magnets and three heaters and a cooling chamber and the flow loop contains Mn-Zn ferrite fluid. By changing the positions of magnets, one can control the flow of the magnetic fluid. Xuan and Lian (2011) reported the physical application of the AETD by designing a cooling device for electronics cooling.

(a)   (b)
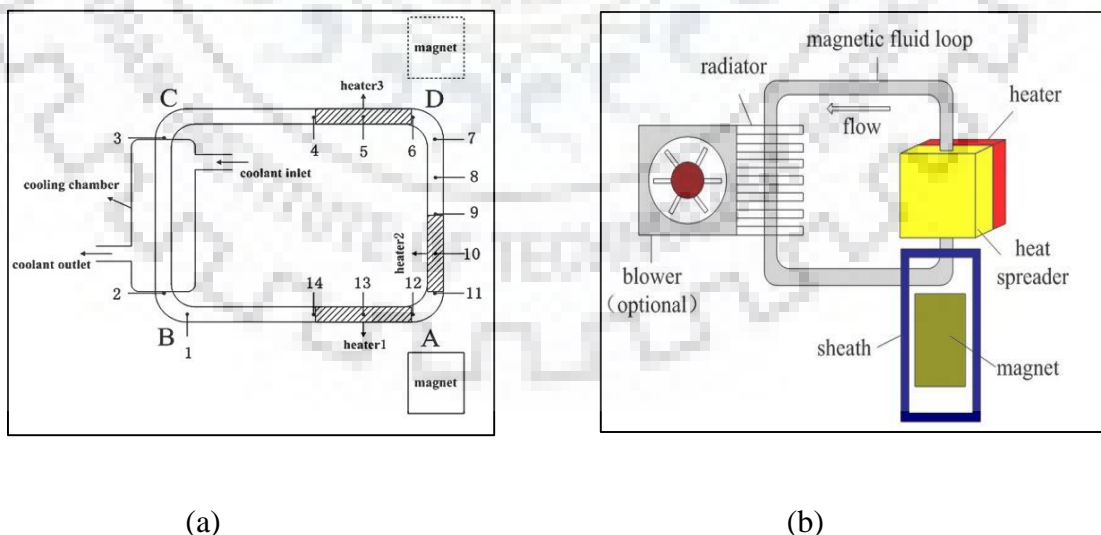
Figure 1. 1 Schematic diagram for automatic cooling devices: (a) a miniature automatic cooling device (Li et al., 2008) (b) thermomagnetic cooler based on AETD (Xuan & Lian, 2011).

Apart from thermomagnetic convection, magnetic nanofluids have a number of applications in forced convection. Moreover, magnetic nanofluids are used in the cooling of loud speakers. Furthermore, Stoian and Holotescu (2014) evaluated the cooling potential of transformer oil (TO-40 A) based Fe_3O_4 nanofluid. From the results, the magneto convection inside the coil core decreased the rate of rising temperature under the presence of a magnetic field. At low intensity or in the absence of a magnetic field, it was showing a similar trend.

In medical science, magnetic nanofluids are used and have shown significant results. So many diseases like cancer, hyperthermia, and amyloid-related diseases can be cured by using magnetic nanofluids (Antosova et al., 2010; Scherer & Neto, 2005). The magnetic nanofluids are also used in dynamic sealing and inertial & viscous damper (Raj & Moskowitz, 1990; Scherer & Neto, 2005).

1.4 Present Study

In this experimental work, the behaviour of natural convection heat transfer in an open cavity heated from below is studied with the variations of different parameters. Unlike Rayleigh-Bénard convection, very few investigations have been reported on the temperature and heat transfer behaviour in an open cavity. So, this parametric experimental study will provide a handful of information about temperature fluctuations, thermal boundary layer thickness and heat transfer in this domain of natural convection. The study also comprises the synthesis, characterization and stability analysis of the magnetic nanofluids. The different parameters included in the present work are stated below.

1.4.1 Heat Flux

In this work, the heat flux varies from 200 to 10500 W/m^2 for all the cases, including water and magnetic nanofluids. The range of Rayleigh numbers noted in the turbulent regime of natural convection for all the cases is reported.

1.4.2 Magnetic Nanofluids

Fe_3O_4-water magnetic nanofluids have nanoparticles concentration in the range of 0.01 to 0.1 vol. % are studied. The effects of particle concentrations on thermophysical properties and natural convection heat transfer are reported and discussed.

1.4.3 Magnetic Field

The study reports the effect of externally applied magnetic field on the thermophysical properties and natural convection heat transfer. The magnetic field in the present study varies in the range 200 -800 Gauss.

1.5 Objectives

Based on the above brief discussion and a broad literature review (chapter 2), the present work is planned for an extensive range of experiments. Following are the major objectives planned for the present work:

- To prepare the stable magnetic nanofluids by the two-step method using different types of surfactants and additives.
- To conduct the experiments on the prepared magnetic nanofluids to measure the different thermophysical properties like thermal conductivity, viscosity and density with variations in different parameters such as temperature, nanoparticles concentrations and externally applied magnetic field.
- To develop the correlations for the prediction of different thermophysical properties with the various parameters.
- To perform the experiments on the open cavity natural convection with water and magnetic nanofluids as working fluids in a controlled experimental facility.
- To investigate the temperature fluctuations and thermal boundary layer properties in the open cavity convection at various heat fluxes for water as well as magnetic nanofluids.
- To investigate the effects of nanoparticle concentrations and externally applied magnetic fields on the open cavity convection.
- To develop the empirical correlations for global heat transfer in the open cavity convection based on the different dimensionless numbers.

1.6 Methodology

The flow chart of the methodology adopted in the present work is shown in Figure 1.2.

Figure 1. 2 Flow Chart of the methodology adopted in the present work.

1.7 Organisation of the thesis

The remaining chapters of the thesis are structured as follows; In the next chapter 2, the literature review regarding the present work is epitomized comprehensively and it also includes the recently published research. Chapter 3 deals with the synthesis, characterization and stability analysis of the magnetic nanofluids. It also includes the comparisons of the various thermophysical properties of magnetic nanofluids with the existed theoretical models. Based on the measured data, the new empirical correlations have been developed and discussed. The experimental facility has been discussed systematically in Chapter 4. Chapter 5 reports the data collection techniques and various dimensionless numbers along with the uncertainty analysis in the experiments and results. Chapter 6 reports the results and a comprehensive discussion on the various trends obtained in the open cavity convection from the results. In the last chapter 7, the conclusion is drawn for discussion and findings of this work and report the various suggestions for future study.
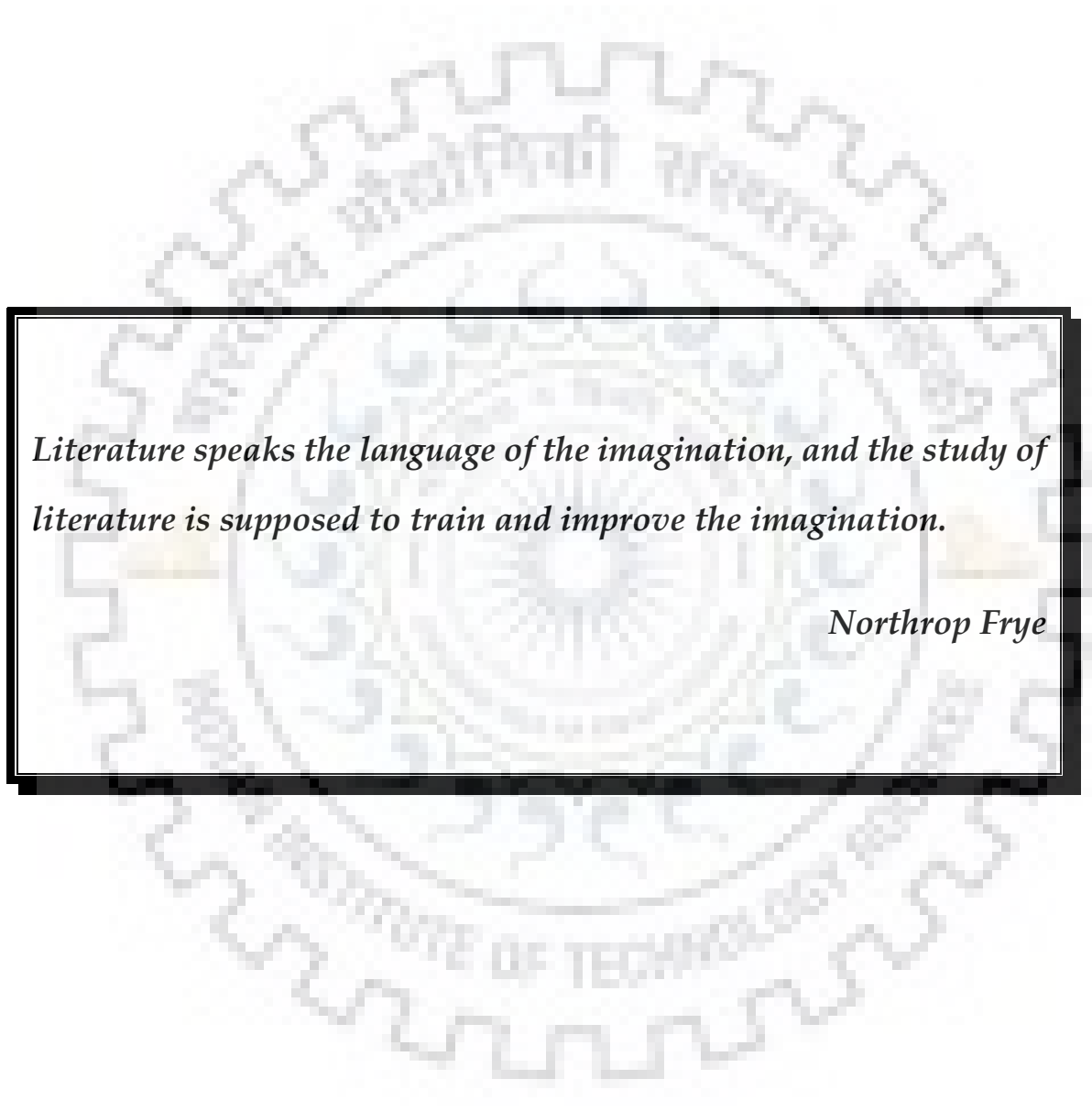
Chapter 2: Literature Review

Index

Literature speaks the language of the imagination, and the study of literature is supposed to train and improve the imagination.

Northrop Frye

2

Literature Review

Nanofluids have diverse applications in nature and technology. There are many different categorized nanofluids have been reported by the researchers. This chapter epitomizes and peruses the research work done on the nanofluids, including synthesis, characterization and applications of the nanofluids. Moreover, both numerical and experimental approaches have been included for the insightful analysis of the nanofluids. The chapter first underlines the different types of nanofluids based on the different categories and then the importance of appropriate methods of preparation of magnetic nanofluids as well as its effects on the thermophysical properties. Subsequently, the chapter comprehends the descriptive analysis of augmentation of natural convection heat transfer and the effect of externally applied magnetic field on the behaviour of magnetic nanofluids. The studies associated with the present area of research conducted so far, existing in the literature, are concise and presented in the succeeding.

2.1 Types of nanofluids

Nanofluids can be classified into several categories based on different parameters. The researchers use different solid materials to manufacture nanoparticles for the nanofluids. These nanoparticles material can be metals (Cu, Ag, Au), metal oxides (Al_2O_3, CuO, TiO_2, Fe_3O_4), metal carbides (SiC, TiC, ZrC), metal nitrides (AlN, SiN, TiN), alloys (Cu-Zn, Fe-Ni, Ag-Cu) and carbon materials (Graphite, Carbon Nanotube, Diamond). The nanoparticles suspended in the base fluids, the common basefluids for the nanofluids are water, ethylene glycol, ethanol, transformer oil, engine coolant and refrigerants. Mainly nanofluids can be classified into two main categories: single material nanofluids and hybrid nanofluids

2.1.1 Single material Nanofluids
Single material nanofluids are the conventional form of nanofluids, in which only a single type of nanoparticles is suspended into the base fluids. Many authors have

reported that the single material nanofluids are superior in performance due to more improvement in the favourable thermophysical properties (Modak et al., 2018; Reddy et al., 2017; Yang & Du, 2017).

2.1.2 Hybrid Nanofluids

These are the advanced nanofluids, which are prepared by the combination of two or more than two material's nanoparticles dispersion into the base fluids. Jana et al. (2007) have studied the hybrid nanofluids and compared them with the single material nanofluid and reported that the hybrid nanofluids do not show as much improvement in the thermal conductivity as found in single or monotype nanofluids. They have also reported that the stability of hybrid nanofluids is more than that of the single material nanofluids, which can lead to preserving the thermal conductivity of nanofluids much longer time before settling of nanoparticles.

2.1.3 Magnetic Nanofluids

Magnetic nanofluids or Ferrofluid are a special class of nanofluids having distinct unique features. These are the suspension of ferromagnetic nanoparticles such as Maghemite, Magnetite, Cobalt, nickel etc., into the nonmagnetic base fluids. In particular, the magnetic nanofluid is a smart fluid magnetically controllable (Engler et al., 2009; Odenbach, 2003; Rosensweig, 1969; Shliomis, 1972; Shliomis & Morozov, 1994; Zablotsky et al., 2009) and has the potential for a variety of applications.

2.2 Synthesis of Magnetic Nanofluids

A uniformly dispersed and stable nanofluid is highly applicable to various categories of applications, so the key step to achieve highly stable nanofluids is the synthesis of nanofluid. Various types of nanofluids are synthesized by different physical and chemical processes. Agglomeration of particles and various other properties depend on the preparation of nanofluids. Broadly there are two methods to synthesize nanofluids viz. one step and two-step method (A. Kumar & Subudhi, 2018, 2019). This study is about magnetic nanofluids and hence the preparation of the same and the method of preparation by researchers are briefly described in Table 2.1.

The single-step method is the process of combining the manufacturing of nanoparticles and synthesis of nanofluids in one step only. In this method, simultaneously making and dispersing of the particles in the basefluid, avoid the drying, transportation and

storage problems of nanoparticles. A two-step method is mostly used in the making of nanofluids. In this method, the previously prepared nano-powder is get dispersed by ultra-sonication. Although the one-step method has some advantages over the two-step method, the researchers prefer the two-step method. The two-step method involves two steps to prepare magnetic nanofluids. The first step includes the preparation or purchasing of nanoparticles and the second step is comprising the dispersion of nanoparticles into a basefluid by ultra-sonication. A simple and standard method to prepare magnetite nanoparticles is co-precipitation. An aqueous mixture of ferrous and ferric in the form of hydrated chloride salts in the alkaline medium in the ratio of $Fe3^+$/ $Fe2^+ :: 2/1$ is used for the preparation of magnetic nanoparticles. The flow diagram of the procedure of the co-precipitation method is shown in Figure 2.1 (Laurent et al., 2008; Peternele et al., 2014 and Saien et al., 2015). Ultra-sonication is the process used to disperse nanoparticles into the base fluid in two-step methods (shown in Figure 2.1 inset). For the sake of uniformity and homogeneity, a high degree of steadiness is required. Oleic acid is one of the most commonly used surfactants in magnetic nanofluids for high stability.

Table 2. 1 Reported synthesis of magnetic nanofluids over the last few years.

Authors	Material of nanoparticles	Base fluid	Concentration	Particle size (nm)	Process
Aksenov et al.(2003)	Fe_3O_4 & $CoFe_2O_4$	Water	6.5 vol% & 2 vol%	-	Two step
Li et al. (2005)	Fe_3O_4 & Fe	Water	1 to 5 vol %	20 & 26	One step & two step
Bica et al. (2007)	Fe	Water	0.15 vol %	Less than 10	One step
Hong et al. (2007)	Fe_2O_3	DI water	0.02 wt.%	5–25	Two step
Singh et al. (2009)	Cr_2O_3	Distilled water	0.1 wt.%	30–80	Two step
Li & Xuan (2009)	Fe_3O_4	Water	1.0 vol %	10	One step
Abareshi et al. (2010)	Fe_3O_4	Water	0 to 3 vol%	10	Two step
Yu et al. (2010)	Fe_3O_4	Kerosene	1.0 vol.%	15	Two step
Kudelcik et al. (2010)	Fe_3O_4	Transformer oil ITO 100	0.2, 1 & 2 vol.%	10.6	Two step
Lajvardi et al. (2010)	Fe_3O_4	Water	5 vol. %	10±5	Two step
Abareshi et al. (2011)	α-Fe_2O_3	Glycerol	0.125 to 0.75 vol. %	5	Two step

Nabeel Rashin & Hemalatha (2012)	Fe_3O_4	Water	0.2, 0.4, 0.6, 0.8 & 1 vol.%	11	One step
Syam Sundar et al. (2012)	Fe_3O_4	EG-water	0 to 1 vol%	11.42	Two step
Syam Sundar et al. (2012)	Fe_3O_4	Distilled water	0.02 to 0.6 vol%	36	Two step
Gavili et al. (2012)	Fe_3O_4	DI water	5 vol %	10±3	Two step
Gu et al. (2013)	Fe_3O_4	DI water	0.5 to 2.5 vol%	8 to 12	Two step
Nabeel Rashin & Hemalatha (2014)	$CoFe_2O_4$	Water	0.2 to 1 vol %	14	Two step
Karimi et al. (2014)	Fe_3O_4 & $CoFe_2O_4$	DI water	0 to 4.8 vol %	10 &15	Two step
Goharkhah et al. (2015)	Fe_3O_4	Water	1 to 2 vol %	30	Two step
Bagheli et al. (2015)	Fe_3O_4	DI water	0.1 to 0.5 vol %	14.2	Two step
Wang et al. (2016)	Fe_3O_4	Water	0.5 to 5 vol %	7.5	Two step
Sundar et al. (2014)	Nano diamond and nickel	EG-water	0 to 3.03 wt. %	30	Two step
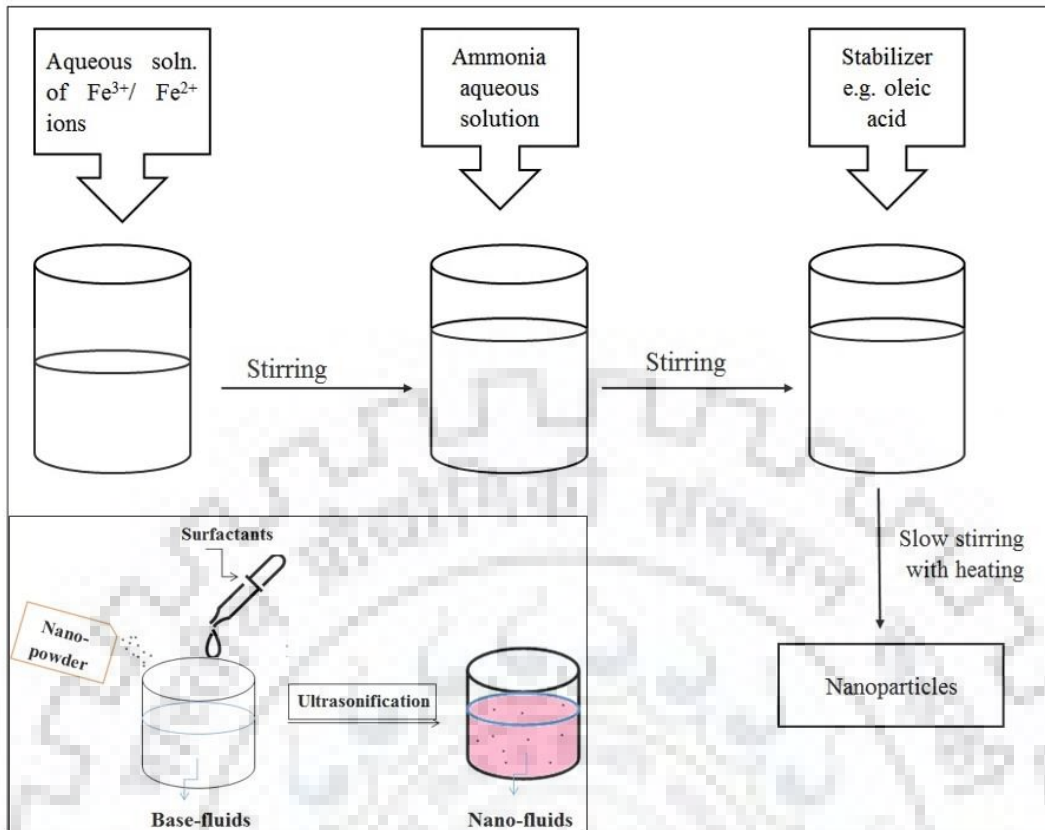
Figure 2. 1 Flow diagram of Co-precipitation method to prepare magnetite nanoparticles, inset shows the two-step method to prepare nanofluids.

2.3 Thermophysical properties of magnetic nanofluids

A colloidal suspension of magnetic nanoparticles into the base fluid can adjust the thermophysical properties to the desired requirement. The thermophysical properties mainly comprise thermal conductivity, viscosity, heat capacity and density. Thermal conductivity and viscosity play a vital role in enhancing convection heat transfer, especially in magnetic nanofluids. Magnetic nanofluids (which are sensitive to temperature) are severely dependent on thermal conductivity.

2.3.1 Thermal Conductivity

As mentioned in the first chapter, in 1995, S U S Choi comes up with the term Nanofluid after mixing the nano-sized particles into the convectional base fluids to enhance the thermal conductivity of the fluid (Choi & Eastman, 1995). Later many studies investigated and reported similar trends about the thermal conductivity of nanofluids. The thermal conductivity of nanofluid depends on various factors such as shape, size, concentration, temperature, dispersion of nanoparticles in the base fluid, the stability of a suspension, nanoparticles clustering, pH variation, chemical additives and surfactant

(Khurana et al., 2016 & Puliti et al., 2011). However, in the case of magnetic nanofluid, thermal conductivity also depends on the applied magnetic field. The scientists have studied the thermal conductivity of nanofluids by changing these above mentioned pertinent parameters and they have found impressive & exciting results. The correct measurement and prediction of the thermal conductivity of nanofluids is always a challenging task for researchers due to the involvement of numerous different parameters.

Many researchers have developed theoretical models and correlations by considering various factors to find thermal conductivity. Maxwell (1873) has reported the first theoretical correlation for the thermal conductivity of solid-liquid mixture considering the concentration of solids. Table 2.2 reports these significant theoretical correlations developed by the researchers. The Maxwell model is representative of all the theoretical models for thermal conductivity.

The effect of volume fraction on the thermal conductivity of magnetic nanofluids is shown in Figure 2.2. Figure 2.2 shows the graph between thermal conductivity ratio (thermal conductivity of nanofluids/thermal conductivity of the base fluid, k/k_0) and volume fraction (Vol. %) at room temperature. Abareshi et al. (2010) and Khedkar et al. (2013) have experimentally revealed that the thermal conductivity of water-based Fe_3O_4 magnetic nanofluids is a function of volume fraction. Enhancement in thermal conductivity is more pronounced at higher concentrations because of the reduced distance between nanoparticles. Similar kinds of trends have been noticed by Philip et al. (2007) & Parekh and Lee (2010) in the kerosene-based Fe_3O_4 magnetic nanofluids. Thermal conductivity may be different for different base fluids, but it is always increased with volume fraction. Perhaps, this difference for different base fluids could be attributed to the surface interaction among base fluid and nanoparticles. Figure 2.3 shows the effect of temperature on the thermal conductivity of the magnetic nanofluids. The temperature rises of the magnetic nanofluids lead to an increment in the Brownian motion of the nanoparticles, which enhances the thermal conductivity of magnetic nanofluids. The temperature effect could be different for using the same particles in different base fluids because the Brownian motion of nanoparticles may be different in the different base fluids. As shown in Figure 2.3 (a), the water-based Fe_3O_4 magnetic nanofluids show the dependence of the thermal conductivity on temperature and Figure 2.3 (b) shows kerosene-based Fe_3O_4 magnetic nanofluids. The effect of temperature is

21

more significant at higher volume concentration. The size of the nanoparticles also plays a vital role to change the thermal conductivity of magnetic nanofluids along with the presence of the magnetic field. Shima & Philip (2011) have revealed that the thermal conductivity is a function of the magnetic field and the particle size, higher enhancement in thermal conductivity with large size particles at the strong strength of the magnetic field, as shown in Figure 2.4. The enhancement in thermal conductivity at 2.8 and 9.5 nm size particles with at 300 G magnetic strength is 16 and 240 %, respectively. Larger size particles show higher enhanced dipolar interaction and the aspect ratio of the chain.
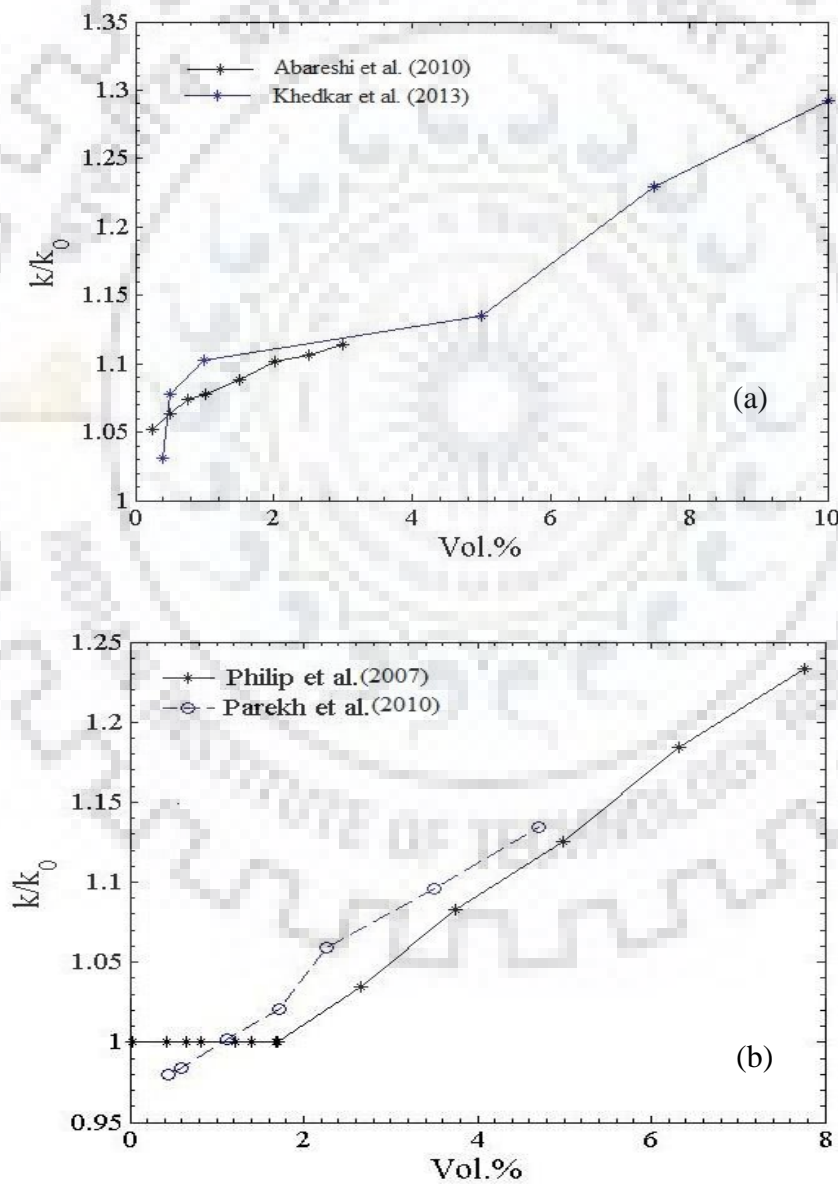
Figure 2. 2 Effect of concentration of Fe_3O_4 nanoparticles on thermal conductivity (a) water-based magnetic nanofluids. (b) kerosene-based magnetic nanofluids.
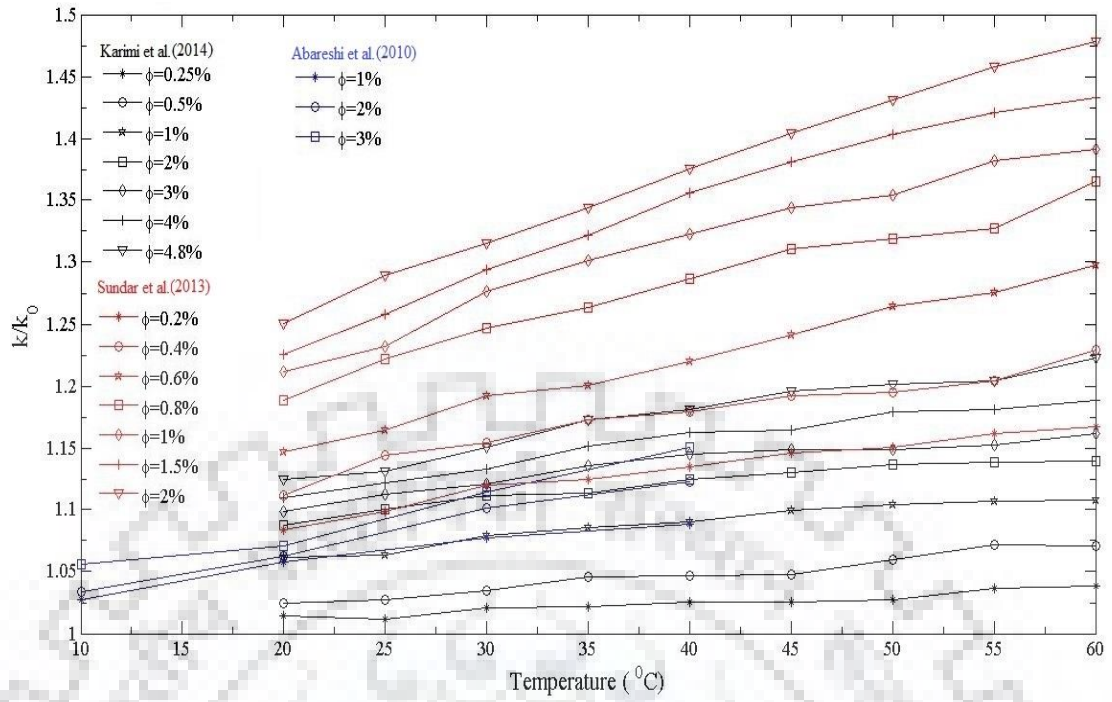
(a)
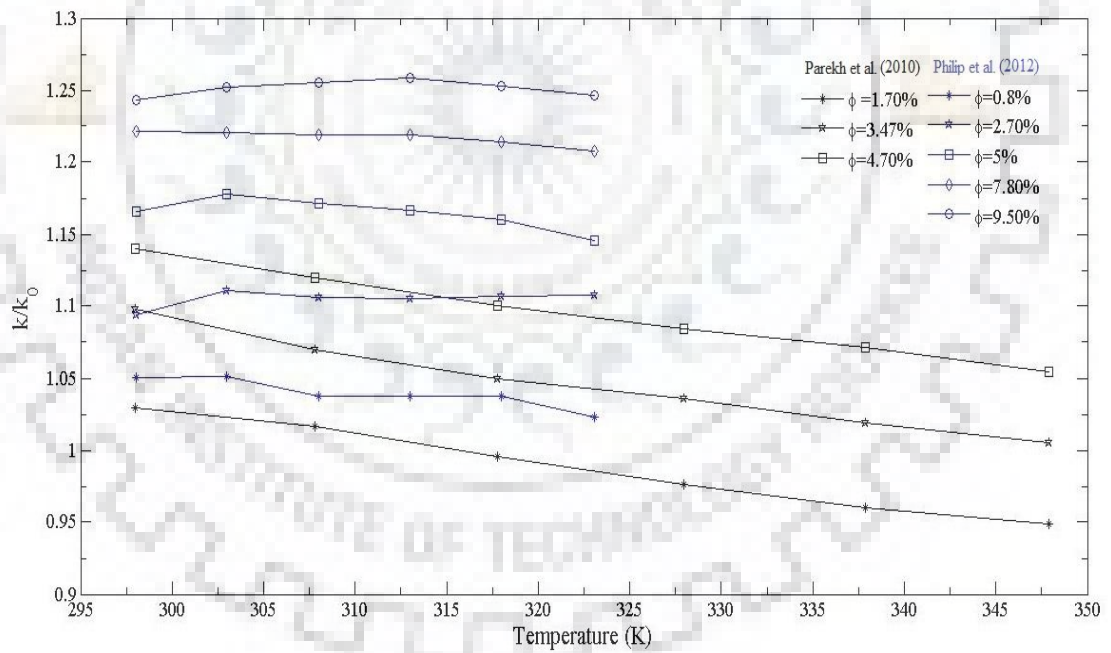
(b)

Figure 2. 3 Effect of temperature on the thermal conductivity of (a) water-based Fe₃O₄ nanofluids. (b) kerosene-based Fe₃O₄ nanofluids.

23
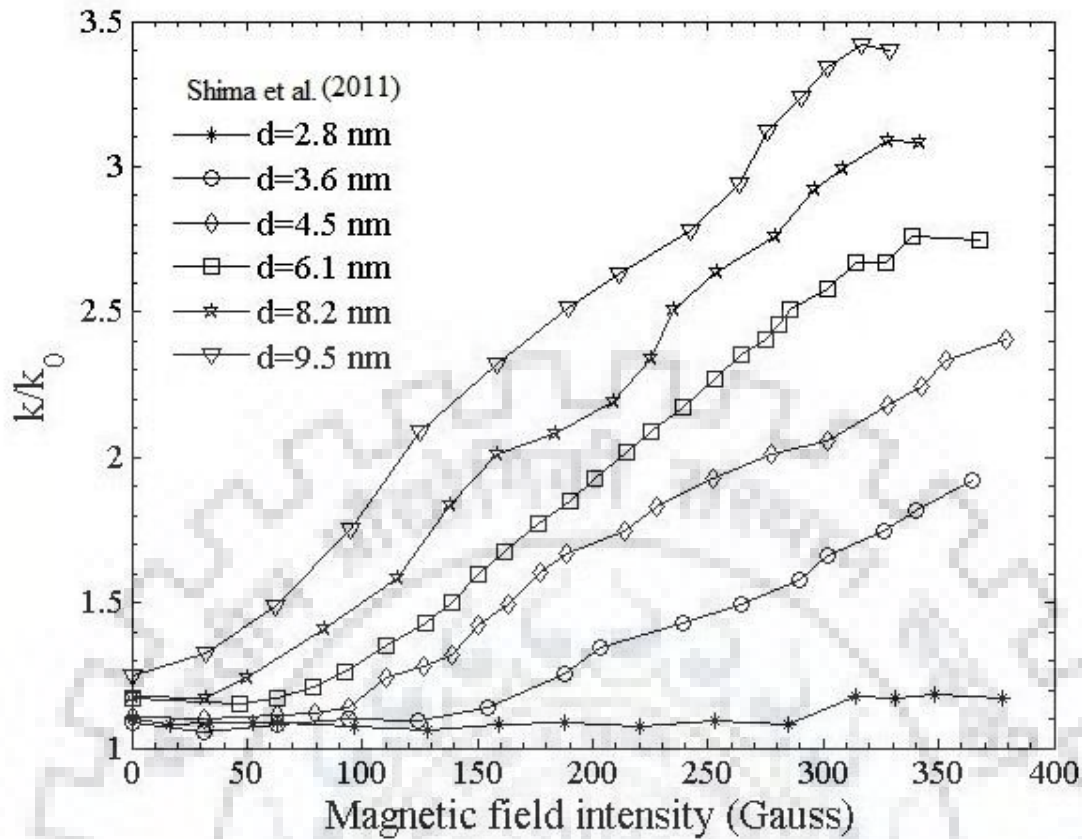
Figure 2. 4 Effect of Fe₃O₄ nanoparticles size on the thermal conductivity of magnetic nanofluids (Shima & Philip, 2011).

Figure 2.5 (a), (b) and (c) show the effect of the magnetic field on the thermal conductivity at different volume fractions of magnetic nanofluids. In Figure 2.5 (a), the water-based Fe_3O_4 magnetic nanofluids show that with the magnetic field, the thermal conductivity is increased. Karimi et al. (2014) have used Fe_3O_4 nanoparticles of 8-10 nm and found that thermal conductivity is increased with the magnetic field before reaching its maximum value. The magnetic dipolar interaction energy aggregates the nanoparticles in chain form under the presence of an external magnetic field. These chains lead to high conductive paths in magnetic nanofluids for high heat transfer. The zippering of chains has occurred at a higher magnetic field, which results in a decrease of the magnetic field. Later, Karimi et al. (2015) have used nanoparticles of 20-40 nm, which show enhancement in thermal conductivity even in the strong magnetic field. Similar kinds of results are revealed by Philip et al. (2007) and Katiyar et al. (2016) for kerosene-based Fe_3O_4 magnetic nanofluid and ethylene glycol-based Fe_3O_4 magnetic nanofluid.

(a)

(b)

25
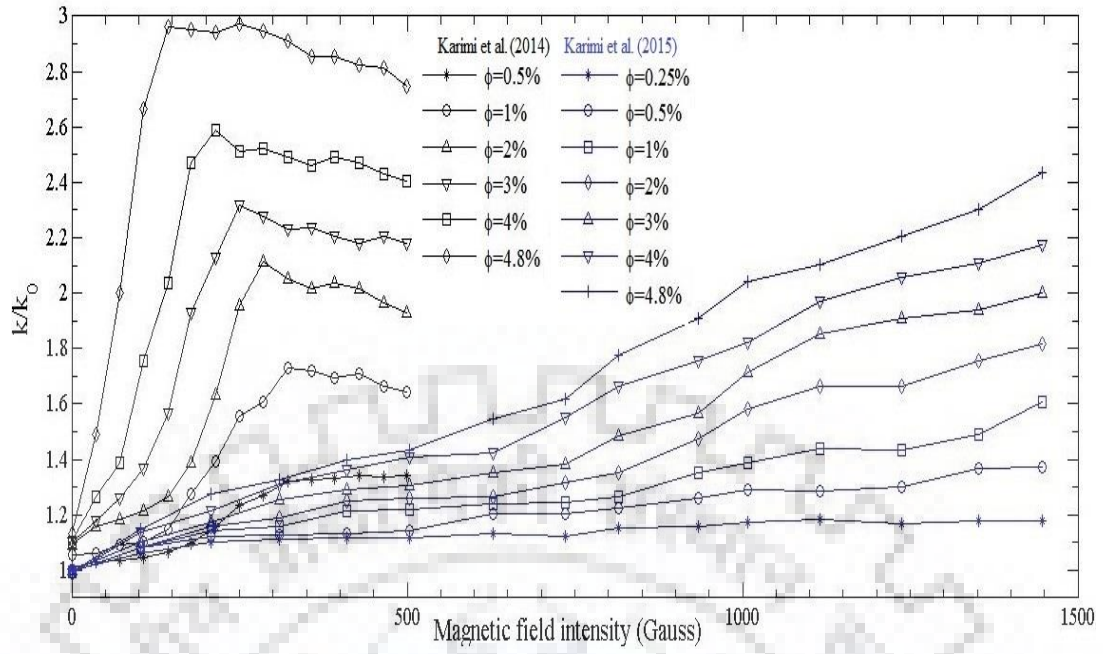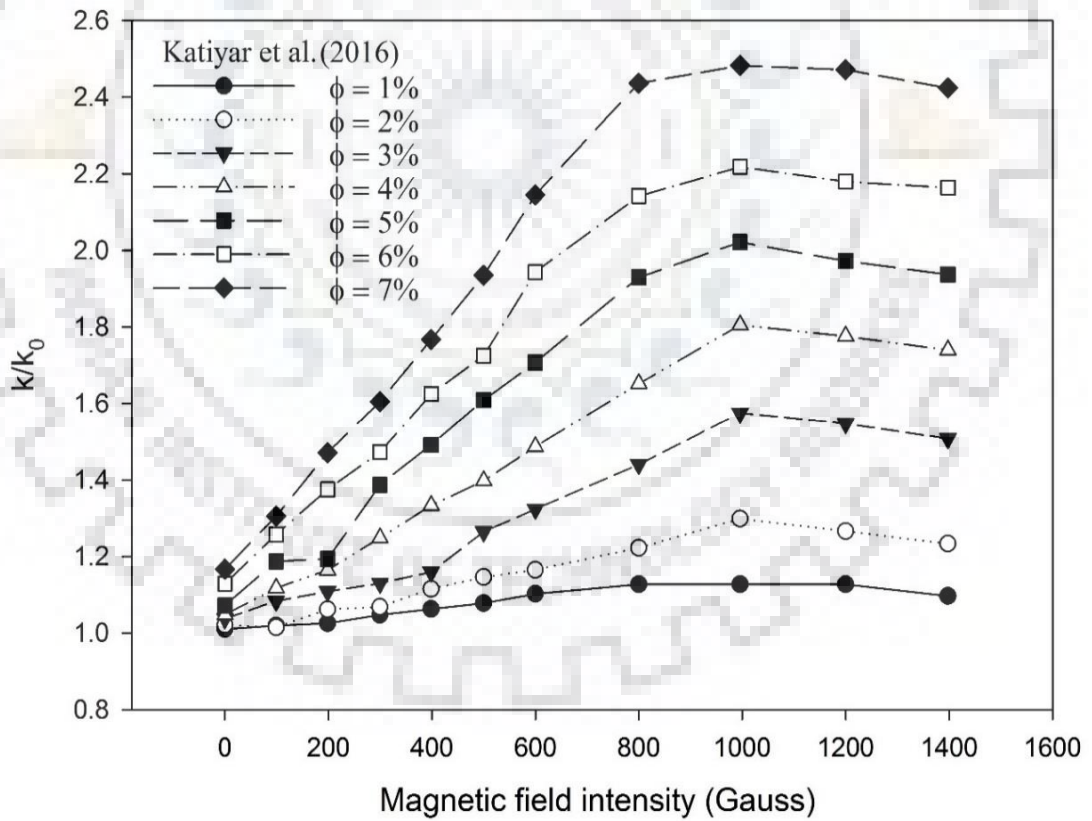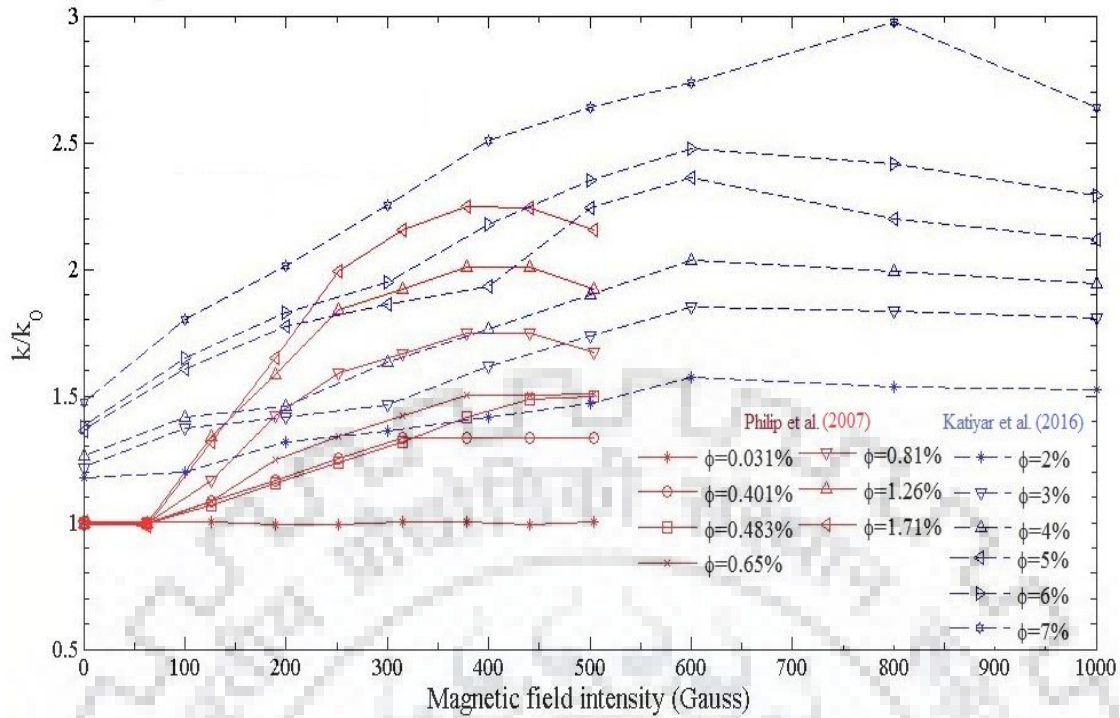
(c)

Figure 2. 5 Effect of applied magnetic field on the thermal conductivity of (a) water-based Fe₃O₄ nanofluids, (b) ethylene glycol-based Fe₃O₄ nanofluids, (c) kerosene-based Fe₃O₄ nanofluids.

2.3.2 Viscosity

A small increment in the viscosity (η) due to the dispersion of nanoparticles can affect processes like natural convection. Therefore, it's mandatory to consider it a key parameter to investigate the heat transfer for magnetic nanofluids. Perhaps the viscosity of magnetic nanofluids in the absence of magnetic field changes, as in the case of other nanofluids. Einstein equation (Einstein, 1906) of viscosity shows the dependence of viscosity on volume concentrations of nanoparticle, which is given by:

$$\eta_{nf} = \eta_f (1 + 2.5 \, \phi) \tag{2.1}$$

The Einstein correlation (equation 2.1) has been valid for the only low solid volume fractions of nanoparticles, and it is based on the Brownian motion of the particles inside the base fluid. Kunitz (1926) has set a new correlation, equation (2.2), to determine the viscosity of the colloidal suspension, which has a higher volume fraction of particles (up to 50%).

$$\eta_{nf} = \eta_f (1 + 0.5 \, \phi)/(1 - \phi)^4 \tag{2.2}$$

26

Several other correlations are listed in Table 2.3 to determine the viscosity of nanofluids. These models are generally based on certain parameters like shape, size, volume fraction, Brownian motion and interaction between particles. These models can be valid for magnetic nanofluids in the absence of the external magnetic field.

Figure 2.6 shows the effect of the magnetic field on the viscosity of water-based Fe_3O_4 magnetic nanofluids at different volume fractions of the nanoparticles. Yang et al. (2014), Wang et al. (2016) and Malekzadeh et al. (2016) have studied the viscosity of water-based Fe_3O_4 magnetic nanofluids and found that as the concentration of nanoparticles increases, there is a decrement in the distance between nanoparticles and increment in the interactions among particles. As a result, the viscosity has continuously increased with concentration. In the presence of a magnetic field, the nanoparticles have oriented in the direction of the magnetic field and formed a chain-like cluster. Hence, this obstruction blocks the flow and is more enhanced with the strength of the magnetic field and resulted in a higher viscosity of magnetic nanofluids. Patel (2012) shows that in the absence of a magnetic field, the nanoparticles in nanofluids roll freely and the magnetic field creates a hindrance to the rotation of nanoparticles, which increases the frictional coupling between nanoparticles and base fluid layers. Therefore, the viscosity of the magnetic nanofluids increases and the study also reveals that for a parallel magnetic field, the viscosity increases more to the perpendicular direction of the magnetic field. The viscosity of magnetic nanofluids also depends upon the selection of base fluid; magnetic nanofluids having different base fluids may have different viscosity although all other parameter and factors are the same. The effect of magnetic field on the viscosity of magnetic nanofluids having base fluid other than water is shown in Figure 2.6. McTague (1969) has studied the viscosity of cobalt particles dissolved in toluene and found that viscosity is a function of both the magnitude and direction of the magnetic field. The magnetic field application hinders the rotation of particles and this hindrance causes extra friction between fluid layers and resulted in an increment in viscosity. Similar kinds of results are obtained by Shima et al. (2009), Sundar et al. (2015) and Nurdin et al. (2016) for water-based γ- Fe_2O_3, kerosene-based magnetite and vacuum pump oil-based Fe_3O_4 magnetic nanofluids, respectively.
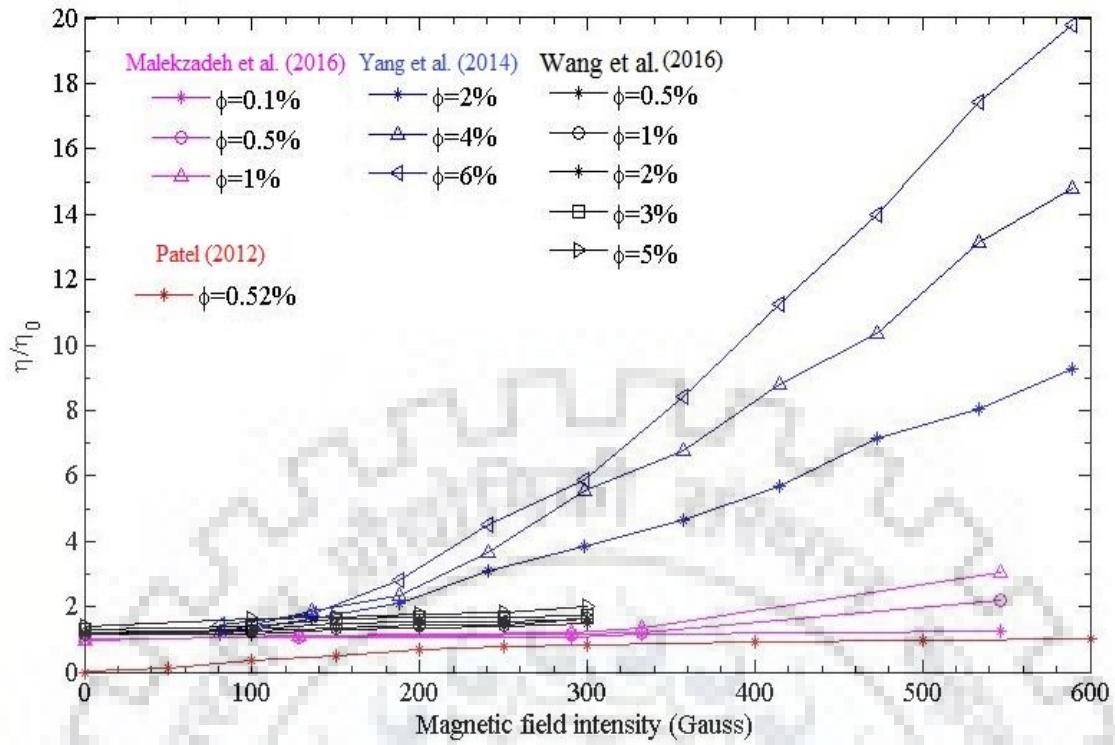
(a)
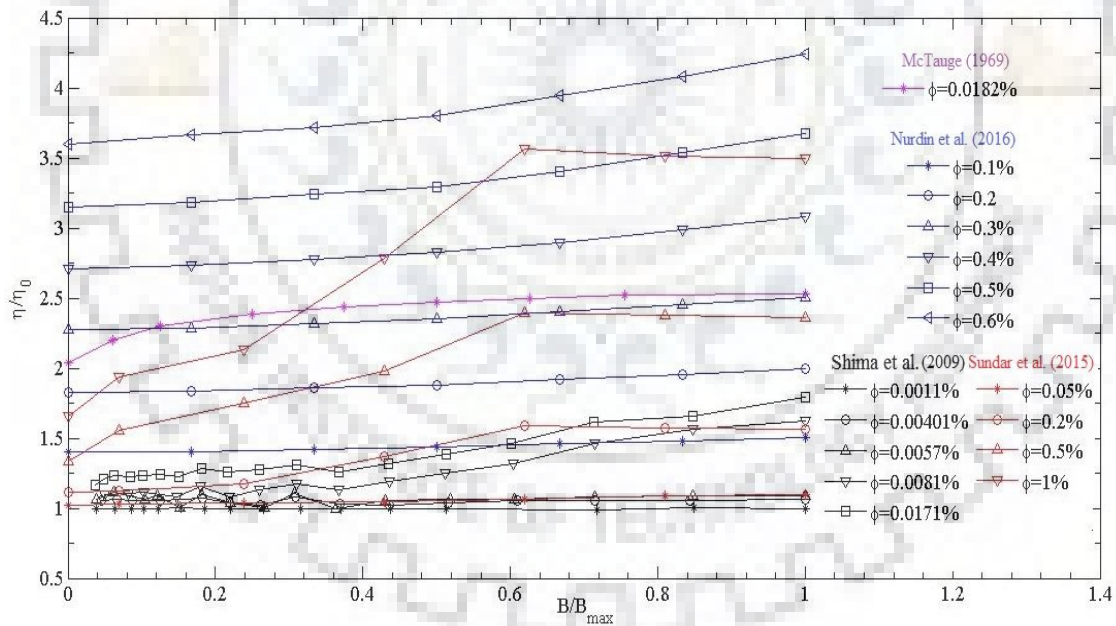
(b)

Figure 2. 6 Effect of magnetic field intensity on the viscosity of magnetic nanofluid (a) Water-based Fe₃O₄ MNfs (b) Oil-based Fe₃O₄ MNfs.

Rosensweig (1969) has predicted that the viscosity of the magnetic fluid in the magnetic field is a function of the ratio of hydrodynamic stress to magnetic stress and verified it experimentally. For the specific range of this ratio, the viscosity is a function of both the magnetic field and shear. McTague (1969) has observed that the viscosity of dilute magnetic colloids is a function of both the magnitude and direction of the applied magnetic field. The viscosity increment in the parallel applied magnetic field is twice compared to that of perpendicular. The experimental data of McTague strongly contradicts the calculated data of Hall & Busenberg (1969). McTague (1969) states correctly that the cause for the disagreement between experimental and calculated data is due to the neglected rotational Brownian motion of the particle. Shliomis (1972) has presented a theory considering the effect of a homogeneous magnetic field on the viscosity of the magnetic suspension. This theory has shown a more significant match to the experimental data of McTague (1969). Later in 1994, Shliomis & Morozov (1994) have proved that the effective viscosity got a decrement in an alternating magnetic field at a higher frequency. Wagh & Avashia (1996) have derived a formula for the viscosity (η_m) of magnetic fluid in terms of microscopic parameters and the magnetic field gradient and which is given by

$$\eta_m = \frac{m_1 \overline{C_1}}{12\sqrt{2}\,\pi a^2}\left\{1 + \frac{n_2}{n_1}\sqrt{\frac{m_1}{m_2}}\left[\frac{m_2/m_1\,(\lambda^2-1)+\delta(\lambda^2 m_2/m_1 -1)-1}{\lambda\sqrt{1+\frac{m_2}{m_1}+\delta}}\right]\right\} \tag{2.3}$$

where, $\lambda = \frac{4\sqrt{2}\,a^2}{(a+b)^2}$ and $\delta = \frac{\mu_0\,M\,\tau_2}{\overline{C_2}\,m_2}\left\{\left(\frac{\partial H}{\partial x}\right)^2 + \left(\frac{\partial H}{\partial y}\right)^2 + \left(\frac{\partial H}{\partial z}\right)^2\right\}$

m_1 is the mass of each fluid molecule and m_2 is the mass of each suspended magnetic particle. $\overline{C_1}$ & $\overline{C_2}$ are the mean speed of fluid molecule and solid particle, respectively. τ_2 is the average time between two successive collisions.

Shima et al. (2009) have reported that for magnetic nanofluids (with nanoparticles size <10 nm), the viscosity enhancement at low concentration is negligible in the presence of a magnetic field, while thermal conductivity shows relatively significant (about 50 %) enhancement. This makes them an ideal candidate for a heat transfer application. Yang et al. (2014) have observed that the viscosity of Fe_3O_4 aqueous nanofluids increases with the increasing intensity of the magnetic field. The reason suggested by them for increasing viscosity is that with increasing magnetic field intensity, the arrangement and interaction of the particles become stronger under the externally

applied magnetic field. Katiyar et al. (2015) have observed the same phenomenon among the magnetic nano colloids comprising of Fe_3O_4 nanoparticles dispersed in Polyethylene Glycol and developed an analytical model for viscosity, which is given by

$$\eta_m = a_1 B^2 + a_2 B + \eta_{m,zf} \qquad (2.4)$$

where, $\quad a_1 = \left(\frac{\tau_N}{2\mu_0}\right)\left(\frac{A_s}{L_c d_p \emptyset^n}\right)\left(\frac{d_{sep,\emptyset}}{d_{sep,opt}}\right) \quad \& \quad a_2 = H_{sat} \tau_N \emptyset^2$

B is magnetic flux density, $\eta_{m,zf}$ is viscosity for zero magnetic flux density, τ_N is Neel relaxation time, H_{sat} is a saturated magnetic field and A_s, d_p, L_c, $d_{sep,opt}$ & $d_{sep,\emptyset}$ represent the average surface area of the nanoparticles, the average nanoparticle diameter, the critical chained structure length under the magnetic field's influence, the interparticle separation within the chained structure at the optimal concentration and the separation at the required concentration, respectively. The exponent 'n' relates the magnitude of the coefficient to the concentration of nanoparticles.

Sundar et al. (2015) have investigated the viscosity and thermal conductivity of magnetic nanofluids with and without the presence of a magnetic field. At 1 % particle concentration and the magnetic field 1300 Gauss, viscosity enhancement is 256% and 298% at 20 and 60 ^{0}C, which is twice of enhancement in thermal conductivity. The formation of the chain-like structure under the magnetic field causes the increment in thermal conductivity and viscosity of nanofluids. Shahsavar et al. (2016) have studied the viscosity pattern of magnetic nanofluid loaded with carbon nanofluid and found that viscosity is increasing with the magnetic field and decrease with temperature. The prepared magnetic nanofluid follows the power-law viscosity model, given as follows:

$$\tau = c\gamma^n \qquad (2.5)$$

where 'c' and 'n' are correlated as:

$$c = 24.769 \left[\frac{1+608891214B-7813611.9\,B^2}{1-621740.5B-24961.852\,B^2}\right]\left[\frac{1+8.08\,\emptyset}{1+6.949\emptyset-.083\,\emptyset^2}\right]$$

$$n = \left[\frac{1+0.063202B-0.000407\,B^2}{1+0.030380B-0.000212\,B^2}\right]\left[\frac{0.651+1.59\,(\emptyset-0.45)}{1+2.464\,(\emptyset-0.45)+0.05\,(\emptyset-0.45)^2}\right]$$

Where B is magnetic field strength and $\emptyset$ is volume concentration.

Nurdin et al. (2016) have reported that the viscosity of maghemite (γ-Fe$_2$O$_3$) increases with magnetic field strength for all particle volume fractions, regardless of the direction of the applied magnetic field. Wang et al. (2016) have reported that the viscosity of water-based Fe$_3$O$_4$ magnetic fluid increases with magnetic induction and decreases with the temperature. Based on experimental data, a correlation has been developed, which is given by

$$\eta_{nf} = (0.035\,H^2 + 3.1\,H - 27886.4807\,\emptyset^2 + 4263.02\,\emptyset + 316.0629)\,e^{-0.02T} \quad (2.6)$$

where H is magnetic induction and $\emptyset$ is the volume concentration of nanoparticles.

Table 2. 2 Mathematical models for the thermal conductivity of solid-liquids suspensions.

Authors	Mathematical expression	Remarks
Maxwell (1873)	$$\frac{k_{nf}}{k_{bf}} = \left[\frac{k_p + 2k_{bf} + 2(k_p - k_{bf})\phi}{k_p + 2k_{bf} - (k_p - k_{bf})\phi}\right]$$	It did not consider the shape of suspended solid particles.
Hamilton & Crosser (1962)	$$k_{nf} = k_{bf}\left[\frac{k_p + (n-1)k_{bf} - (n-1)\phi(k_{bf} - k_p)}{k_p + (n-1)k_{bf} + \phi(k_{bf} - k_p)}\right]$$	n represents the shape
Jefferey (1973)	$$\frac{k_{nf}}{k_{bf}} = 1 + 3\beta + \phi^2\left(3\beta^2 + \frac{3\beta^3}{4} + \frac{9\beta^3}{16}\frac{\alpha+2}{2\alpha+3} + \frac{3\beta^4}{2^6}\right)$$	Extension of the Maxwell model
Bruggeman (1936)	$$k_{eff} = \frac{1}{4}\left[(3\phi-1)\,k_p + (2-3\phi)\,k_b\right] + \frac{k_b}{4}\sqrt{\Delta}$$	$\Delta = \left[(3\phi-1)^2(k_p/k_b)^2 + (2-3\phi)^2 + 2(2 + 9\phi - 9\phi^2)(k_p/k_b)\right]$
W Yu & Choi (2003)	$$k_{nf} = \left[\frac{k_p + 2k_{bf} + 2(k_p - k_{bf})\left(1+\frac{h}{r}\right)^3\phi}{k_p + 2k_{bf} - (k_p - k_{bf})\left(1+\frac{h}{r}\right)^3\phi}\right]k_{bf}$$	Include the effect of nanolayer, the solid-like layer of base fluid molecules around the suspended solid particle, into the Maxwell equation.
Leong et al. (2006)	$$k_{nf} = \frac{(k_p-k_{nl})\phi\left(\left(1+\frac{h}{r}\right)^3-1\right)k_{nl}\left[2\left(1+\frac{h}{2r}\right)^3-\left(1+\frac{h}{r}\right)^3+1\right]+(k_p+2k_{nl})\left(1+\frac{h}{2r}\right)^3\left[\phi\left(\left(1+\frac{h}{r}\right)^3-1\right)\left(1+\frac{h}{r}\right)^3(k_{nl}-k_f)+k_f\right]}{\left(1+\frac{h}{2r}\right)^3(k_p+2k_{nl})-(k_p-k_{nl})\phi\left(\left(1+\frac{h}{r}\right)^3-1\right)\left[\left(1+\frac{h}{2r}\right)^3+\left(1+\frac{h}{r}\right)^3-1\right]}$$	
Xue & Xu (2005)	$$\left(1 - \frac{\phi}{k_p/k_{bf}}\right)\frac{k_{nf} - k_{bf}}{2k_{nf} + k_{bf}} + \frac{\phi}{k_p/k_{bf}}\frac{(k_{nf} - k_p)(2k_p + k_{nl}) - \frac{k_p}{k_{bf}}(k_{nl} - k_p)(2k_p + k_{nf})}{(k_p + 2k_{nf})(2k_p + k_{nl}) + 2\frac{k_p}{k_{bf}}(k_{nl} - k_p)(k_p - k_{nf})} = 0$$	
Jang & Choi (2004)	$$k_{nf} = k_{bf}(1-\phi) + k_p\phi + 3C_1\frac{d_{bf}}{d_p}k_{bf}Re_{d_p}^2 Pr\,\phi$$	Role of Brownian motion taken into consideration

Koo & Kleinstreuer (2005)	$k_{TP} = \dfrac{1}{6\pi}\dfrac{\phi k_b}{\mu_{bf}}\dfrac{3k_{bf}}{k_p + 2k_{bf}}\left(1 \times 10^5 \rho_{bf} c_{p_{bf}}\right)\Delta T$	Effect of thermophoresis on the thermal conductivity of nanofluids with the Brownian motion and osmophoresis.
Gharagozloo & Goodson (2010)	$k_{nf} = k_{bf}\dfrac{k_{agg} + (n-1)k_{bf} - (n-1)\phi_{agg}(k_{bf} - k_{agg})}{k_{agg} + (n-1)k_{bf} + \phi_{agg}(k_{bf} - k_{agg})}$	The influence of aggregates have been taken into consideration

Table 2. 3 Mathematical models for the viscosity of the solid-liquid mixture.

Reference	Correlations	Remarks
Einstein (1956)	$\eta_{nf} = \eta_0\,(1 + 2.5\,\phi)$	Based on the Brownian motion and valid for low particle concentration
Kunitz (1926)	$\eta_{nf} = \eta_0\,(1 + 0.5\,\phi)/(1 - \phi)^4$	Valid for high particle concentration (up to 50%)
Robinson (1949)	$\eta_{nf} = \eta_0\left(1 + \dfrac{2.5\phi}{(1 - S'\phi)}\right)$	Extension of Einstein's equation; for higher concentration
Batchelor (1977)	$\eta_{nf} = \eta_0\,(1 + 2.5\phi + 6.2\phi^2)$	Brownian motion and valid for Homogenous solution;
Brinkman (1952)	$\eta_{nf} = \eta_0\left(\dfrac{1}{(1-\phi)^{2.5}}\right)$	Assumed the mixture as continuum
Masoumi et al. (2009)	$\eta_{nf} = \eta_0\left(1 + \dfrac{1}{\mu_0} \times \dfrac{\rho_p V_B d_p^2}{72C\left(\sqrt[3]{\dfrac{\pi}{6\phi}}\right)d_p}\right)$ $C = \left[(0.09d_p - 0.393) - (1.133d_p + 2.771)\phi\right]/\eta_f$	Based on Brownian motion and function of particle diameter and concentration.

2.3.3 Density

Sundar et al. (2013) have calculated the density of water-based Fe_3O_4 nanofluid at the concentrations range of 0 - 2.0 vol. % between the temperature range of 20 - 60 ℃ by the following equation.

$$\rho_{nf} = (1 - \emptyset)\rho_{bf} + \emptyset\, \rho_{np} \tag{2.7}$$

Later, Askari et al. (2016, 2017) have measured the density of Fe_3O_4 nanofluids at different concentrations and reported that the density is increased by the increment in the concentrations of nanoparticles. However, the increment in density is noted as very small and can be negligible; for instance, at 1 wt. % nanoparticle concentration, only 0.13 % increment in density is reported. They have also reported the theoretical models given in equations (2.8 & 2.9). These correlations are shown excellent consistency with the experimental data.

$$\rho_{nf} = 1003.4 + 30\,\emptyset - 0.18\,T \tag{2.8}$$

$$\rho_{nf} = \frac{\rho_f}{(1 - 2.6\,\emptyset)^{0.01}} \tag{2.9}$$

2.4 Natural Convection heat transfer

The copious literature comprising of theoretical and experimental work has been published on the natural convection in water or gasses using many geometrical shapes, size and various other parameters. The cause behind the natural convection heat transfer is the gravitational force, macroscopically similar everywhere. However, the control and enhancement of natural convection heat transfer is a challenging task. Even the addition of nanoparticles into the base fluids don't remark any significant enhancement of natural convection heat transfer. Choudhary & Subudhi (2016), Hu et al. (2014) and Putra et al. (2003) have observed that at low concentration, there is an enhancement in the heat transfer while at higher concentration, the heat transfer starts deteriorating because of increment in density and viscosity. A new method of using magnetic nanofluid attracts much attention of the researcher. This method allows controlling the fluid motion by the application of the external magnetic field. Along with natural convection, a magnetic field can exert a force that can control fluid motion in the magnetic field. Moreover, some magnetic nanofluids are temperature sensitive, i.e., magnetization decreases with an increase in temperature. When such type of magnetic nanofluids experience a temperature gradient in the presence of a magnetic field

34

(besides gravitational and buoyancy force), a net magnetic driving force exists, which induces the flow of the fluids entitled thermomagnetic convection.

For analysis of natural convective heat transfer, the researchers use different geometries and the most and generally used geometry is shown in Figure 2.7.

The magnetic nanofluid is filled in the test section. The test section generally includes the heating surface, plate heater and cooling chamber. The thermocouples mounted on an insulated rod at different locations are used to find the temperatures at different locations in the test section. The temperatures of the cooling and heating surface are measured using thermocouples mounted on them. A constant temperature bath is generally used to circulate cold water in the cooling chamber. The electromagnets are used to generate the magnetic field across the test section. Different dimensional and non-dimensional parameters are used by researchers to study the natural convective heat transfer. These parameters are generally based on temperature difference (ΔT) between heating and cooling surface temperatures of plates. Rayleigh number (Ra), Thermomagnetic Rayleigh number (Ram), Prandtl number (Pr) and Nusselt number (Nu) are used to analyse natural convective heat transfer. Table 2.4 provides the parameters used by different researchers to analyse the natural convective heat transfer.

Völker et al. (2007) and Engler et al. (2009) have studied the heat transfer by thermomagnetic convection and they have explained that when a Ferrofluid is subjected to the magnetic field and temperature gradient simultaneously then there exists a net driving force, called thermomagnetic convection. To understand it better, consider two parallel plates (as shown in Figure 2.7) containing magnetic nanofluid between them. A temperature gradient is applied by simultaneous heating of one plate and cooling of another plate, density difference within the fluid is created when there is the temperature gradient in the fluids. In the presence of the gravitational field, this density gradient leads to convective flow called Rayleigh- Bénard convection (shown in Figure 2.9 (a)). Moreover, magnetic nanofluids change their magnetization according to the temperature, called temperature-sensitive magnetic nanofluid (TSMNF). Aquino et al. (2005), Yamaguchi et al. (2010) and Aursand & Lund (2016) have reported the decrement in the magnetization with the increase of temperature of magnetic nanofluids, as shown in Figure 2.8. When there is an external magnetic field and a temperature gradient, there is a change in magnetization of particles, leading to

thermomagnetic convection. In Figure 2.9 (b), to avoid the gravitational effect, the temperature gradient is in the opposite direction and only thermomagnetic convection is present there. When both are considered (shown in Figure 2.9 (c)), then there is a presence of current between two plates, which enhances the convective heat transfer prominently. Furthermore, the Rayleigh number is obtained in the presence of both natural and thermomagnetic convection as given by

$$Ra_{total} = Ra + Ra_m \qquad (2.10)$$

where, Ra represents natural convection Rayleigh number and Ra_m is thermomagnetic Rayleigh number. (Reported in Table 2.4)
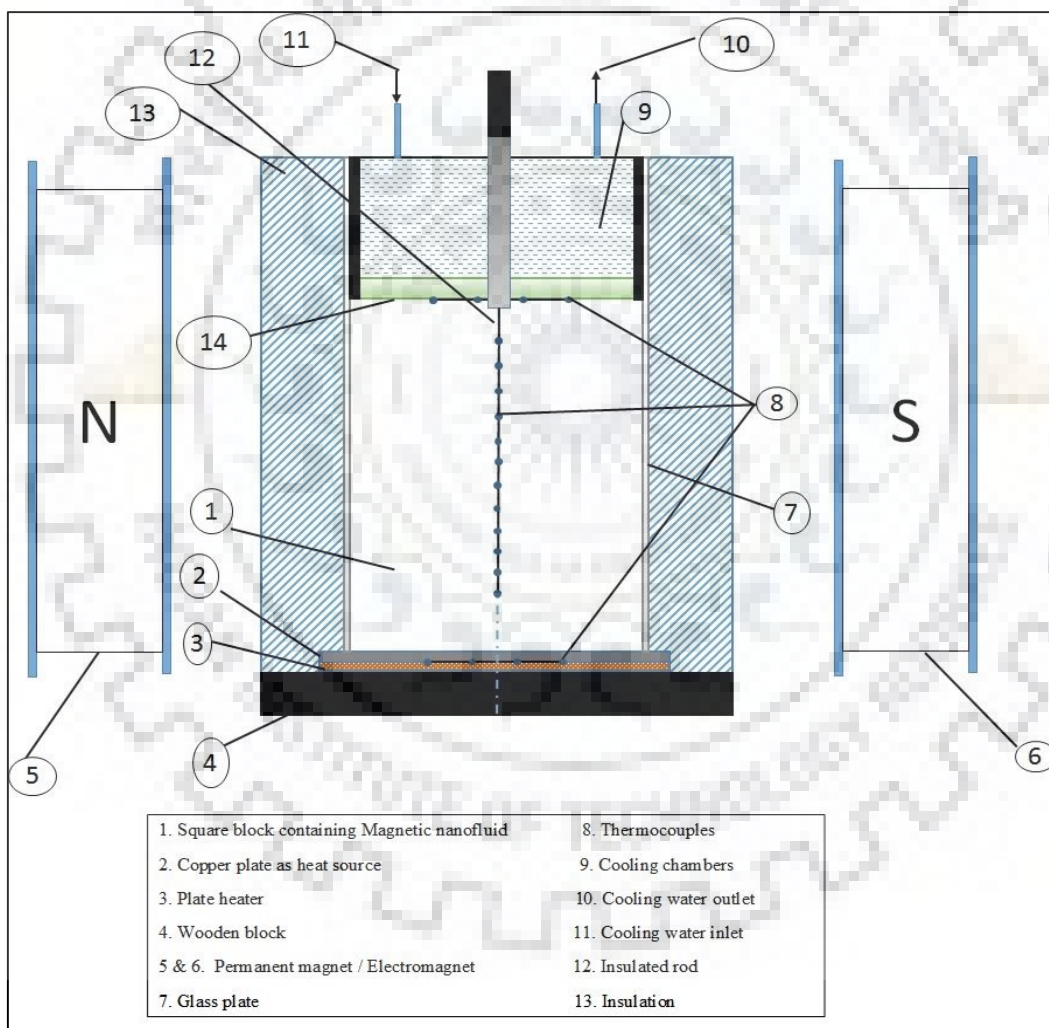
Figure 2. 7 Generalised schematic diagram of test section for natural convective heat transfer in magnetic nanofluids using an external magnetic field.
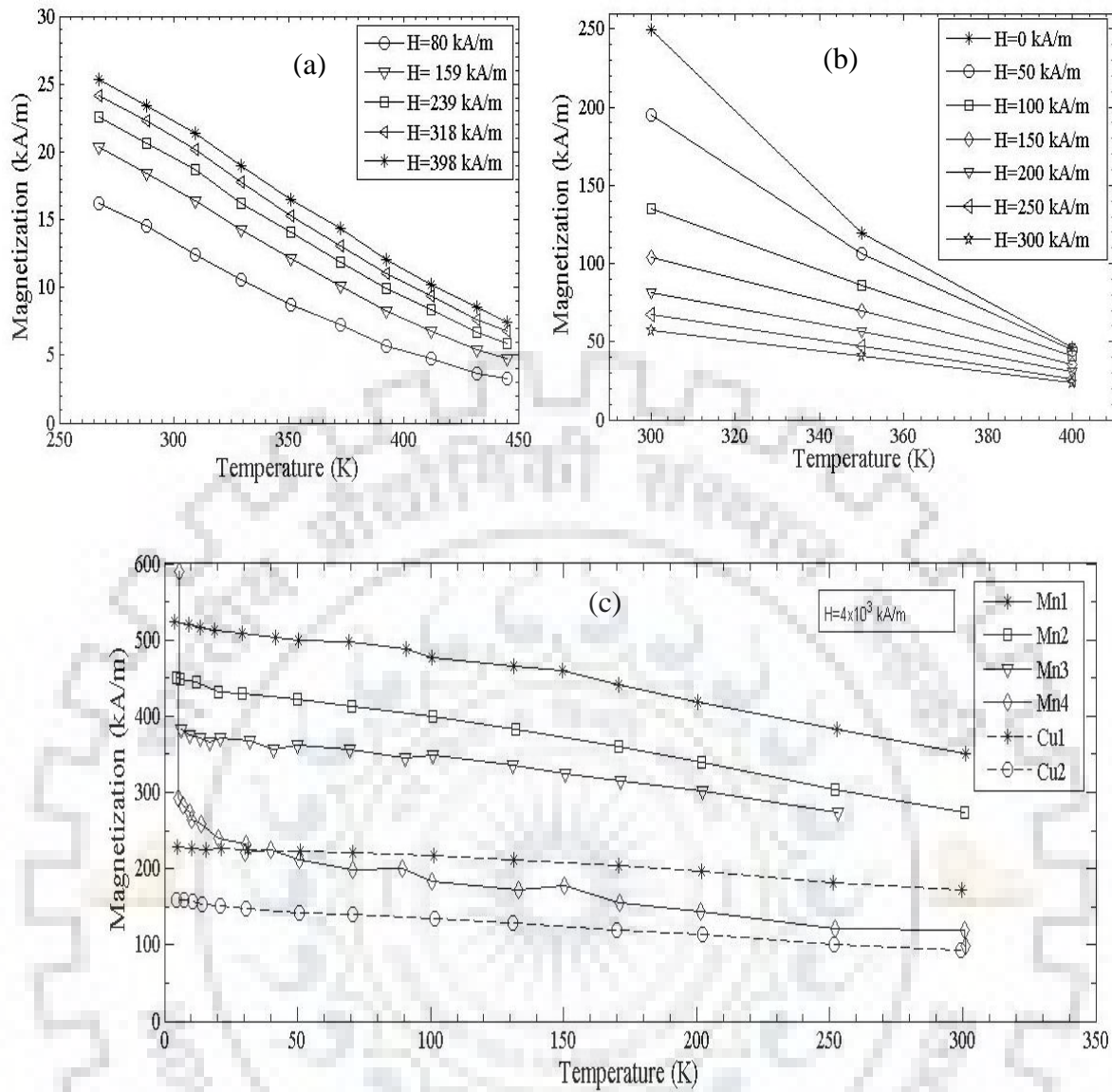
Figure 2. 8 Showing the temperature dependence of the magnetization of magnetic nanofluids (a) Kerosene based Mg-Zn, (b) Kerosene (TS50K) based Mg-Zn, (c) Mn samples based on MnFe$_2$O$_4$ and Cu samples based on Cu Fe$_2$O$_4$.

Table 2. 4 Reported various parameters and correlations used to investigate heat transfer characteristics in natural convection with thermomagnetic convection.

Authors	Parameters	Remarks
Völker et al. (2007)	Magnetic Rayleigh no., $Ra_m = \frac{\mu_0 K \, \Delta T \, \nabla H \, d^3}{k \, \eta}$ Where, $K = \left\lvert \frac{\partial M}{\partial T} \right\rvert$ $\mu_0 =$ Magnetic permeability	Destabilizing force is counteracted by two stabilizing effects: the thermal conductivity and the viscous friction of the fluid.
Yamaguchi et al. (2010)	Grashof No., $Gr = \frac{\rho^2 \, g \, \beta \, \Delta T \, d_C^3}{\eta^2}$ Magnetic Grashof no., $Gr_m = \frac{\rho^2 \, \mu_0 \, \chi_0 \, H_0^2 d_C^2}{\eta^2}$ $Nu^* = \frac{k \, \beta_c \, d_s \, \theta^{1/3}}{k \, \Delta T} \quad \theta = \frac{d_c}{d_s}$	Nu^* is the effective Nusselt number, d_c and d_s are the side length of the cubic container and heating generating stick, respectively. $\beta_c =$ Slope of approximated linear temperature distribution
Jin & Zhang (2013)	Rayleigh No., $Ra = \frac{\rho \, g \, \beta \, \Delta T \, L^3}{k \, \eta}$ Magnetic Rayleigh no., $Ra_m = \frac{\mu_0 \, H_0 \, M_s \, L^2}{k \, \eta}$	Natural convection in a porous cavity with different Darcy numbers.
Blums et al. (2008)	Total Rayleigh no., $Ra_{tot} = Ra + Ra_m$ $Ra_{tot} = \frac{\rho \, C_T \, \Delta T \, d^3}{\eta \, k} (\beta_T \rho \, g \, \pm \, \mu_0 \beta_m M \, \nabla H)$	Magneto convective heat transfer in a cylinder using both uniform and non-uniform acting transversally to the axis.
Zablotsky et al. (2009)	$Ra = \frac{\rho \, C_p \beta \, \Delta T \, L^3}{\eta \, k} \rho \beta_T \, g$ $Ra_m = \frac{\rho \, C_p \Delta T \, L^3}{\eta \, k} \, \mu_0 \beta_m M \, \nabla H$	Surface cooling in the non-uniform magnetic field in a rectangular cell.
Engler et al. (2009)	$Ra = \frac{\rho \, g \, \beta \, \Delta T \, L^3}{k \, \eta}$ $Ra_m = \frac{\mu_0 K \, \nabla H \, \Delta T \, d^3}{k \, \eta} = \frac{\mu_0 K^2 \, \Delta T^2 \, d^2}{k \, \eta}$ $Ra_{tot} = Ra_m + Ra$	Stabilizing effects of thermal diffusivity and viscous friction act contrary to this destabilizing force. All three effects are combined in the magnetic Rayleigh number
Ganguly et al. (2004)	$Ra_m = \frac{\mu_0 \, \rho \, \beta_\rho \, \chi_0 \, m^2 \Delta T \, Pr}{\eta^2 \, H^2}$	There is an empirical equivalence between buoyant and thermomagnetic convection based on their respective Rayleigh number correlations.
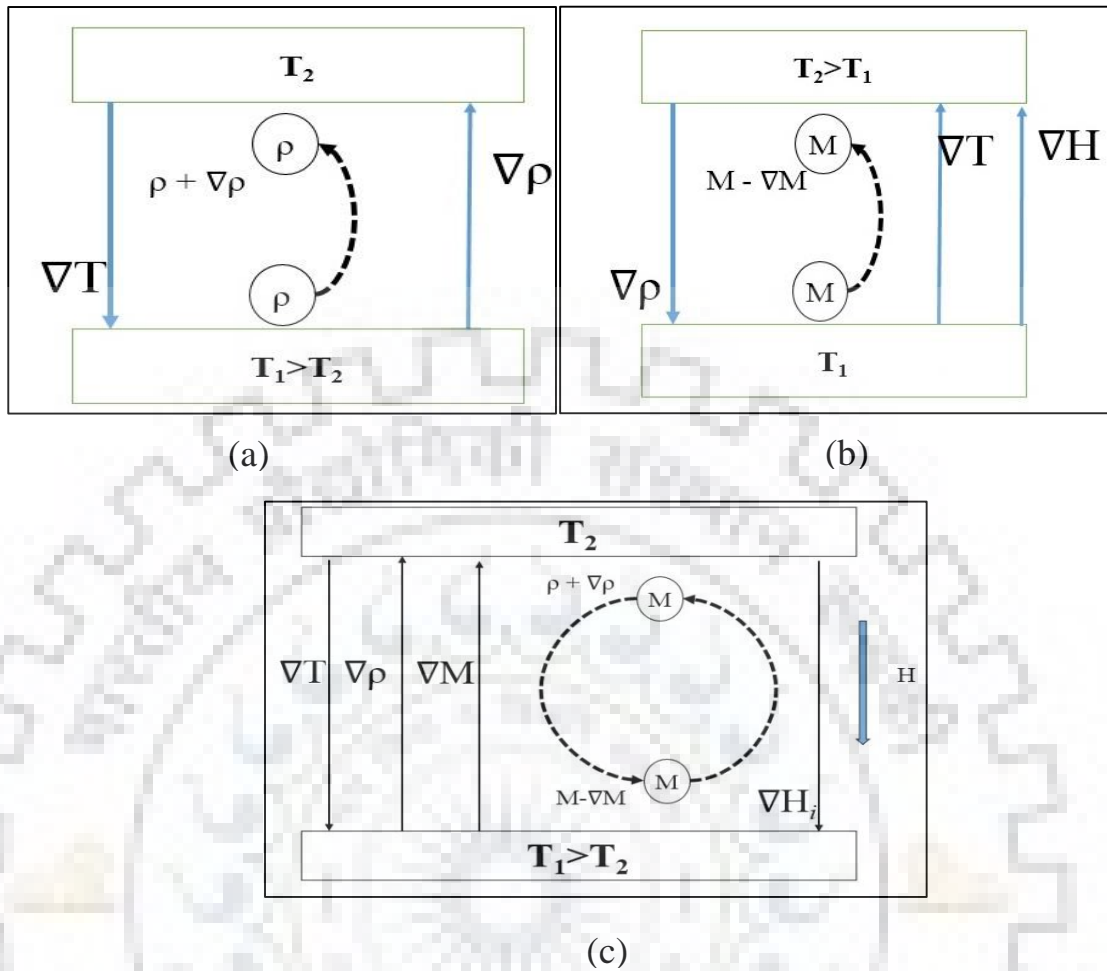
Figure 2. 9 The principal sketch of (a) Rayleigh Bénard convection (b) thermomagnetic convection (c) combination of Rayleigh Bénard convection and thermomagnetic convection (Engler et al., 2009; Völker et al., 2007).

Here, the applied external magnetic field is uniform and the fluid exhibits a magnetization and its magnetization decreases with the increase in temperature. An inner magnetic field gradient produced in the fluid which is given by

$$\nabla H_i = H - D\nabla M \tag{2.11}$$

where *D* denotes the demagnetization factor. When there is a non-uniform magnetic field, there are imbalance forces in the magnetic nanofluids.

Moreover, Sawada et al. (1993) have studied the natural convective heat transfer of magnetic fluid in concentric horizontal annuli experimentally. The study confirms that the magnetic field can control natural convection heat transfer in the magnetic fluid and it may get enhanced if the application of the magnetic field is adjusted according to the gravitation force. It also indicates that applied magnetic field direction also plays an

essential role in enhancing convective heat transfer naturally. Krakov & Nikiforov (2001) have numerically studied the influence of uniform magnetic field on thermomagnetic convection using a square cavity. The governing equations are Maxwell, Navier-stokes and energy equations for the magnetic field, fluid flow and temperature, respectively, in the frame of Boussinesq approximation. The angle between temperature gradient and magnetic field influences the convection structure. Ganguly et al. (2004) have studied thermomagnetic convection in a differentially heated square cavity, experiencing two dimensions of the magnetic field. The colder fluid with higher susceptibility is attracted towards the high magnetic field region and displaced warmer fluid. The thermomagnetic convection can be correlated with dimensionless magnetic Rayleigh number and heat transfer by thermomagnetic convection ($Ra_m=10^4$-10^7) as effective as in buoyancy-driven convection ($Ra=10^3$-10^6). Jafari et al. (2008) have numerically investigated the effect of the controllable parameters on thermomagnetic convection in Ferrofluid by the Taguchi method. A cylindrical geometry with different parameters including temperature difference across the layer, initial magnetic phase concentration, the aspect ratio of the geometry, magnetic field magnitude and diameter of magnetic particles are examined using L16 orthogonal array of Taguchi at four levels. The analysis of the simulation data indicates that the magnetic Soret effect could even be higher than the conventional one and its strength depends on the magnetic field strength. Mahmoudi et al. (2014) have numerically investigated the natural convection in a cavity filled with the nanofluid and experienced magnetic field. The Lattice Boltzmann simulation method is applied to study two dimensional square cavity heated uniformly from the base and linearly from sides and insulated from the top. Hartman and Rayleigh number are taken from 0 to 60 and 10^3 to 10^6, respectively. The magnetic field controls the effects of nanoparticles in the nanofluids and strongly affects the convection flow. Yamaguchi et al. (1999; 2002; 2010) have investigated the thermomagnetic natural convection in temperature-sensitive magnetic fluid both experimentally and numerically with a cubic container containing a heat-generated cylinder under the presence of the magnetic field. Mg-Zn ferrites nanoparticles are suspended in kerosene, and suspension has significant temperature dependence under a uniform magnetic field. The experimental result shows that the heat transfer characteristics using temperature-sensitive fluid are enhanced, shown in Figure 2.10. As the size of the heat-generating unit increases, the heat transfer decreases because of the flow obstruction. Numerically, the Lattice Boltzmann method confirms the

experimental findings. Wen et al. (2002) have reported natural convection experimentally in rectangular Hele-Shaw cell using magnetic fluid. Figure 2.11 shows that convective heat transfer is enhanced using a magnetic field. Figure 2.12 shows the effect of the direction of the applied magnetic field. Fornalik-Wajs et al. (2014) have reported that the Nusselt number is proportional to the thermomagnetic Rayleigh number raised to a power of 0.25, shown in Figure 2.13. Many researchers have studied the thermomagnetic convection with magnetic nanofluids in different geometries and found many interesting results summarized in Table 2.5.
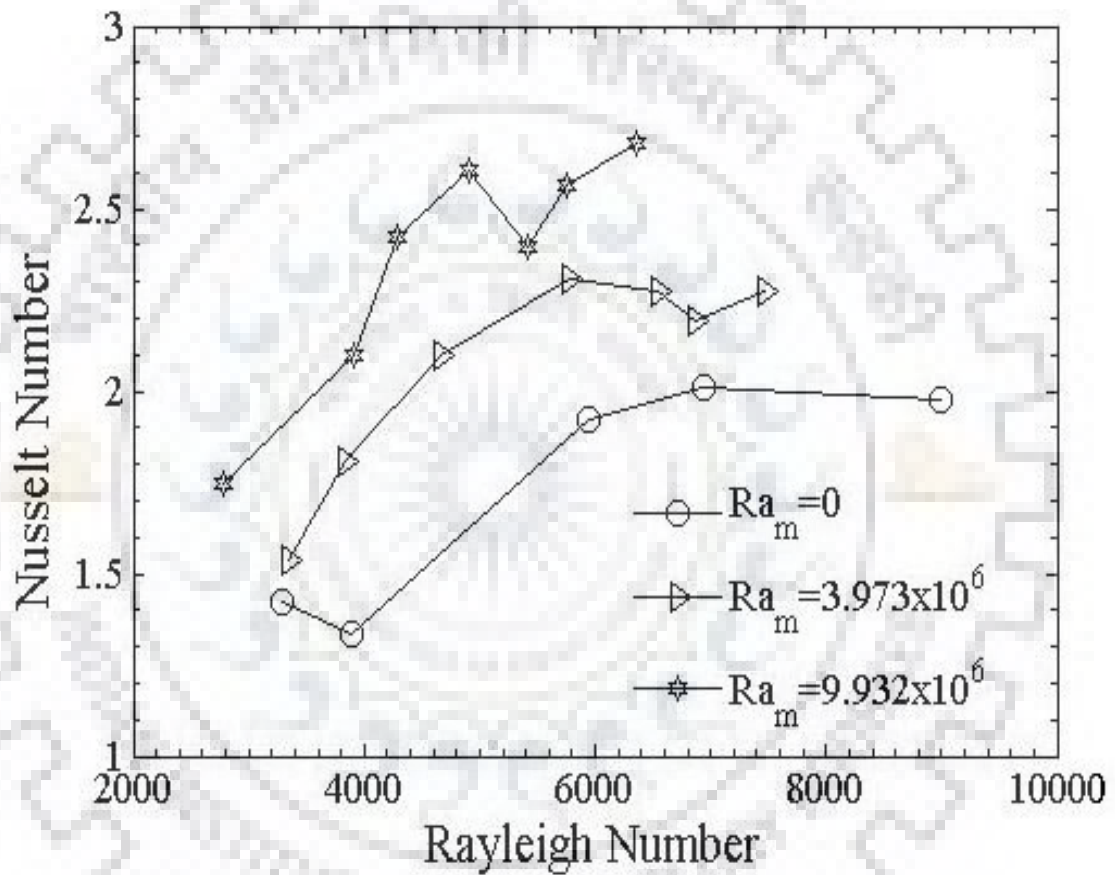
Figure 2. 10 The effect of magnetic Rayleigh number on the average Nusselt number in the magnetic nanofluids for the natural convection reported by Yamaguchi et al. (2002; 1999)
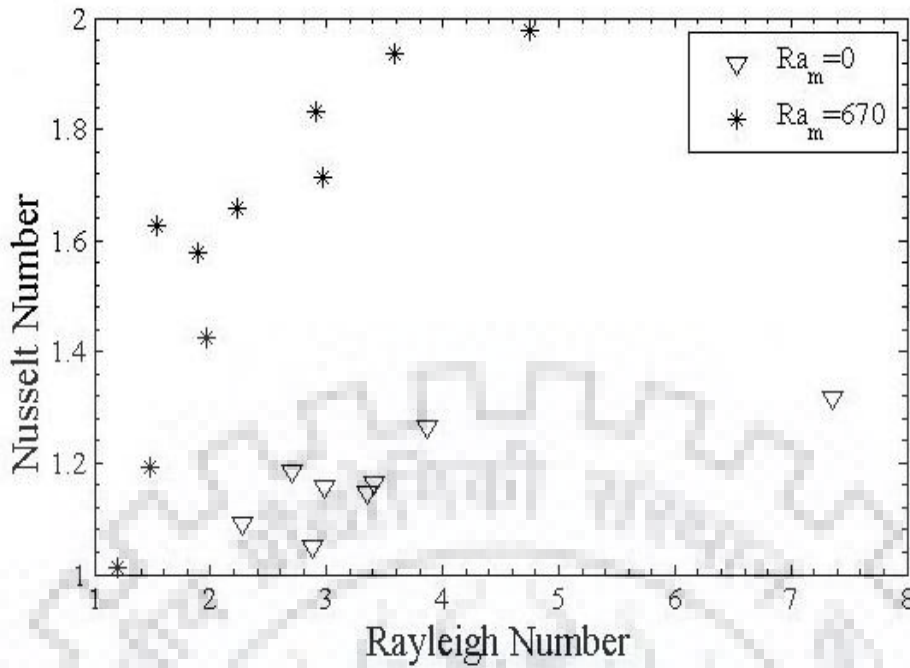
Figure 2. 11 The effect of low magnetic Rayleigh number on the average Nusselt number in the magnetic nanofluids for the natural convection reported by Wen et al. (2002).
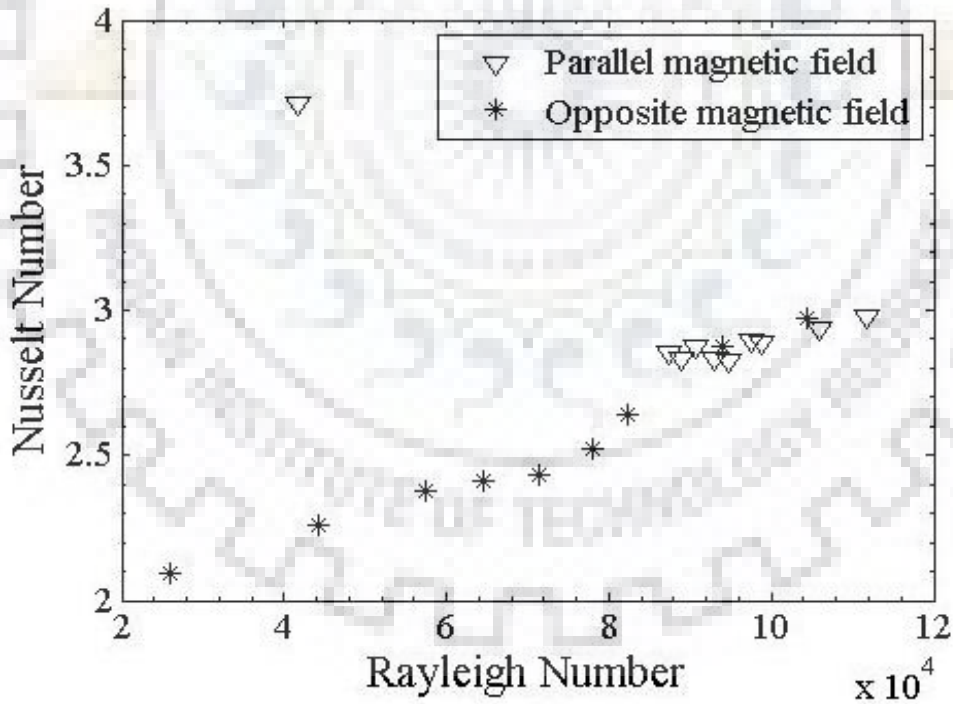
Figure 2. 12 The effect of direction of applied magnetic field on the average Nusselt number in natural convection for magnetic nanofluid reported by Sawada et al. (1993).
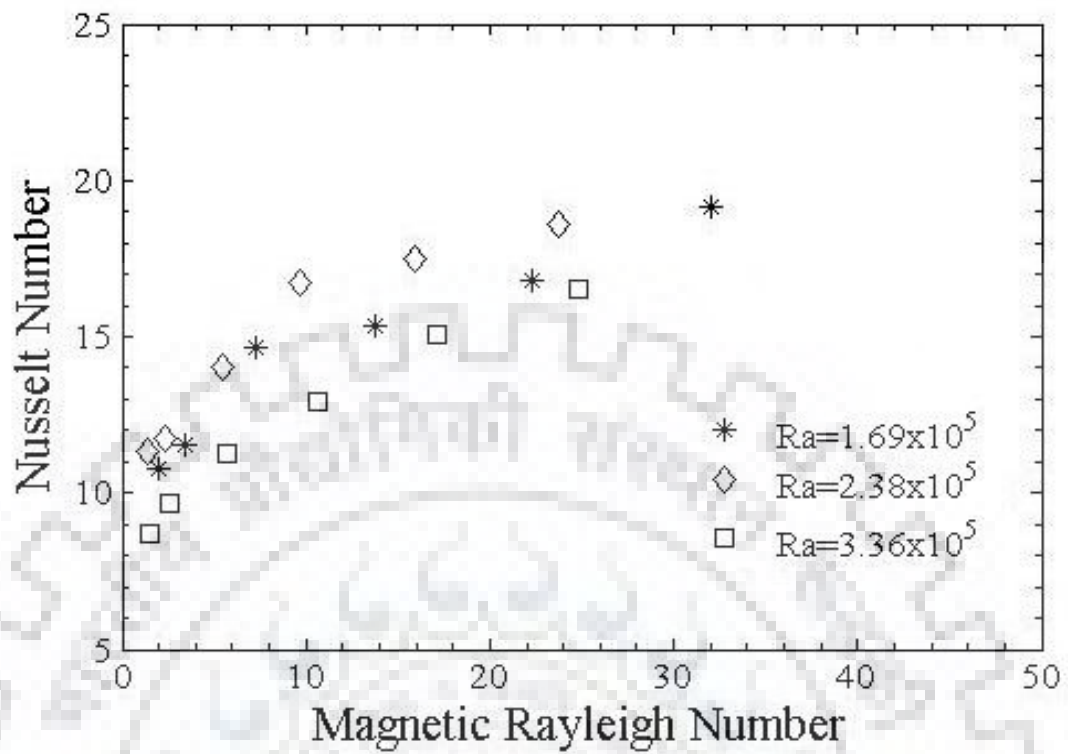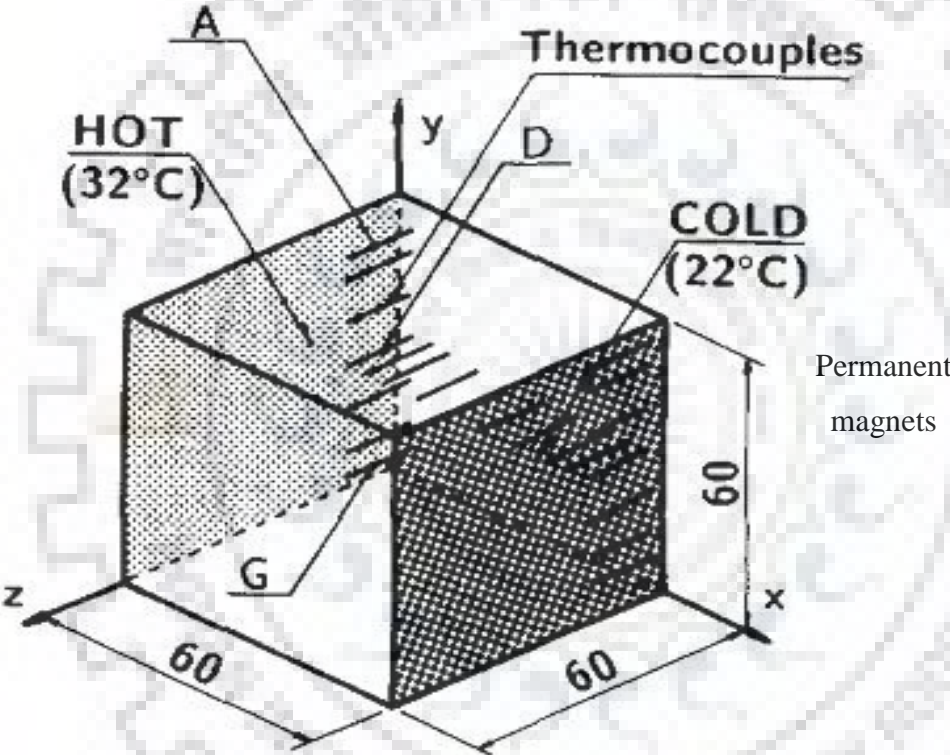
Figure 2. 13 The effect of magnetic Rayleigh number on average Nusselt number for different Rayleigh number in magnetic nanofluid reported by Fornalik-Wajs et al. (2014).

Table 2. 5 The experimental and numerical investigations on thermomagnetic convection.

Authors	Approach	Geometry	Magnetic field	Results/Remarks
Kikura et al. (1993)	Experimental			Wall temperature distribution is visualised with different placements of the magnet. Local and average Nusselt number and revised Grashof number are analysed for each case. It is concluded that the convection heat transfer can be controlled by changing the magnetic field. The water-based magnetic field is used as the working fluid in the experiment. Impressive thermomagnetic convection has been observed during the horizontal magnetic field case. Interestingly a rapid steady-state and effective heat transfer are observed in thermomagnetic convection.

Wen et al. (2002)	Experimental		Electromagnet Vertically	Hele-Shaw cell ($15 \times 15 \times 0.3$ mm^3) with water-based Fe$_3$O$_4$ magnetic fluid is used in the experiment. From heat transfer measurement and by visualizing shadowgraph, it is revealed that the magnetic field has a destabilizing hydrodynamic effect on the flow. It reflects as an increment in the heat transfer. Critical Rayleigh number is reduced to half of the without magnetic field state.
Yamaguchi et al. (1999, 2010)	Experimental and Numerical		Electromagnet vertically	Mn-Zn ferrite in alkyl naphthalene base fluid as a magnetic fluid is used in a two-dimensional cell for natural convection experiment. Enhancement in the heat transfer rate at the supercritical state is noted by the increasing magnetic field. Chain formation of nanoparticles causes this enhancement of heat transfer at the higher magnetic field. Observation reveals the destabilizing effect on hydrodynamic instability in a magnetic field. In numerical analysis, it is observed that heat
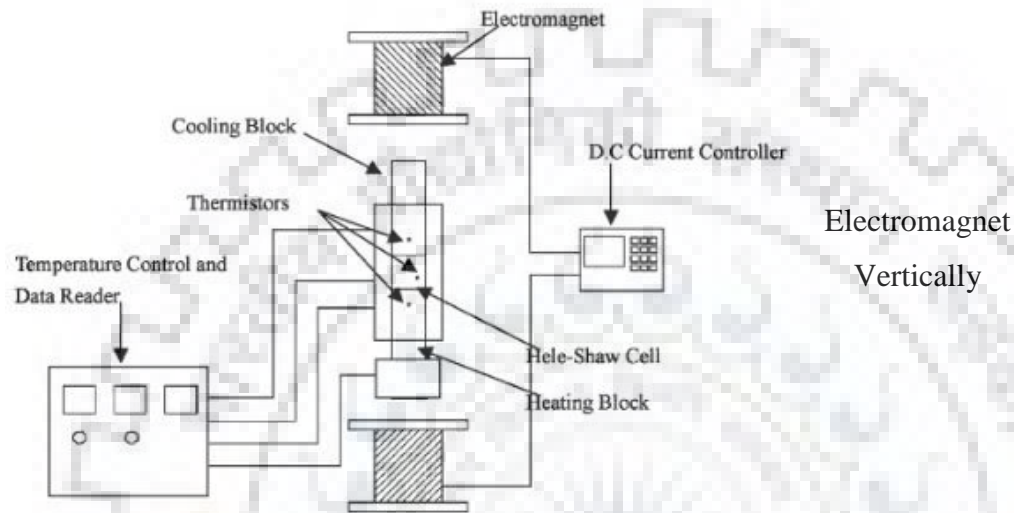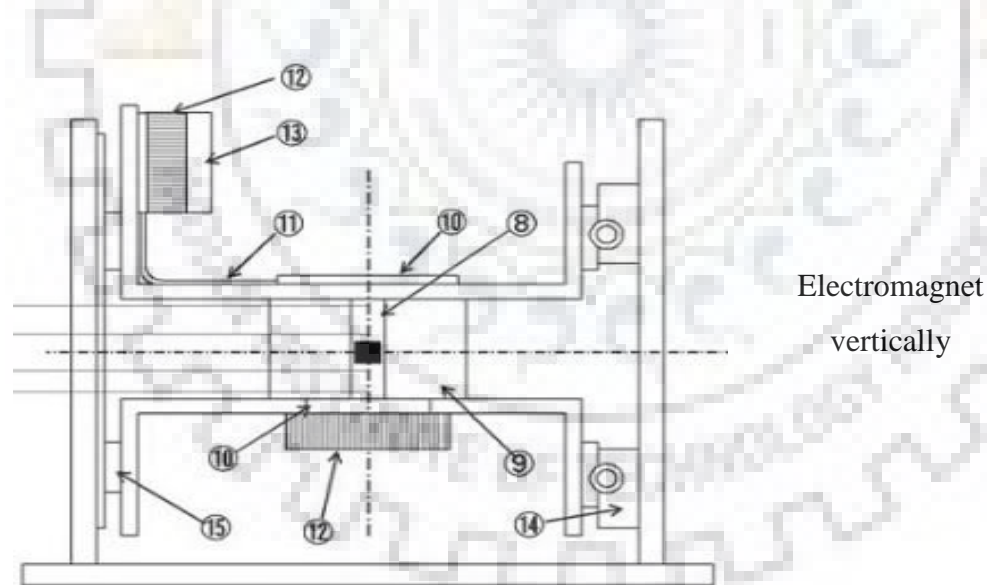
transfer strongly depends on the applied magnetic field strength. For the low Rayleigh number regime, the heat transfer is low; on the other hand, at higher Rayleigh number heat transfer shows significant improvement and intense dependence on the magnetic field.

Snyder et al. (2003)

Numerical

$$\frac{\partial T}{\partial z} = 0$$
$$u = 0$$

T_2
$u = 0$

T_1
$u = 0$

symmetry

$$\frac{\partial T}{\partial z} = 0$$
$$u = 0$$

Magnetic field gradient with permanent magnet
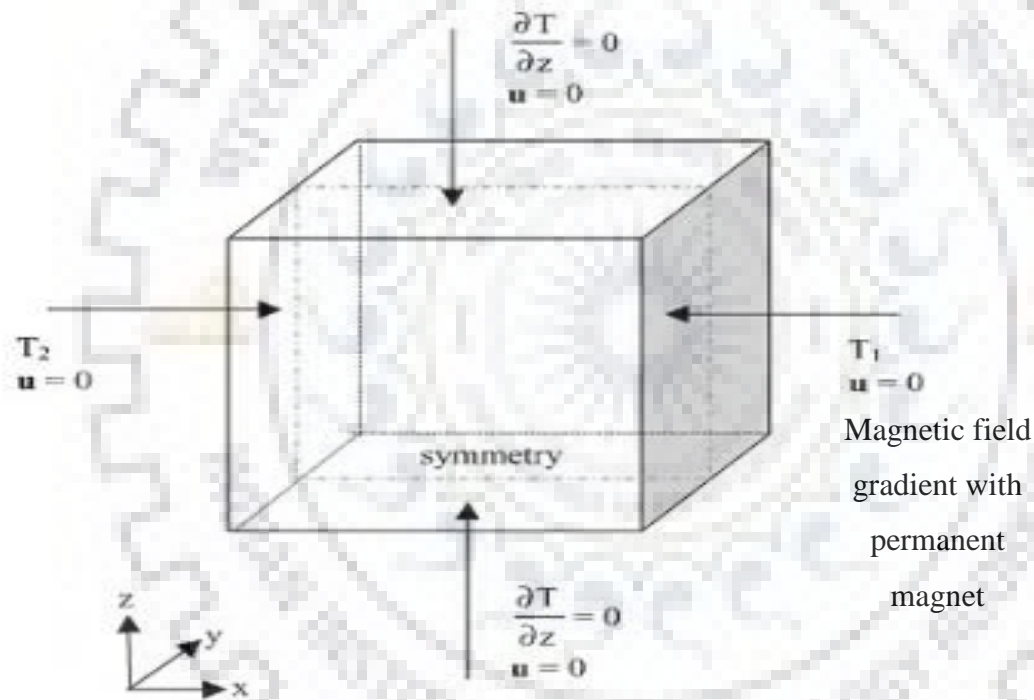
Magneto convection is predicted numerically and the standard theory of convection is confirmed. The model is validated with the experimental work.

Mahmoudi et al. (2014, 2015, 2016,)   Numerical
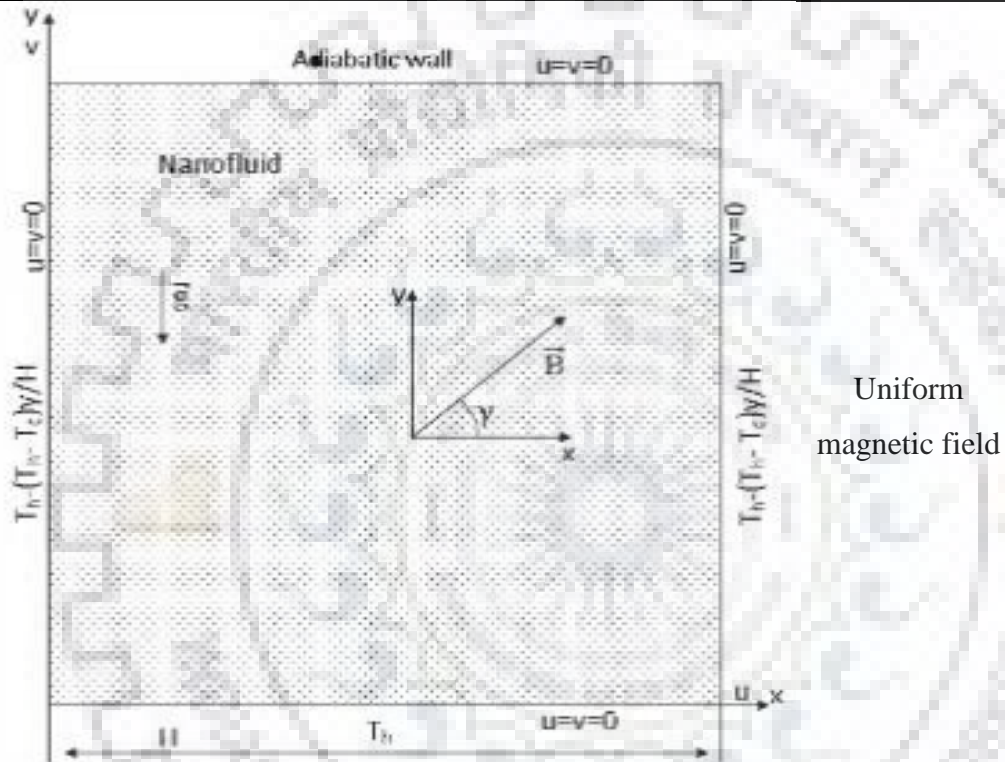
Lattice Boltzmann method has been applied to analyse the effect of magnetic field on nanofluids in a cavity. Rayleigh number, Ra $=10^3$-10^5 Hartmann number Ha = 0 to 60 and volume fraction of alumina nanofluid from 0 to 0.06 at 0 to 1800 magnetic field direction were the pertinent parameters. Heat Transfer is declined with an increase in Hartmann number for all magnetic field direction. The direction of the applied magnetic field controls the effects of nanoparticles in the nanofluid. The nanoparticle concentration improves the heat transfer at a higher Hartmann number.

Roszko et al. (2014, 2018)	Experimental	Superconducting magnet	Low concentration nanofluid has been investigated for thermomagnetic convection. Magnetic field direction and position of the experimental setup. Nusselt number increases in low magnetic induction values and the decrease in higher magnetic induction. Copper nanoparticles having a size range 40-60 nm are used here for the nanofluid.
Mansour et al. (2013)	Numerical	Vertical magnetic field	The trapezoidal cavity is filled with water-based Copper nanofluid in the presence of a magnetic field. Inclination helps to vanish the viscous effect. The rate of increment of Hartman number leads to an increase in the temperature gradient, hence an increase in diffusion heat transfer at higher Rayleigh number. In the absence of a magnetic field the heat transfer increases with volume fraction and Rayleigh number.
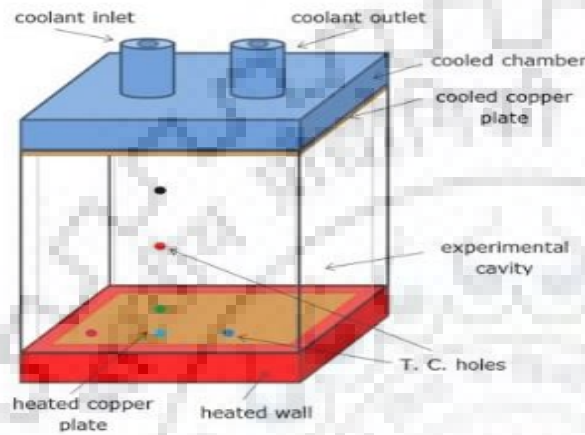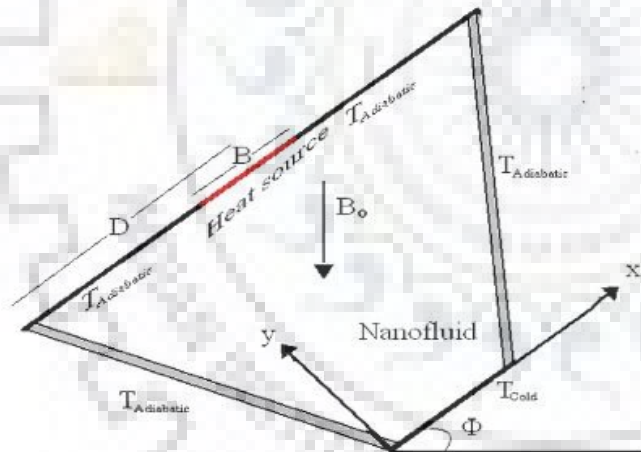
Sourtiji & Hosseinizadeh (2012)	Numerical	Uniform magnetic field	L-shaped cavity is filled with alumina nanofluid and has been analyzed in the presence of the uniform magnetic field. Different parameters imprinted distinctive marks on the heat transfer. The increment in the volume fraction of nanoparticles leads to the enhancement of heat transfer. A similar kind of results is obtained for increasing the Rayleigh number. The increment in Hartmann number increases the Nusselt number significantly, but in a higher regime of Rayleigh number, Nusselt number is decreased.
Ece & Büyük (2006)	Numerical	Uniform magnetic field	Characteristics of laminar natural convection flow show interesting results in the inclined rectangular enclosure in the presence of a magnetic field. The increment in Grashof number significantly increases the convection but suppresses under the presence of a strong magnetic field. Nusselt number decreases in the strong magnetic field.

Ashorynejad et al. (2013, 2018)	Numerical		Static radial magnetic field	The lattice Boltzmann method is used to investigate the effect of the presence of a magnetic field on heat transfer by natural convection. Particle volume fraction and Rayleigh number increase the Nusselt number, but it decreases with the Hartmann number. Perhaps, Radial magnetic field suppresses the flow oscillation effectively.
Battira & Bessaih (2016)	Numerical		Radial/ Axial magnetic field	A vertical cylinder having alumina nanofluid has been studied for natural convection heat transfer characteristics. In a stronger magnetic field, circulation in the cavity reduces significantly in the axially oriented magnetic field. In a convection dominating regime at low Hartmann number, the increment in volume fraction deteriorates the heat transfer under the axially applied magnetic field.
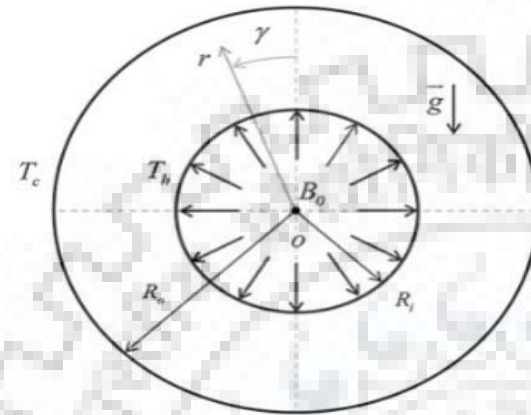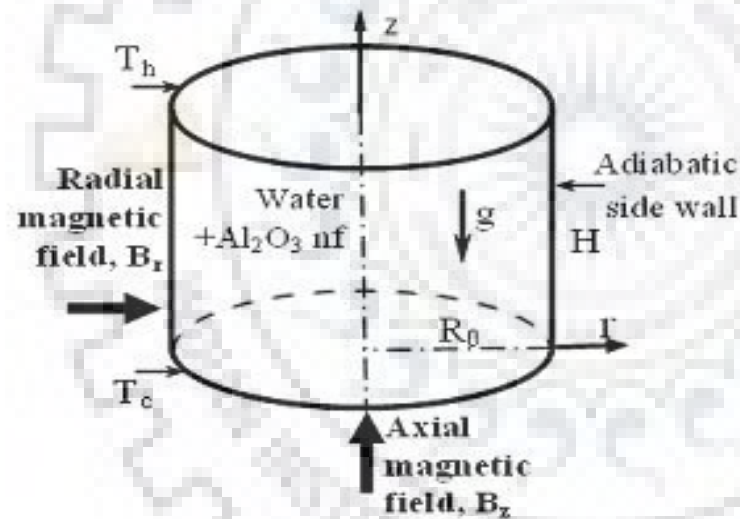
| Mahmoudi et al. (2012) | Numerical | | Uniform magnetic field | The triangular cavity is filled up with the copper-water nanofluid. The location of two identical heat sources at the bottom of the cavity changes to measure the change in heat transfer. The heat transfer is more when the sources are parted by some distance. At a high Hartmann number, the flow in the cavity is reduced, which leads to a reduction in heat transfer. In the conduction dominating regime, nanoparticle concentration increases the heat transfer rate. |
| Bahiraei & Hangi (2014) | Numerical | | Non-uniform magnetic field | Two phase Euler- Lagrange method is used to assess natural convection in water-based Mn-Zn ferrite MNfs. The square cavity under the non-uniform magnetic field has been analyzed. In the presence of a magnetic field, flow near walls increased, which increases the Nusselt number and at a particular field, convection is intensified for bigger particles. Large particles significantly increase the magnetic force. |

2.5 Remark
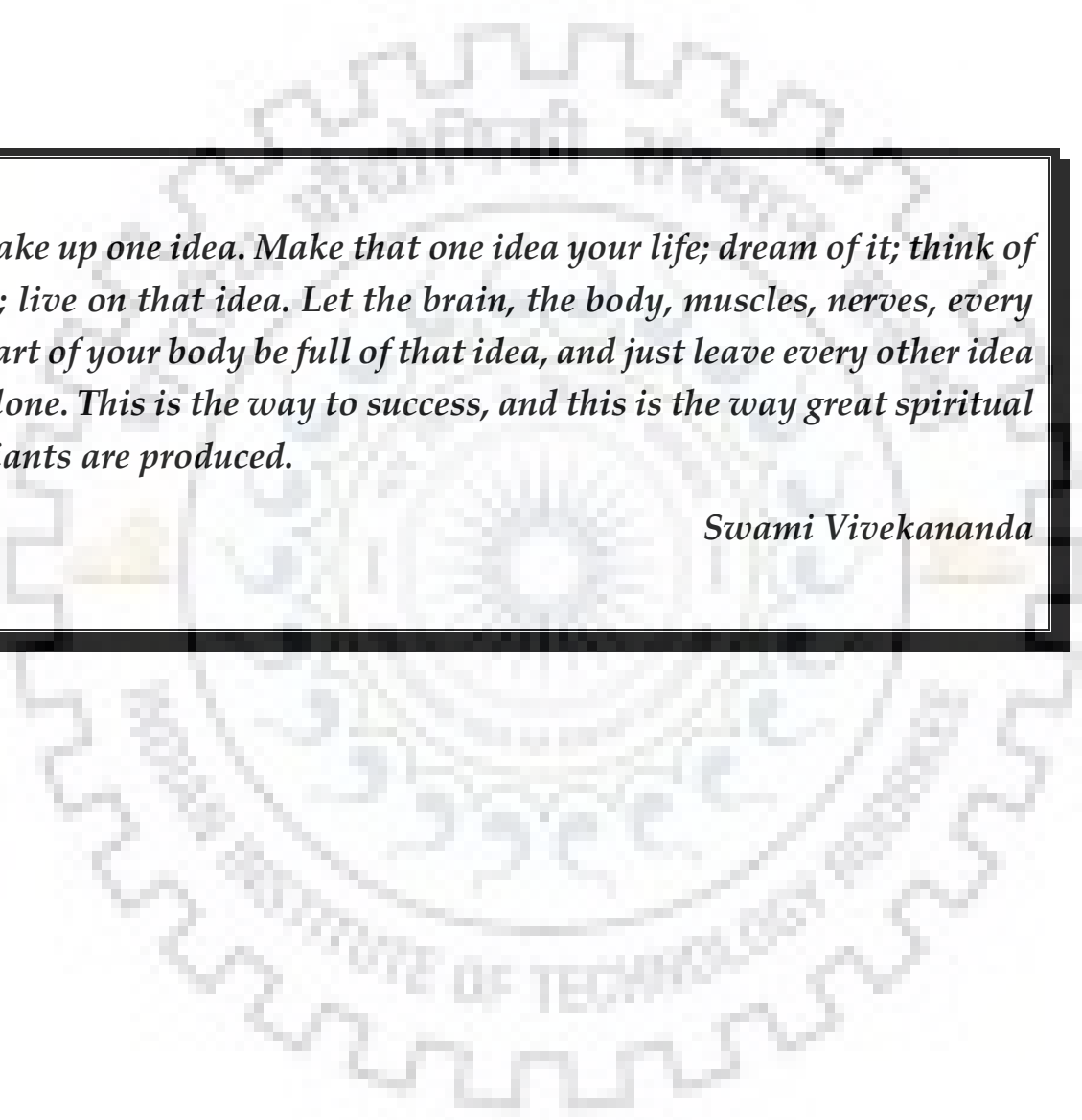
A detailed literature review is done in the current chapter to understand the effect of various parameters and thermophysical properties of magnetic nanofluids on the natural convection heat transfer. A robust fundamental foundation has been made to understand the characteristics of magnetic nanofluid in natural convection through the current chapter.

Chapter 3: Synthesis and Characterization of Magnetic Nanofluids

Index

Take up one idea. Make that one idea your life; dream of it; think of it; live on that idea. Let the brain, the body, muscles, nerves, every part of your body be full of that idea, and just leave every other idea alone. This is the way to success, and this is the way great spiritual giants are produced.

Swami Vivekananda

3

Synthesis and Characterization of Magnetic Nanofluids

Water based Fe_3O_4 magnetic nanofluid is used in the investigation as a working fluid. The present chapter is dedicated to synthesis, characterization and stability analysis of the magnetic nanofluids.

3.1 Materials & apparatus

Commercial spherical shaped; Fe_3O_4 nanoparticles of average particle size of 40-60 nm have been purchased from the USA based company, Nanoshell. The properties of the nanoparticles are summarized in Table 3.1. We have independently characterized these nanoparticles by X-ray diffraction and scanning electron microscope (SEM) performed on Powder X-ray diffractometer make of Bruker (Model: D8-Advance) using Cu-Kα source in angular range 10 to 90º and Carl-Zeiss Make Field-Emission Scanning Electron Microscope (Model: Carl-Zeiss Ultra plus). The purified water is having TDS value of 0 and electrical conductivity of 0.9 µ S/cm is prepared by Elix® Essential 3 Water Purification System, Merck, USA. Other chemicals like oleic acid, N-cetyl- N N N Trimethylammonium bromide (NNN), NaOH and HCl are purchased from Himedia laboratories. All chemicals are used without further purification.

The schematic view of the thermal conductivity measurement setup is shown in Figure 3.1 and the photographic view is shown in Figure 3.2. The intrinsic thermal conductivity of the magnetic nanofluids is measured by using the thermal property analyser, KD2 pro (Decagon Devices, Inc.) and the transient line heat source method is used in the instrument to measure thermal conductivity. KS-1, 1.3 mm diameter × 6 cm long sensor with ± 5 % accuracy is used to measure the thermal conductivity. All measurements are performed at least 5 times and averaged. The electromagnet used to apply a uniform magnetic field has an iron core of 4.5 cm diameter. The vile having 2.5

cm diameter × 7 cm length containing magnetic nanofluids is used to measure the thermal conductivity inside the 8 cm air gap between the iron core tips of the electromagnet. The electromagnet is connected to the constant current power source and the digital gauss meter DGM-100 is used to measure the intensity of the magnetic field with an accuracy of ± 0.5 %. To ensure constant temperature to the sample, a programmable circulating constant temperature bath of Koehler Instrument Company Inc., USA (Model: K33085) is used. The thermal conductivity is measured after achieving the steady-state temperature and each interval of measurement has a 15-minute window to dissipate any thermal gradients due to KD2 pro.

Table 3. 1 Properties of Fe$_3$O$_4$ nanoparticles.

Properties	Fe$_3$O$_4$ nanoparticles
Average Particle size	40-60 nm
Colour	Dark brown
pH Value	6.7
Odour	Odourless
Fe$_3$O$_4$ content	99.99 %
Morphology	Powder
Density, g/cm^3	5
Specific Surface Area, m^2/g	45
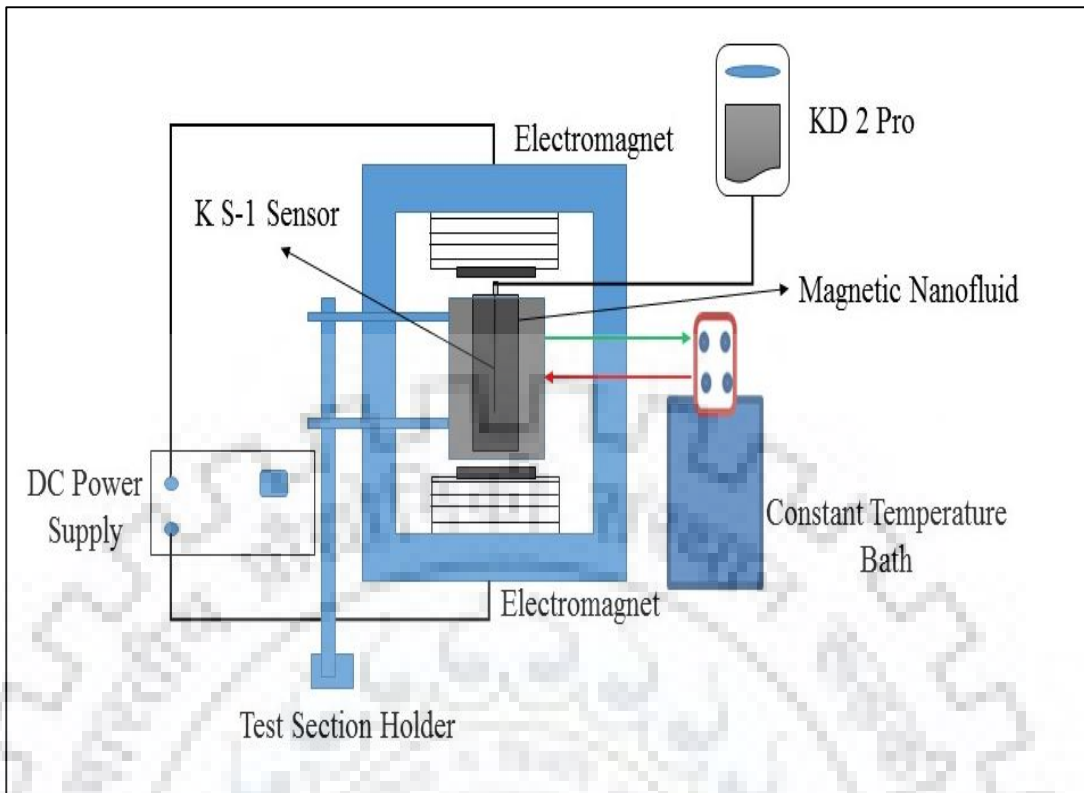
Figure 3. 1 Schematic view of the experimental set up for the thermal conductivity at different parameters.
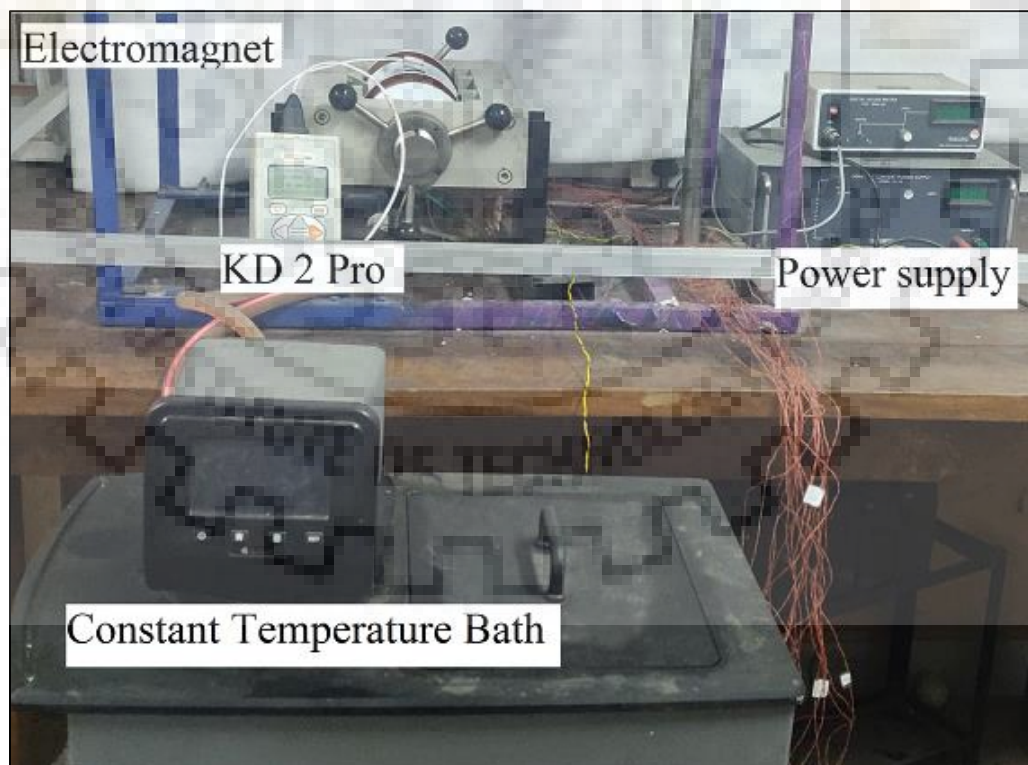
Figure 3. 2 Photographic view of the experimental setup for thermal conductivity measurement by KD2 Pro.

The viscosity in the present study is measured by the Modular Compact MCR 102 Rheometer (Make Anton Paar GmbH, Austria, Europe) as shown in Figure 3.3 with the accuracy ± 5 %. The rheometer has a two-cylinder arrangement; the liquid is placed inside the annulus of one cylinder and the other cylinder is rotated to give us the shear rate. The liquid inside the cylinder exerts the force on the rotating cylinder which is converted into shear stress.
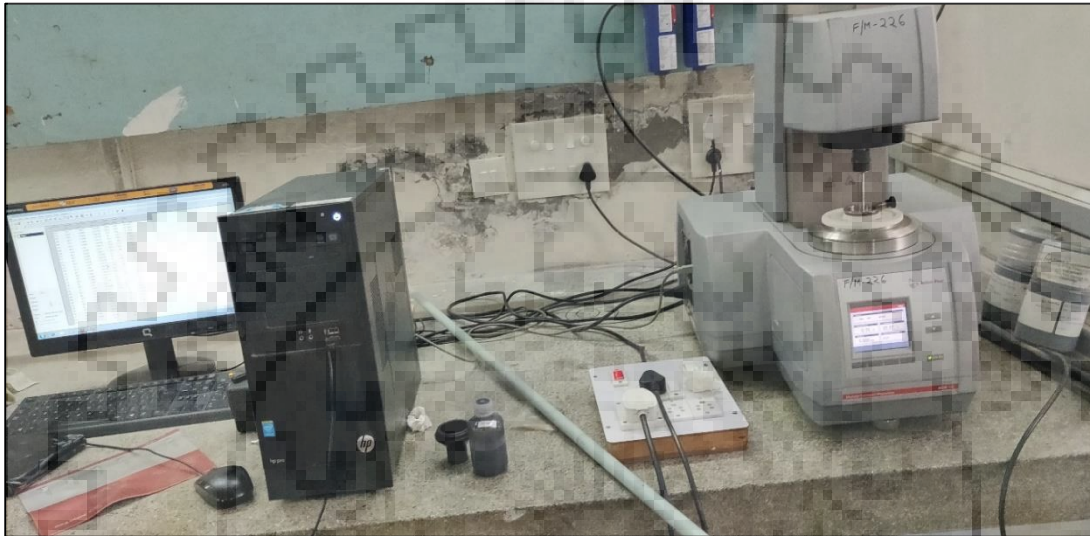
Figure 3. 3 Photographic view of the viscosity measurement by the rheometer MCR 102.

The density of the liquids is measured by the weighing machine (Digital Analytical Balance, DAB 220 (Wensar Weighing Scale Ltd., India) and the Pycnometer (50 ml), as shown in Figure 3.4. The instruments are calibrated against the standard liquids (water and ethylene glycol). The basic principle for the density is to measure the mass in the fixed volume of the Pycnometer.

Figure 3. 4 Photographic view of the weighing machine and Pycnometer.

3.2 Synthesis of magnetic nanofluids

The commonly used two-step method is used here to prepare magnetic nanofluids, as discussed comprehensively in the literature review chapter. The liquid & particle mixture is continuously ultra-sonicated for 1 to 2 h by the probe sonicator purchased from Biomatrix Inc., USA. The surface modification of Fe_3O_4 nanoparticles with oleic acid and NNN has been done to avoid the settlement of the nanoparticles into the base fluids. Distilled water is used as base fluids and the nanoparticles are dispersed with the concentrations of 0.01, 0.05, 0.08, 0.1, 0.5, 0.8, 1 vol.% in the base fluids. The concentration in the base fluid of the nanoparticles is calculated from the weight of dry nanoparticles and the true density of nanoparticles is provided by the supplier, as mentioned in equation 3.1. Digital Analytical Balance, DAB 220 (Wensar Weighing Scale Ltd., India) is used to measure the weight of the nanoparticles with the readability

and repeatability of 0.1 mg and ±0.1 mg, respectively. The schematic diagram to depicts the synthesis of magnetic nanofluids by the two-step method is shown in Figure 3.5.

Volume concentration (Vol.%), $\varphi = \dfrac{\{W_{Fe_3O_4}/\rho_{Fe_3O_4}\}}{\{W_{Fe_3O_4}/\rho_{Fe_3O_4}\}+\{W_{water}/\rho_{water}\}} \times 100$ \hfill (3.1)
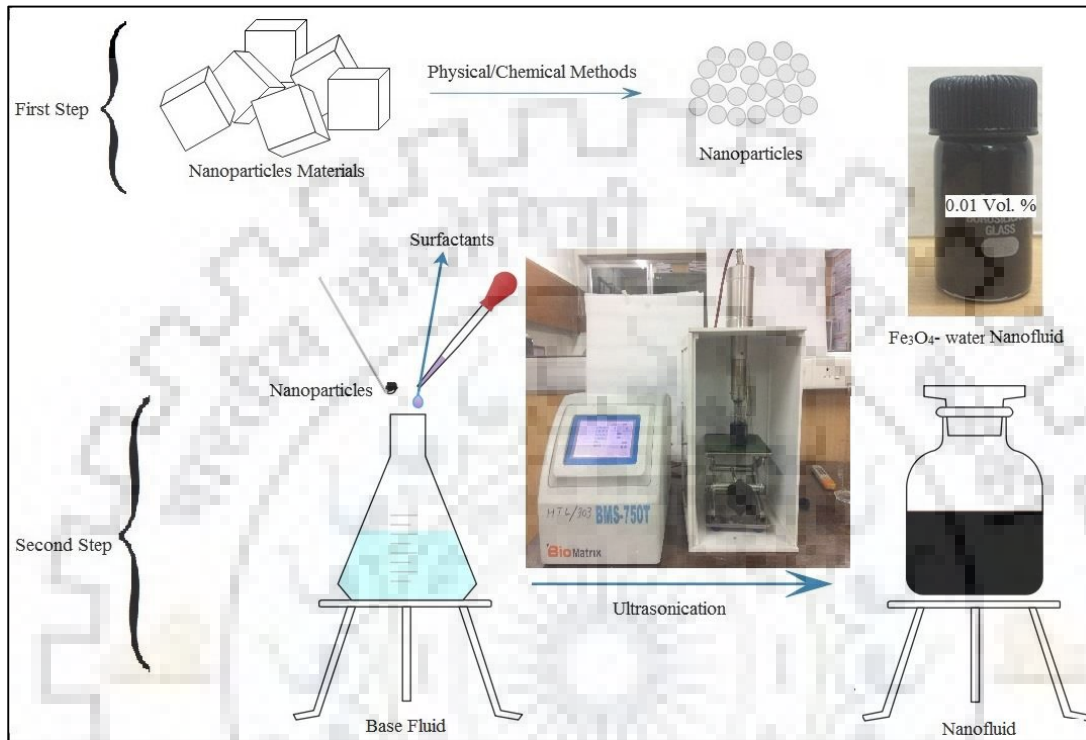
Figure 3. 5 Two-step method for the synthesis of Fe₃O₄ magnetic nanofluids.

3.3 Characterization of magnetic nanoparticles

The X-ray diffraction pattern of the Fe₃O₄ magnetic nanoparticles is shown in Figure 3.6. The different characteristic peaks are consistent with the JCPDS (Joint Committee on Powder Diffraction Standards) file number 82-1533 of Fe₃O₄ nanoparticles. Figure 3.7 shows the curve of magnetization for Fe₃O₄ nanoparticles at room temperature. The magnetic nanoparticles show superparamagnetic behaviour with almost zero coercivity. The saturation magnetization is 80 emu/g for the Fe₃O₄ nanoparticles.
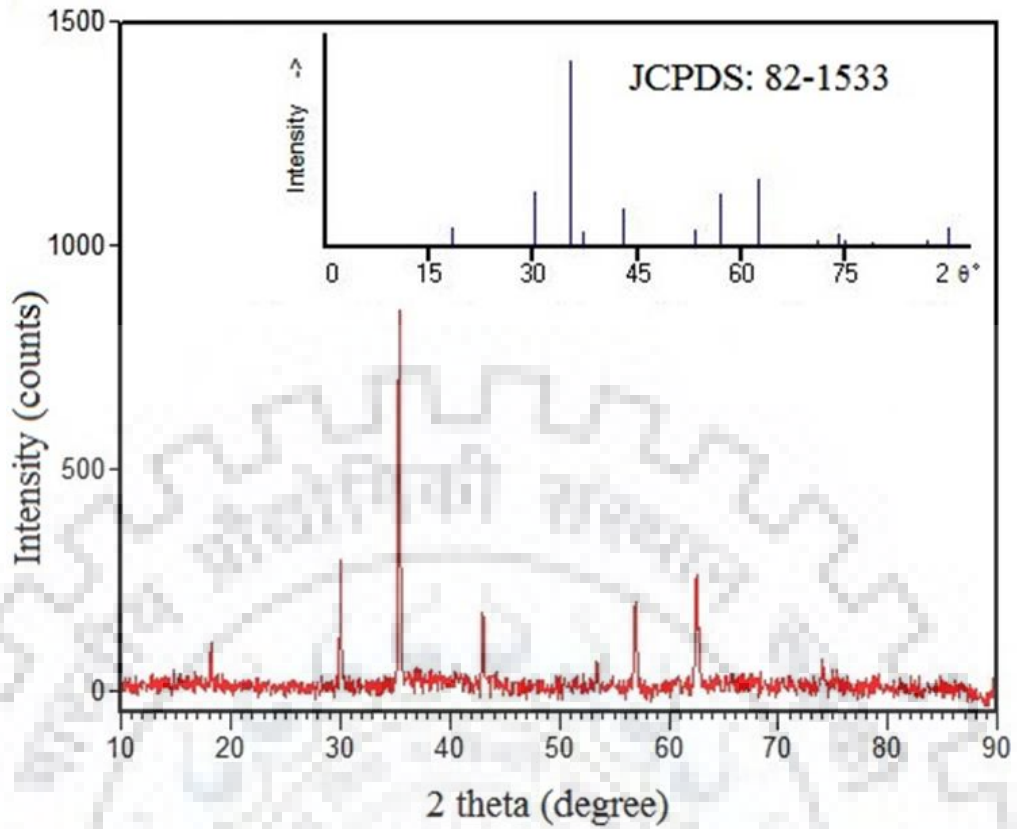
Figure 3. 6 XRD pattern of the Fe₃O₄ nanoparticles. The inset shows the JCPDS (Joint Committee on Powder Diffraction Standards) data for the Fe₃O₄ nanoparticles.
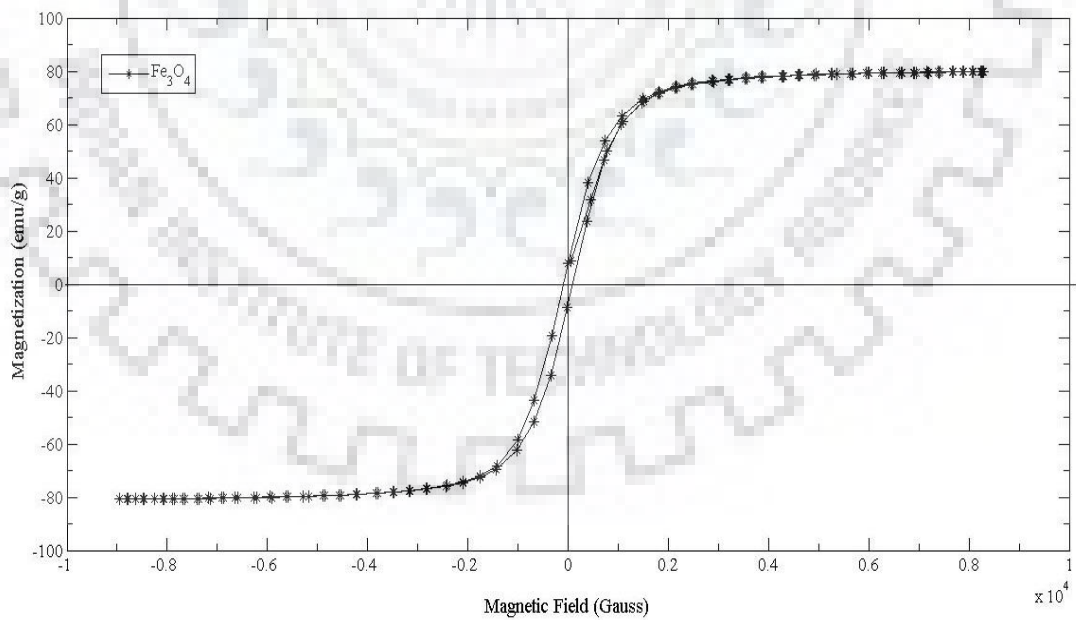
Figure 3. 7 Magnetization curve of the Fe₃O₄ nanoparticles.

<div style="text-align:center">(a)   (b)</div>
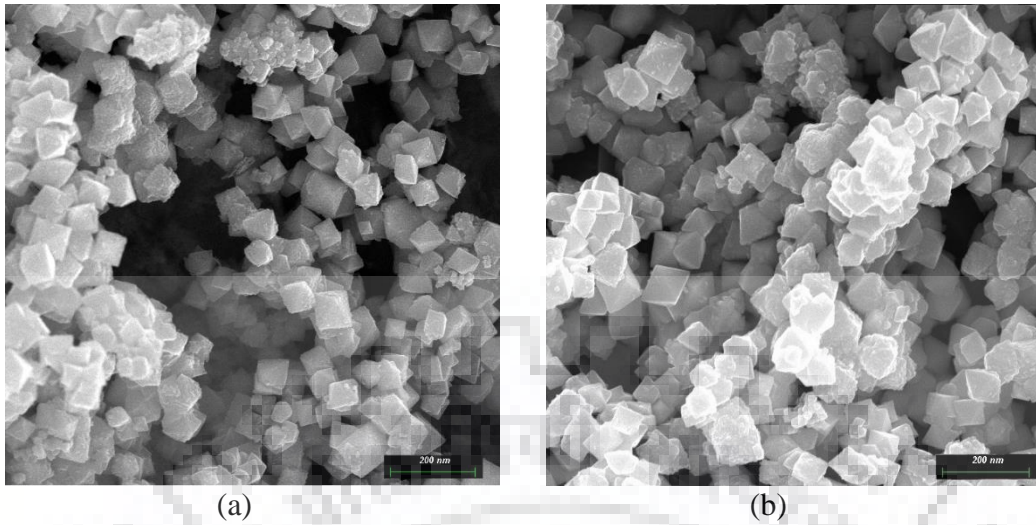
Figure 3. 8 SEM (Scanning Electron Microscope) images of Fe₃O₄ nanoparticles (a) Purchased Fe₃O₄ nanoparticles (b) Fe₃O₄ nanoparticles with the oleic acid coating.

Figure 3.8 shows the scanning electron microscope images of Fe_3O_4 nanoparticles. The images reveal that the average size of the nanoparticles is in the range of 60-80 nm. Figure 3.8 (a) shows the image of nanoparticles purchased from the manufacturing company, Nanoshell. These purchased nanoparticles are processed further for surface modification. Figure 3.8 (b) shows the image of Fe_3O_4 nanoparticles coated with oleic acid by processing the purchased nanoparticles. The particles are first dispersed in methanol by ultrasonication and then oleic acid is added during constant stirring at 80 °C. The nanoparticles particles are then filtered through Whatman filter paper and washed with distilled water several times. After that, with the help of acetone, the nanoparticles are separated from the filter paper and dried at room temperature (Shete et al., 2015).

3.4 Thermophysical properties of Magnetic nanofluids

3.4.1 Thermal Conductivity

The validation of the experimental setup for measuring thermal conductivity (k) is done by measuring the thermal conductivity of the water at different temperatures and comparing them with existing experimental values (Sengers & Watson, 1986) and theoretical model (Popiel & Wojtkowiak, 1998) given in equation (3.2)

$$k = a + bT + cT^{1.5} + dT^2 + eT^{0.5} \tag{3.2}$$

where $a = 0.5650285$, $b = 0.0026363895$, $c = -0.00012516934$, $d = -1.5154918 \times 10^{-6}$ and $e = -0.009412945$

Figure 3.9 shows that the experimental setup to measure thermal conductivity is valid as the experimental results are consistent with the theoretical as well as previous experimental results. Figure 3.10 shows the effect of the concentration of the magnetic nanoparticles on the thermal conductivity of the magnetic nanofluids. The maximum enhancement of around 15 % has occurred at the highest concentration of 0.1 vol. %. The results are consistent with the previously published investigations (Karimi et al., 2014 and Zhu et al., 2006).
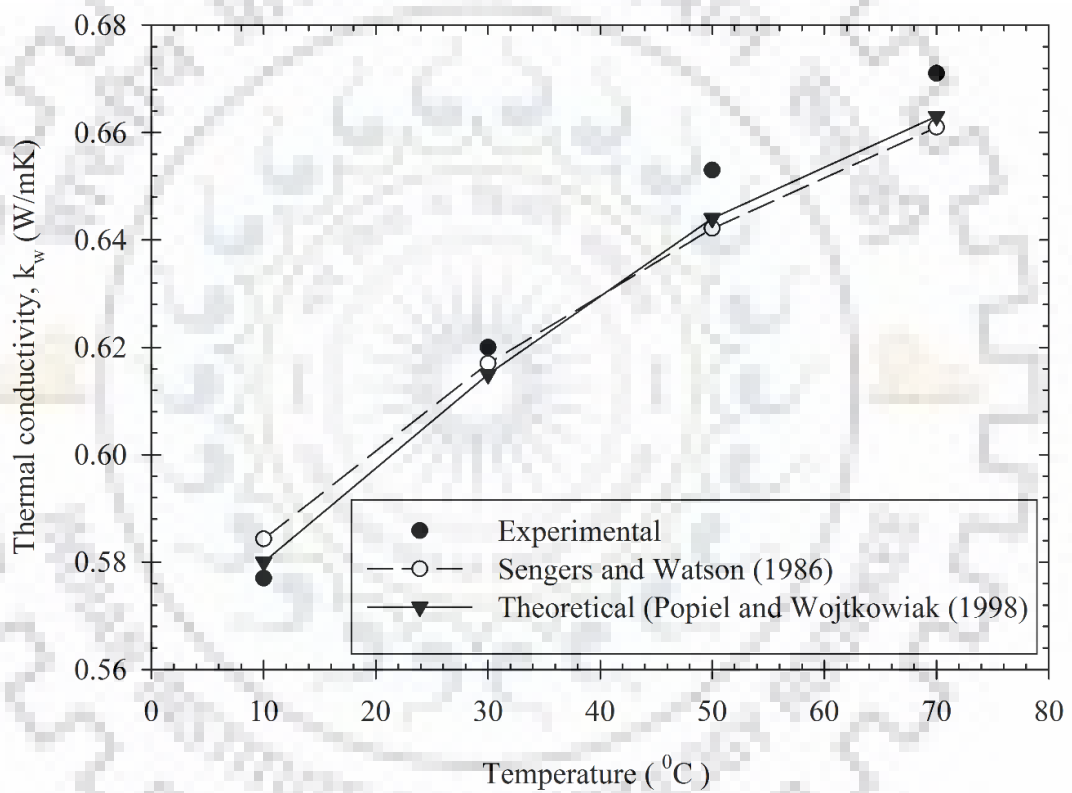
Figure 3. 9 Thermal conductivity of the water with different temperatures and comparison with the existing classical theoretical models (Popiel & Wojtkowiak, 1998) and the previous experimental values (Sengers & Watson, 1986).

Figure 3.11 shows the effect of the temperature on the thermal conductivity of the Fe_3O_4/Water magnetic nanofluid. The thermal conductivity of the magnetic nanofluid is shown the increment trend with the temperature. The thermal conductivity at the nanoparticles concentration of 0.1 vol. % is enhanced from 3 to 18 % in the temperature range of 10 to 70 ^{0}C. The Brownian motion enhancement with the temperature is one

of the possible explanations for the increment of the thermal conductivity with temperature.
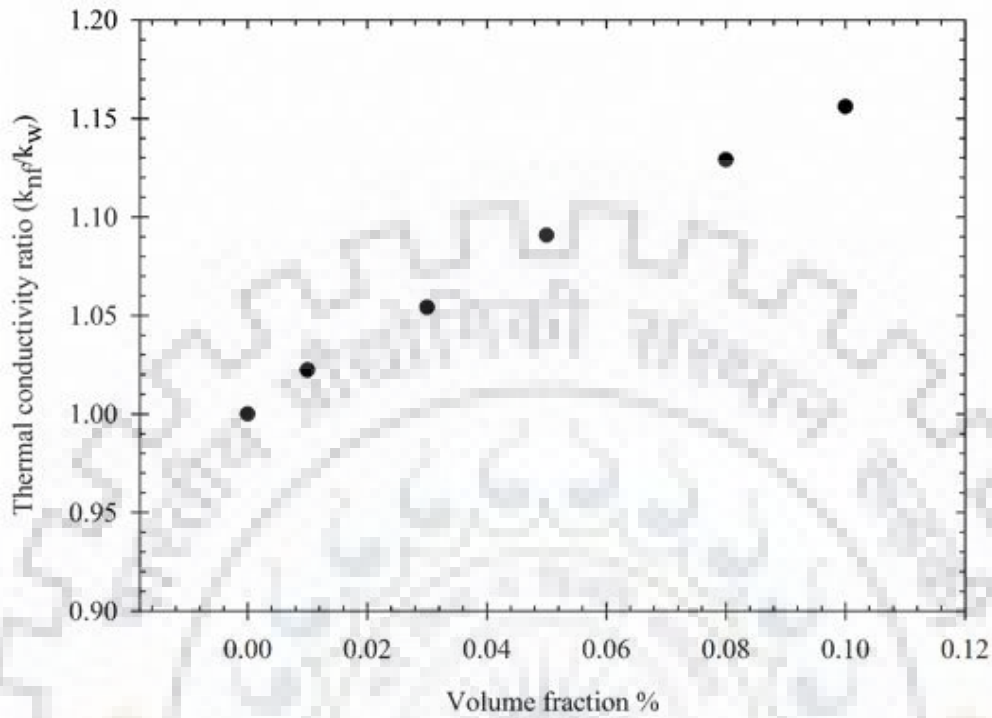
Figure 3. 10 Thermal conductivity ratio of Fe_3O_4/Water magnetic nanofluid and water with the concentration of nanoparticles.
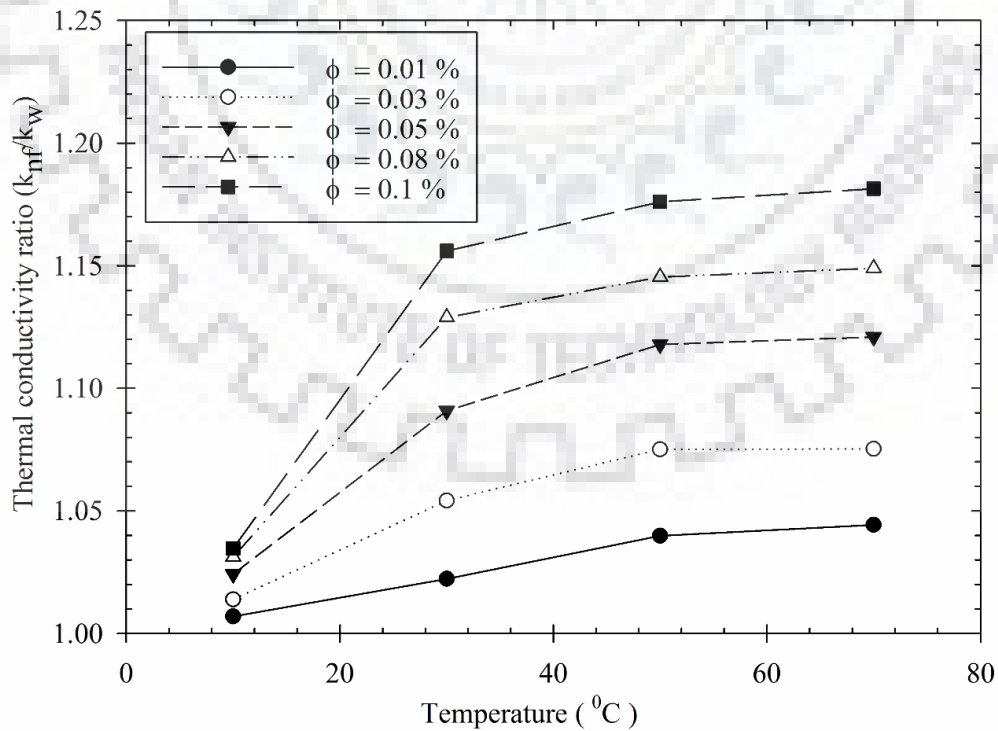
Figure 3. 11 Thermal conductivity ratio versus the temperature of the Fe_3O_4/ Water magnetic nanofluids.
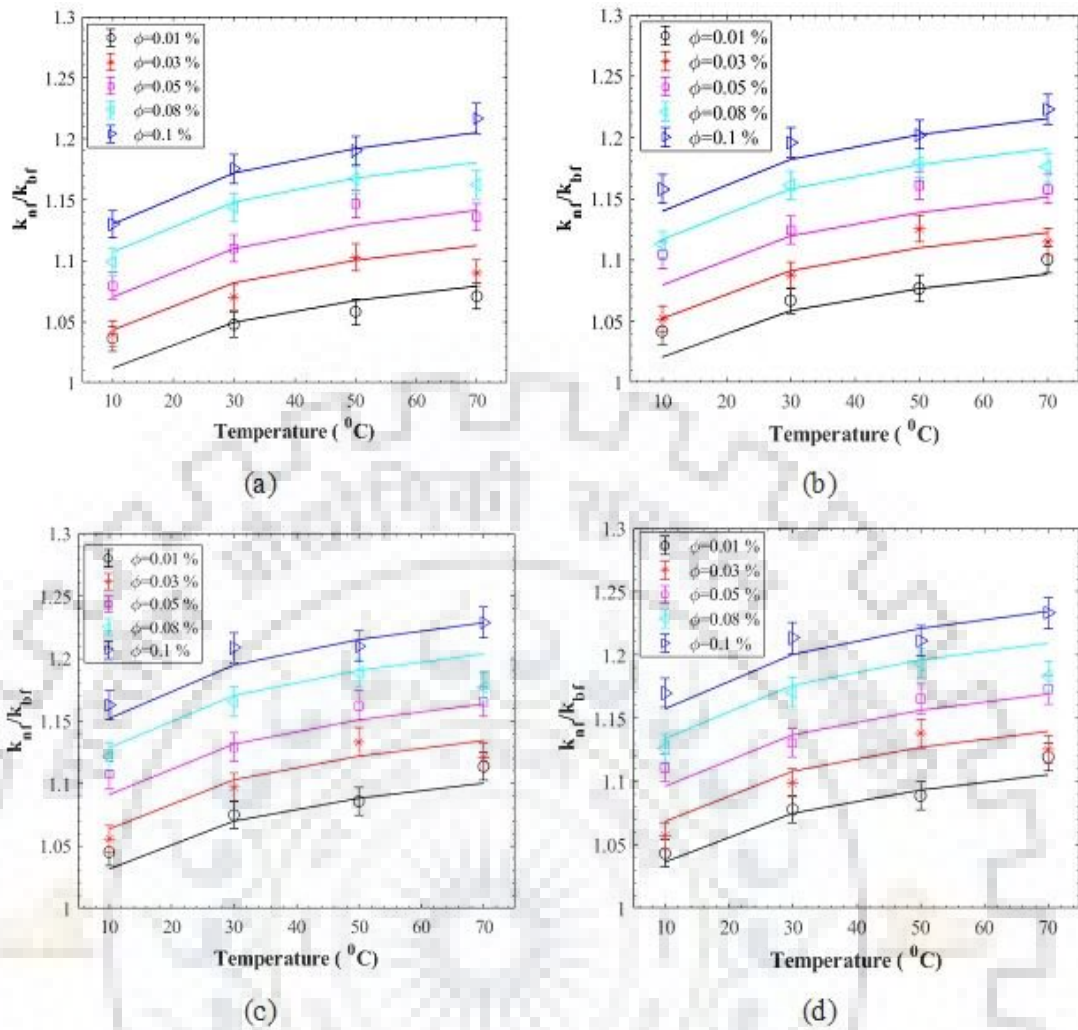
Figure 3. 12 Thermal conductivity ratio versus temperature at various magnetic field (a) 200 G (b) 300 G (c) 600 G (d) 730 G; the solid lines show the developed empirical correlation presented in the equation (3.3).

Figure 3.12 shows the variation in the thermal conductivity of Fe_3O_4/ Water magnetic nanofluids with the temperature at the various magnetic field, the markers show the experimentally obtained data, while the solid lines show the developed empirical correlation. The correlation is developed based on experimental data with 1.2 % standard deviation from the experimental data is presented in the equation (3.3). The ratio of the thermal conductivity of magnetic nanofluids and water is plotted versus the magnetic field at different concentrations and different temperatures. The maximum enhancement of 22 % is observed at the highest concentration, temperature and magnetic field of 0.01 vol. %, 70 ^{0}C and 730 Gauss, respectively. The enhancement in the thermal conductivity in the presence of a magnetic field is caused by the alignment

of the nanoparticles in the direction of the magnetic field (Shima et al., 2014; Shima & Philip, 2011).

$$\frac{k_{nf}}{k_{bf}} = (1 + 35.88\,\emptyset^{0.801}) \left(1 + 0.051 \left(\frac{B}{B_{max}}\right)^{0.51}\right) \left(\frac{k_p}{k_{bf}}\right)^{0.012} \left(\frac{T}{T_{max}}\right)^{0.034} (Pr_{bf})^{0.0001} \quad (3.3)$$

3.4.2 Viscosity

The validation of the experimental measurements of the rheometer for viscosity is presented in Figure 3.13. The water is used for the validation, the measured experimental value of viscosity of the water is compared with previously published experimental values (Sengers & Watson, 1986) and theoretical model (Popiel & Wojtkowiak, 1998) given in equation (3.4). The experimental value is well consistent with the compared theoretical and experimental data.

$$\eta = \frac{1}{a + bT + cT^2 + dT^3} \quad (3.4)$$

where, $a = 557.82468$, $b = 19.408782$, $c = 0.1360459$ and $d = -3.1160832 \times 10^{-6}$
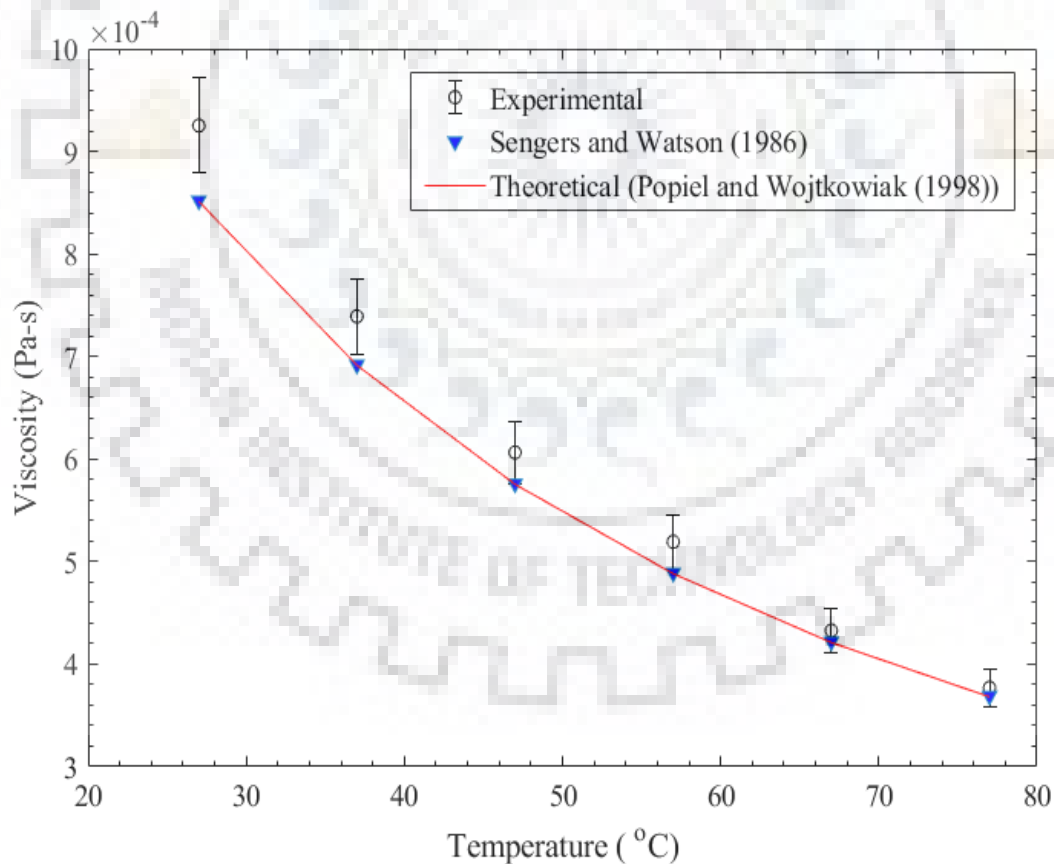
Figure 3. 13 Viscosity of the water with different temperatures and comparison with the existing classical theoretical model (Popiel & Wojtkowiak, 1998) and the previous experimental values (Sengers & Watson, 1986).
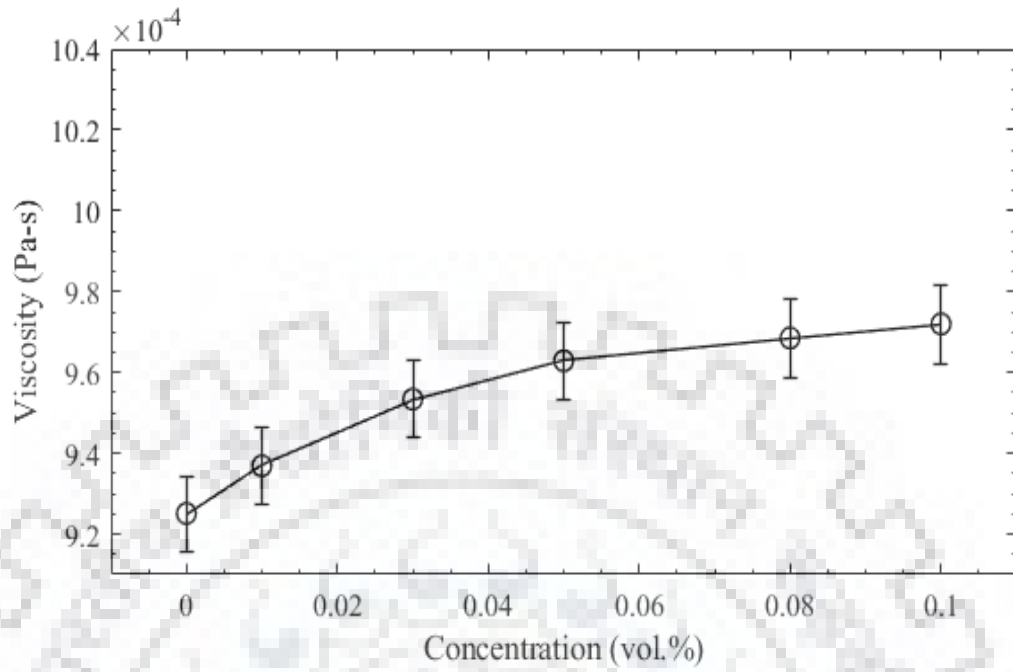
Figure 3. 14 Viscosity of the Fe₃O₄/ Water magnetic nanofluid with the concentration of the nanoparticles.
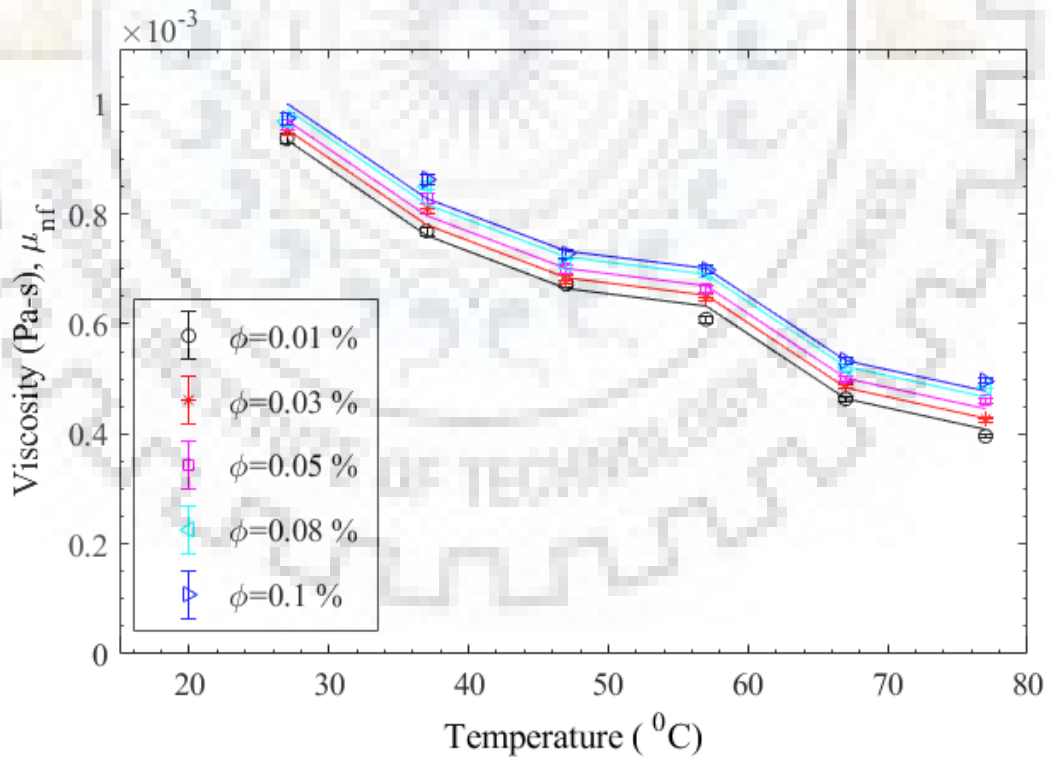
Figure 3. 15 Viscosity of the Fe₃O₄/ Water magnetic with the temperature at various concentrations of the nanoparticles. The solid lines represent the developed empirical correlation presented in equation (3.5).

The effect of the concentration of the nanoparticles on the viscosity is shown in Figure 3.14. The viscosity of the magnetic nanofluids is showing an increasing trend with the concentration of the nanoparticles. The viscosity of Fe_3O_4/ Water magnetic nanofluids is enhanced up to 5 % at the highest concentration of the magnetic nanofluid compared to water. Figure 3.15 shows the effect of temperature on the viscosity of Fe_3O_4/ Water magnetic nanofluids, and the solid lines represent the developed empirical correlation presented in equation (3.5). The correlation is developed based on the experimental data and shows around 2 % standard deviation from the actual experimental data. The viscosity of the magnetic nanofluids is showing a decreasing trend with the temperature but with concentration, the viscosity is enhanced compared to water. At a concentration of 0.1 vol. %, the viscosity increases from 5 to 30% in the temperature range of 27 to 77 °C.

$$\mu_{nf} = 2.41 \left(0.43\, \mu_{bf} - 13.32\, \emptyset^2 + 0.0467\, \emptyset \right) \left(\frac{T}{T_{max}} \right)^{0.051} \tag{3.5}$$

3.4.3 Density

The experimental setup for the density measurement is first validated with the theoretical model and previously published experimental results for the water. Figure 3.16 shows the density of the water at different temperatures and it consists of the theoretical model. The experimental values of the density are compared with the theoretical model (Popiel & Wojtkowiak, 1998) given in equation (3.6) and the previously published experimental values (Sengers & Watson, 1986).

$$\rho = a + bT + cT^2 + dT^{2.5} + eT^3 \tag{3.6}$$

where, a = 999.79684, b = 0.068317355, c = -0.010740248, d = 0.00082140905 and e = -2.3030988 × 10^{-5}

Figure 3.17 shows the density of the Fe_3O_4/ Water magnetic nanofluids with concentrations of nanoparticles. The thermal conductivity ratio is increased with the concentration of the nanoparticles. The maximum enhancement of 0.8 % in the density value is measured at the concentration of 0.1 vol. %. Figure 3.18 shows the density of the magnetic nanofluids with the temperature, and the solid lines show the correlation developed based on the experimental data. The correlation is represented in equation (3.7), the standard deviation for the correlation is 0.04 % from the actual experimental data. The density ratio is first decreased with temperature and then started to increase.

The enhancement in the density value changes from 1.2 to 0.7 % in the range of 10 to 70 ℃ for the 0.1 vol. %.

$$\frac{\rho_{nf}}{\rho_{bf}} = (1 + 61.29\,\emptyset^{1.13})\ T^{-0.34} \tag{3.7}$$
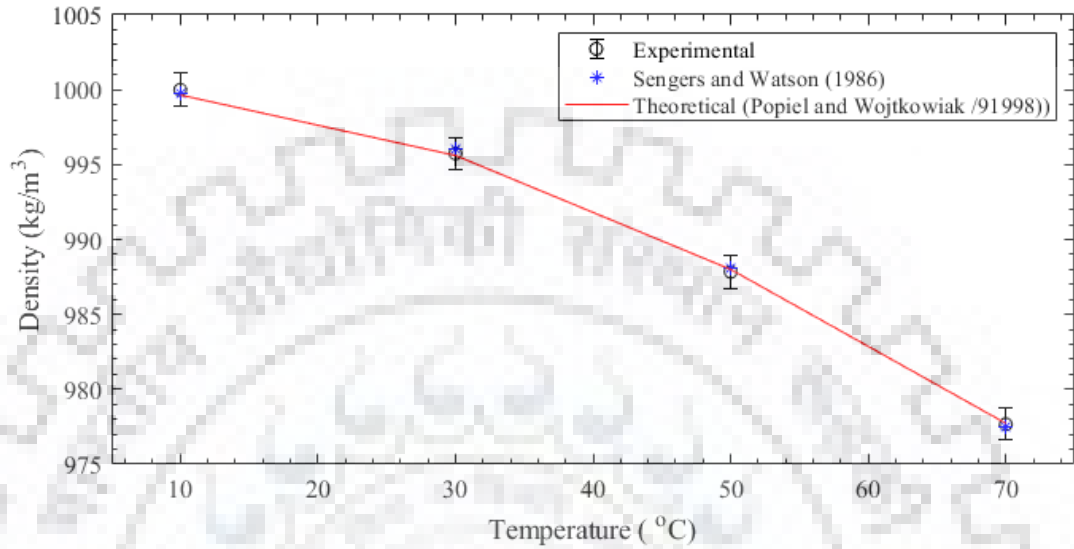
Figure 3. 16 Density of the water with different temperatures and comparison with the existing classical theoretical model (Popiel & Wojtkowiak, 1998) and the previous experimental values (Sengers & Watson, 1986).
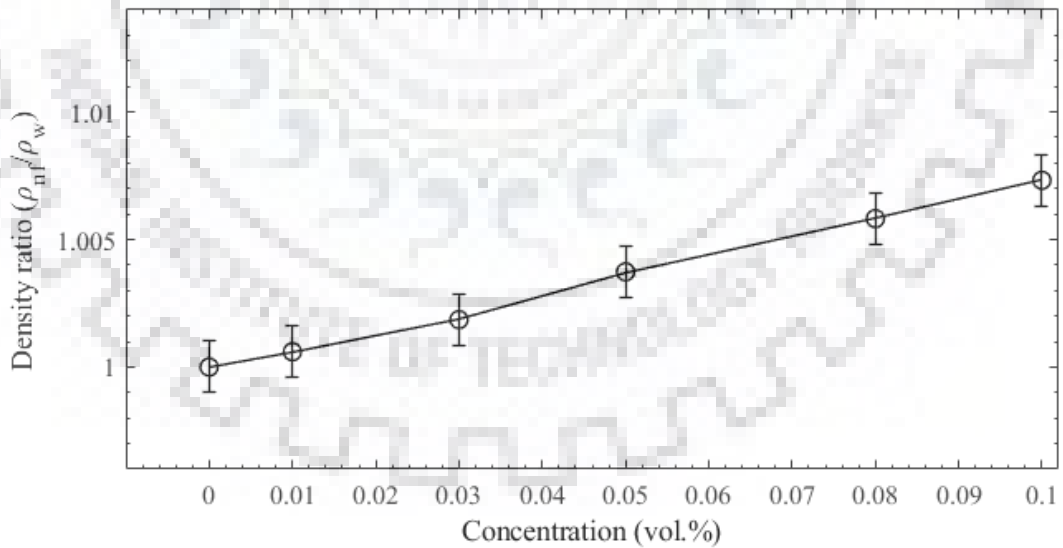
Figure 3. 17 Density ratio of magnetic nanofluids and water with the concentration of nanoparticles.
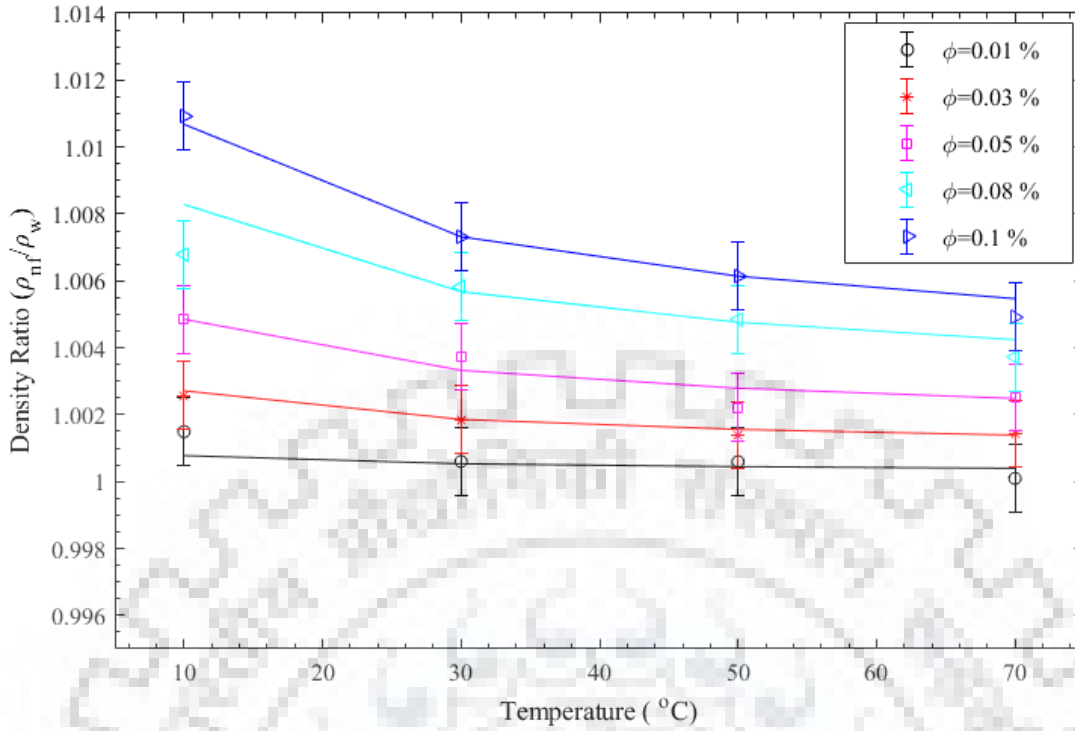
Figure 3. 18 Density ratio of magnetic nanofluids and water with the temperature at various concentrations of nanoparticles. The solid lines represent the developed empirical correlation presented in equation (3.7).

3.4.4 Other properties

The other thermophysical properties like specific heat and the thermal expansion coefficient are estimated in the study by the mathematical correlations. These mathematical correlations are tabulated in Table 3.2.

Table 3. 2 Mathematical correlations used to estimate different properties in the current study.

Property	Correlation	Reference
Specific Heat	$\rho_{nf}C_{p,nf} = (1-\emptyset)\rho_{bf}C_{p,bf} + \emptyset\rho_{np}C_{p,np}$	(Xuan & Roetzel, 2000)
Thermal Expansion Coefficient	$\rho_{nf}\beta_{p,nf} = (1-\emptyset)\rho_{bf}\beta_{p,bf} + \emptyset\rho_{np}\beta_{p,np}$	(Khanafer et al., 2003)

70

Remarks

The experiments are performed on the Fe_3O_4/ Water magnetic nanofluids to study the effect of temperature and magnetic field on the thermal conductivity. Different samples of magnetic nanofluids have been prepared by the two-step method after characterizing the magnetic nanoparticles with XRD, VSM and SEM for structure, magnetic properties and size. The magnetic nanofluids' thermal conductivity is affected by the concentration, temperature, and externally applied magnetic field.

The results show that the thermal conductivity is increased with concentration. The maximum enhancement in the study is observed at the highest concentration, which is around 15% compared to water at 0.1 vol.% of nanoparticle concentration. The temperature also enhances the thermal conductivity of the magnetic nanofluids samples. The maximum enhancement from 3 to 18 % is observed at the 0.1 vol.% in the temperature range 10 to 70 ℃, compared to water. The externally applied magnetic field is playing an imperative role in the thermal conductivity behaviour because of the ferromagnetic nanoparticles. The particles seem to align during the magnetic field application in a chain-like structure, which leads to an increment in the thermal conductivity of the magnetic nanofluids. The maximum enhancement of 22% is observed at 730 G magnetic field intensity and 70 ℃ for 0.1 vol.% concentration as compared to water. The other thermophysical properties like viscosity and density are measured at different concentrations and temperatures. The viscosity has shown a decrement trend with the temperature, however, it is increased with the concentration. At the 0.1 vol.% concentration of magnetic nanofluids the viscosity enhances from 5 to 30 % in the range 27 to 77 ^{0}C as compared to water. The slight enhancement is observed in the density of the magnetic nanofluids with concentration and with temperature, the density is shown a decrement trend. The maximum enhancement of only 0.8% occurs at 0.1 vol.% concentration at room temperature. The enhancement in the density is decreasing from 1.2 to 0.6 % in the range of temperature 10 to 70 ℃.
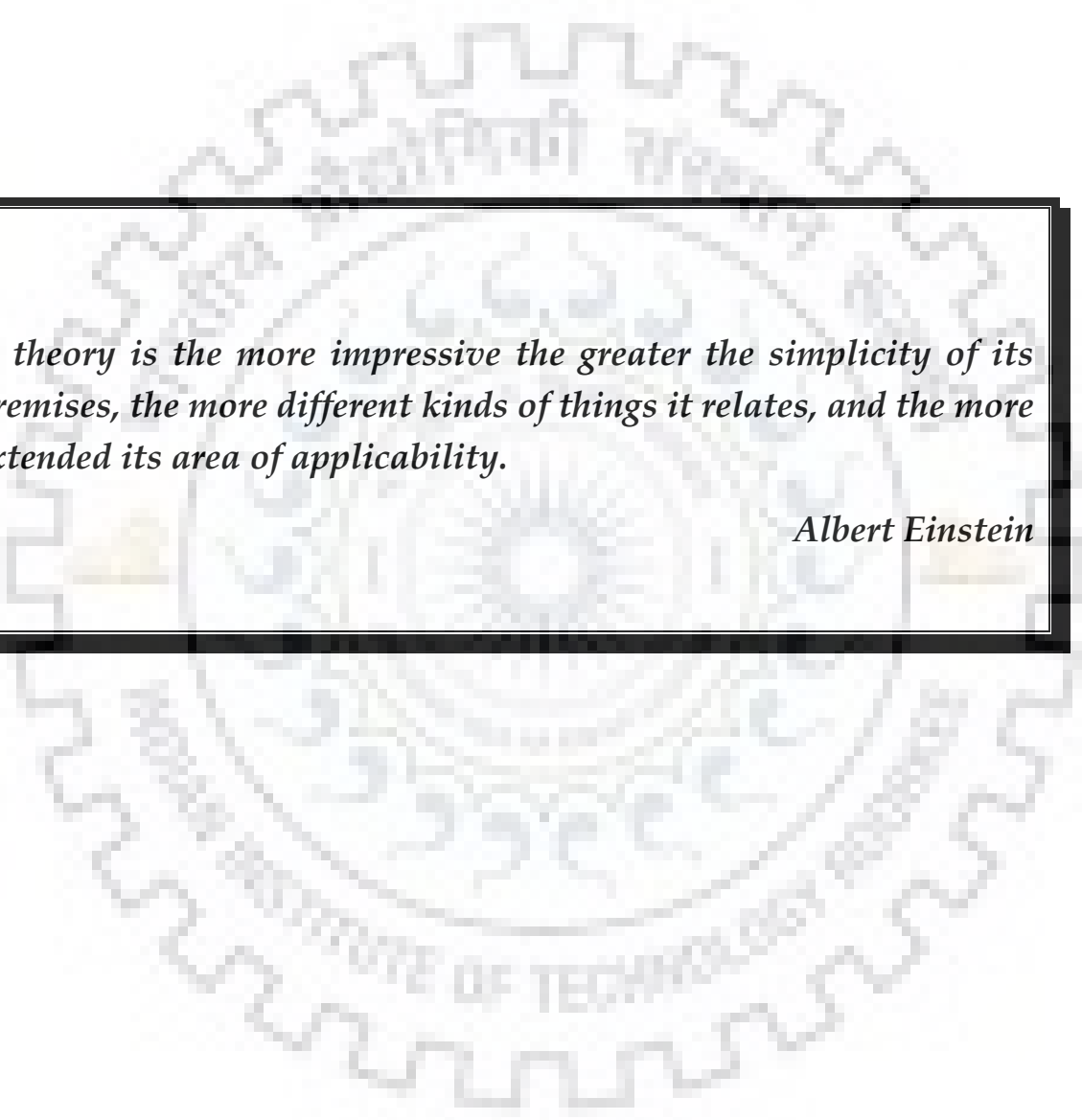
The new empirical correlation is developed and reported for thermal conductivity, viscosity and density with different parameters. The developed correlation shows a perfect fit with the experimental data by considering all the parameters.

Chapter 4: Experimental Facility, Data Reduction & Statistical Analysis

Index

A theory is the more impressive the greater the simplicity of its premises, the more different kinds of things it relates, and the more extended its area of applicability.

Albert Einstein

4

Experimental Facility, Data Reduction & Statistical Analysis

To achieve the different objectives of the study, different instruments are used to prepare the experimental setup. This chapter deals with the information about the various devices, apparatus and data analysis techniques used to achieve the objectives of the study.

4.1 Experimental Set up

In order to study the natural convection heat transfer in an open cavity, the test cavity is prepared. This schematic and photographic view of the experimental setup is outlined in Figures 4.1 and 4.2, respectively, consisting of a small cubic cavity of side 30 mm, insulated from sides. The aspect ratio (width/height) of the test section is one for all the experiments. In the present experiment, the bottom of the cavity is made of a 5 mm thick copper plate and the top is open to the environment. Oxygen-free high conductive annealed copper having a thermal conductivity of 350 W/m K at room temperature is used here. The thin plate heater of thickness 5 mm, specially designed for this application, is attached to the bottom copper plate and perfectly insulated by ceramic wool and wood from the sides and the bottom side, respectively. The side walls are made up of a 5 mm thick transparent perspex sheet and insulated with thick ceramic wool. The open environment is maintained at a temperature of 20 ℃ and the relative humidity of 45 to 55 % during the experiment. The water in the cavity is purified water having TDS value 0 and electrical conductivity 0.9 μS/cm prepared by Elix® Essential 3 Water Purification System, Merck, USA. The plate temperature distribution is measured by highly accurate, four calibrated copper-constantan thermocouples (OMEGA), inserted horizontally up to half the distance from the center from each side inside the copper plate (Figure 4.3 (b)).

To record thermal fluctuation inside the cavity, there are fifteen very thin thermocouples having bead thickness of 0.25 mm placed along the centreline (Figure 4.3 (a)). Testo 605i thermohygrometer is used to measure the relative humidity and temperature inside the room. Each thermocouple is initially calibrated to minimize the error in measurement. The different Rayleigh numbers are achieved by adjusting the heat flux with the variation of the power and the steady-state is achieved after about one hour. The temperature data series are recorded on a PC using a data logger (Keysight Tech.) with 0.004 % dcV accuracy.

1. Test Section
2. Electromagnet (Helmholtz coil)
3. Horizontal stand to hold Helmholtz coil
4. Constant current supply (0- 6 Amp)
5. Gauss meter
6. Intermediate rod holding thermocouples
7. Copper plate
8. Heater
9 Data logger
10. Computer
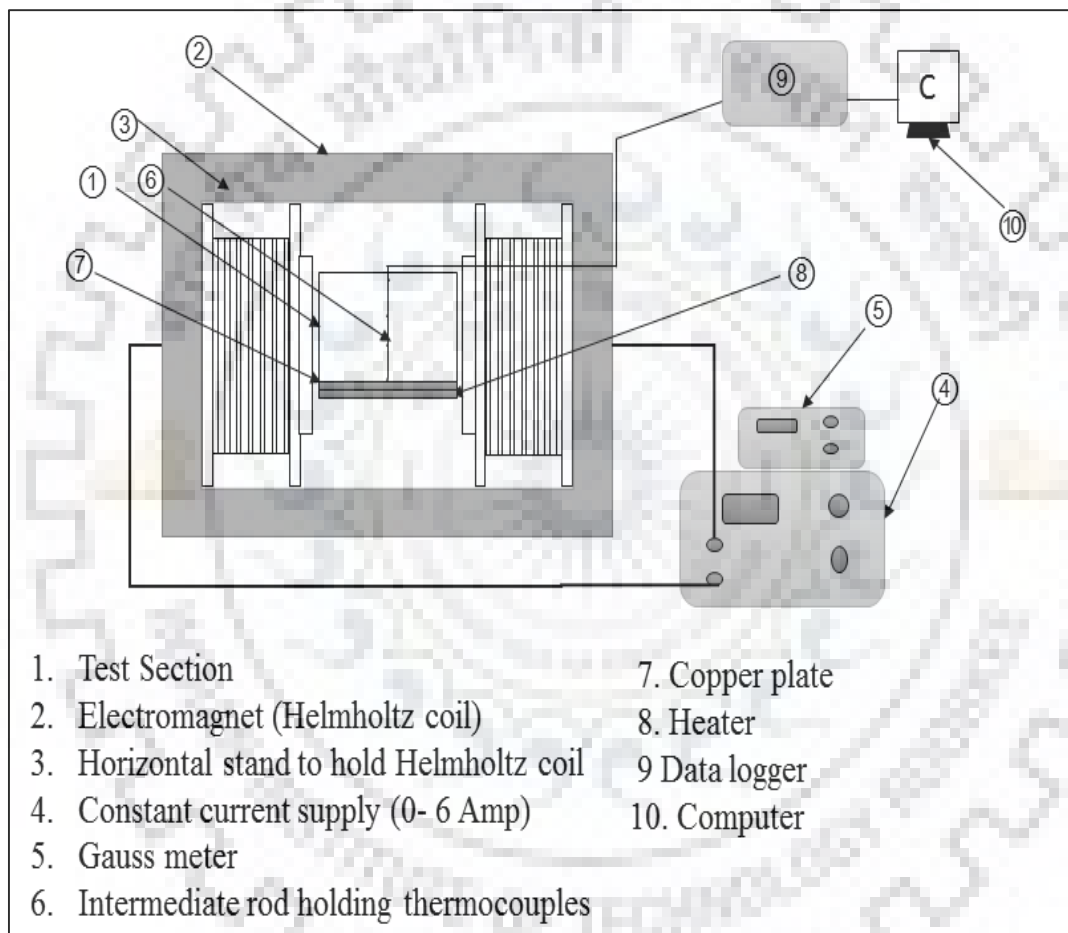
Figure 4. 1 Schematic figure of the experimental test setup.
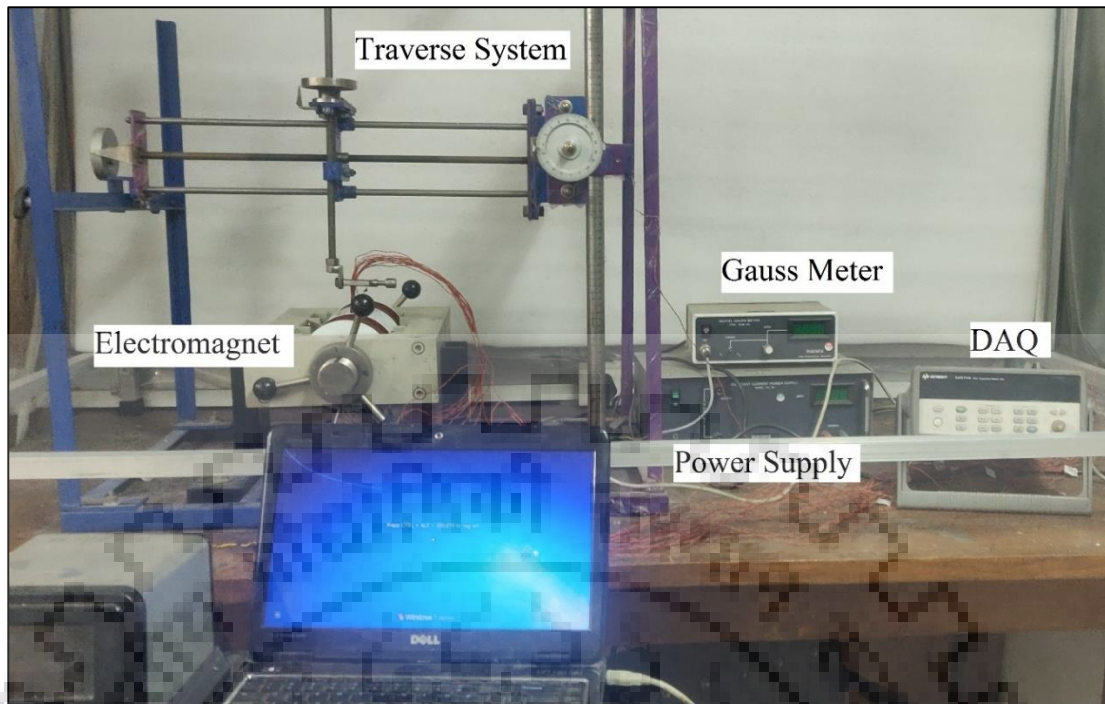
Figure 4. 2 Photographic view of the experimental setup.

4.1.1 Major parts of the experimental setup

The experimental setup is consisting of a number of parts and instruments. A detailed explanation about these parts and instruments is presented below.

A. Test section

The test section shown in Figure 4.3 includes the open cubic cavity contained the working fluid. The dimensions of the different parts of the cubic cavity is summarized in Table 4.1. The cubic cavity of the side 30 mm is open to the environment. The sides of the cavity are fabricated by the Perspex sheet and perfectly insulated by the ceramic wool. The bottom of the cavity is made of oxygen-free high conductive annealed copper having a thermal conductivity of 350 W/mK at room temperature. The bottom of the cavity is heated by the specially designed plate heater fabricated in the Arihant Electricals, Maharashtra, India. The plate heater is electrically insulated by the mica sheet and provides the constant heat flux to the bottom of the cubic cavity. To make the perfect contact between the bottom heated plate and the plate heater for perfect thermal contact conductance, the viscous fluid glycerine is used as a thermal interface material. The plate heater, along with the cubic cavity, is placed on the wooden block to minimizes the heat losses from the bottom. The T type thermocouples are used to measure the time series of the temperatures along the centreline of the cubic cavity, as shown in Figure 4.3 (a). The positions of thermocouples from the bottom plates are at

0, 0.5, 1, 2, 3, 4, 5, 7, 10, 15, 20, 25 and 30 mm. One thermocouple is placed to measure the temperature just above the water surface and one is placed near the test section inside the room to measure the ambient temperature. The temperature of the bottom heated plate is measured by the four T-type thermocouples inserted at a distance of 7.5 mm from the sides, as shown in Figure 4.3 (b).

Table 4. 1 Dimensions of the components of the open cubic cavity.

Components	Dimensions
Cavity (water layer)	30 mm × 30 mm × 30 mm
Bottom heated plate (copper plate)	30 mm × 30 mm × 5 mm
Sidewalls (Perspex sheet)	30 mm × 30 mm × 5 mm
Plate Heater	35 mm × 35 mm × 5 mm
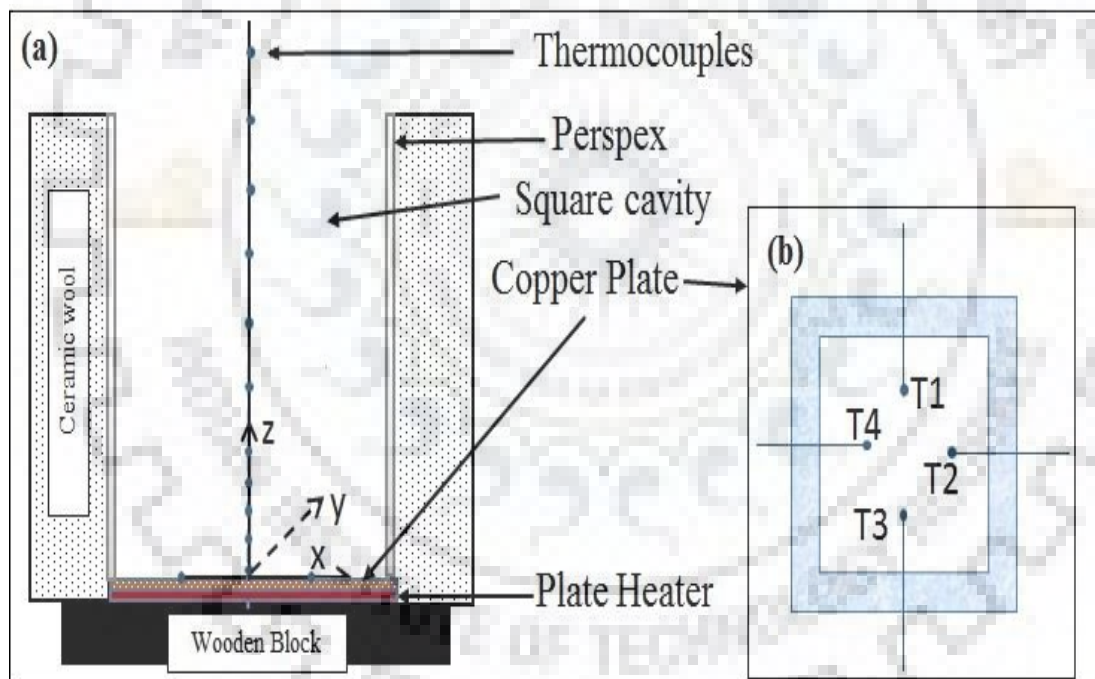
Figure 4. 3 Schematic of the experimental test setup: (a) the top surface is open to the environment and the cavity is filled with water up to 30 mm height and (b) thermocouple positions inside the copper plate.
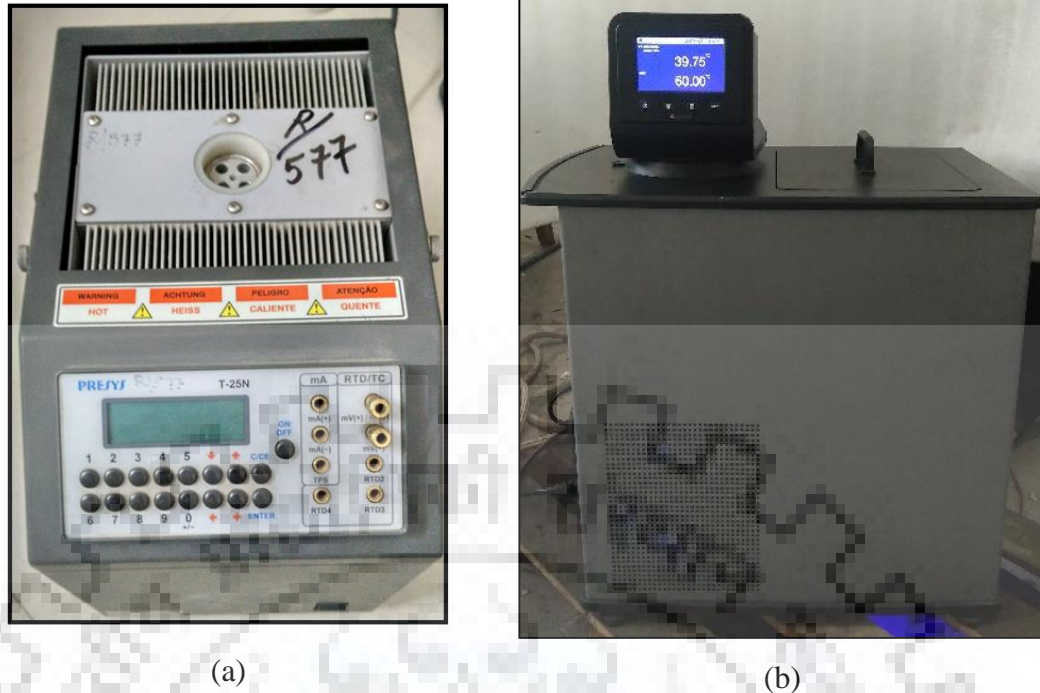
Figure 4. 4 Photographic view of (a) Presys T-25 N calibrator and (b) Constant Temperature Bath.

B. Thermocouples & Traverse System

As the temperature in the present study is varied from the 10 ℃ to 90 ℃, T-type thermocouples are used to measure the temperature with minimum error in this range. As mentioned above, the total number of thermocouples at different locations is 18 in the experimental setup. These thermocouples are first calibrated with the Presys T-25N calibrator and constant temperature bath in the range 10 ℃ to 90 ℃ and these instruments are shown in Figure 4.4.

C. Data Logger

The voltage output data of thermocouples is converted into digital values by the data acquisition system (DAQ). The DAQ system purchased from Keysight Technologies, USA is shown in Figure 4.5. The thermocouples are directly connected to the multiplexer (Model: 34901A), which is connected in the DAQ (Model: 34970A). The DAQ system is connected to the computer with the help of the Agilent Bench Link Data Logger (Version 4.3) software.

D. Electromagnets & Gaussmeter

The external magnetic field is applied by the H-shaped electromagnets, as shown in Figure 4.6. The poles of the electromagnets have diameters of 50 mm and are made from soft iron. The electromagnet is connected with the constant current power supply. Gaussmeter is used to measure the magnetic field between the two poles of

electromagnets. The specifications of the electromagnets, power supply and gaussmeter are given in Table 4.2. The electromagnets are fabricated by the Vijayanta Technology Pvt. Ltd. Roorkee, India.

E. Hygrometer

The relative humidity of the room is measured by the testo 605 i Thermohygrometer, shown in Figure 4.7, purchased from Testo India Pvt. Ltd., Maharashtra, India. The instrument is probe type and connected with the smartphones via testo app. The specifications of the product are given in Table 4.3.

Table 4. 2 Specifications of the testo 605 i smart probe Thermohygrometer.

Parameters	Specifications
Measuring Range	0 to 100 % Relative Humidity (RH)
Accuracy	± 3 % RH (10 to 35 % RH) at 25 ℃
	± 2 % RH (35 to 65 % RH) at 25 ℃
	± 3 % RH (65 to 90 % RH) at 25 ℃
	± 5 % RH (<10 or > 90 % RH)
Resolution	0.1 % RH
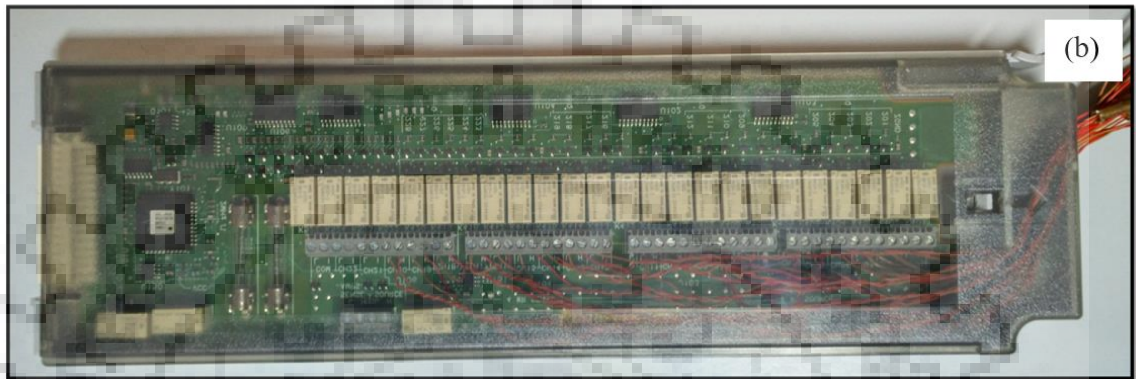
Figure 4. 5 Photographic view of (a) Data Logger, Model: 34970A (b) Multiplexer, Model: 34901A, Make: Keysight Technologies, USA.
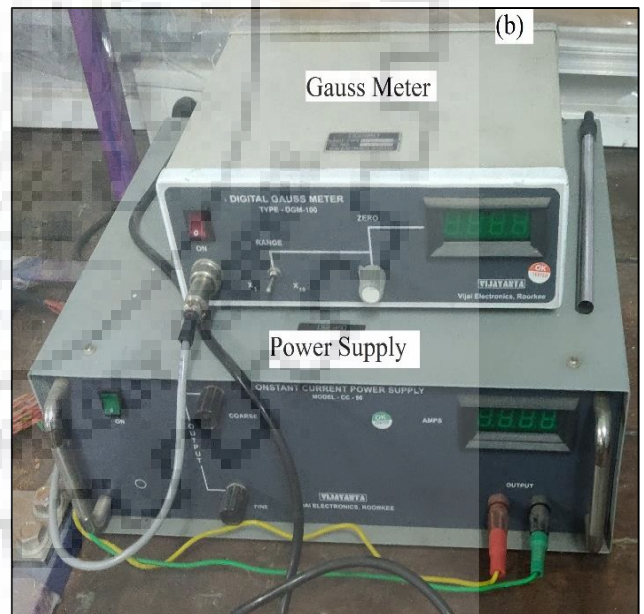
Figure 4. 6 Photographic view of the (a) Electromagnet (b) Power supply and Gaussmeter.

Figure 4. 7 Photographic view of Thermohygrometer.

4.2 Data Reduction

4.2.1 Data Collection

The measured data from the experiments is converted into various dimensional and non-dimensional numbers. A number of experiments are conducted over the range of various parameters. The following are the different data collected for each of the experiments.

- The power supply in the form of current and voltage from ammeter and voltmeter, respectively.
- Time series of temperature at the bottom heated surface.
- Time series of temperature at various locations at the centreline of the open cubic cavity.
- Time series of the temperature of the room temperature
- The humidity of the room.

4.2.2 Data Reduction

Each experiment is started from the initial point and a steady state is achieved after some time. The steady-state data for each experiment is used to calculate various parameters given below:

A. Heat flux at the bottom heated surface

The heat flux at the surface of the bottom heated plate is assumed to be the same as at the plate heater due to high thermal contact conductance between the plate heater and the bottom heated plate. The voltage (V) from the voltage variac, the resistance (R) of the plate heater and surface area (A_c) of the bottom heated plate are used to measure the heat flux at the surface of the bottom heated plate.

$$q = \frac{V^2}{R\, A_c} \tag{4.1}$$

B. Average Temperature and Temperature difference

The average temperature ($<T>$) inside the cavity is calculated by averaging the temperature obtained inside the cavity at different positions along the centreline. The thermophysical properties of the working fluids are calculated at the average temperature.

$$<T> = \frac{T_1+T_2+T_3+T_4+T_5+T_7+T_{10}+T_{15}+T_{20}+T_{25}}{10} \tag{4.2}$$

The temperature difference (ΔT) is calculated as the difference between the surface temperature of the bottom heated plate (T_h) and the temperature of the bulk fluid (T_b) at the center of the cavity.

$$\Delta T = T_h - T_b \tag{4.3}$$

C. Rayleigh Number

The Rayleigh Number (Ra) governing the convection state is defined as the ratio of buoyancy force to the product of viscous force and rate of heat diffusion. The mathematical form of the Rayleigh number is given as:

$$Ra = \frac{g\beta\,\Delta T L^3}{\nu\alpha} \tag{4.4}$$

where g is the acceleration due to gravity, β is the isobaric thermal expansion coefficient, ΔT is the temperature difference across the vertical layer between the heated bottom surface and bulk fluid, ν is the kinematic viscosity and α is the thermal diffusivity of the fluid.

D. Nusselt Number

The global heat transfer is defined by dimensionless Nusselt number (Nu) is defined as the ratio of convective heat transfer to conductive heat transfer at a boundary of the fluid. The Nusselt number is given as follows:

$$Nu = \frac{hL}{k} = \frac{Q\,L}{k\,A\,\Delta T} \tag{4.5}$$

where h is the heat transfer coefficient. In the open cavity, the convection assumed to be quasi-steady and the heat input into the convecting layer (Q) is related to heat output from the heater (Q_h)

$$Q = Q_h - M_s C_{ps}\frac{dT}{dt} - Q_l \tag{4.6}$$

The $M_s C_{ps}$ is the effective product of mass and specific heat of the bottom copper plate. The heat losses (Q_l) from the vertical side walls are estimated by the thermal conductance ($C=0.00116 \pm 0.0001$) from the series combination of conduction through the perspex sheet, conduction through the ceramic wool insulation and convection from the outer surface of the insulation. Assuming the steady and equal heat transfer from each sidewall, the different values estimated of thermal conductance for each side wall are 0.0342, 0.00135 and 0.0109 W/^{0}C for conduction through the perspex sheet, conduction through the ceramic wool insulation and convection from the outer surface of the insulation, respectively.

E. Prandtl Number

The Prandtl number (Pr) is the ratio of the viscous diffusivity to the thermal diffusivity. The Prandtl number is given as follows:

$$Pr = \frac{\mu\,C_p}{k} = \frac{\nu}{\alpha} \tag{4.7}$$

where C_p is the specific heat capacity.

F. Thermal Boundary Layer thickness

The thermal boundary layer thickness (δ_{th}) is the vertical distance measured from the bottom heated plate to the point where linear temperature profile encounters with the tangent of bulk fluid temperature. The thermal boundary layer thickness is calculated from the graph of the temperature versus the height inside the cavity. Mathematically, the thermal boundary layer thickness can be calculated as follows:

$$\delta_{th} = \frac{k\,\Delta T}{Q} = \frac{H}{2\,Nu} \tag{4.8}$$

4.3 Statistical Analysis

Statistical data analysis is involved in the presentation and exploration of the collected extensive sampled data to discover the underlying patterns and trends. Statistical data analysis provides us the in-depth information about the heat transfer phenomena inside the open cubic cavity. The techniques of the statistical analysis thoroughly examine the trends about the temperature fluctuations inside the cavity at various locations. In this study, the following are the primary statistical analysis techniques used.

4.3.1 Temperature Time Plot

The time series of the temperature is recorded in the experiments at the various locations of the cubic cavity across the centreline. The fluctuations in the temperature change according to various parameters in the cavity. The thermal activities can be visualized comprehensively in the temperature versus time graph. The normalized mean temperature is given in the equation (4.8) used to characterize the temperature fluctuations inside the open cubic cavity.

$$\theta = \frac{[T_h - \langle T \rangle (z)]}{\Delta T} \tag{4.9}$$

where, $\langle T \rangle (z)$ is the average temperature of the steady state at a vertical distance (z) from the bottom heated surface.

4.3.2 Probability Density Function

The probability density function (*pdf*) of a random variable defines the probability distribution, or in other words, it is the function that provides the probability occurrence of the random phenomena in an experiment. In more simple words, the *pdf* defines the likelihood of outcomes for a random variable. The area under the graph of *pdf* shows the probability of a discrete random variable. In this study, the *pdf* of the temperature fluctuations at the center of the cavity is plotted for different Rayleigh numbers.

4.3.3 Root Mean Square

The root mean square (r.m.s or σ) value is the second-order moment defined as the square root of the mean squared deviation of the collected data. The mathematical form of the r.m.s is given in equation (4.10).

$$\sigma_T = \langle (T - \langle T \rangle)^2 \rangle^{1/2} \tag{4.10}$$

where $< >$ operator indicate the mean value.

The r.m.s value indicates the deviation of the data around the mean value; r.m.s value is always greater than or equal to zero. The r.m.s value closed or equal to zero indicates that the data is concentrated about the mean.

4.3.4 Power Spectral Distribution

The power spectral distribution (*psd*) at a given location is the squared magnitude of the time Fourier transformation of the measured data. The *psd* shows the strength of the energy transformation with frequency. In simple words, it shows at which frequency the variation in the energy transformation is stronger. The spectra of the temperature variance are defined as:

$$E_\sigma = \frac{1}{2}\langle \sigma^2 \rangle = \int_0^\infty E_\sigma(k)\, dk \qquad (4.11)$$

Remarks
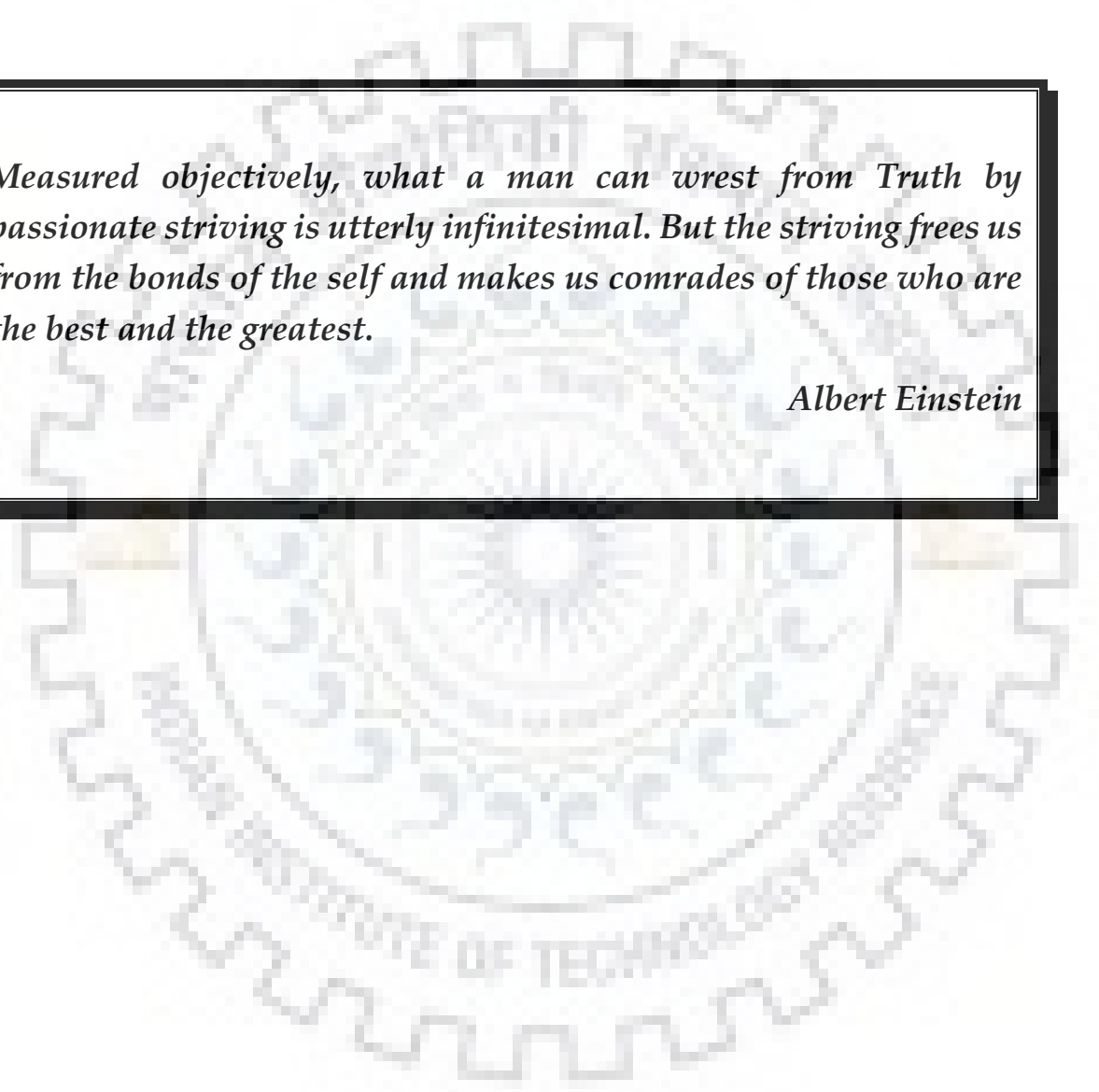
A detailed description of the experimental setup is presented. The major components and instruments with the technical specifications are elaborated. The procedures followed to conduct the experiments for various parameters are also presented. It has been attempted to cover all the parts and deliver information related to the experimental setup, procedures and data reduction techniques.

Chapter 5: Calibration & Uncertainty Analysis

Index
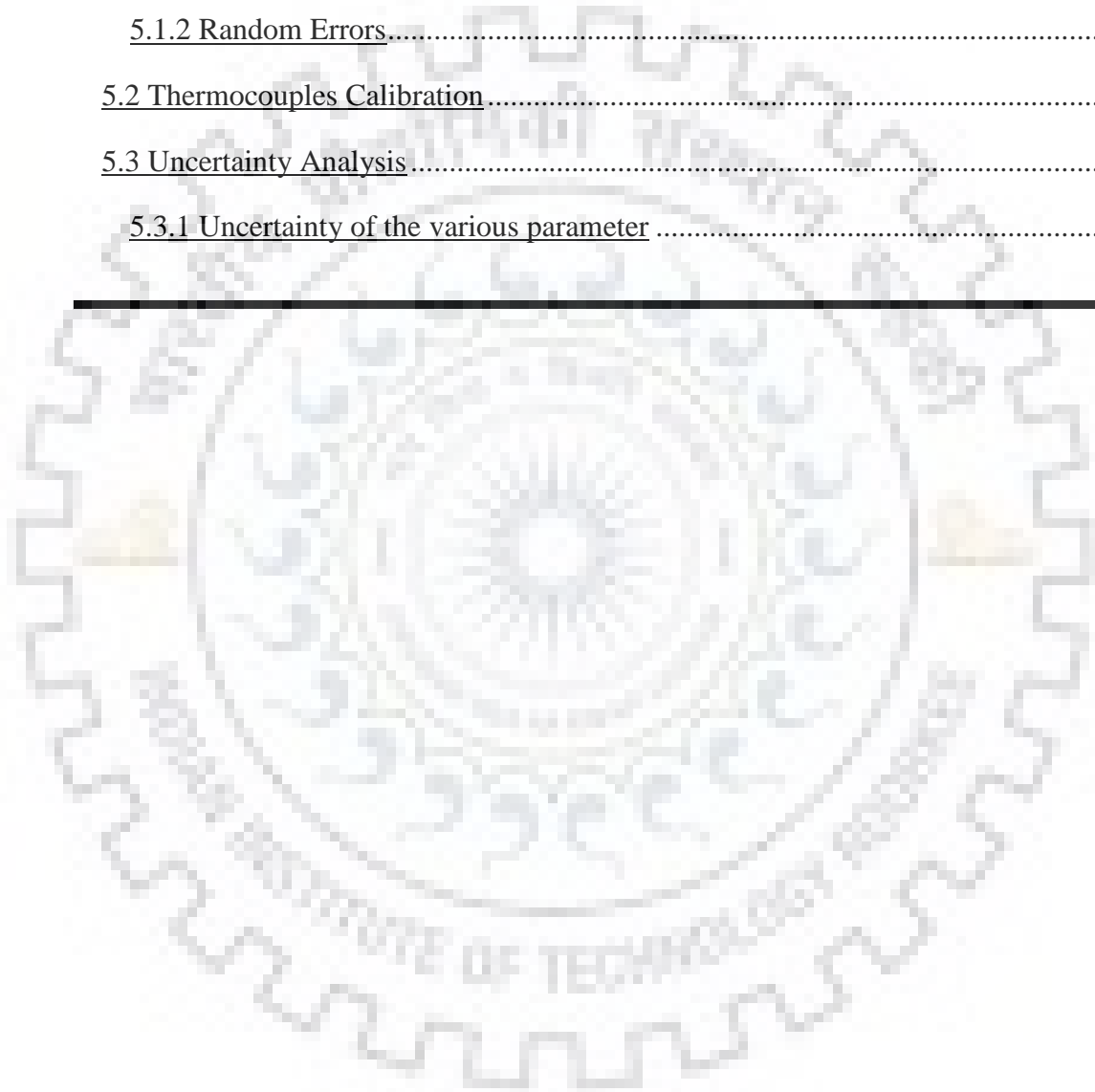
Measured objectively, what a man can wrest from Truth by passionate striving is utterly infinitesimal. But the striving frees us from the bonds of the self and makes us comrades of those who are the best and the greatest.

Albert Einstein

5

Calibration & Uncertainty Analysis

As explained in the earlier chapter, the experiments are done using various tools and instruments. The errors and the uncertainties in the experiments are inevitable parts of any measurement. There are various errors and uncertainties present in the visible or invisible form in the experiments. In this chapter, various types of errors and uncertainties are discussed, followed by the calibrations of the various instruments used during the experiments.

5.1 Errors

Error is the deviation of the measured value from the true value of the property being measured. If possible, the known errors are corrected by the applications of corrections from the calibrations certificates or data. The errors in the measurement are categorised into various parts, but based on the origin, the errors are categorised into two parts viz. systematic errors and random errors.

5.1.1 Systematic Errors

The systematic errors are originated due to fault in the measuring instrument. Systematic errors can be occurred due to various reasons like improper handling of instruments, external environment conditions and wrong observations of the reading. The repetition of the experiment can't detect systematic error. These errors are challenging to eliminate, but these errors can be avoided by identifying and restoring the instruments.

5.1.2 Random Errors

The random errors occurr by the impulsive fluctuations in the experimental conditions. Other than systematic errors, all errors fall in this category of measurement errors. The random errors can be avoided by taking the average value of many repeated experiment values.

The errors in the measurement can be avoided or minimized by applying the calibrations certificate to the instruments. The present study deals with many instruments such as thermocouples, data logger, electromagnet, gaussmeter, power supply etc. Most of the instruments are calibrated against the standard values. The calibration of thermocouples was done with the thermocouple calibrator. However, many errors originated whose values are unknown, so the uncertainty analysis for such errors quantifies the doubt about the experimental measurement results.

5.2 Thermocouples Calibration

The calibration is the comparison of a standard value against the measured value from the instrument. The accuracy of the standard should be very high compared to the measuring instrument. However, the accuracy of the standard should be three times the measuring instrument, which is acceptable for the calibration. The usefulness of the data is dependent on the accuracy of the measuring instruments. Calibration of the instruments over a period of time, as mentioned in the instructions by the manufacturing company or observed by the instrument operator, leads to achieving accuracy in the measuring instrument. In this study, to prevent errors in the temperature measurement and make the experimental data highly accurate, the T-type thermocouples are calibrated in the range of 10 ℃ - 90 ℃. The highly accurate standard instrument Persys T-25N calibrator and another instrument, Constant temperature bath (CTB), are used to calibrate the thermocouples in the present study. Figure 5.1 and 5.2 shows the graph for the calibration curve for Persys T-25N calibrator and Constant temperature bath, respectively. The correlation between the standard value and the measured value is established by the regression analysis. The correction is made on the measuring values by thermocouples by using this regression correlation to achieve high accuracy in the results.
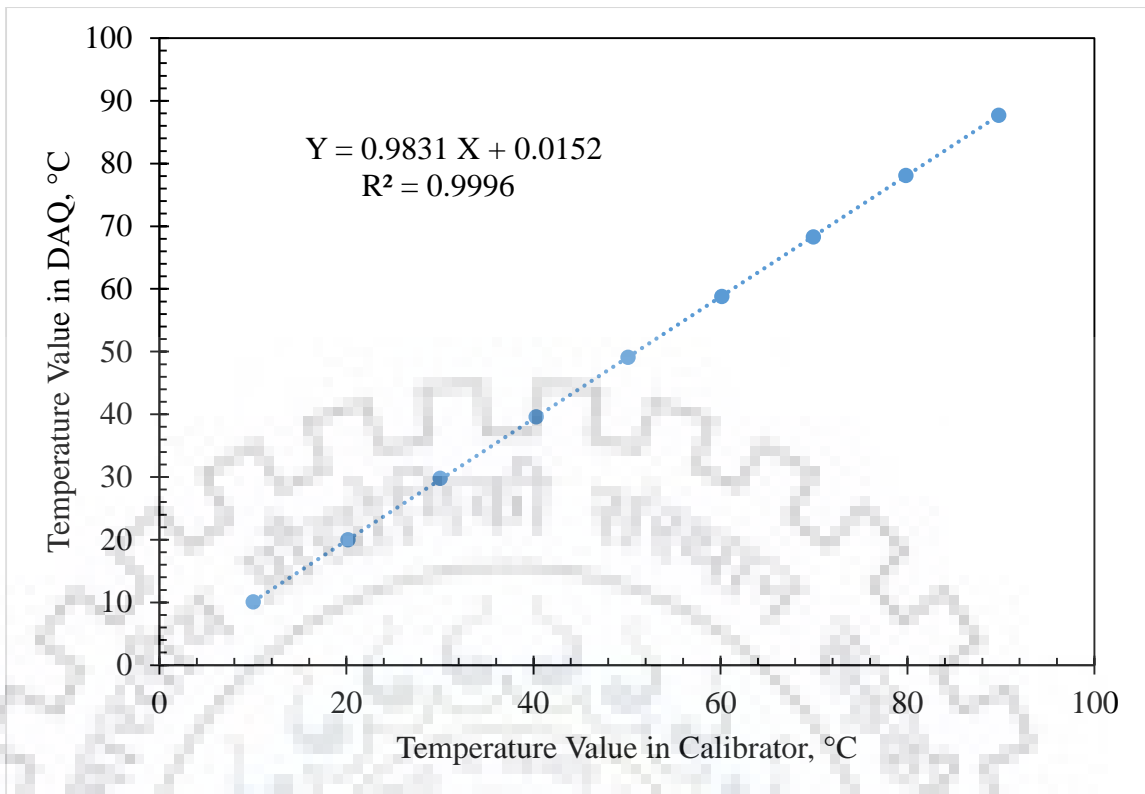
Figure 5. 1 Calibration graph for T-types thermocouples against the Persys T-25N calibrator, the blue circle indicates the measured experimental data and the dotted line is a correlation.
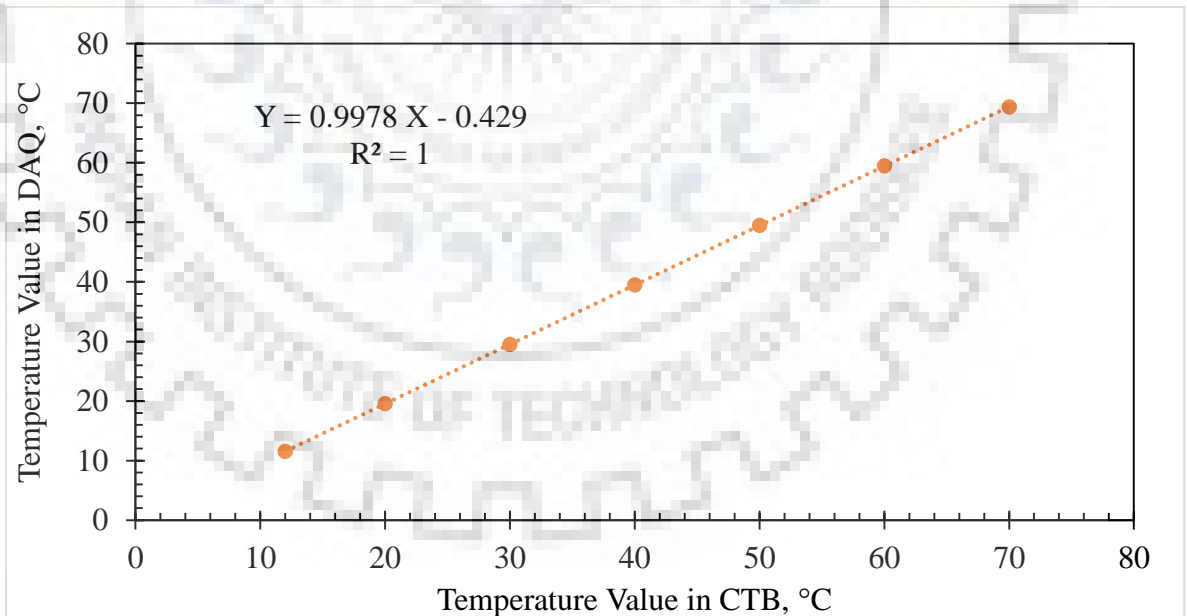
Figure 5. 2 Calibration graph for T-types thermocouples against the Constant Temperature Bath , the orange circle indicates the measured experimental data and the dotted line is a correlation.

5.3 Uncertainty Analysis

The doubt about the measurement results is the uncertainty definition in simple worlds. The uncertainty shows the quality of the results. It is the quantification of the doubt about the measured results. The unknown error in the experiments is also the source of uncertainty. Uncertainty is the statistical interpretation of the errors in the experiments. Kline and McClintock (1953) describe the uncertainty "a possible value that an error may have." Bell (2001) describes the two way to estimate uncertainties in the experiment: Type A and Type B. Uncertainty estimated using the statistics (from repeated experimental values) fall into the Type A category, while type B category involves the uncertainty calculated from experience, from manufacture specification, from calibration data or certificates of calibration provided by the manufacturer and from previously published data. Type A uncertainty (u_A) is calculated from the standard deviation (σ) of a set of experimental data repeated n times.

$$u_A = \frac{\sigma}{n} \tag{5.1}$$

where standard deviation (σ) is estimated as

$$\sigma = \sqrt{\frac{1}{n-1} \sum_i^n (x_i - \bar{x})^2} \tag{5.2}$$

where $\bar{x}$ is the mean of n experimental readings.

The information in Type B uncertainty (u_B) is more scarce, the upper and lower limit of uncertainty is only possible to estimate. The values of uncertainty have to be assumed between the upper and lower limit. The rectangular or uniform distribution is used to calculate the uncertainty between the upper limit. From the view of uniform distribution, the uncertainty of type B is found:

$$u_B = \frac{a}{\sqrt{3}} \tag{5.3}$$

where a is the half-width of the upper and lower limit.

The combined or total uncertainty (u_c) of the experimental measurement is calculated by the root sum of Type A and Type B uncertainty.

$$u_c = \pm \sqrt{u_A^2 + u_B^2} \tag{5.4}$$

5.3.1 Uncertainty of the various parameter

The combined uncertainty (u_c) of the temperature is measured as

$$u_c = \pm \sqrt{\left(u_{A,\sigma_{\bar{T}}}^2 + u_{B,\bar{T},Resolution}^2 + u_{B,\bar{T},Calibration}^2 + u_{B,\bar{T},DAQ}^2\right)} \qquad (5.5)$$

On the right-hand side, the first term represents the Type A uncertainty and the remaining terms are Type B uncertainties. The second term is uncertainty in the resolution of the Persys T-25N calibrator, having a value of 0.01 °C, the third term is uncertainty due to calibration and the fourth term is uncertainty in the data logger.

$$u_T(T) = \pm \sqrt{\left((0.094)^2 + 0.01^2 + 0.058^2 + 0.001^2\right)} = \pm 0.15\,°C$$

The uncertainties of other measured parameters such as voltage, current and relative humidity etc., are summarized in Table 5.1.

Table 5. 1 Measured parameters of uncertainty.

S. No.	Parameter	Range	Expanded Uncertainty
1	Voltage	0-240 volts	0.08 %
2	Current	0-2 amp	0.18 %
3	Temperature	10-90 °C	± 1.084 °C
4	Relative Humidity	0-100 %	± 3.01 %

Uncertainty in the derived parameters is calculated according to the number of parameters it depends upon. The uncertainty for various derived parameters are as follows:

A. Heat Flux
The heat flux is calculated as:

$$q = \frac{VI}{A} = \frac{Q}{A} \qquad (5.6)$$

The uncertainty in the heat flux is calculated as:

$$u_c(q) = \frac{\delta q}{q} = \pm\sqrt{\left(\frac{\delta Q}{Q}\right)^2 + \left(\frac{\delta A}{A}\right)^2} = \pm 0.033\%$$

B. Nusselt Number (Nu)

$$Nu = \frac{qH}{k\Delta T} \tag{5.7}$$

The uncertainty in the Nusselt number is calculated as:
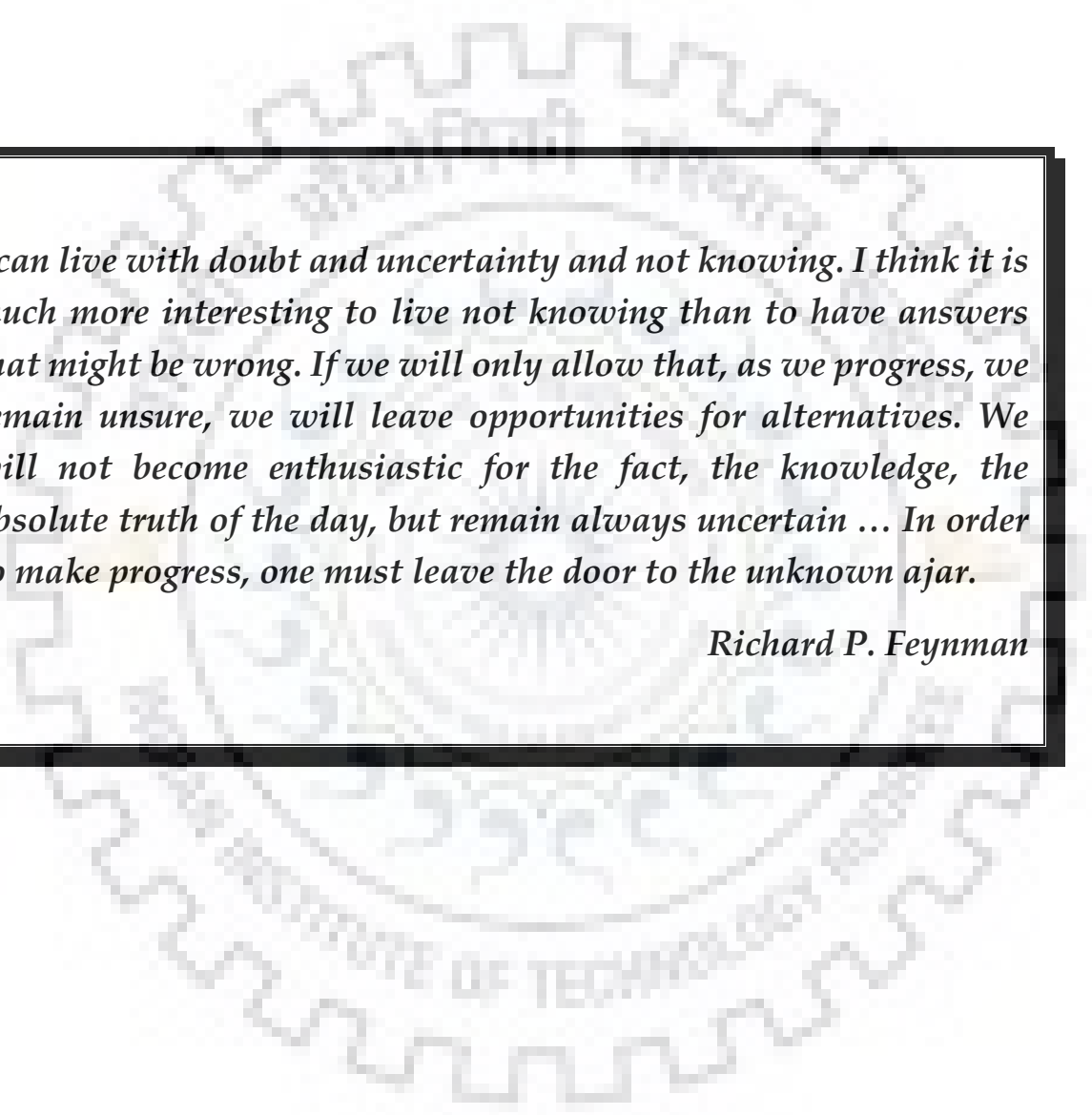
$$u_c(Nu) = \frac{\delta Nu}{Nu} = \pm\sqrt{\left(\frac{\delta q}{q}\right)^2 + \left(\frac{\delta H}{H}\right)^2 + \left(\frac{\delta k}{k}\right)^2 + \left(\frac{\delta \Delta T}{\Delta T}\right)^2} = \pm 2.16\%$$

Chapter 6: Results & Discussions

Index

I can live with doubt and uncertainty and not knowing. I think it is much more interesting to live not knowing than to have answers that might be wrong. If we will only allow that, as we progress, we remain unsure, we will leave opportunities for alternatives. We will not become enthusiastic for the fact, the knowledge, the absolute truth of the day, but remain always uncertain … In order to make progress, one must leave the door to the unknown ajar.

Richard P. Feynman

6

Results & Discussions

6.1 Water

The experimental measurement of the temperature fluctuation in the vicinity of different zones of the thermal boundary layer in water-filled open cubic cavities heated from below and open at the top has been studied. The experiments are performed on the cubic cavity of aspect ratio 1 and lateral dimension of 30 mm, also, the results of our previously reported open cubic cavities of aspect ratio 1 and lateral dimensions (120mm and 240 mm) are considered here. The transient nature of the temperature has been measured from the temperature time-series recorded across the central axis of the cavity at different vertical positions z from the heated bottom plate. The Prandtl number and Rayleigh number range reported in this work are $4 \leq Pr \leq 6$ and $10^5 \leq Ra \leq 10^9$, respectively. The different basic statistical properties, such as mean temperature, root mean square (r.m.s.) and probability density function (*pdf*) of temperature fluctuation, are studied and discussed. The power law of power spectral density of the temperature fluctuations at the different regions of the thermal boundary layer is studied and the different rolls of rate is compared with the previously established theories and models. The validity criteria for the Oberbeck-Boussinesq approximation is fulfilled. The trend of dimensionless Nusselt number (*Nu*), representing global convective heat transfer is obtained and discussed. The variation of $\left(Ra_{\delta_{th}} \right)^{-1/3}$ for heat transfer representation is noted in the range of 0.04 to 0.24, where δ_{th} is the boundary layer thickness.

6.1.1 Temperature series

All the experiments are carried out with the water as a working fluid. The values of the dynamic Bond number, B_d calculated for all the experiments are higher than 30 and the value of Crispation number, $Cr < 10^{-4}$, which means surface tension effects are negligible. Figure 6.1 shows the variation of temperature with time during the experiment for $Ra = 8.38 \times 10^5$. The total duration of the experiments is 120 minutes and during the experiments, the temperatures inside the cavity at all locations are varied with the time. However, the temperature difference between the bottom heated surface

and bulk fluid was found to be constant about 30-40 minutes after the starting of the experiment (as shown in the bottom side inset of Figure 6.1). So, the experiments are treated as a quasi-steady, the bulk fluid temperature in a quasi-steady state varies within ± 4.5% of the mean bulk temperature. The bottom plate mean temperature, $<T_b>$, and bulk fluid temperature at the centre of the cavity, $<T_0>$ are 26.8 and 25.1 °C for this *Ra*, respectively. The non-dimensional parameters such as *Ra*, *Pr* and *Nu* are calculated using the thermophysical properties of water at the average value of all the mean temperatures across the cubic cavity. The graph agrees with the previous observations of Kumar et al. (2016) and Choudhary et al. (2019) measured in the open cavity experimental setups.
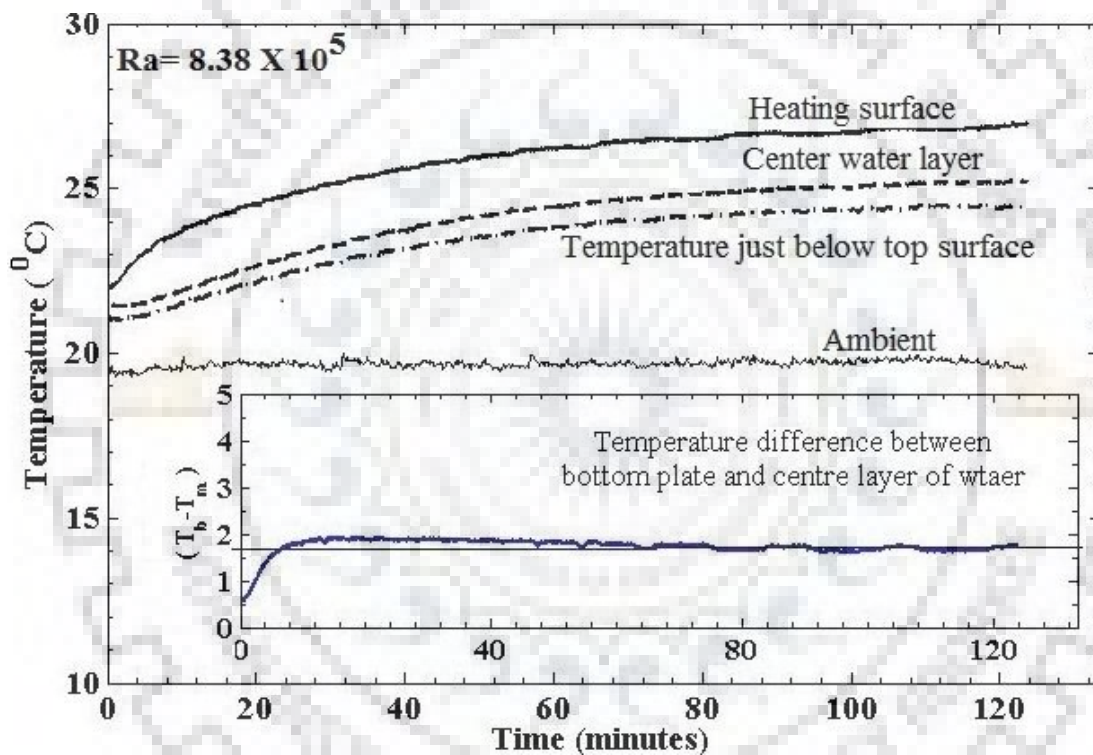
Figure 6. 1 The variation of temperature from the starting of the experiment for Ra = 8.38 ×10^5 at the bottom heating surface (continuous thick line), the centre of the cavity (dashed line), just below the open top surface (dashed line with dots) and the environment (continuous thin line). The inset shows the variation in the difference of temperatures of the bottom heated surface and bulk fluid at the centre of the cavity.

6.1.2 Thermal boundary layer

Figure 6.2 shows the temperature profile results at different locations across vertical heights from the heated bottom surface at different *Ra*. The mean temperature of steady-state data shows the boundary profiles at each *Ra*. The decrement in temperature profile is followed by a thin linear trend from bottom plate ($z=0$) to the thermal boundary layer

thickness ($z \leq \delta_{th}$), then a little transition and finally constant to bulk fluid temperature. The observations agree well with the experiment of R-B convection conducted by Lui & Xia (1998), Wang & Xia (2003) and Zhou & Xia (2013) in turbulent convection at different Pr and Ra numbers. The thermal boundary layer thickness is the vertical distance measured from the bottom plate to the point where linear temperature profile encounters with the tangent of bulk fluid temperature (Zhou et al., 2011; Zhou & Xia, 2013; Vishnu et al., 2019). In the present experiment, the linear profile of temperature is estimated by the 3 to 7 points best fit and extrapolated up to the intersection point with bulk fluid constant temperature profile. The profile of the temperature near the bottom heated surface is linear for about 50-60% of the boundary layer thickness. The uncertainty associated with the estimation of thermal boundary layer thickness is ± 0.7 mm to ± 0.1 mm. For the present experiment, the dependence of the thermal boundary layer thickness (δ_{th}) on Ra is measured with the temperature profile at the centreline of the cubic cavity can be fitted to a power-law which is, $\delta_{th}= 703\ Ra^{(-1/3)}$ (mm) with 5 % standard deviation of data. For the cubic cavity of Choudhary (2015, 2019) and Kumar et al. (2016) the δ_{th} power law can be fitted to $\delta_{th}= 615\ Ra^{(-1/3)}$ (mm) and $\delta_{th}= 1540\ Ra^{(-1/3)}$ (mm) with 15 % and 17 % standard deviation from the experimental data, respectively. Figure 6.3 plots the Ra and normalized boundary layer thickness (normalized by cavity height H). The height is used here to normalize thermal boundary layer thickness because the geometrical confinement of the fluid might be affecting the nature of the convection. The symbols represent the measured experimental values and the different lines represent the developed correlations based on the experimental data. The correlations for the boundary layer thickness for different cavities are given as

$$\frac{\delta_{th}}{H} = \ 23.44\ Ra^{-1/3} \tag{6.1}$$

$$\frac{\delta_{th}}{H} = 5.31\ Ra^{-1/3} \tag{6.2}$$

$$\frac{\delta_{th}}{H} = 6.41\ Ra^{-1/3} \tag{6.3}$$

Equation (6.1), is based on the present experiment and equations (6.2 & 6.3) are based on the experimental data of Choudhary (2015, 2019) & Kumar et al. (2016), respectively. It is measured that the standard deviation of equations (6.1, 6.2 & 6.3) is 5.8, 18 and 16%, respectively. The inset of Figure 6.3 shows the compensated plot for

the $\delta_{th}/H \propto Ra^{-1/3}$, showing the similar exponent obtained by Zhou & Xia (2013) in R-B convection. The compensated plots for different dimension cavities are drifted apart, one of the possible explanations for this deviation is the boundary condition at the free surface of the cavities. The rate of heat loss to the environment from the open cavities is highly dependent upon the boundary conditions at the top open surface. And the other may be the geometrical confinement of the fluid.
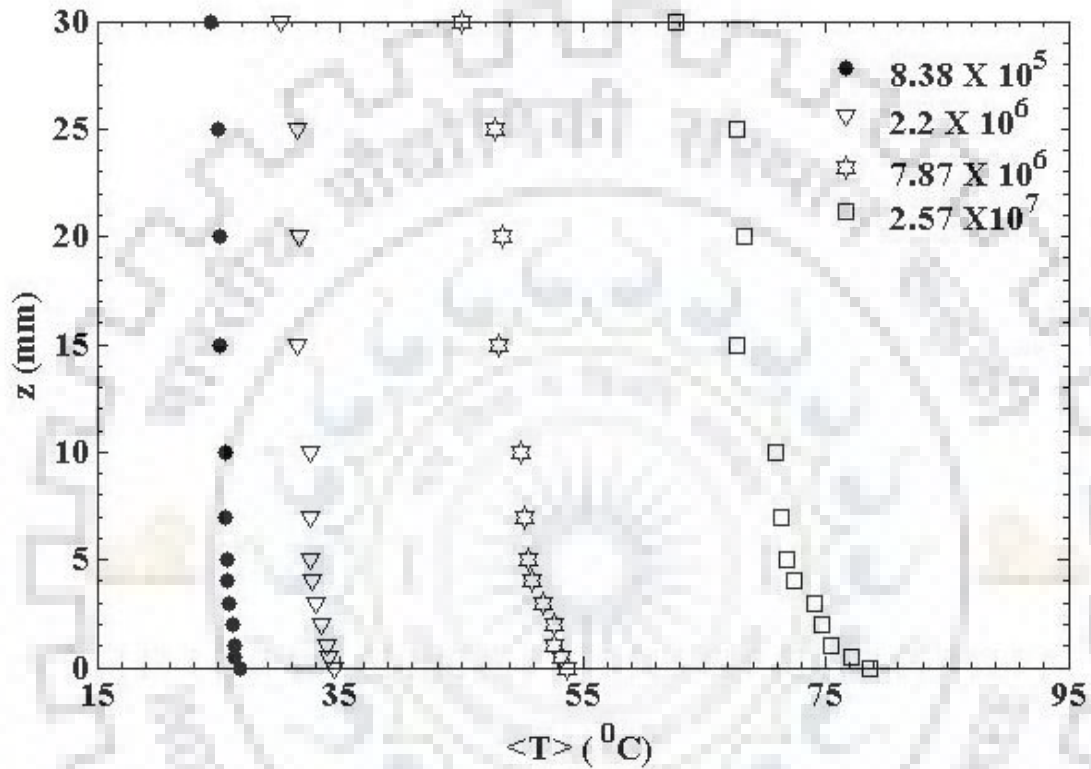
Figure 6. 2 Mean temperature profile measured across vertical distances from the heated bottom surface at different Ra.

6.1.3 Temperature fluctuations

In Figure 6.4, the temperature time series for about 500 seconds after steady state at different distances from the heated bottom surface across height have been shown for $Ra = 7.86 \times 10^6$. The thermal boundary layer thickness δ_{th} for this Ra is 3.48 ± 0.09 mm. Figure 5 shows the local temperature fluctuation at (1) the bottom heated surface of the cavity, $z/\delta_{th}=0$, (2) inside the thermal boundary layer, $z/\delta_{th}= 0.57$, (3) at the edge of the thermal boundary layer, $z/\delta_{th}=0.87$, (4) outside the thermal boundary layer, $z/\delta_{th}=1.15$, (5) far away from the thermal boundary layer, $z/\delta_{th}=2.87$, (6) at the center and very far away from the thermal boundary layer, $z/\delta_{th}= 4.31$ & 5.74 and (7) at the top layer of water in the cavity which is open to ambient, $z/\delta_{th}=8.62$. The temperature

at the bottom heated surface (z=0) is almost constant for the entire time interval, however moving away from the heated surface, the fluctuations in the temperatures are increased, and it shows maximum fluctuations near to boundary layer thickness. These temperature bursts near the edge of the thermal boundary layer thickness specify the presence of thermal plumes as reported and explained in the R-B convection by Zhou & Xia (2002), Xi et al. (2009) and Zhou & Xia (2013). The temperature fluctuations are reduced a lot at the center of the cavity as there is a decrease in the thermal plumes with the height, z. These fluctuations in temperature after the δ_{th} start decreasing as thermal plumes start mixing, merging and clustering in this region, called mixing zone (Castaing et al. 1989; Zhou et al. 2007). The thermal boundary layer thickness δ_{th} value is calculated by the distance from the bottom surface to the point at which the linear part of temperature profile intersects with the constant bulk fluid temperature.
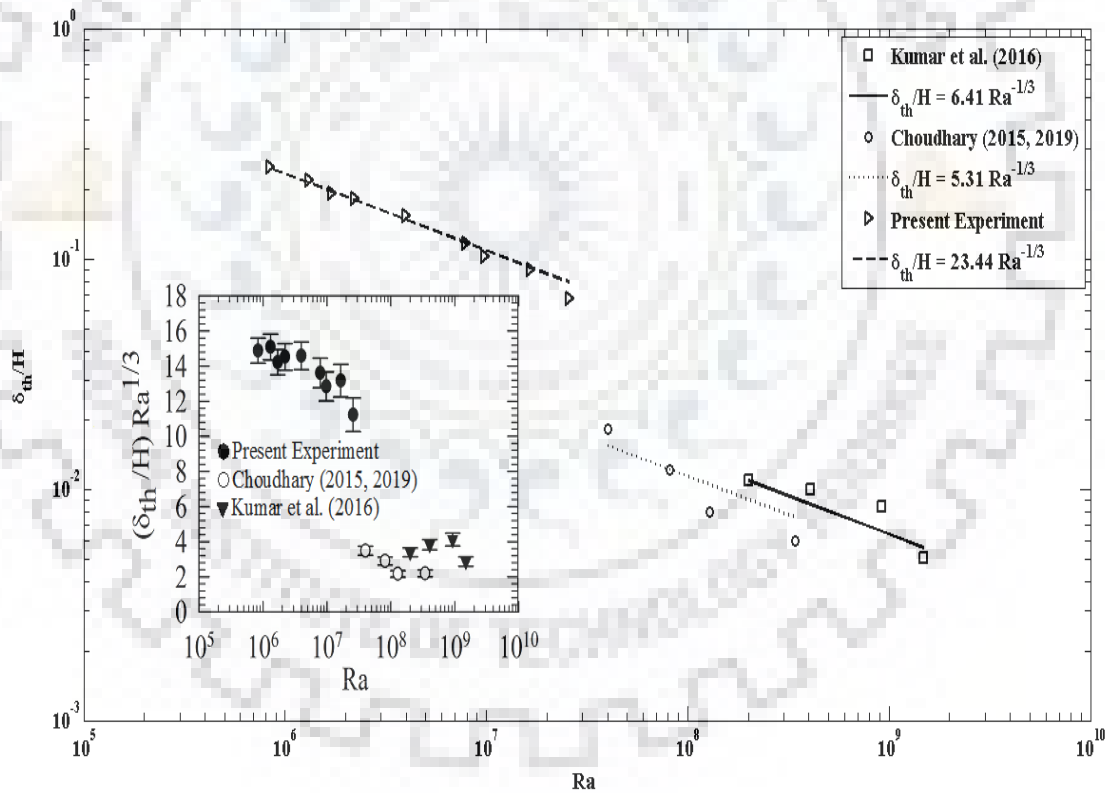
Figure 6. 3 Thermal boundary layer thickness normalized by cavity height H, δ_{th}/H as a function of Ra, the different kinds of lines show the δ_{th}/H dependence. The inset is the compensated plot represents $\delta_{th}/H\ Ra^{1/3}$.
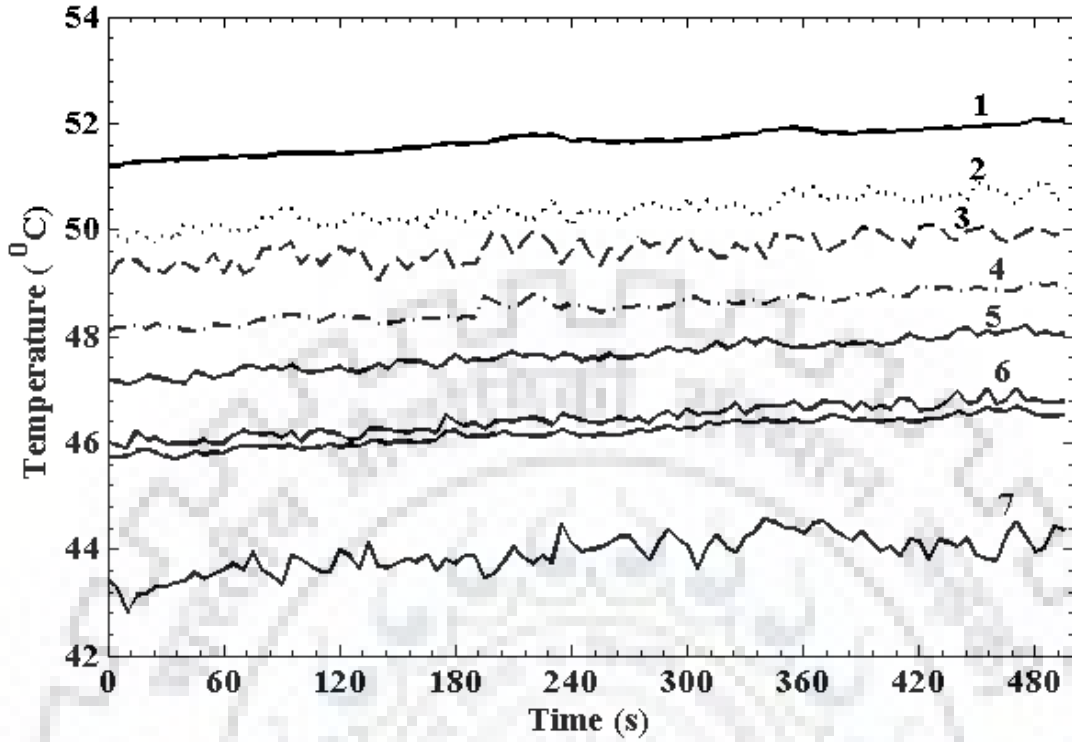
Figure 6. 4: Temperature time series measured at Ra = 7.86 × 10⁶ along the centreline at different locations, (1) z/δth=0, (2) z/δth= 0.57, (3) z/δth=0.87, (4) z/δth=1.15, (5) z/δth=2.87, (6) z/δth= 4.31 & 5.74 and (7) z/δth=8.62.

Figure 6.5 shows the detail about the normalized mean temperature distribution for different Ra plotted as a function of z normalized by δ_{th}. The temperature profile is normalized by the ΔT, so the profiles of normalized temperature at various Ra show values 0 and 1 at the bottom heated surface and center of the cavity, respectively. The profiles of the normalized temperature show a linear trend up to the boundary layer ($z/\delta_{th}=1$, shows by the dotted line in Figure 6.5) and shows nearly constant values at the center of the cavity. The normalized temperature shows more than one value at the open surface because the temperature at the open surface decreases. The graph confirms the linear deterioration of the temperature near the bottom heated surface and finally ends up constant at the very far away from δ_{th} at the center of the cavity. The graph of the normalized temperature confirms the existence of different regions in the turbulent convection. The first region is following the linear decrement of the temperature when moving across the height from the bottom heated surface, the second one is after the thermal boundary layer, as mentioned above, the mixing zone and the third one is the

constant temperature region. Apart from these different regions, one can observe another region at the top end of open cavity experiments, where temperature fluctuation is far more than any other region because the energy from the cavity is leaving into the environment. Near the heated surface, the no-slip condition prevails and the velocity became zero, the heat transfer is by conduction only, at the centre of the cavity convection mode of heat transfer prevailed as the temperature gradient became almost zero. The change in the profile near or at the edge of the boundary layer thickness may indicate the presence of rapid mixing, and this zone is also called a transitional zone (Belmonte et al., 1993, 1994; Lui & Xia, 1998; Vouros & Panidis, 2012). The increment in Ra leads to the less steep in the shape of the normalized temperature profile because the values of δ_{th} is decreasing with Ra. The trend of the graphs agrees well with Vouros & Panidis (2012).

In Figure 6.6, the probability density function (*pdf*) of temperature difference from the mean temperature at the cavity centre *((T- <T>)/ ΔT)* for the different Ra is plotted. This basic simple statistics technique shows how drastically the fluctuations in temperature are changed with different Ra at the centre of the cavity. The *pdf* for the temperature fluctuations at the centre is following nearly Gaussian behaviour, shown in the inset (a-d) of Figure 6.6. In the inset Figure 6.6 (a-d), the log of *pdf* is plotted against the temperature fluctuations, (a, b) for the current experiment, and (c, d) for Choudhary (2015). Figure 6.6 (e) shows the log of pdf versus temperature fluctuations at different heights across the centreline of the cubic cavity at $Ra = 2.57 \times 10^7$ for the current experiment. The data points at the centre of the cavity are less scattered as compared to the near boundary layer. At these moderate Rayleigh numbers of the turbulent convection regime, the shape of the temperature fluctuations shows symmetric and nearly Gaussian-shaped at the centre of the open cavity. Figure 6.6 shows that the width of the measured *pdf* profile at the cavity centre changes with Ra. In the present experiment, the width of *pdf* profiles becomes constant after the $Ra = 1.31 \times 10^6$ and folded to a single systematic Gaussian-shaped curve. Similar results are obtained for the Choudhary (2015) data for moderate Ra, and at higher $Ra = 1.48 \times 10^9$, the shape of the *pdf* is contracted to the exponential shape, indicating that the transition to higher-order turbulence at higher Ra. A similar kind of shape for the *pdf* is obtained in the R- B convection by Wang et al. (2019).
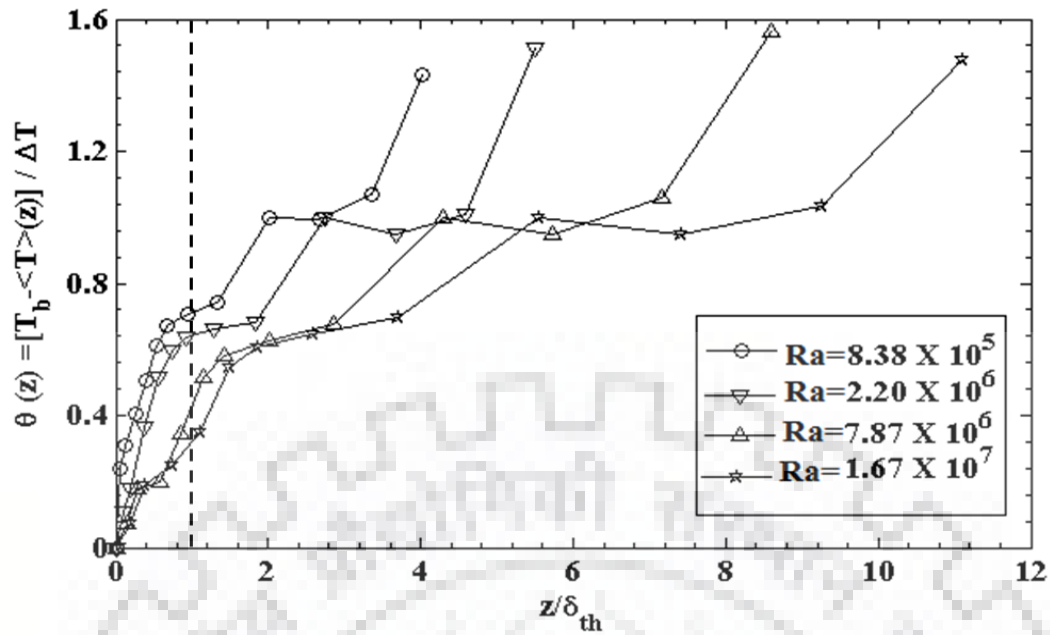
Figure 6. 5 The normalized difference between the temperature of bottom heated plate (T_b) and mean temperature ($<T>$ (z)) across the centreline of the cavity as a function of distance from the bottom heated surface normalized by boundary layer thickness at different Rayleigh numbers, as indicated.
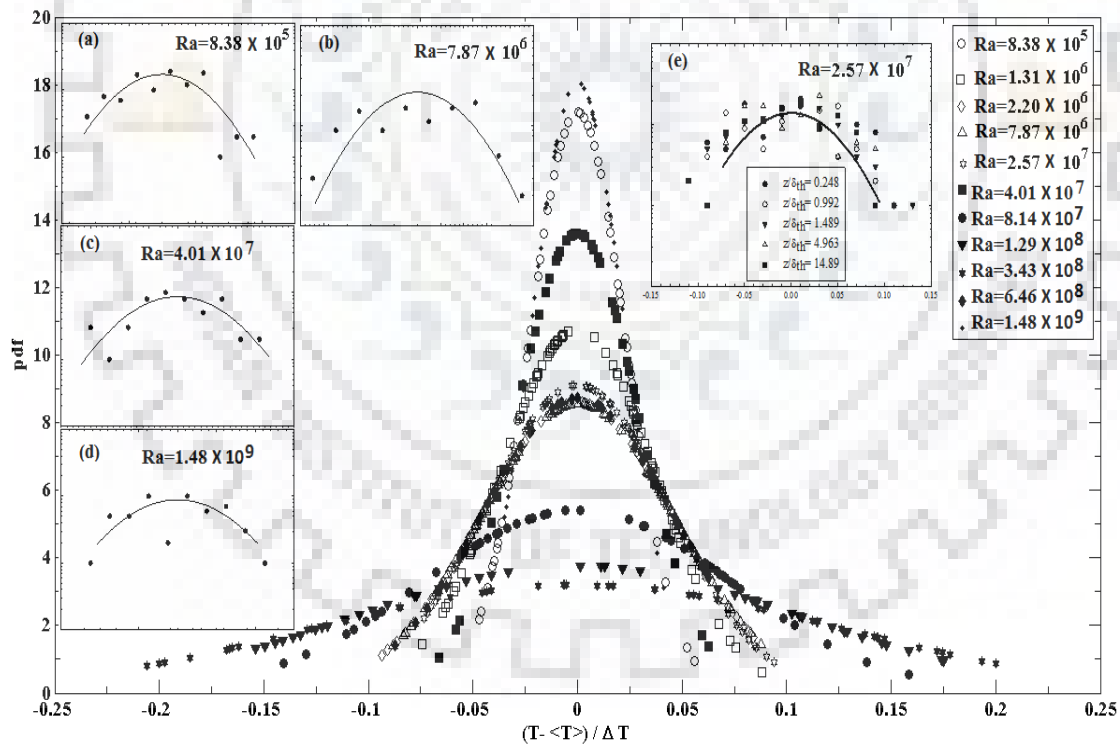
Figure 6. 6 The probability density function (pdf) of the temperature fluctuation at the center of the cavity along the centreline at different Rayleigh numbers (filled symbols are from Choudhary (2015)). The inset, (a, b) log of pdf plotted against the temperature fluctuations for current experiments, (c, d) log of pdf for temperature fluctuations in Choudhary (2015), similarly, (e) the log of pdf at different vertical positions across the centreline at Ra = 2.57 × 10^{7} for the current experiment. The solid line in the insets shows the Gaussian shape.

In the Figure 6.7 (a), r.m.s temperature fluctuations (σ_T) at the center of the cavity normalized by the ΔT is plotted against the Ra. The results for the r.m.s fluctuations are found similar to those observed by Sano et al. (1989) in R-B convection. The r.m.s temperature fluctuation $\sigma_T/\Delta T$ increase in Rayleigh number range $8.38 \times 10^5 \leq Ra \leq 2.2 \times 10^6$. In this regime the fluid is circulating from bottom to top, the hot fluid is going up and the cold fluid is going down as observed by the Chu & Goldstein (1973) in R-B thermal convection for water. The hot thermals (mass of fluid-driven by buoyancy) after bursting out from the boundary layer travel vertically through the bulk fluid reached the top and referred as stable blobs. The large-scale circulation of the fluid causes the adverse pressure gradient, which then creates instability in the thermal boundary layer at the bottom of the cavity (Sano et al., 1989). As the Rayleigh number increases more than $Ra > 2.2 \times 10^6$ the thermal boundary layer nucleates the hot thermals and the presence of stable blobs observed rarely at the surface (Chu & Goldstein 1973), these hot thermals are the main source of temperature fluctuations. After $Ra = 2.2 \times 10^6$, the r.m.s temperature fluctuation shows, $\sigma_T/\Delta T \sim Ra^{-0.17 \pm 0.05}$ as shown by solid line in Figure 8(a) with a standard deviation of 24%. Sun & Xia (2007) and Shang et al. (2008) reported the power law as, $\sigma_T/\Delta T \sim Ra^{-0.14 \pm 0.02}$ and $\sigma_T/\Delta T \sim Ra^{-0.14 \pm 0.03}$, respectively, at the centre of the cavity. Grossmann & Lohse (2004) theoretically predicted the exponent value is varied in the range -0.11 to -0.09, near the heat conducting plate in the cavity where plume dominated fluctuation is dominated for all the Pr. Figure 6.7 (b) shows the r.m.s temperature fluctuations at the $Ra = = 2.57 \times 10^7$ and it shows the r.m.s value is linearly increasing in the boundary layer region and above the boundary layer it is showing some fluctuations and then become the constant at far away from the boundary layer.

The power spectral density (PSD) of temperature fluctuation $((T - <T>)/ \Delta T)$ is demonstrated for the higher $Ra = 2.57 \times 10^7$ at a different height (z) from the heated bottom surface in Figure 6.8. In the plot of PSD, the low and high frequency shows the region of larger and smaller-scale motions, respectively. The straight line region indicates the developed power-law among the flat low frequency and sharp drop at high frequencies (Wu et al. 1990). The centre region in the cavity is the place of homogenous motion and shows the characteristic of the free convection. The PSD shows an increment in the power-law exponent from bottom to boundary layer thickness and attains a maximum value of 2.28 $\pm$0.05 at the mixing zone at $z/\delta_{th} = 1.48$. This maximum

value of the exponent indicates that the energy transformation from a larger to a smaller scale is maximum near the boundary layer thickness in the mixing zone. At the centre layer of the cavity, the energy transformation barely fluctuates and keeps at a constant power-law exponent. This region of constant exponent characterizes the motion in free convection. The power-law exponent shows a value of 1.478 ±0.03, consistent with 7/5 predicted by Bolgiano (1959) and Obukhov (1959). The same vale 7/5 also reported by Wu et al. (1990) and Niemela et al. (2000) in the R-B convection experiment for different *Ra* with the helium gas as a fluid. At the top cold layer, the efficiency of energy transformation reduces as approaching the top cold layer, the power-law exponent shows a minimum value at the top (Zhang et al. 2016).
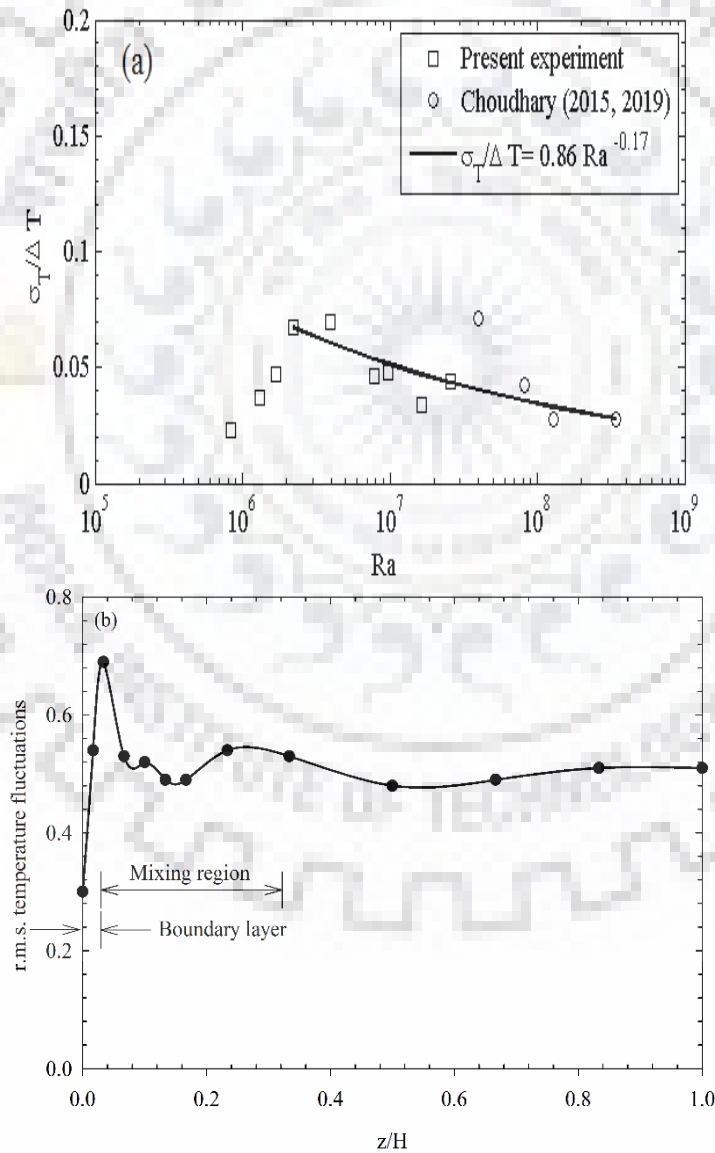
Figure 6. 7 (a) The r.m.s (σ_T) values normalized by the temperature difference at center of cavity is plotted against the Rayleigh number. (b) r.m.s temperature fluctuations across the centreline of the open cavity at Ra = 2.57 × 10⁷.
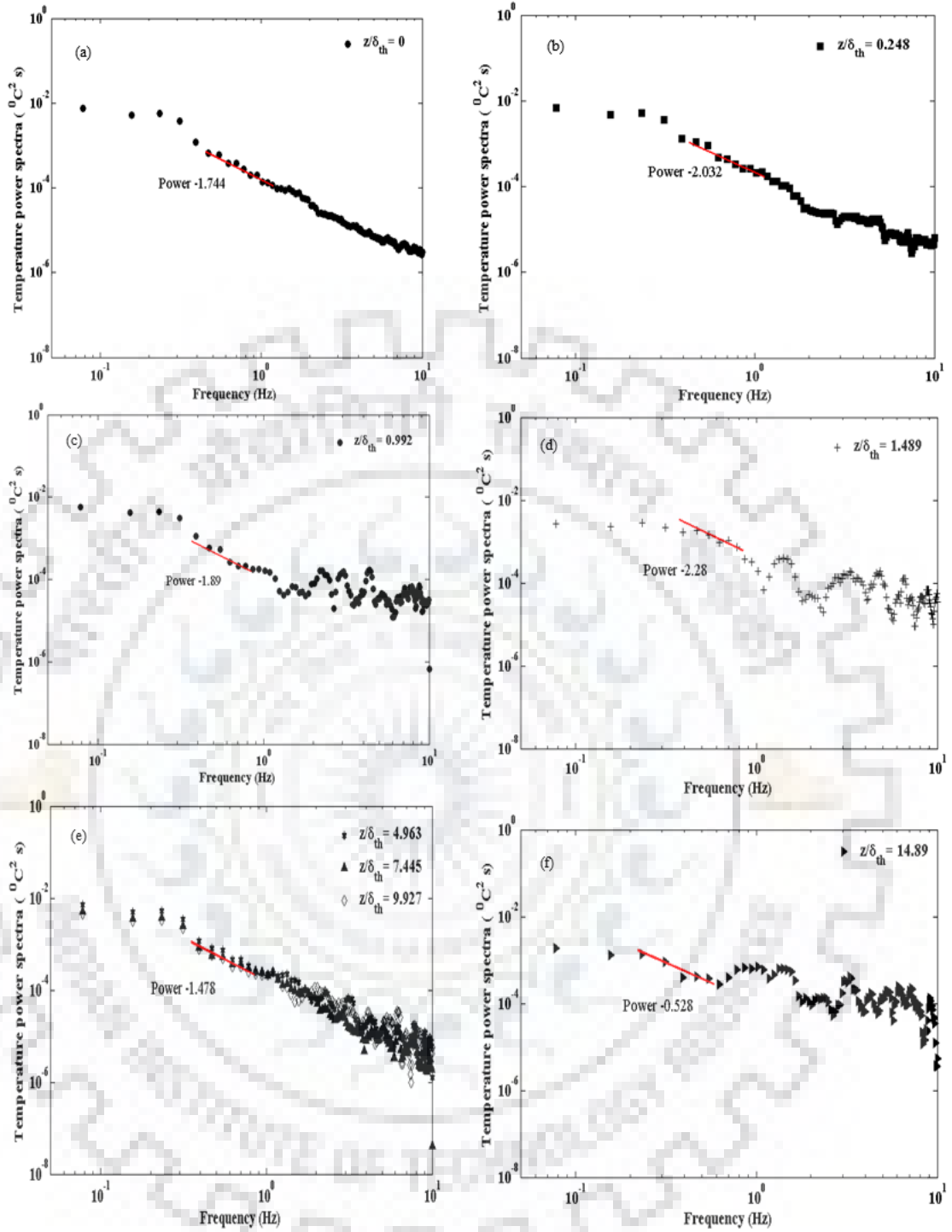
Figure 6. 8 The distribution of the power spectrum of temperature fluctuations at different positions along the centreline of the cavity for Rayleigh Number, Ra= 2.57 × 10⁷. (a) z/δ_th= 0, Power law: 1.744±0.03, (b) z/δ_th= 0.248, Power law: 2.032±0.05 (c) z/δ_th= 0.992, Power law: 1.89±0.05 (d) z/δ_th=1.489, Power law: 2.28±0.06 (e) z/δ_th= 4.963,7.445,9.927, Power law: 1.478±0.03 (f) z/δ_th= 14.89, Power law: 0.528±0.07

6.1.4 Heat transfer and *Ra* dependence on *Nu*

The Prandtl number for the present experiment is varied from 4 to 6 (as shown by the filled square in Figure 6.9) over the range of *Ra*. The non-Boussinesq effects are neglected here as the empirical criteria for the validity of Oberbeck-Boussinesq approximation, the product of $\beta \Delta T < 0.2$, (Niemela & Sreenivasan 2003) is fulfilled (for the present experiment shown by filled circles in Figure 6.9) for all the experimental data. Figure 6.10 shows the proportions of conductive $(-k\,\partial T/\partial Z)$ and convective heat transfer for the minimum and maximum *Ra* measured from the experimental data along the centreline of the cavity with the combined uncertainty of $\pm$ 2 %. Near the bottom heated surface, the conduction heat transfer dominates over the convection heat transfer and for z/H > 0.2, almost all the heat is transported by the convection mode. Figure 6.11 shows the variation in *Nu* with the function of *Ra,* the figure is plotted as the $Nu \times Ra$ versus *Ra* to exclude the temperature difference between the bottom surface and water layer. The developed correlations based on the present experimental data given as

$$Nu = 0.138\,Ra^{0.30} \tag{6.4}$$

$$Nu = 0.033Ra^{0.384}\,Pr^{0.066} \tag{6.5}$$

Equation (6.4) is the power-law correlation developed between *Nu* and *Ra* with a standard deviation of about 10 %. On the other hand, when *Pr* is considered here, the correlation for *Nu* is presented in equation (6.5) with a standard deviation of 5.9 %. The behaviour of *Nu* appears to be strongly dependent on *Pr* at the low *Ra* in the turbulent convection. The scaling of the above equations is showing similar trends obtained by Di Federico & Foraboschi (1966) in an open tank heated from below at $Ra > 2.2 \times 10^4$ and by Zhou & Xia (2013) in R-B convection inside a water-filled rectangular cell. However, Niemela et al. (2000) reported the value of scaling of *Ra,* 0.3089 ±0.0043 and ruled out the 1/3 value in R-B convection for $10^6 \le Ra \le 10^{17}$. Figure 6.11 shows the different trend follows by the correlations developed by the data of different cavities as explained in the previous studies (Choudhary, 2015, 2019; Kumar et al., 2016) and these correlations and the experimental data are compared with the correlations of Di Federico & Foraboschi (1966) & Theerthan & Arakeri (2000) according to the range of *Ra* as summarized in Table 1. The product of *Nu* and *Ra* (in Figure 6.11) is noted

relatively lower compared to other authors. This may be partly because of the geometrical confinement of the cavities; the other possible reason may be the effect of different boundary conditions at the open end of the cavities. The compensated plot (Figure 6.11: inset) for Nu with the scaling $Ra^{-0.30}$ quantifies the dependence of Nu on the ambient conditions. Furthermore, the coefficients for the different $Nu \sim Ra^{0.30}$ equations of these experimental studies are interestingly divergent so much because these cavities used in the different experiments have been subjected to different ambient conditions. Consequently, the rate of heat losses from each cavity's top is varied according to the ambient conditions fixed for each experiment. We have also calculated the Nusselt number based on thermal boundary layer thickness Nu_{th}, which is defined as, $Nu_{th} = 0.5H/\delta_{th}$ (Belmonte et al. 1994), plotted in Figure 6.11 with the red filled markers. It is seen clearly from the figure that the Nu_{th} values are departed from the actual experimental data. As the temperature is constant after the boundary layer thickness for all the open cavities except close to the open surface. This means that the height H of the cavities does not play a significant role in calculating Nu_{th}. So, as suggested by Grossmann & Lohse (2003) that the relevant length scale for the plate should be the width of plate l, which is equal to $l = \sqrt{2} H$ for the cubic cavity. Based on the value of l, the Nu_{th} is plotted and shown by the filled blue colour markers in Figure 6.11. It seems the new Nu_{th} is agreed with the experimental data for all cavities. Theerthan & Arakeri (2000) adopted another approach to distinguish the heat flux, which based on the $\left(Ra_{\delta_{th}}\right)^{-1/3}$ in place of Nu. $Ra_{\delta_{th}}$ is the Rayleigh number based on thermal boundary layer thickness δ_{th} and the temperature difference across the thermal boundary layer (г). The heat flux defined as

$$q = k\,\text{г}\,\left(\frac{g\,\beta\,\text{г}}{\nu\,\alpha}\right)^{1/3}\left(Ra_{\delta_{th}}\right)^{-1/3} \tag{6.6}$$

The main advantage of the non-dimensional parameter $\left(Ra_{\delta_{th}}\right)^{-1/3}$ is that it does not contain the length scale. So the heat transfer rate does not vary much for a given temperature difference and given fluid in turbulent free convection. The Nu and the $\left(Ra_{\delta_{th}}\right)^{-1/3}$ are mathematically can be written as in equation (6.7) and given as

$$Nu = \left(Ra_{\delta_{th}}\right)^{-1/3}Ra^{1/3} \tag{6.7}$$

Figure 6.12 shows the variations in the values of $\left(Ra_{\delta_{th}}\right)^{-1/3}$ in the range of 0.04 - 0.3 for present experiments and for previous experiments (Choudhary, 2015; Kumar et al., 2016) which almost similar to the range 0.1-0.3 reported by Theerthan & Arakeri (2000). The solid line in Figure 6.12 shows the $Nu \propto Ra^{1/3}$ for all the experimental data (including Choudhary, 2015, 2019; Kumar et al., 2016), as the Ra is increasing the value of the $\left(Ra_{\delta_{th}}\right)^{-1/3}$ is also increasing. Moreover, the values of $\left(Ra_{\delta_{th}}\right)^{-1/3}$ for the present experimental data is less comparatively, the possible reason for this occurrence may be in the present experiment the ambient conditions (as explained in the experimental section) are allowed more heat losses from the top of the open cavity, compared to our previous studies.
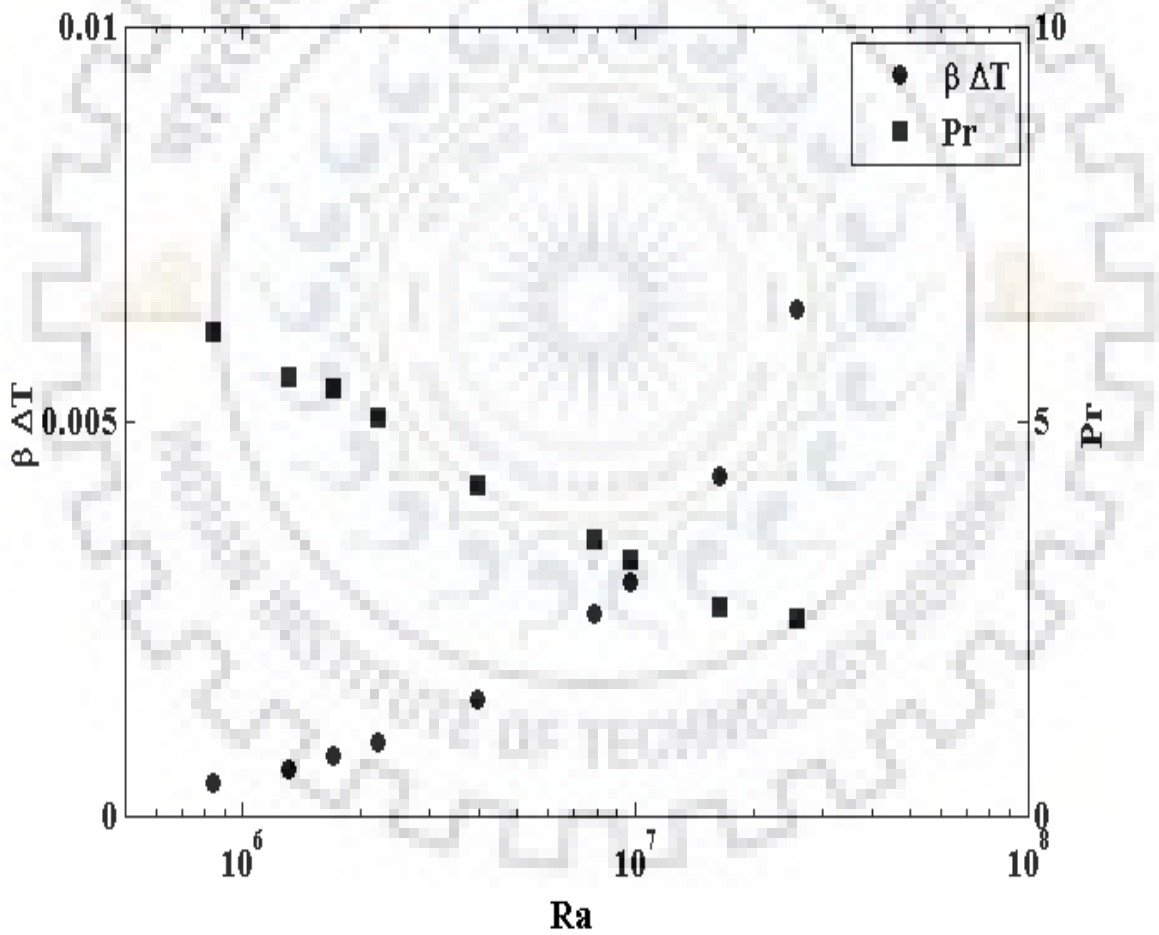
Figure 6. 9 The filled circle is $\beta\Delta T$, a parameter measure of the non- Boussinesq effect considered to be less than 0.2. The filled square shows the variation of the Prandtl number over the range of Ra.
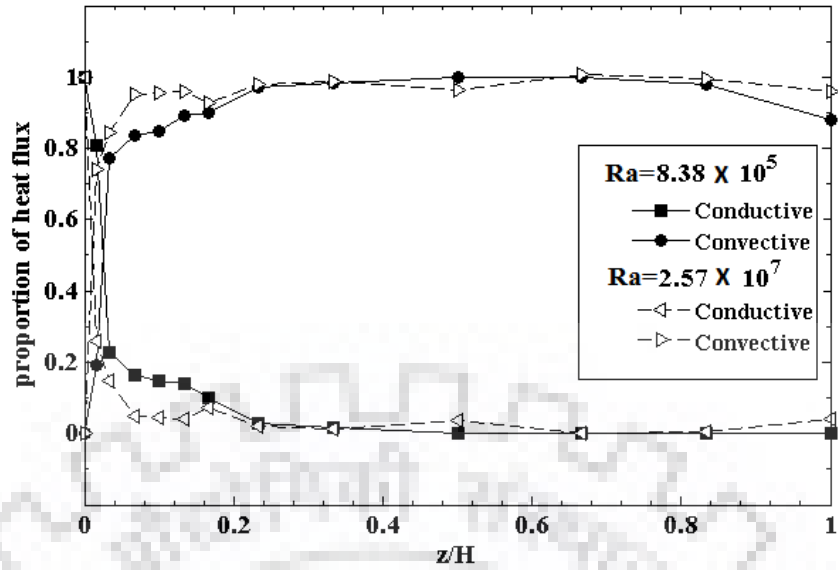
Figure 6. 10 The proportions of the conductive and convective heat transfer measured in the experiment from the temperature gradient with the total uncertainty of ±2%.
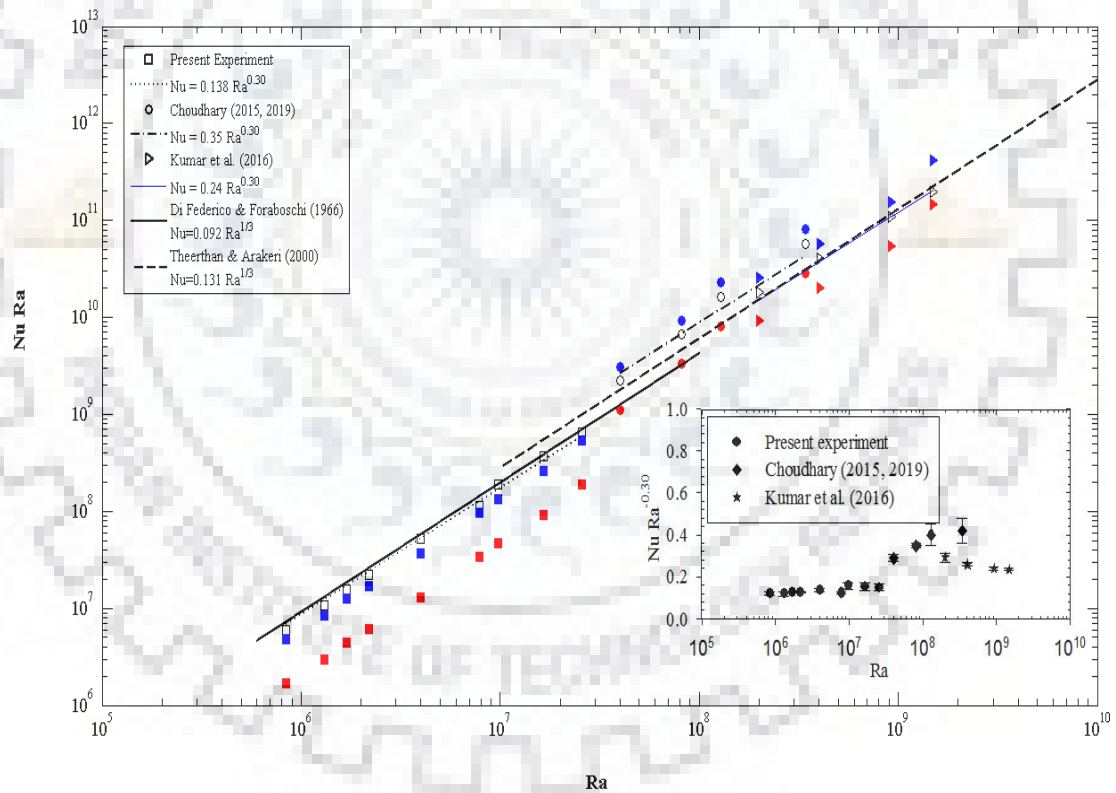
Figure 6. 11 Logarithmic plot of the product of Nusselt Number and Rayleigh Number versus Rayleigh Number, Square marker for present experiment, circle marker for Choudhary (2015, 2019) "reproduce with permission from Heat Mass Transfer 55, 2095–2102 (2019)" and triangle marker for Kumar et al. (2016) "reproduce with permission from Heat Mass Transfer 52, 245–253 (2016)". The open marker represents the experimental Nu data with the uncertainty of 2-4 %. The red colour filled marker represents the $Nu_{th}=0.5H/\delta_{th}$ and the blue colour filled marker shows $Nu_{th}= \sqrt{2} H/\delta_{th}$. Inset: compensated plot of Nu $Ra^{-0.30}$ for the same set of data.
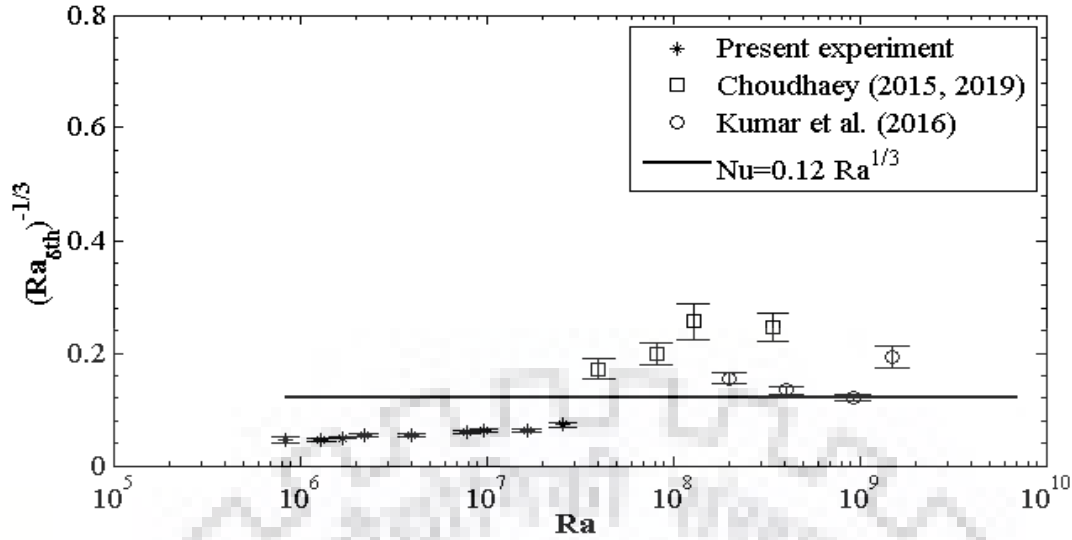
Figure 6. 12 Another parameter to represent heat transport, $\left(Ra_{\delta_{th}}\right)^{-1/3}$ versus Ra, the continuous solid line shows the Nu correlation.

6.2 Magnetic Nanofluids under the presence of horizontal magnetic field

6.2.1 Time series of Temperature

All the experiments are carried out with the Fe_3O_4-water magnetic nanofluids as a working fluid with and without the presence of magnetic field parallel to bottom surface. The values of the dynamic Bond number, B_d calculated for all the experiments are higher than 30 and the value of Crispation number, $Cr < 10^{-4}$, which means surface tension effects are negligible. The variation in the temperature at bottom heated surface and the bulk fluid is shown in Figure 6.13 for $Ra = 8.04 \times 10^5$ in Fe_3O_4-water magnetic nanofluids at $\phi = 0.01$ vol. %. Similar trend has been followed by the other Ra for other concentrations of the Fe_3O_4-water magnetic nanofluids. The duration of the experiment is about 120 minutes for all the experiments with the Fe_3O_4-water magnetic nanofluids. The inset of Figure 6.13 shows that the temperature difference for $Ra = 8.04 \times 10^5$ between the bottom heated surface and bulk fluid became constant after some time. Hence, the experiments are treated as in the quasi-steady after the temperature difference between bottom heated surface and bulk fluid became constant. Similar kind of trend are observed with the other concentrations of the Fe_3O_4-water magnetic nanofluids.
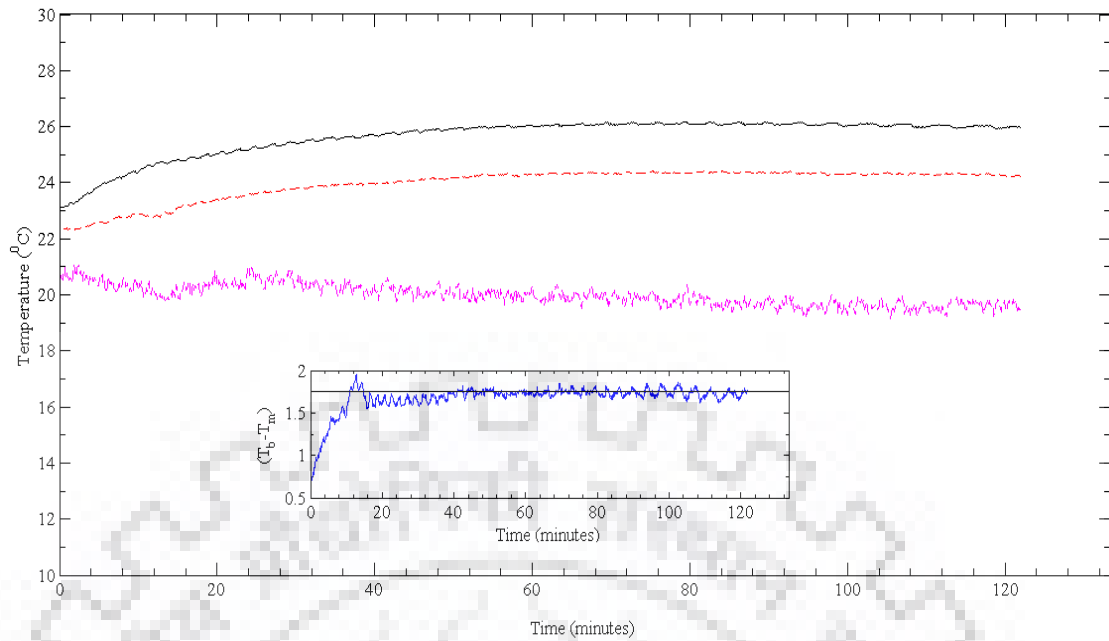
Figure 6. 13 Variation of temperature from the starting of the experiment for Ra = 8.04 × 10⁵, *Fe₃O₄-water magnetic nanofluids at* ϕ = 0.01 vol. %. *The inset: the difference between the temperature at the bottom heated surface and bulk fluid in the cavity.*

6.2.2 Oberbeck-Boussinesq approximation

The thermophysical properties are varied in the experiments for the different concentrations of the Fe_3O_4-water magnetic nanofluids. However, the change in the thermophysical properties due to temperature difference across the fluid is assumed negligible under the Oberbeck-Boussinesq approximation. In the Oberbeck-Boussinesq approximation, the change in the thermophysical properties such as thermal conductivity, viscosity, thermal expansion coefficient etc. of fluids are assumed to constant except the density. As mentioned earlier, for the validation of Oberbeck-Boussinesq approximation, the product of $\beta \Delta T < 0.2$, (Niemela & Sreenivasan 2003). Figure 6.14 shows that for all the volume concentrations and Ra the $\beta \Delta T < 0.2$.
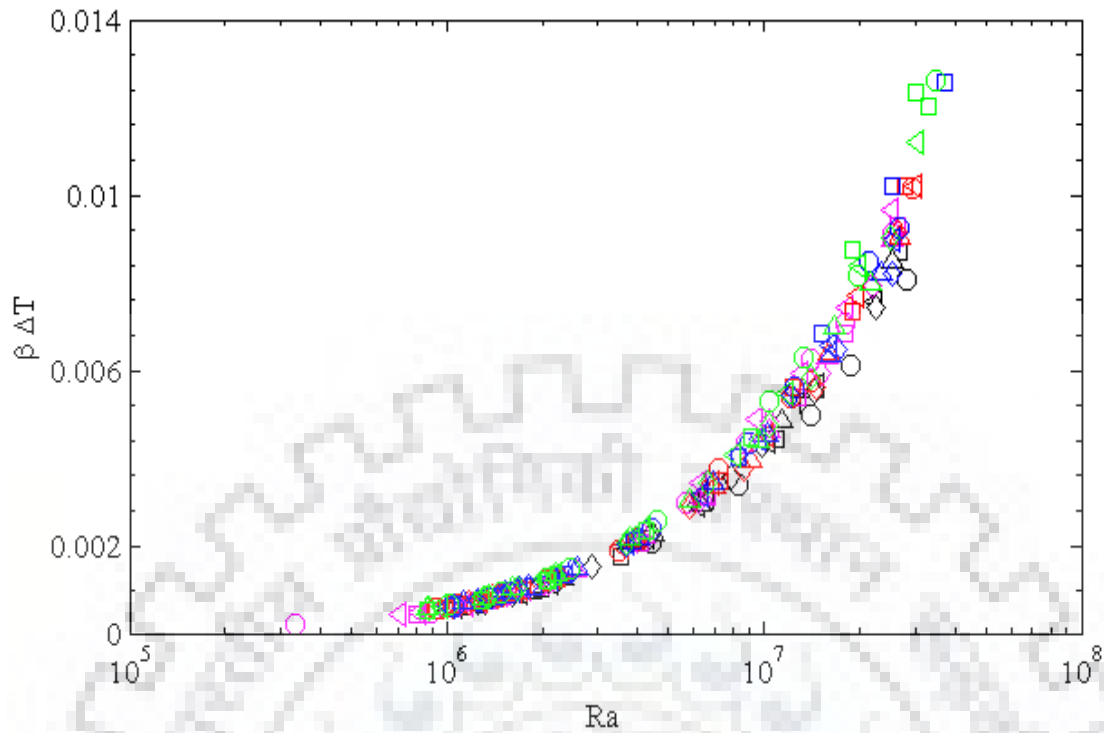
Figure 6. 14 Variation of $\beta\Delta T$ with the Ra *for all the concentration of Fe₃O₄-water magnetic nanofluids.*

6.2.3 Variations in Nusselt Number

The global heat transfer in the cavity is represented by the Nusselt number (*Nu*) at various Rayleigh number (*Ra*) is estimated by the formulas or equations mentioned in Chapter 4. The experimental results were plotted in the form of *Nu* and *Ra* for different concentrations of magnetic nanofluid and externally applied magnetic fields. In Figure 6.15, the *Nu* is plotted against the *Ra* for the concentration, $\phi = 0.01$ vol. % of Fe₃O₄-water magnetic nanofluid at the various externally applied magnetic field. The *Nu* is increased with the *Ra* for the concentration of the magnetic nanofluid. The Nu is decreased with the externally applied magnetic field.

To examine the enhancement or deterioration in the heat transfer compared to water by magnetic nanofluid is carried out by plotting the ratio of *Nu* of magnetic nanofluid to *Nu* of water with *Ra* in Figure 6.16. For all the *Ra* the values of *Nu* are less than 1, showing the deterioration in the heat transfer for the magnetic nanofluid at the $\phi = 0.01$ vol. % compared to water.
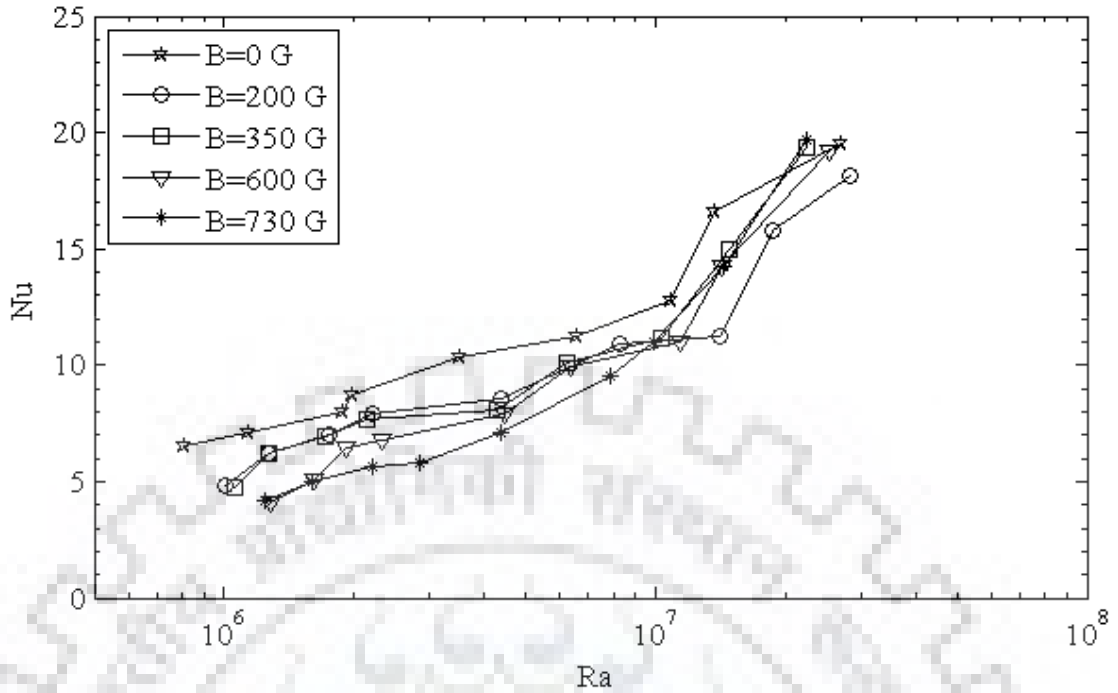
Figure 6. 15 A semi log plot of the experimental Nu versus Ra *for ϕ = 0.01 vol. %*
concentration of Fe_3O_4-water magnetic nanofluids at various magnetic fields.
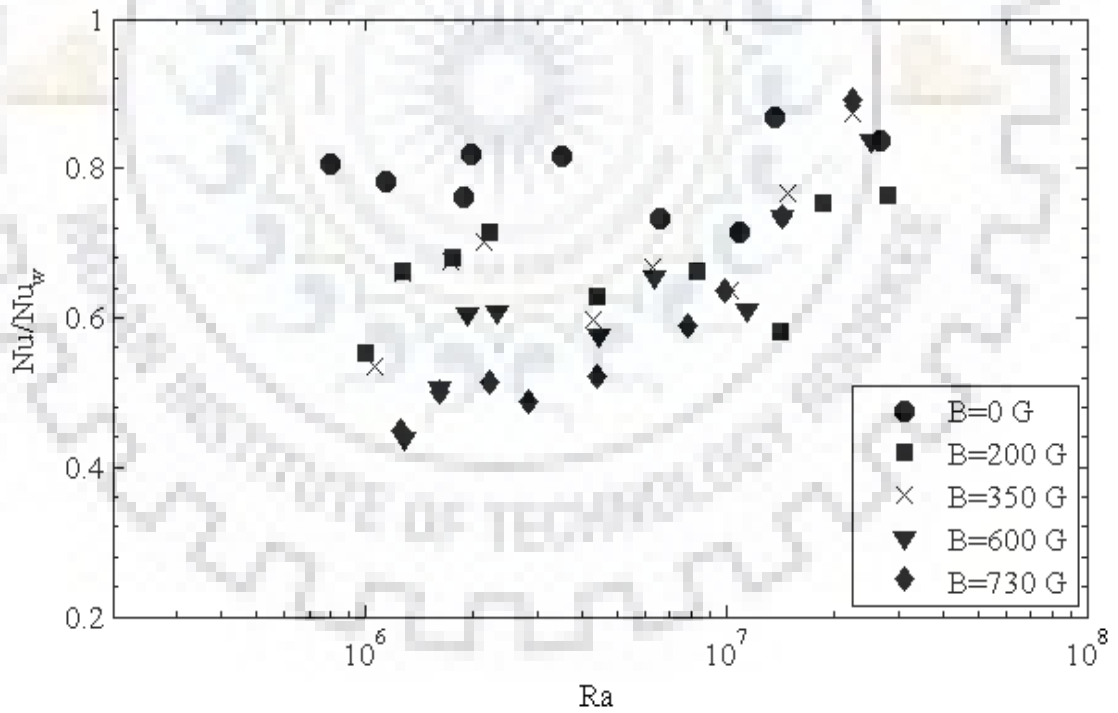
Figure 6. 16 A semi log plot between ratio of experimental Nu of magnetic nanofluids
at ϕ = 0.01 vol. % to the water and Ra.

In Figure 6.17, the *Nu* is plotted against the *Ra* for the concentration, $\phi = 0.03$ vol. % of Fe_3O_4-water magnetic nanofluid at the various externally applied magnetic field. The *Nu* is enhancing with the *Ra* but showing deterioration with the magnetic field. For comparison with water, the ratio of *Nu* to water is plotted in Figure 6.18. The values of the ratio of *Nu* magnetic nanofluid to *Nu* water lie below 1, which means the deterioration in the magnetic nanofluid. The deterioration is higher with the *Ra* and at a higher magnetic field.
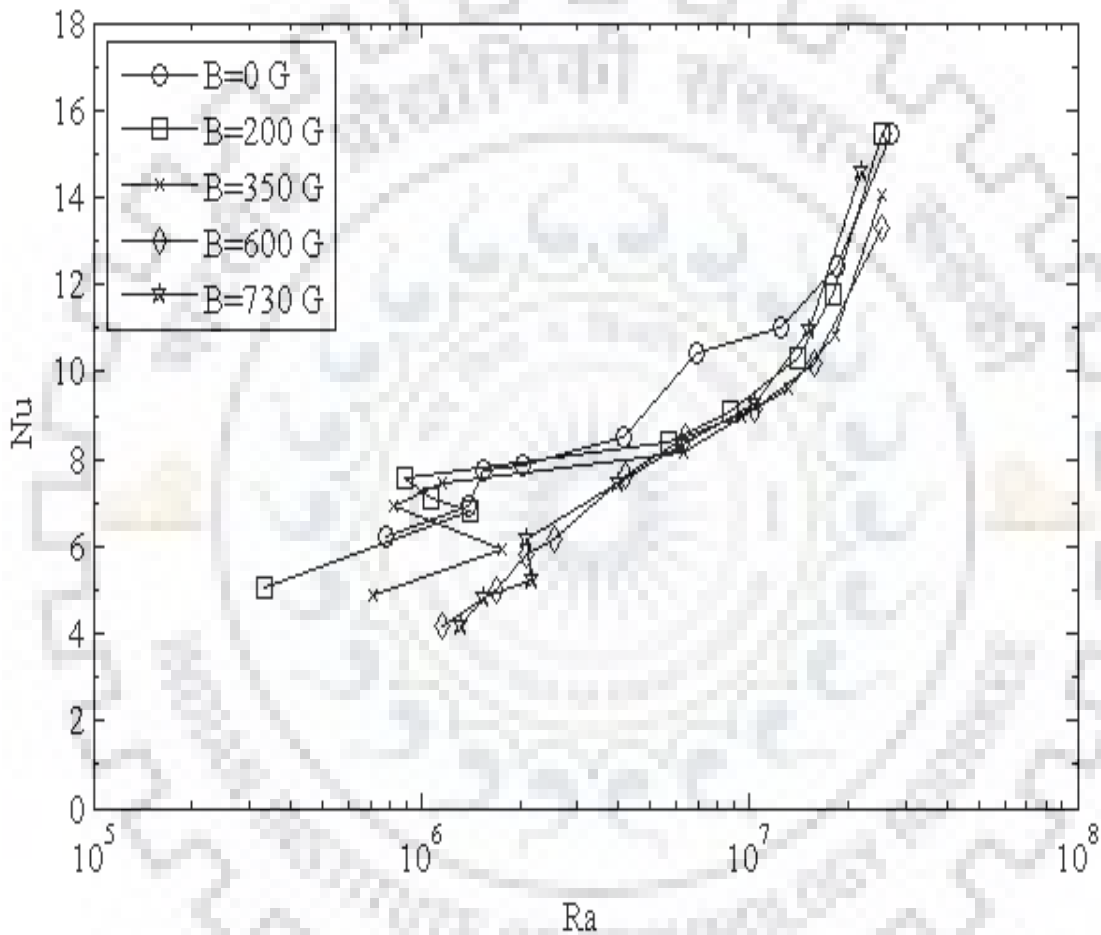
Figure 6. 17 A semi log plot of the experimental Nu versus Ra *for φ = 0.03 vol. %
concentration of Fe₃O₄-water magnetic nanofluids at various magnetic fields.*
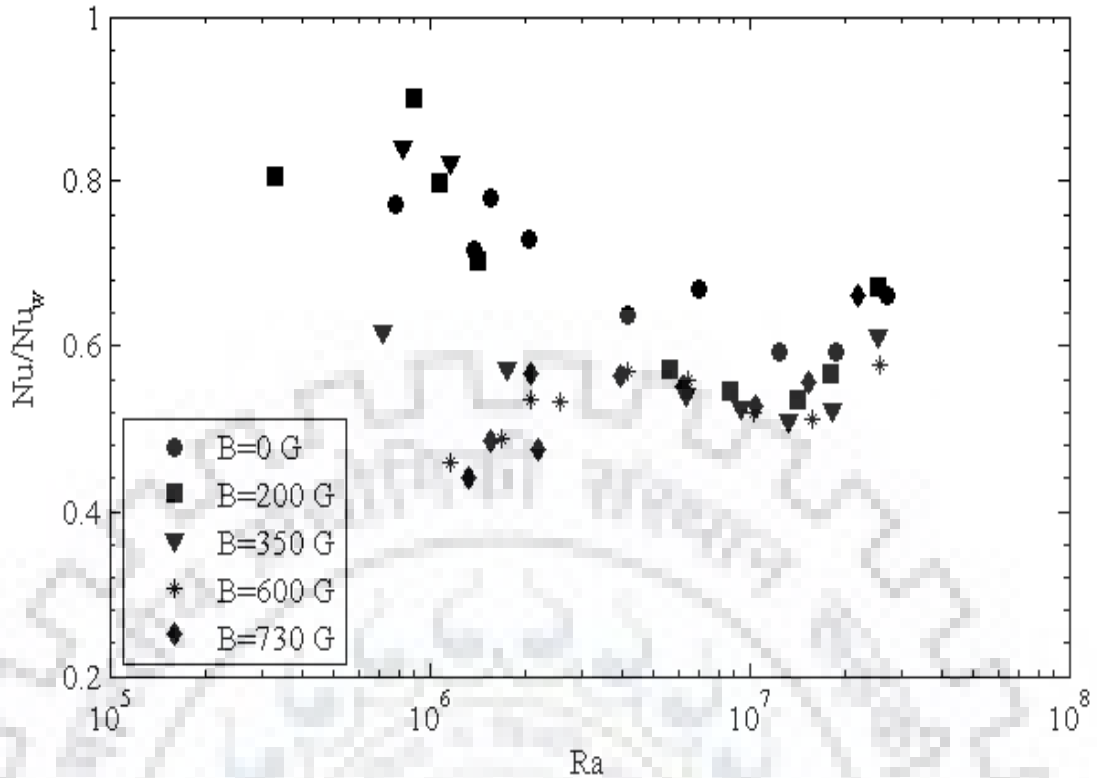
Figure 6. 18 A semi log plot between ratio of experimental Nu of magnetic nanofluid at ϕ = 0.03 vol. % to the water and Ra.

Similar kind of results has been observed with the higher concentrations of the nanoparticles in the Fe_3O_4-water magnetic nanofluid. For the concentration, ϕ = 0.05 vol. %, the results for *Nu* are shown in Figure 6.19 showing that the externally applied traverse magnetic field has less effect on the *Nu* values. However, in Figure 6.20, the *Nu* values are shown more deterioration compared to water. The one possible reason for the more reduction in the heat transfer values is the enhancement in viscosity of the magnetic nanofluids with nanoparticles concentrations. Figure 6.21 shows the values of *Nu* for the concentration, ϕ = 0.08 vol. %, and shows similar results and Figure 6.22 shows that at this higher concentration, the *Nu* values show more deterioration compared to the previous lesser concentration. Figure 6.23 shows the *Nu* versus *Ra* plot for the concentration, ϕ = 0.1 vol. %, the values of the *Nu* at the higher magnetic field is showing a significant enhancement comparatively. This leads to that the magnetic field might plays a role to enhance the heat transfer at the higher concentration of magnetic nanofluids. However, in Figure 6.24 it is observed that though there is an enhancement in the *Nu* values at the higher magnetic field but the *Nu* values are still less than water.

The nanoparticles have imposed a resistance to the convection currents, therefore the *Nu* is showing the deteriorating trend with the concentration. The externally applied magnetic field has less effect at the lower concentrations of the magnetic nanofluid but at higher concentrations, the *Nu* values are increasing with *Ra*. This may be the intensification of turbulence at a higher concentration with a high magnetic field.
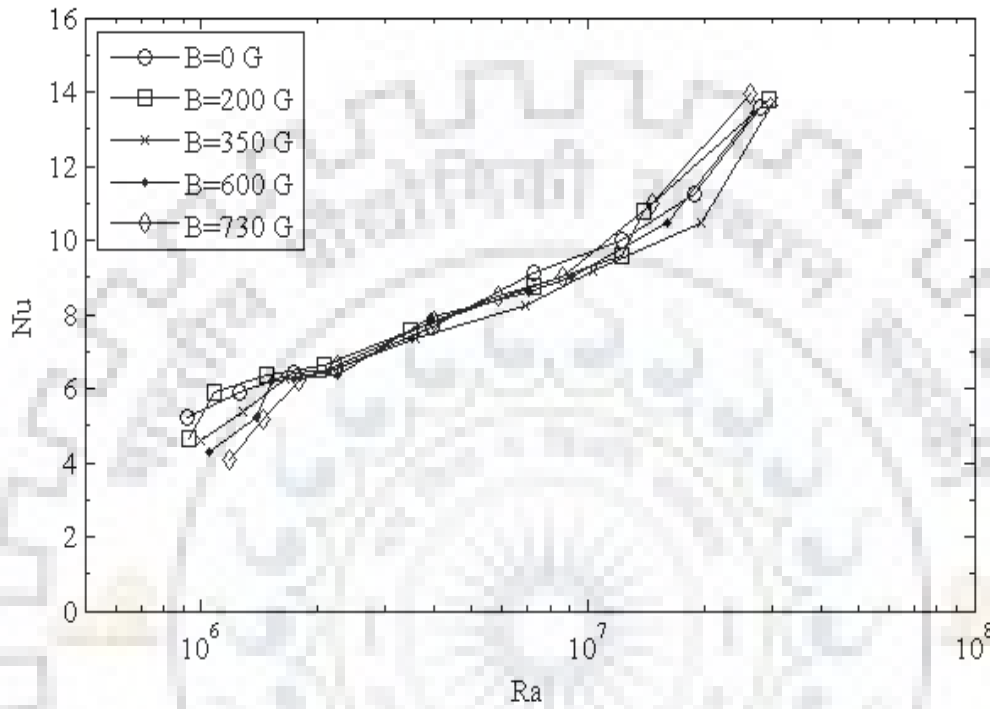
Figure 6. 19 A semi log plot of the experimental Nu versus Ra for $\phi = 0.05$ vol. % concentration of Fe$_3$O$_4$-water magnetic nanofluids at various magnetic fields.
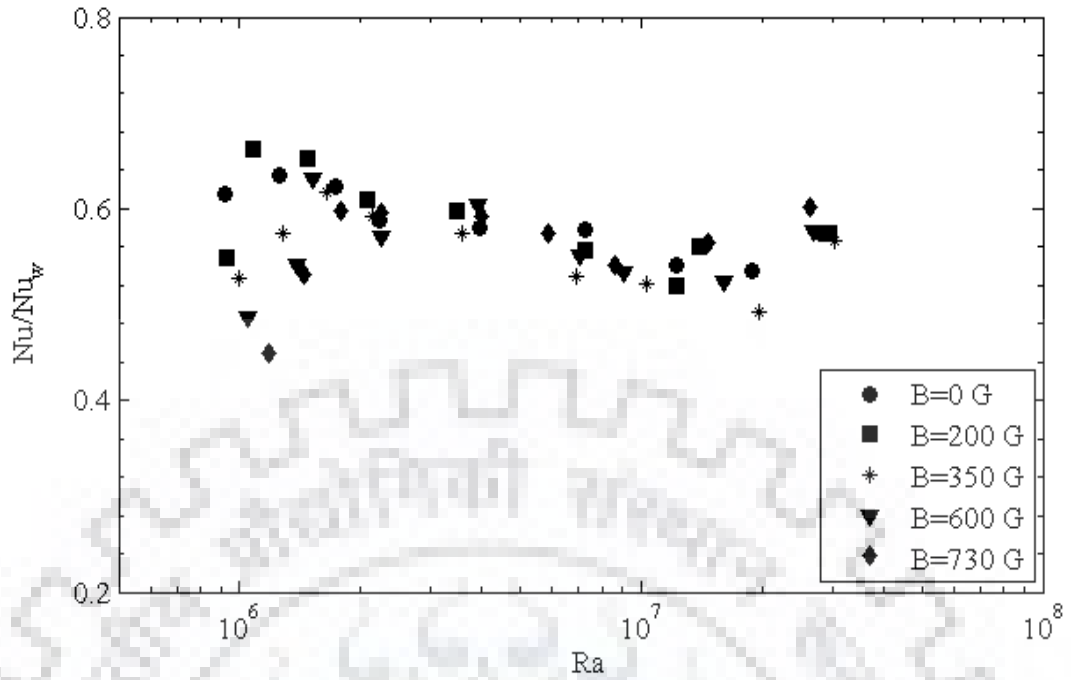
Figure 6. 20 A semi log plot between ratio of experimental Nu of magnetic nanofluids at ϕ = 0.05 vol. % to the water and Ra.
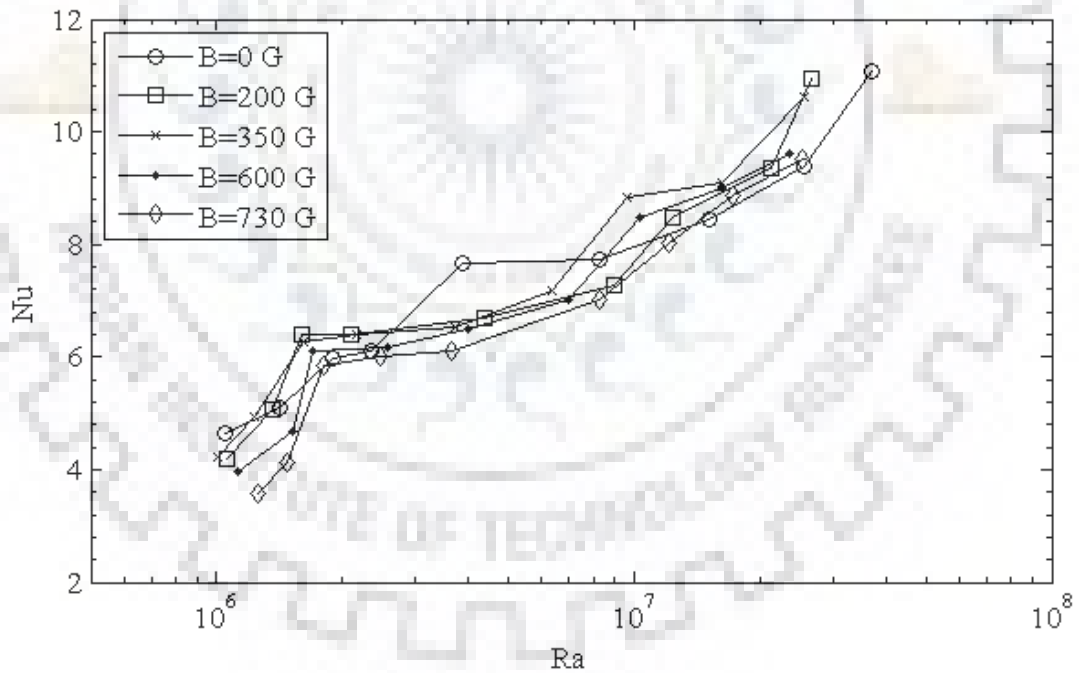
Figure 6. 21 A semi log plot of the experimental Nu versus Ra for ϕ = 0.08 vol. % concentration of Fe₃O₄-water magnetic nanofluids at various magnetic fields.

119
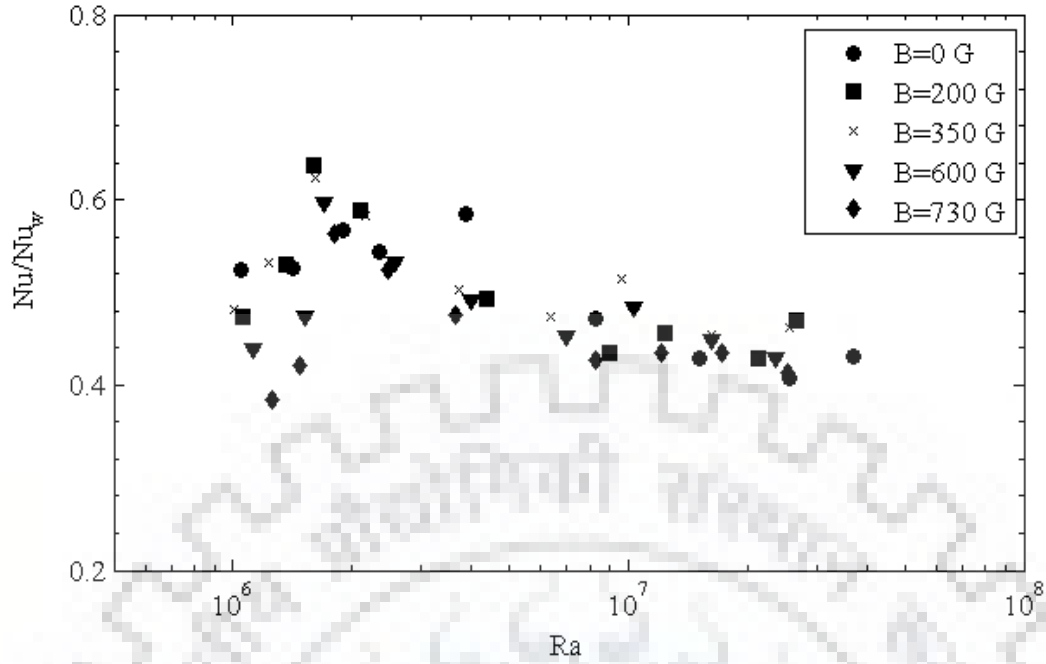
Figure 6. 22 A semi log plot between ratio of experimental Nu of magnetic nanofluid at $\phi = 0.08$ vol. % to the water and Ra.
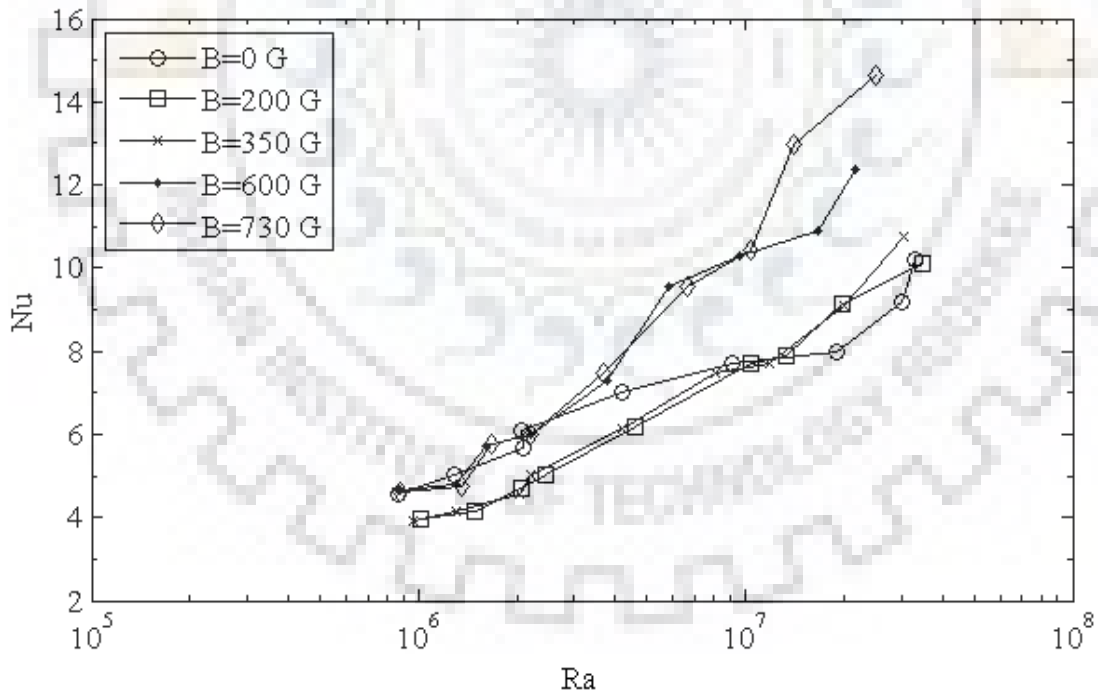
Figure 6. 23 A semi log plot of the experimental Nu versus Ra for $\phi = 0.1$ vol. % concentration of Fe_3O_4-water magnetic nanofluids at various magnetic fields.
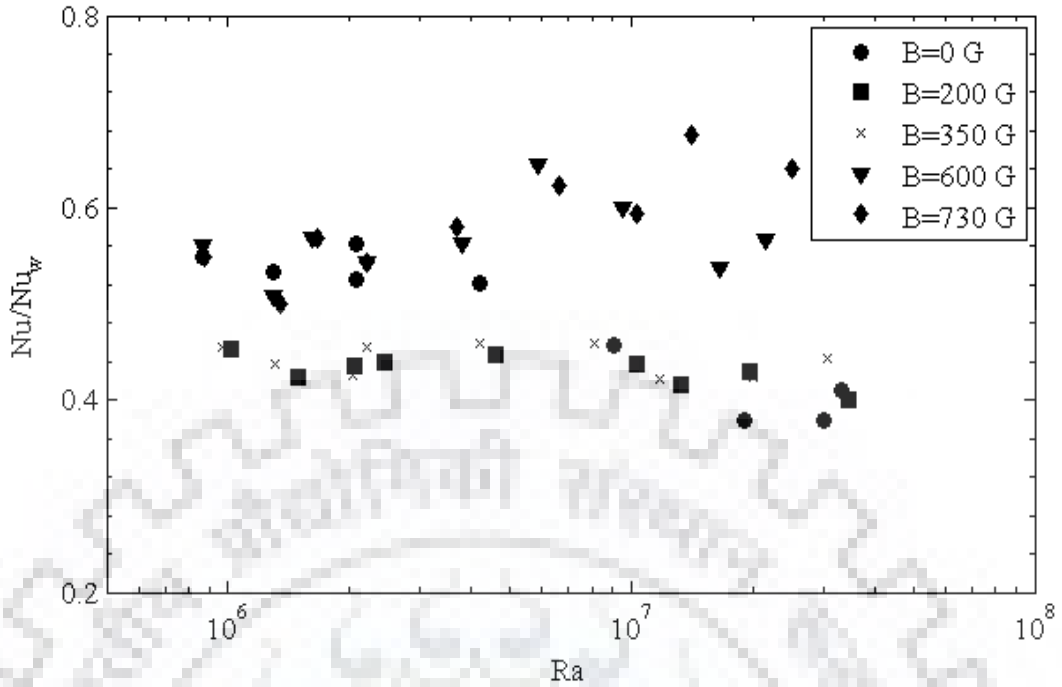
Figure 6. 24 A semi-log plot between ratio of experimental Nu of magnetic nanofluids at ϕ = 0. 1 vol. % to the water and Ra.

6.2.4 Thermal Boundary Layer Thickness

The thermal boundary layer thickness normalized by the height of the test section against the *Ra* is examined for the different magnetic nanofluids under the presence of various intensities of magnetic field and the power-law relations are established in between the thermal boundary layer and *Ra*.

The thermal boundary thickness for water as working fluid is discussed earlier in section 6.1.2 and the power-law developed between the thermal boundary thickness and *Ra* is presented by Equation 6.1. The thickness of the thermal boundary layer is decreased with the *Ra*, indicated the heat transfer augmentation with the *Ra* for water. As per the best knowledge of the author, no study has been reported in the literature to investigate the thermal boundary layer in the magnetic nanofluids for an open cubic cavity. Therefore, in the present study, the experimental facility is validated for the water with the reported results in the literature (section 6.1.2).

For the Fe_3O_4-water magnetic nanofluid $\phi = 0.01$ vol.%, the thickness of the thermal boundary layer normalized by the height of enclosure, corresponding to the aspect ratio 1 and under the presence of externally applied traverse magnetic field is depicted in

Figure 6.25. The power-law relation for predicting the thickness of the thermal boundary layer based on the Ra is formulated as given in Equation 6.8.

$$\left(\frac{\delta_{th}}{H}\right)_{MNF} = 16.41\, Ra^{-1/3} \tag{6.8}$$

The slope of the normalized thickness of the thermal boundary layer is decreased for Fe_3O_4-water magnetic nanofluid $\phi = 0.01$ vol.%, compared to water, which can be observed from Equations 6.1 and 6.8. The slope of decrement is higher for the water than the magnetic nanofluid, which depicted the enhancement in the thermal boundary layer thickness for the magnetic nanofluid.

For the Fe_3O_4-water magnetic nanofluid $\phi = 0.03$ vol.%, the thickness of the thermal boundary layer plotted against Ra is depicted in Figure 6.26. The power-law relation to predicting the thickness of the thermal boundary layer based on the Ra is formulated as given in Equation 6.9.

$$\left(\frac{\delta_{th}}{H}\right)_{MNF} = 17.88\, Ra^{-1/3} \tag{6.9}$$

The slope for the thermal boundary layer thickness enhanced with the concentration but compare to water it is less.
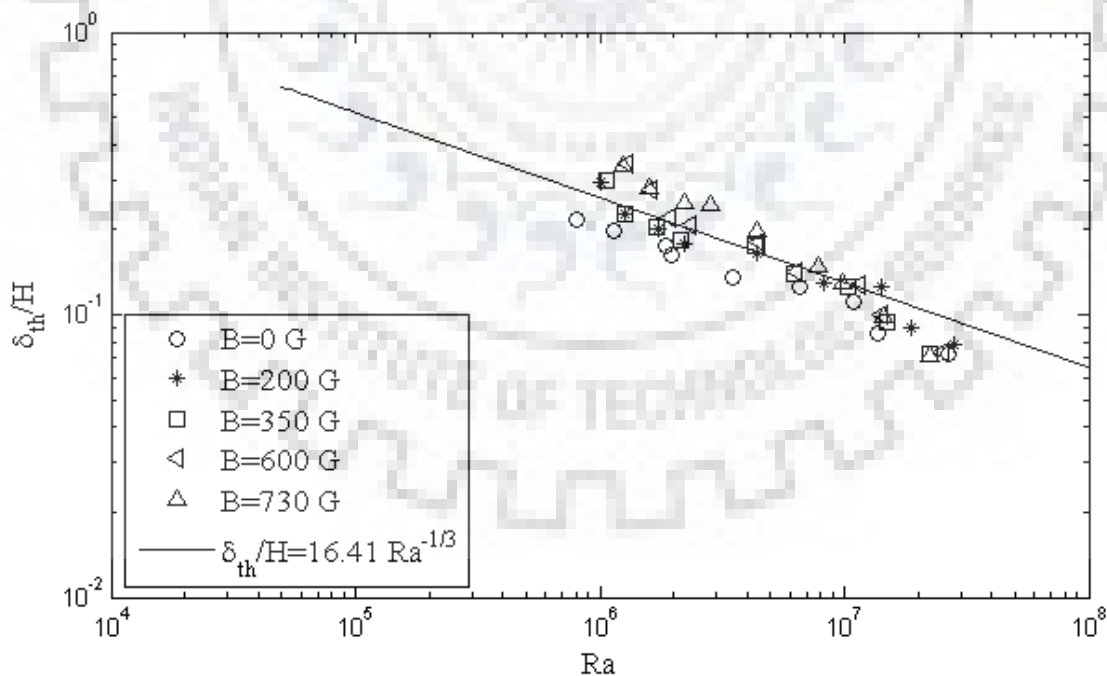
Figure 6. 25 A log-log plot of the normalized thermal boundary layer thickness with respect to Ra for φ = 0.01 vol. % concentration of Fe₃O₄-water magnetic nanofluids at various magnetic fields.

For Fe_3O_4-water magnetic nanofluids with $\phi = 0.05$ vol. %, the normalized thermal boundary layer thickness is plotted against Ra in Figure 6.27. The thermal boundary layer thickness is decreasing with the Ra and the developed power law is present in Equation 6.10.

$$\left(\frac{\delta_{th}}{H}\right)_{MNF} = 17.82\ Ra^{-1/3} \tag{6.10}$$

The power-law developed between previous and this case is almost the same and less than the water. It means the thermal boundary layer thickness is not changing much between these concentrations of magnetic nanofluids.

Similar kinds of results are obtained in the $\phi = 0.08$ vol. % and $\phi = 0.1$ vol. % of Fe_3O_4-water magnetic nanofluid for normalized thermal boundary layer thickness, as shown in Figure 6.28 and 6.29, respectively. The developed power law based on the experimental data is presented in Equations 6.11 and 6.12 for the $\phi = 0.08$ vol. % and $\phi = 0.1$ vol. % of Fe_3O_4-water magnetic nanofluid, respectively.

$$\left(\frac{\delta_{th}}{H}\right)_{MNF} = 20.83\ Ra^{-1/3} \tag{6.11}$$

$$\left(\frac{\delta_{th}}{H}\right)_{MNF} = 20.2\ Ra^{-1/3} \tag{6.12}$$

The slopes for Equations 6.11 and 6.12 are almost the same and increased from the previous cases but compared to water, the slopes are still lower. These observations of the thermal boundary layer thickness show that the thermal boundary layer thickness decrease with the Ra and with the concentration it is increasing but compare to water, the thermal boundary layer thickness is lower.
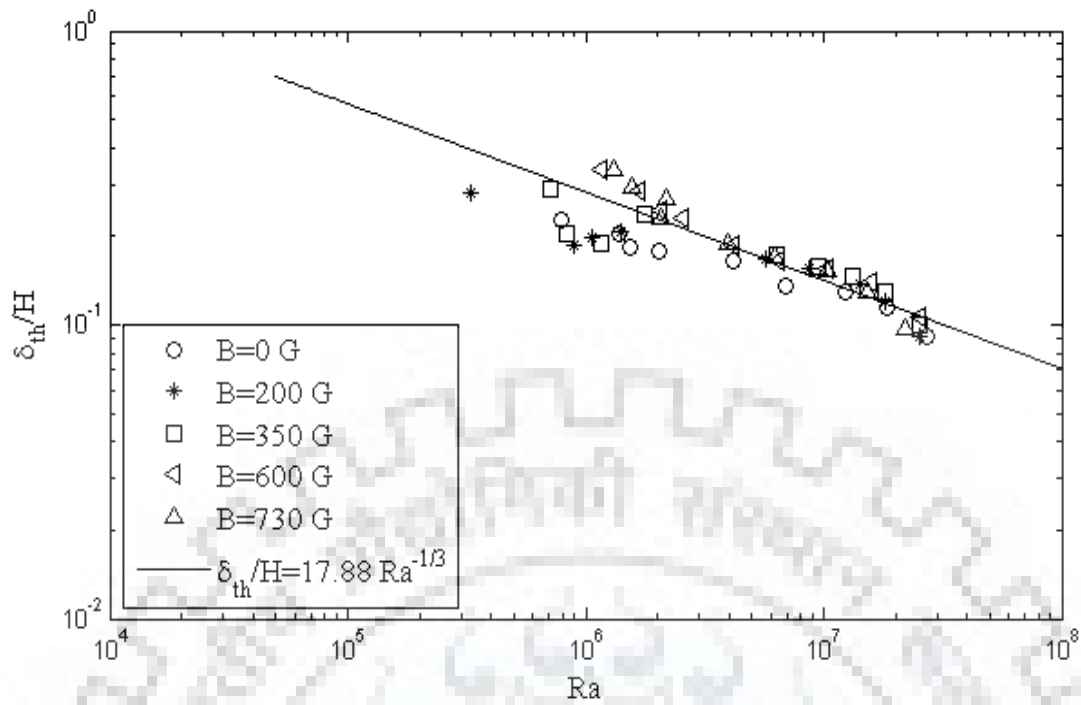
Figure 6. 26 A log-log plot of the normalized thermal boundary layer thickness with respect to Ra for ϕ = 0.03 vol. % concentration of Fe₃O₄-water magnetic nanofluids at various magnetic fields.
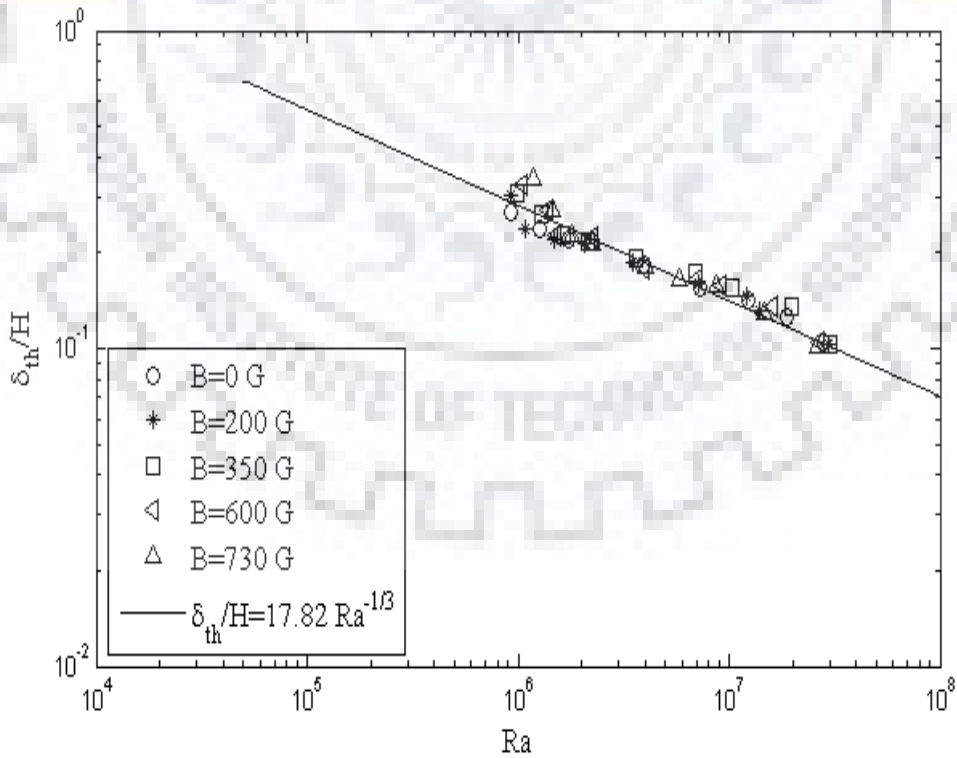
Figure 6. 27 A log-log plot of the normalized thermal boundary layer thickness with respect to Ra for ϕ = 0.05 vol. % concentration of Fe₃O₄-water magnetic nanofluid at various magnetic fields.

124
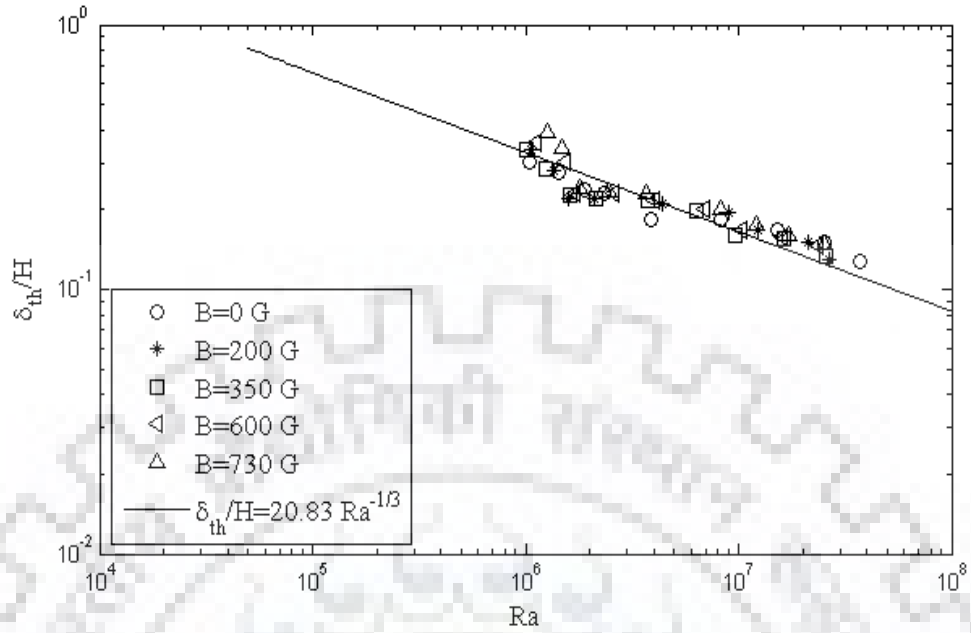
Figure 6. 28 A log-log plot of the normalized thermal boundary layer thickness with respect to Ra for ϕ = 0.08 vol. % concentration of Fe_3O_4-water magnetic nanofluid at various magnetic fields.
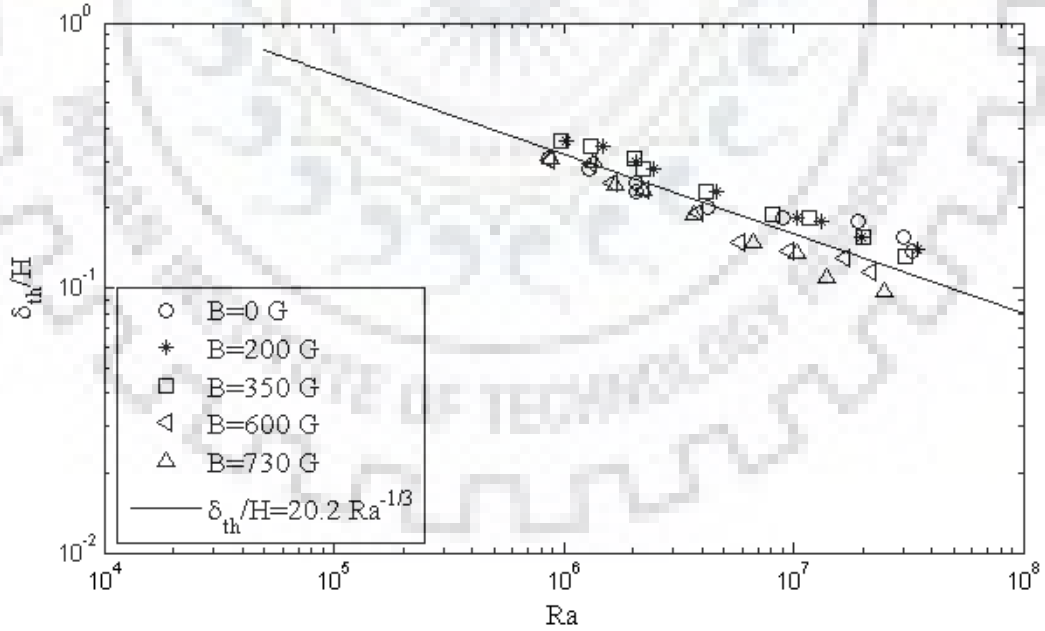
Figure 6. 29 A log-log plot of the normalized thermal boundary layer thickness with respect to Ra for ϕ = 0.1 vol. % concentration of Fe_3O_4-water magnetic nanofluid at various magnetic fields.

6.2.5 Statistical Analysis of Temperature Fluctuations in Magnetic Nanofluids

As discussed in chapter 4, a statistical approach is applied in the current section to obtain deep knowledge about the mechanisms involved in the alteration of heat transfer in the different Magnetic nanofluids. Different techniques are applied, such as histogram, probability density function (*pdf*), power spectral density (*psd*) profiles for the various groupings of particle concentration and magnetic field. For the water, the temperature fluctuations analysis is presented earlier in section 6.1.3.

For the $\phi = 0.01$ vol. % concentration of Fe_3O_4-water magnetic nanofluid at various magnetic fields, Figure 6.30 shows the probability density function (pdf) of temperature difference from the mean temperature at the cavity centre ($(T - <T>)/ \Delta T$) for the different *Ra*. This basic simple statistics technique shows how drastically the fluctuations in temperature are changed with different *Ra* at the centre of the cavity. The solid line in Figure 6.30 shows the Gaussian distribution. Generally, the temperature pdf profile is symmetric at the centre of the cavity and follows the Gaussian profile at the moderate regime of the turbulent convection. In Figures 6.30 (a), (c), (e), (g) and (i) the pdf profile shows the multimodal behaviour at lower Ra, indicating that the presence of regime transition to intensive turbulence. The other Figures 6.30 (b), (d), (f), (h) and (j) show the temperature fluctuations profile follows the Gaussian trend indicating the turbulence regime of the convection.

Figure 6.31 shows the pdf versus temperature fluctuation for the $\phi = 0.05$ vol.% concentration of Fe_3O_4-water magnetic nanofluid at various magnetic fields. The temperature fluctuation profile for low *Ra* are following the multimodal trends under the presence of the magnetic field. At the higher *Ra* the profile of temperature fluctuation follows the Gaussian trends. Similar kinds of results have been observed with $\phi = 0.1$ vol. % concentration of Fe_3O_4-water magnetic nanofluid at various magnetic fields in Figure 6.32.

The multimodal behaviour of temperature pdf indicates the convection is in transition regime and the Gaussian behaviour indicates the turbulence regime (Xu et al., 2019) (Niemela et al., 2000).
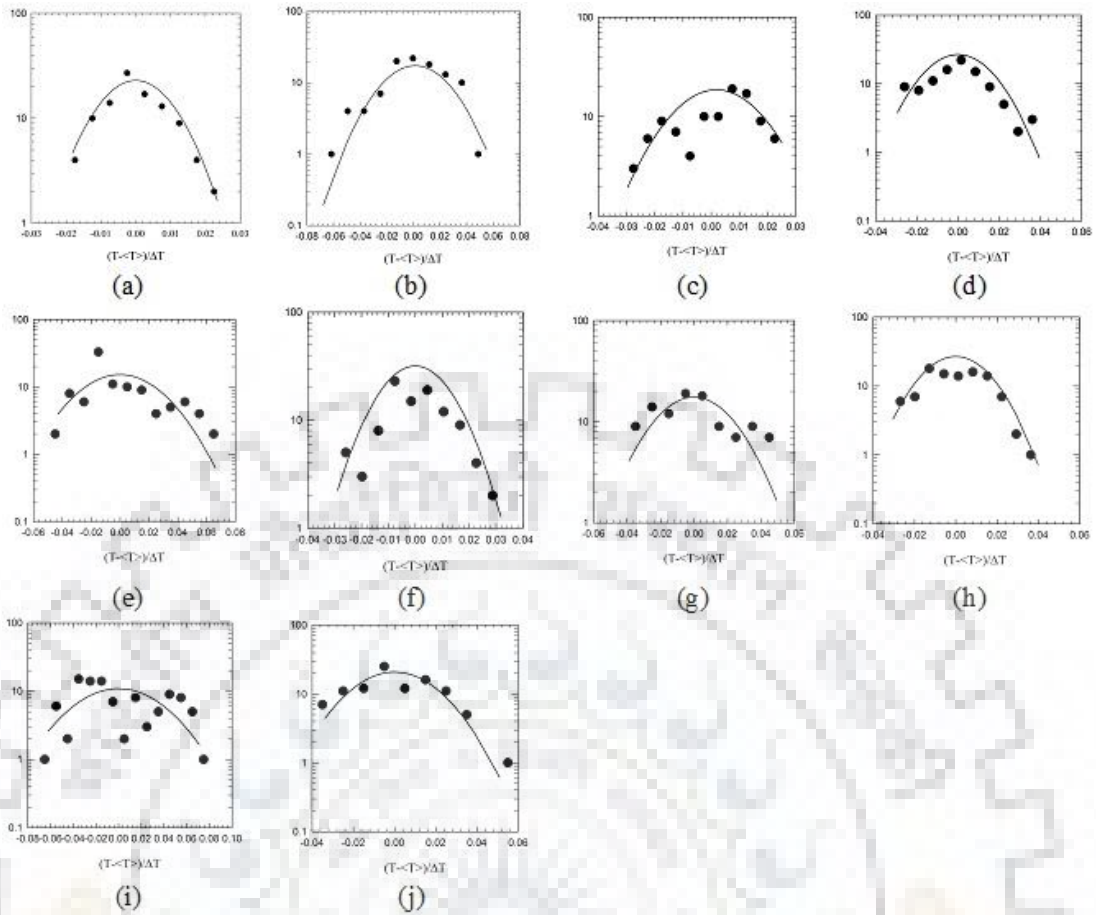
Figure 6. 30 The probability density function (pdf) of the temperature fluctuation at the center of the cavity along the centreline at different Rayleigh numbers for ϕ = 0.01 vol. % concentration of Fe₃O₄-water magnetic nanofluid at various magnetic fields. (a) B= 0 Gauss, Ra= 8.04 ×10⁵ (b) B= 0 Gauss, Ra= 1.37×10⁷ (c) B= 200 Gauss, Ra= 1.27 ×10⁶ (d) B= 200 Gauss, Ra= 1.87×10⁷ (e) B= 350 Gauss, Ra= 1.06 ×10⁶ (f) B= 350 Gauss, Ra= 2.23× 10⁷ (g) B= 600 Gauss, Ra= 1.29 ×10⁶ (h) B=600 Gauss, Ra= 2.53×10⁷ (i) B= 730 Gauss, Ra= 1.60 ×10⁶ (j) B= 730 Gauss, Ra= 2.24×10⁷
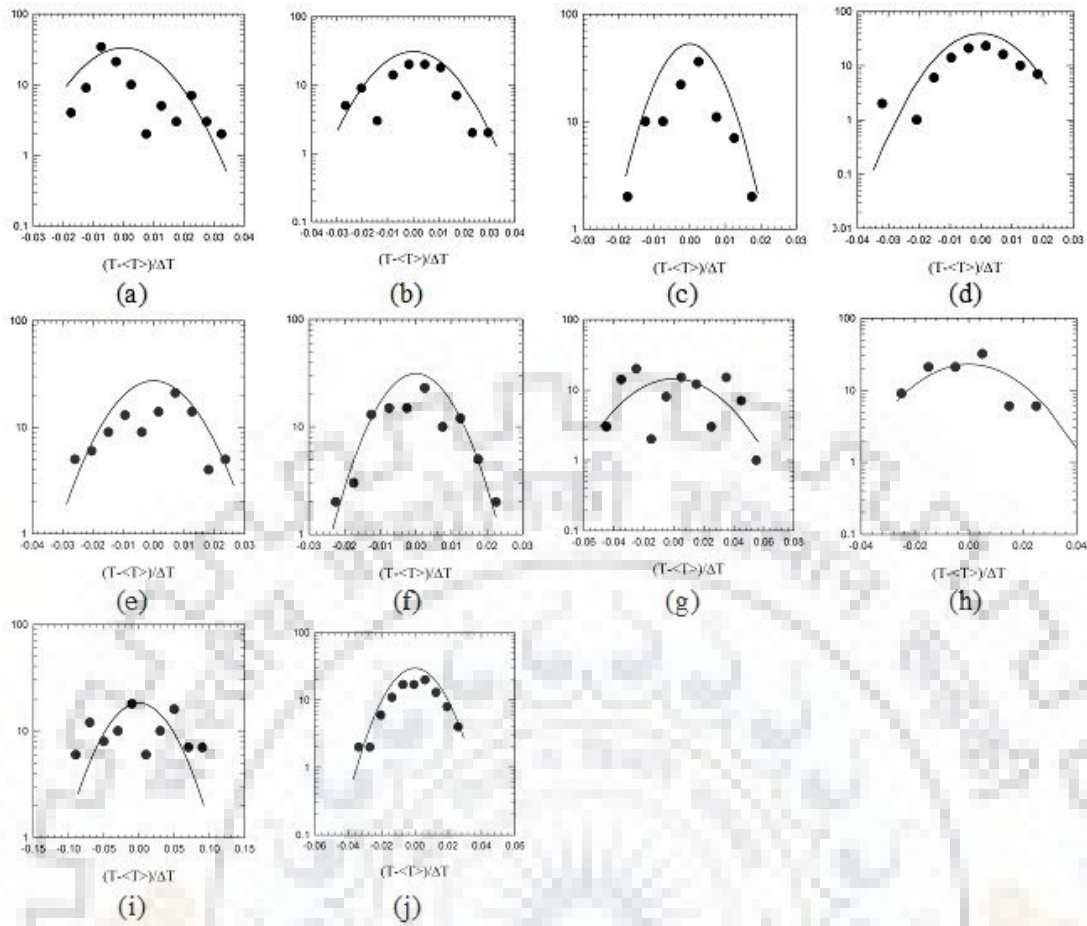
Figure 6. 31 The probability density function (pdf) of the temperature fluctuation at the center of the cavity along the centreline at different Rayleigh numbers for $\phi = 0.05$ vol. % concentration of Fe_3O_4-water magnetic nanofluid at various magnetic fields. (a) B= 0 Gauss, Ra= 9.24 $\times 10^5$ (b) B= 0 Gauss, Ra= 1.89 $\times 10^7$ (c) B= 200 Gauss, Ra= 9.25 $\times 10^5$(d) B= 200 Gauss, Ra= 2.95$\times 10^7$ (e) B= 350 Gauss, Ra= 9.98$\times 10^5$ (f) B= 350 Gauss, Ra= 3.02$\times 10^7$ (g) B= 600 Gauss, Ra= 1.05 $\times 10^6$ (h) B=600 Gauss, Ra= 2.69 $\times 10^7$ (i) B= 730 Gauss, Ra= 1.18 $\times 10^6$ (j) B= 730 Gauss, Ra= 2.64 $\times 10^7$

128
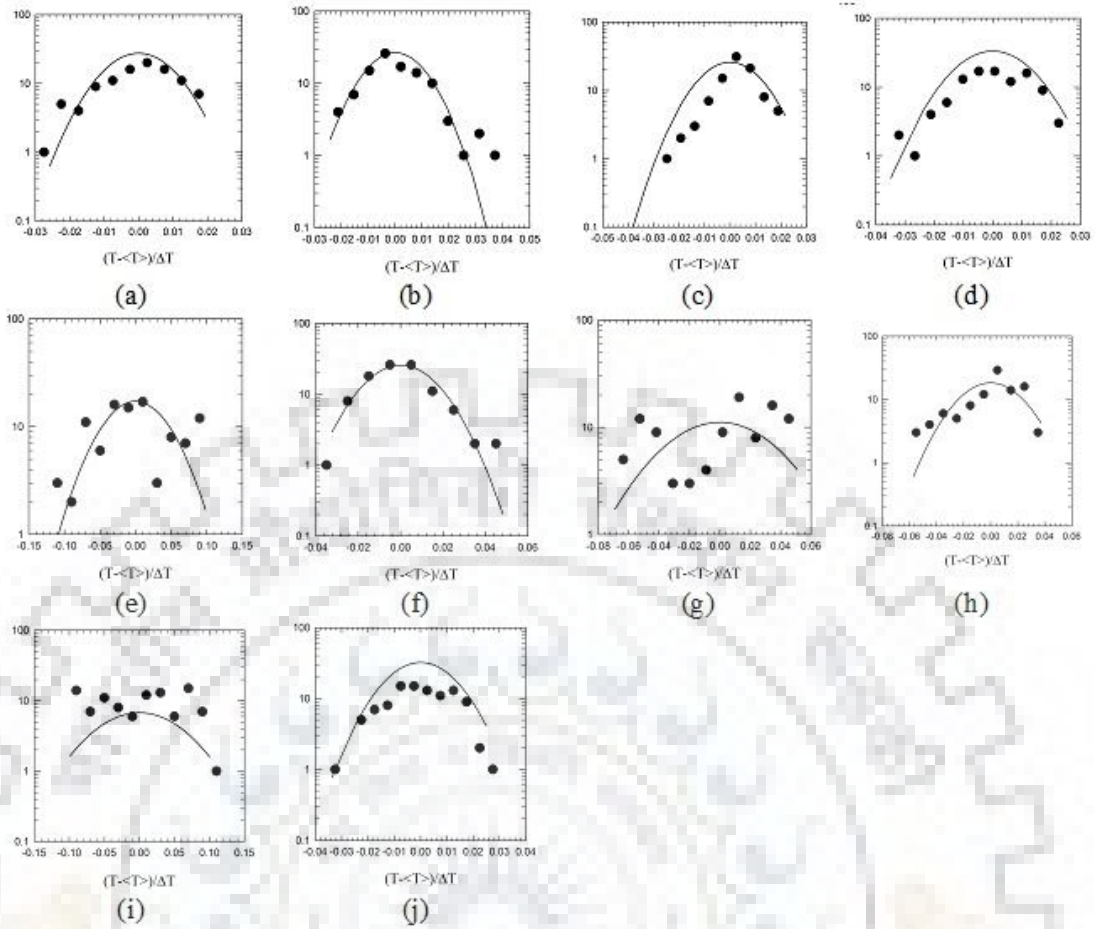
Figure 6. 32 The probability density function (pdf) of the temperature fluctuation at the center of the cavity along the centreline at different Rayleigh numbers for $\phi = 0.1$ vol. % concentration of Fe_3O_4-water magnetic nanofluid at various magnetic fields. (a) B= 0 Gauss, Ra= 8.69×10^5 (b) B= 0 Gauss, Ra= 3.31×10^7 (c) B= 200 Gauss, Ra= 1.02×10^6 (d) B= 200 Gauss, Ra= 3.46×10^7 (e) B= 350 Gauss, Ra= 9.67×10^5 (f) B= 350 Gauss, Ra= 3.06×10^7 (g) B= 600 Gauss, Ra= 8.67×10^5 (h) B=600 Gauss, Ra= 2.16×10^7 (i) B= 730 Gauss, Ra= 8.79×10^5 (j) B= 730 Gauss, Ra= 2.50×10^7

The power spectral density (*PSD*) of temperature fluctuation *((T- <T>)/ ΔT)* is demonstrated for the higher $Ra = 2.68 \times 10^7$ at the center of the cavity in figure 6.33 in the Fe_3O_4-water magnetic nanofluid of $\phi = 0.01$ vol. % concentration. As defined earlier in section 6.1.3 for water, the power spectrum follows the power law for different concentrations of the magnetic nanofluids and under the presence of various magnetic field intensities, summarized in Table 6.1.
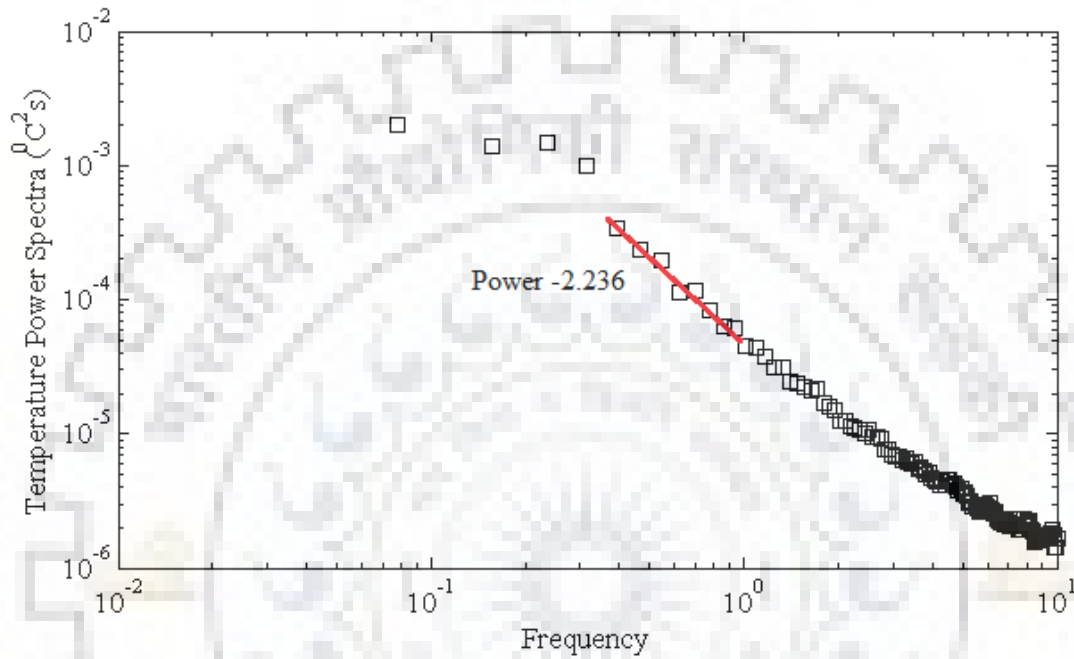
Figure 6. 33 The distribution of temperature fluctuations spectrum at the center of the cavity across the centreline for φ = 0.01 vol. % concentration of Fe₃O₄-water magnetic nanofluid at Ra=2.68 × 10⁷.

Table 6. 1 Power law index of temperature power spectrum.

S. No	Φ (vol.%)	Magnetic Field (Gauss)	Ra × 10⁻⁷	Power Law
1		0	2.68	2.236
2		200	2.81	1.985
3	0.01	350	2.23	1.628
4		600	2.53	1.708
5		730	2.24	2.010
6		0	2.63	2.098
7		200	2.52	1.869
8	0.03	350	2.53	1.967
9		600	2.54	1.829
10		730	2.19	1.482
11		0	2.79	1.118
12		200	2.95	1.903
13	0.05	350	3.02	1.823
14		600	2.69	1.247
15		730	2.64	1.988
16		0	3.69	1.747
17		200	2.66	2.000
18	0.08	350	2.56	1.751
19		600	2.35	2.366
20		730	2.53	3.340
21		0	3.31	1.485
22		200	3.46	1.915
23	0.1	350	3.06	1.749
24		600	2.16	1.998
25		730	2.50	1.824

6.3 Magnetic nanofluids under the presence of vertical magnetic field

In this type of natural convection experiments, the orientation of the externally applied magnetic field is changed into the direction of temperature gradient i.e. in the vertical direction. Figure 6.33 shows that the temperature difference between the bottom plate and the middle layer of water (bulk fluid) became constant, so the experiment is treated as quasi-steady. So, all the analysis has been done on the quasi-steady state only. Figure 6.34 shows the validity criteria ($\beta\Delta T$<0.2) of Oberbeck-Boussinesq is fulfilled for all the experiments. Figure 6.35 illustrated the results of heat transfer measurement for the open cavity natural convection in the magnetic nanofluids having nanoparticles concentration 0.01 vol %. The bottom of the cavity is at constant temperature and the top is open to the environment with temperature 20±2 ^{0}C % RH = 50 ±5 %. All the other sides are perfectly insulated. The Nusselt number is significantly increased compared to water in the case of magnetic nanofluid. The Nusselt number in the

presence of an externally applied magnetic field (260 Gauss) is enhanced more, which means the magnetic field substantially helps to enhance the heat transfer in the magnetic nanofluids.

This is our next step to find out the effect of the presence of the magnetic field in the direction of the temperature gradient on the natural convection heat transfer. As this work is under process, so only few results are presented here.
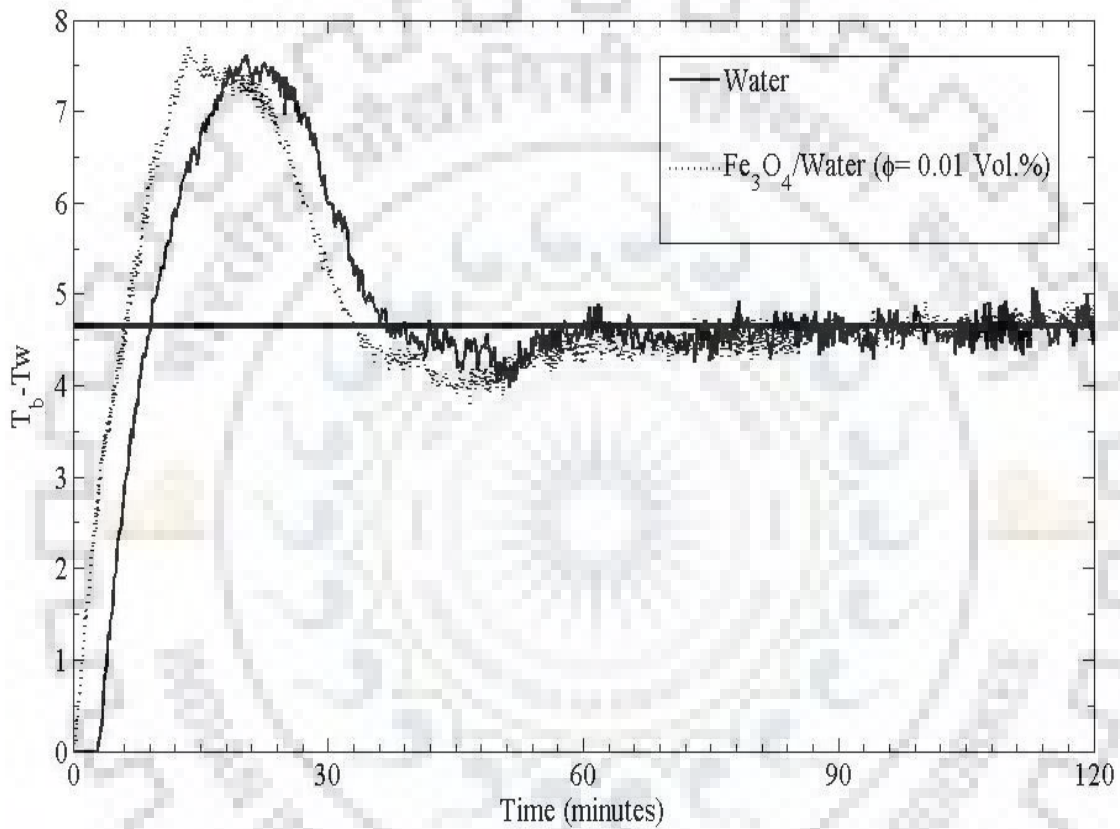
Figure 6. 34 Variation in the temperature difference between bottom surface and bulk fluid, during the experiment for vertical magnetic field.
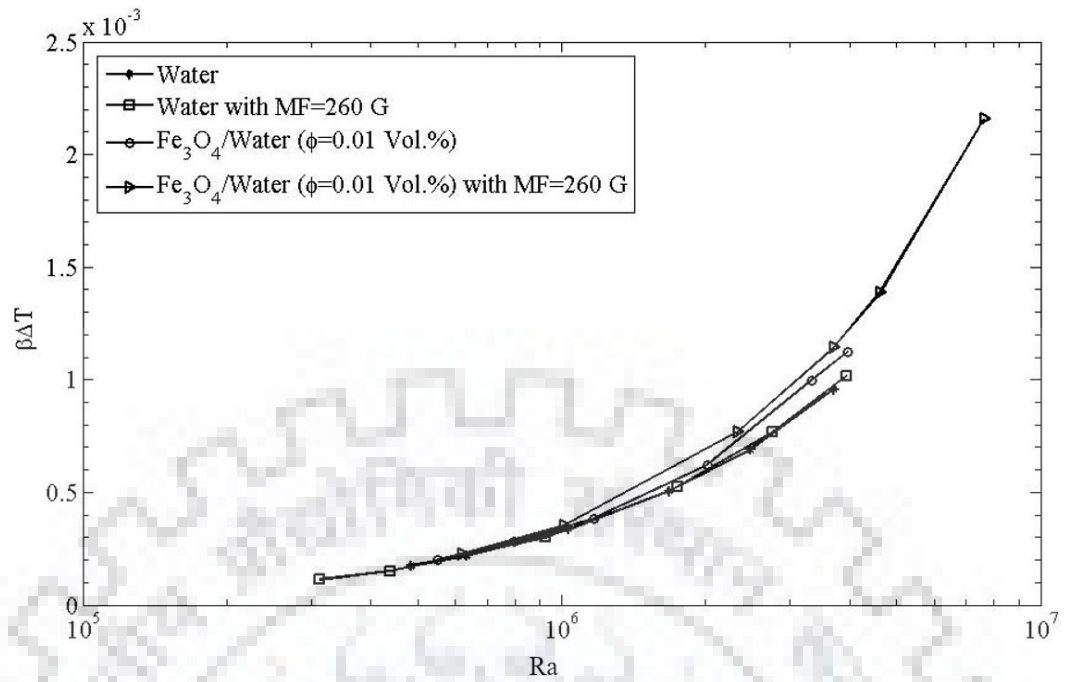
Figure 6. 35 Oberbeck - Boussinesq approximation βΔT<0.2, for the vertical magnetic field experiments.
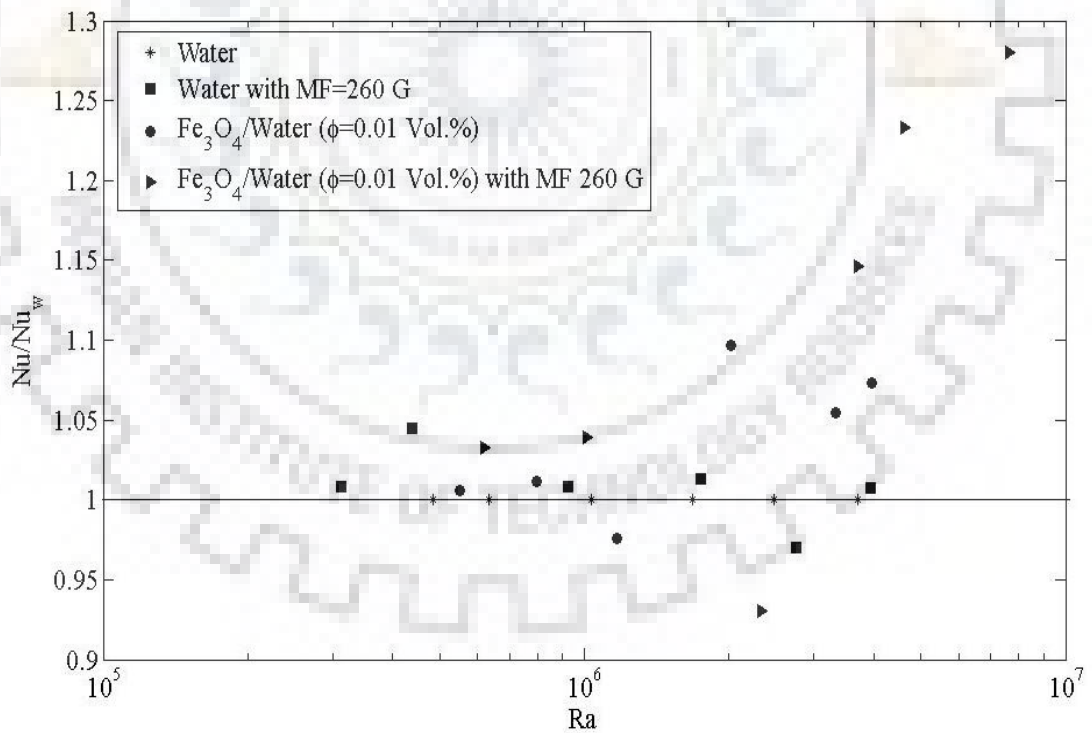
Figure 6. 36 A semi log plot between ratio of experimental Nu of magnetic nanofluids at ϕ = 0.0 1 vol. % to the water and Ra *with magnetic field parallel to the temperature gradient.*
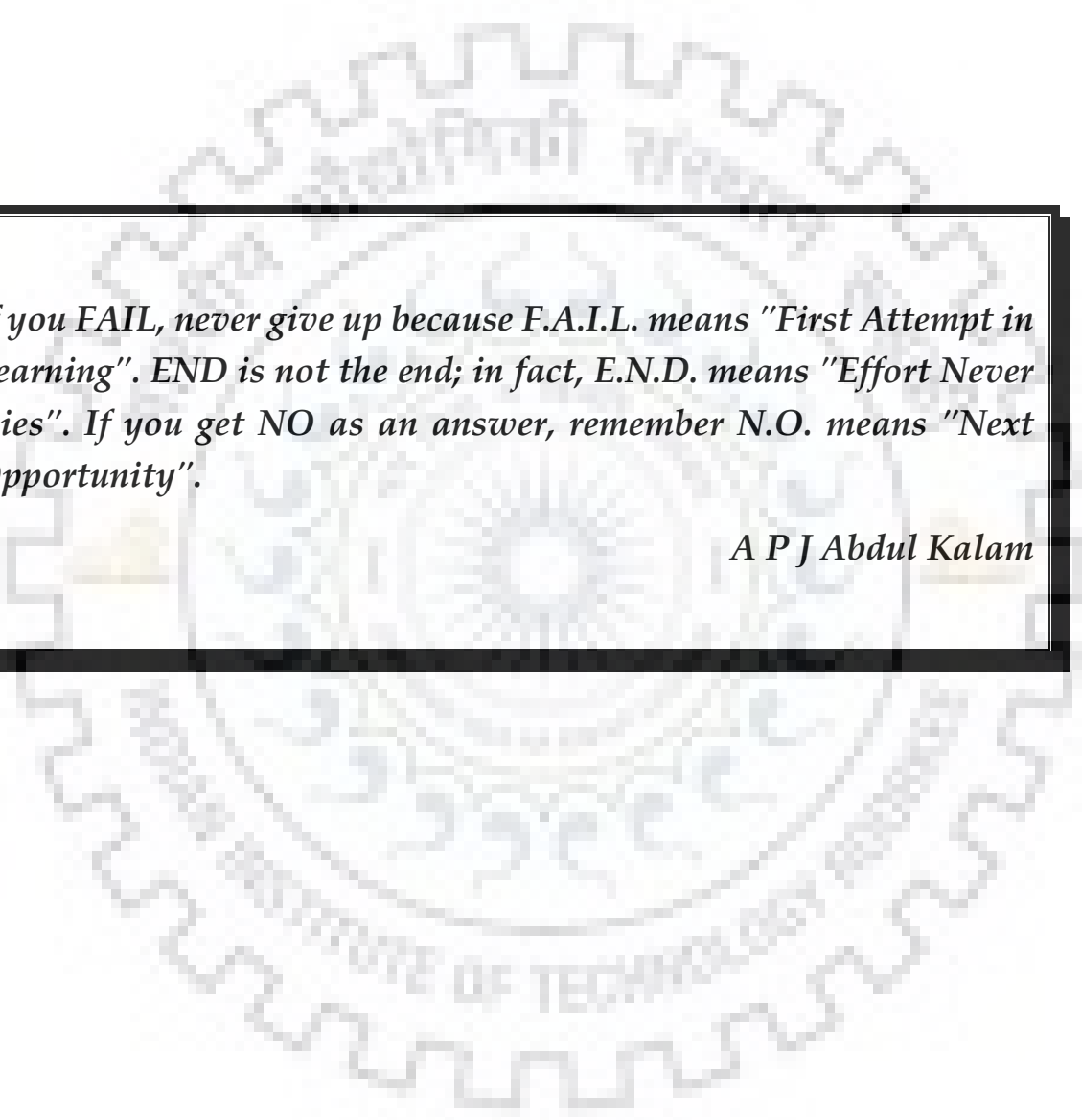
Chapter 7: Conclusions & Future Scope

Index
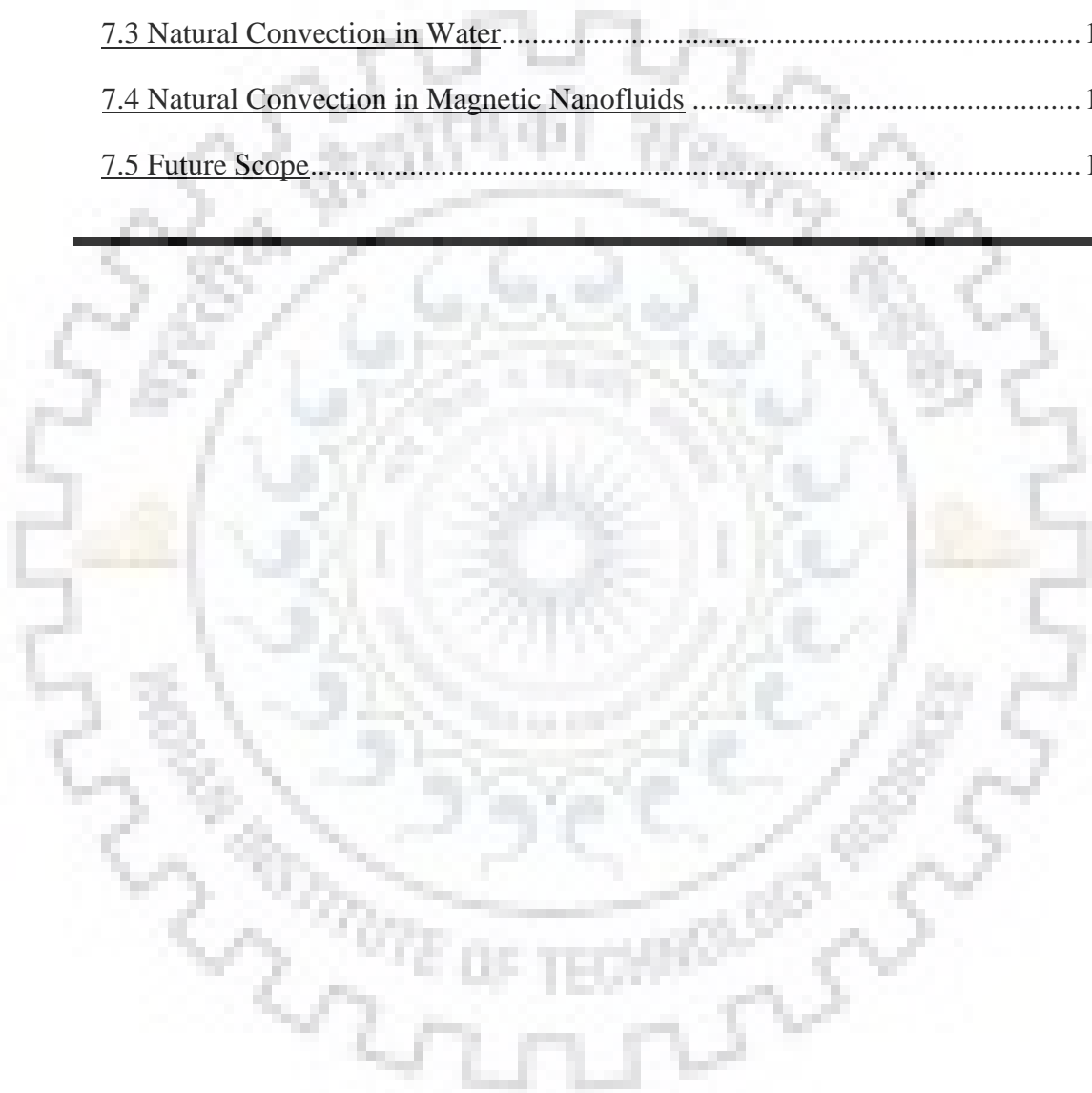
If you FAIL, never give up because F.A.I.L. means "First Attempt in Learning". END is not the end; in fact, E.N.D. means "Effort Never Dies". If you get NO as an answer, remember N.O. means "Next Opportunity".

A P J Abdul Kalam

7

Conclusions & Future Scope

Several numerical studies have been conducted to analyse the natural convection inside an open cavity with magnetic nanofluids and all demonstrated enhancement in the heat transfer performance. While very few experimental investigations have been conducted on the natural convection in magnetic nanofluids using the R-B convection model. The mechanisms involved in the enhancement or deterioration of the natural convection in the magnetic nanofluids were not examined in the open cubic cavity and hence the information on the phenomena was unclear. To establish a clear phenomenon of natural convection in magnetic nanofluids, more experimental investigations were needed. The effect of nanoparticle concentration, externally applied magnetic field in traverse direction to the temperature gradient and Rayleigh number on the open cubic cavity natural convection is investigated in a very narrow range of these parameters.

In the present work, the natural convection phenomena in the water and Fe_3O_4-water magnetic nanofluid were systematically investigated, which include the preparation and characterization of nanofluids. Thermal boundary layer properties and temperature fluctuation for both water and magnetic nanofluids are thoroughly investigated and discussed The principal objective of the present study is to provide more experimental information on the thermal convection turbulent regime in an open cavity heated from below at moderate Rayleigh numbers and compare to the corresponding state observed in the *R–B* convection. Moreover, Nusselt number correlations are developed, and the thermal boundary layer properties are reported and discussed comprehensively.

A literature review is summarized on the various studies conducted involving Fe_3O_4-water magnetic nanofluids, and the thermophysical properties of Fe_3O_4-water magnetic nanofluids, mechanisms responsible for the heat transfer are included in Chapter 2. The findings of the previously studied research on the thermophysical properties of magnetic nanofluids are summarized, and compare graphically by extracting data and plotted collectively. The findings on the natural convection, theoretically and experimentally, are also reviewed and summarized. Chapter 3 is about the preparation

and characterization of Fe_3O_4-water magnetic nanofluids conducted in the present work.

Chapters 4 – 5 are about the experimental facility and procedure, data reduction with the calibration and uncertainty analysis, and statistical analysis techniques. The experimental results are summarized in Chapter 6 and a comprehensive discussion on the results is also included in the same chapter. A sum-up of major findings of the present work as well as propositions for further work are presented.

7.1 Summary of the experimental test results

The present study investigates the effect of Fe_3O_4 nanoparticles concentrations, the intensity of externally applied magnetic field on the temperature fluctuations, thermal boundary properties and natural convection heat transfer inside an open cubic cavity heated from below. The different dimensionless parameters such as Rayleigh number, Nusselt number and Prandtl number are examined in the study.

The two-step approach is used to prepare the nanofluids of different particle concentrations for the optimum sonication time. The different thermophysical properties are measured with high precision in the calibrated instruments.

An enclosure with the bottom side heating and top side open to a controlled environment is used to measure the natural convection heat transfer. All the measuring properties were noted down at the steady-state to prevent errors in the measurements after the proper systematic calibration of instruments and sensors. A thorough analysis was conducted on the experimental results to absorb every bit of information. The dependencies of the Nusselt number on the Rayleigh number were presented in the present work.

7.2 Characterization of the magnetic nanofluids

At present, the fundamental understanding of the effect of temperature on thermal conductivity and density in magnetic nanofluids are in the initial stage. Thermal conductivity and density are the two most important thermal properties which contribute to the convective heat transfer. In the present work the water-based Fe_3O_4 magnetic nanofluid is synthesized by two-step method at different volume percentage

138

concentrations. The density and thermal conductivity of the magnetic nanofluids are measured at different temperatures and compared with water. All the instruments are first calibrated. The results show the concentration of nanoparticles increased both density and thermal conductivity of magnetic nanofluids compared to water. The maximum enhancement in density and thermal conductivity with 0.1 vol % concentration are 0.8 % and 15 % compared to water, respectively. The density of magnetic nanofluids increases more at low temperatures and less at a higher temperature. The maximum enhancement in the density value changes from 1.2 to 0.7 % in the temperature range of 10 to 70 ℃ for the 0.1 vol. % of magnetic nanofluids. The thermal conductivity of magnetic nanofluids shows the increment with the temperature. The thermal conductivity at the nanoparticles concentration of 0.1 vol. % is enhanced maximum from 3 to 18 % in the temperature range of 10 to 70 ℃, respectively. The increment in the thermal conductivity with temperatures is attributed to the Brownian motion increment of nanoparticles at a higher temperature. The application of the external magnetic field also tunes the thermal conductivity of the magnetic nanofluids. The maximum enhancement of 22 % is observed at the highest concentration, temperature and magnetic field of 0.01 vol. %, 70 ℃ and 730 Gauss, respectively. The alignment of the nanoparticles causes the enhancement in the thermal conductivity in the presence of a magnetic field in the direction of the magnetic field (Shima et al., 2014; Shima & Philip, 2011).

Similar kind of results has been discussed on the kinematic viscosity of the Fe_3O_4 magnetic nanofluid. The viscosity is enhanced with the concentration; a maximum of 5 % enhancement is observed with ϕ=0.1 vol. %. However, with temperature, the viscosity is decreased compared to the minimum temperature of the particular fluid. On the other hand, with concentration, the viscosity is enhanced compared to water at a fixed temperature. The maximum enhancement is observed at a concentration of 0.1 vol. %, the viscosity increases from 5 to 30% in the temperature range of 27 to 77 ℃, respectively.

There are several other factors present that may affect these thermal properties like shape, size of nanoparticles, magnetic field, base fluid and the stability of magnetic nanofluids. All these factors should be included in future experiments to achieve a subtle better understanding of the mechanism of changes in thermal properties.

7.3 Natural Convection in Water

In an open cubic cavity heated from below, the behaviour of local temperatures has been recorded and analysed. In this form of thermal convection, the presence of distinct different boundary conditions compared to R-B convection plays an exciting role in the behaviour of the temperature trends. Boundary layer properties in the specific range of $4 \leq Pr \leq 6$ and $10^5 \leq Ra \leq 10^7$ in turbulent convection are observed. Based on the different basic statistical techniques, we can conclude that the temperature fluctuations in the cavity changes with the boundary layer. Based on the boundary layer thickness and temperature fluctuations, the existence of the different zones is confirmed here in the turbulent thermal convection. The power spectrum of temperature fluctuations reported the transformation of energy from larger to smaller scale and reached a maximum value near the thermal boundary layer thickness in the mixing zone of thermal convection. The power spectrum at the central layer of the cavity follows the power law of exponent 7/5, which is consistent with Bolgiano's theory (Bolgiano 1959). Moreover, the Oberbeck-Boussinesq approximation is validated with the value of $\beta \Delta T$. The Nu dependence on Ra and Pr is developed into correlation with the minimum standard deviation over the experimental data.

7.4 Natural Convection in Magnetic Nanofluids

In an open cubic cavity heated from below, the Fe_3O_4 nanoparticles concentrations from 0.01% and 0.1 vol.% in water were investigated for natural convection heat transfer under the presence of a magnetic field. The uniform magnetic field intensity varies from 0 to 730 Gauss in the horizontal direction to the temperature gradient. The deterioration in the heat transfer is observed with the concentration of the nanoparticles. The Nusselt number is increasing with the Rayleigh number. In the lower concentrations of nanoparticles in the Fe_3O_4-water magnetic nanofluids, the Nusselt number shows not much affected by the presence of a magnetic field. However, at 0.1 vol.% the Nusselt number is increasing with the magnetic field. The thermal boundary layer thickness normalized by the height of the test section against the Rayleigh number was investigated and found as given by:

$$\frac{\delta_{th}}{H} \sim ARa^a \tag{8.1}$$

The value of a =-1/3 and A is varied according to the working fluid, given in Table 7.1

Table 7. 1 Value of the constant A

S. No	Φ (vol.%)	A
1	0.01	16.41
2	0.03	17.88
3	0.05	17.82
4	0.08	20.83
5	0.1	20.2

7.5 Future Scope

In the present scenario, to use nanofluids in a wide range of applications, it will be necessary to overcome some of the challenges with nanofluids. High production cost, various difficulties in production, increment in pumping power, the stability of nanoparticle dispersion with time, lower specific heat etc. are some of the challenges to be overcome.

The effect of higher volume concentration of nanoparticles on the natural convection will be necessary to investigate, which may be resulted in the enhancement due to increased thermal conductivity and particle-particle interaction. A more focused study on natural convection in nanofluids is required to reveal the hidden obstacles to the enhancement in natural convection in nanofluids.

➢ List of Publication

Journal

- Aditya Kumar, Sudhakar Subudhi, "Thermal fluctuations and boundary layer properties of turbulent natural convection inside open cavities of different dimensions heated from below" Physics of Fluids **32**, 067114 (2020); https://doi.org/10.1063/5.0008160

- Aditya Kumar, Sudhakar Subudhi, "Preparation, characterization and heat transfer analysis of nanofluids used for engine cooling" Applied Thermal Engineering, 160, (2019), 114092; https://doi.org/10.1016/j.applthermaleng.2019.114092

- Aditya Kumar, Sudhakar Subudhi, "Preparation, characteristics, convection and applications of magnetic nanofluids: A review" Heat and Mass Transfer volume 54, (2018) 241–265. https://doi.org/10.1007/s00231-017-2114-4

- Aditya Kumar, Vivekananda, Sudhakar Subudhi, "Cooling and Dehumidification using Vortex tube" Applied Thermal Engineering 122, (2017).
  DOI: 10.1016/j.applthermaleng.2017.05.015

- Rajesh Choudhary, Deepak Khurana, Aditya Kumar, Sudhakar Subudhi, "Stability analysis of Al2O3 /water nanofluids", Journal of Experimental Nanoscience, 12 (1), (2017). DOI: 10.1080/17458080.2017.1285445

Conferences

- Aditya Kumar, Sudhakar Subudhi, "Experimental investigation on the heat transfer properties of Fe3O4 based magnetic nanofluid" in the 25th National and 3rd International ISHMT-ASTFE Heat and Mass Transfer Conference held during December 28-31,2019, IIT Roorkee.

- Aditya Kumar, Sudhakar Subudhi, "Experimental investigation of convection instability and heat transfer characteristics by Fe3O4-water magnetic nanofluid", in 10th International Conference on Multiphase Flow, ICMF 2019, At: Rio de Janeiro, Brazil, 2019

- Aditya Kumar, Sudhakar Subudhi, "Experimental Investigation of Natural Convection in an Open Cavity with Water and Fe3O4/Water Magnetic

Nanofluid", in 7th International and 45th National Conference on Fluid Mechanics and Fluid Power, At: IIT Bombay , India, 2018

- Aditya Kumar, Sudhakar Subudhi, "Investigation of thermal conductivity of water based Fe3O4 magnetic nanofluids", in COMPFLU-2018: International Conference on Complex Fluids and Soft Matter, At: IIT Roorkee, India, 2018

- Aditya Kumar, Sudhakar Subudhi, "Investigation of stability of water based alumina nanofluids", in 6th International and 43rd National Conference on Fluid Mechanics and Fluid Power, At: MNITA, India, 2016

- Aditya Kumar, Deepak Khurana, Rajesh Choudhary, Sudhakar Subudhi, "Preparation and Stability Analysis of Water Based Aluminum Oxide Nanofluids", in International Conference on Energy Systems and Developments 2015, At: Pune, Maharashtra, India, 2015

Books

- Aditya Kumar, Sudhakar Subudhi, "Thermal Characteristics and Convection in Nanofluids" Book Proposal approved by Editorial Board of Springer Nature, June 2020.

Book Chapters

- Aditya Kumar, Sudhakar Subudhi, "Natural Convection in an Open Cavity Containing Water Based Fe_3O_4 Magnetic Nanofluids" Advances in Engineering Research, Nova Science Publisher, June 2020.

- Sudhakar Subudhi, Aditya Kumar, "Application of Nanofluids for Radiator Cooling ", in Reference Module in Materials Science and Materials Engineering, Elsevier, 2019

References

Abareshi, M., Goharshadi, E. K., Mojtaba Zebarjad, S., Khandan Fadafan, H., & Youssefi, A. "Fabrication, characterization and measurement of thermal conductivity of Fe3O4nanofluids." Journal of Magnetism and Magnetic Materials, *322*(24), 3895–3901. (2010). https://doi.org/10.1016/j.jmmm.2010.08.016

Abareshi, M., Sajjadi, S. H., Zebarjad, S. M., & Goharshadi, E. K. "Fabrication, characterization, and measurement of viscosity of α-Fe2O3-glycerol nanofluids." Journal of Molecular Liquids, *163*(1), 27–32. (2011). https://doi.org/https://doi.org/10.1016/j.molliq.2011.07.007

Aksenov, V. L., Avdeev, M. V, Balasoiu, M., Bica, D., Rosta, L., Török, G., & Vekas, L. "Aggregation in non-ionic water-based ferrofluids by small-angle neutron scattering." Journal of Magnetism and Magnetic Materials, *258*, 452–455. (2003).

Antosova, A., Siposova, K., Koneracka, M., Zavisova, V., Daxnerova, Z., Vavra, I., Fedunova, D., Bagelova, J., Kopcansky, P., & Gazova, Z. "Magnetic fluid- A novel approach to treat amyloid-related diseases." Physics Procedia, *9*, 262–265. (2010). https://doi.org/10.1016/j.phpro.2010.11.058

Aquino, R., Depeyrot, J., Sousa, M. H., Tourinho, F. A., Dubois, E., & Perzynski, R. "Magnetization temperature dependence and freezing of surface spins in magnetic fluids based on ferrite nanoparticles." Physical Review B - Condensed Matter and Materials Physics, *72*(18), 1–10. (2005). https://doi.org/10.1103/PhysRevB.72.184435

Ashorynejad, H. R., Mohamad, A. A., & Sheikholeslami, M. "Magnetic field effects on natural convection flow of a nanofluid in a horizontal cylindrical annulus using Lattice Boltzmann method." International Journal of Thermal Sciences, *64*, 240–250. (2013). https://doi.org/10.1016/j.ijthermalsci.2012.08.006

Ashorynejad, H. R., & Shahriari, A. "MHD natural convection of hybrid nanofluid in an open wavy cavity." Results in Physics, *9*, 440–455. (2018).

Askari, S., Lotfi, R., Rashidi, A. M., Koolivand, H., & Koolivand-Salooki, M. "Rheological and thermophysical properties of ultra-stable kerosene-based Fe3O4/Graphene nanofluids for energy conservation." Energy Conversion and Management, *128*, 134–144. (2016). https://doi.org/10.1016/j.enconman.2016.09.037

Askari, Saeed, Koolivand, H., Pourkhalil, M., Lotfi, R., & Rashidi, A. "Investigation of Fe3O4/Graphene nanohybrid heat transfer properties: Experimental approach." International Communications in Heat and Mass Transfer, *87*(July), 30–39. (2017). https://doi.org/10.1016/j.icheatmasstransfer.2017.06.012

Aursand, E., & Lund, H. *Potential of enhancing a natural convection loop with a thermomagnetically pumped ferrofluid. 7465*. (2016).

Bagheli, S., Fadafan, H. K., Orimi, R. L., & Ghaemi, M. "Synthesis and experimental investigation of the electrical conductivity of water based magnetite nanofluids." Powder Technology, *274*, 426–430. (2015). https://doi.org/https://doi.org/10.1016/j.powtec.2015.01.050

Bahiraei, M., & Hangi, M. "Natural convection of magnetic nanofluid in a cavity under non-uniform magnetic field: A novel application." Journal of Superconductivity and Novel Magnetism, *27*(2), 587–594. (2014). https://doi.org/10.1007/s10948-013-2317-y

Batchelor, G. K. "The effect of Brownian motion on the bulk stress in a suspension of spherical particles." Journal of Fluid Mechanics, *83*(1), 97–117. (1977).

Battira, M., & Bessaih, R. *Radial and Axial Magnetic Fields Effects on Natural Convection in a Nanofluid-filled Vertical Cylinder*. *9*(1), 407–418. (2016).

Bell, S. A. *A beginner's guide to uncertainty of measurement.* (2001).

Belmonte, A., Tilgner, A., & Libchaber, A. "Boundary layer length scales in thermal turbulence." Physical Review Letters, *70*(26), 4067–4070. (1993). https://doi.org/10.1103/PhysRevLett.70.4067

Belmonte, A., Tilgner, A., & Libchaber, A. "Temperature and velocity boundary layers in turbulent convection." Physical Review E, *50*(1), 269–279. (1994). https://doi.org/10.1103/PhysRevE.50.269

Bica, D., Vékás, L., Avdeev, M. V, Marinică, O., Socoliuc, V., Bălăsoiu, M., & Garamus, V. M. "Sterically stabilized water based magnetic fluids: synthesis, structure and properties." Journal of Magnetism and Magnetic Materials, *311*(1), 17–21. (2007).

Blums, E., Mezulis, A., & Kronkalns, G. "Magnetoconvective heat transfer from a cylinder under the influence of a nonuniform magnetic field." Journal of Physics: Condensed Matter, *20*(20), 204128. (2008).

Bolgiano, R. "Turbulent spectra in a stably stratified atmosphere." Journal of Geophysical Research, *64*(12), 2226–2229. (1959). https://doi.org/10.1029/jz064i012p02226

Borkar, S. V, & Choudhary, S. K. *A Literature Review on Use of Nanofluids in*. *6*(Ii), 2307–2312. (2018).

Brinkman, H. C. "The viscosity of concentrated suspensions and solutions." The Journal of Chemical Physics, *20*(4), 571. (1952).

Bruggeman, D. A. G. "Berechnung verschiedener physikalischer Konstanten von heterogenen Substanzen. II. Dielektrizitätskonstanten und Leitfähigkeiten von Vielkristallen der nichtregulären Systeme." Annalen Der Physik, *417*(7), 645–672. (1936). https://doi.org/10.1002/andp.19364170706

Castaing, B., Gunaratne, G., Heslot, F., Kadanoff, L., Libchaber, A., Thomae, S., Wu, X.-Z., Zaleski, S., & Zanetti, G. "Scaling of hard thermal turbulence in Rayleigh-Bénard convection." Journal of Fluid Mechanics, *204*(1), 1. (1989). https://doi.org/10.1017/S0022112089001643

Choi, S. U. S., & Eastman, J. A. *Enhancing thermal conductivity of fluids with nanoparticles*. (1995). Argonne National Lab., IL (United States).

Choudhary, R. *Study of Natural Convection Heat Transfer in Al2O3/Water nanofluids*. (2015). Indian Institute of Technology Roorkee.

Choudhary, R., Saini, A., & Subudhi, S. "Oberbeck-Boussinesq approximations and geometrical confinement effects of free convection in open cavity." Heat and Mass Transfer/Waerme- Und Stoffuebertragung, *55*(8), 2095–2102. (2019). https://doi.org/10.1007/s00231-019-02563-8

Choudhary, R., & Subudhi, S. "Aspect ratio dependence of turbulent natural convection in Al2O3/water nanofluids." Applied Thermal Engineering, *108*, 1095–1104. (2016). https://doi.org/10.1016/j.applthermaleng.2016.08.016

Chu, T. Y., & Goldstein, R. J. "Turbulent convection in a horizontal layer of water." Journal of Fluid Mechanics, *60*(1), 141–159. (1973). https://doi.org/10.1017/S0022112073000091

Colangelo, G., Favale, E., Milanese, M., de Risi, A., & Laforgia, D. "Cooling of electronic devices: Nanofluids contribution." Applied Thermal Engineering, *127*, 421–435. (2017). https://doi.org/https://doi.org/10.1016/j.applthermaleng.2017.08.042

Di Federico, I., & Foraboschi, F. P. "A contribution to the study of free convection in a fluid layer heated from below." International Journal of Heat and Mass Transfer, *9*(12), 1351–1360. (1966). https://doi.org/10.1016/0017-9310(66)90133-5

Ece, M. C., & Büyük, E. *Natural-convection flow under a magnetic field in an inclined rectangular enclosure heated and cooled on adjacent walls*. *564*, 564–590. (2006). https://doi.org/10.1016/j.fluiddyn.2006.04.002

Einstein, A. *Investigations on the Theory of the Brownian Movement*. (1956). Courier Corporation.

Engler, H., Borin, D., & Odenbach, S. *Thermomagnetic convection influenced by the magnetoviscous effect Thermomagnetic convection influenced by the magnetoviscous effect*. (2009). https://doi.org/10.1088/1742-6596/149/1/012105

Fornalik-Wajs, E., Filar, P., Wajs, J., Roszko, A., Pleskacz, L., & Ozoe, H. "Flow structure, heat transfer and scaling analysis in the case of thermo-magnetic convection in a differentially heated cylindrical enclosure." Journal of Physics: Conference Series, *530*(1). (2014). https://doi.org/10.1088/1742-6596/530/1/012041

Fumoto, K., Yamagishi, H., & Ikegawa, M. "A mini heat transport device based on thermo-sensitive magnetic fluid." Nanoscale and Microscale Thermophysical Engineering, *11*(1–2), 201–210. (2007). https://doi.org/10.1080/15567260701333869

Ganguly, R., Sen, S., & Puri, I. K. "Thermomagnetic convection in a square enclosure using a line dipole." Physics of Fluids, *16*(7), 2228–2236. (2004).

Gavili, A., Zabihi, F., Isfahani, T. D., & Sabbaghzadeh, J. "The thermal conductivity of water base ferrofluids under magnetic field." Experimental Thermal and Fluid Science, *41*, 94–98. (2012). https://doi.org/https://doi.org/10.1016/j.expthermflusci.2012.03.016

Gharagozloo, P. E., & Goodson, K. E. "Aggregate fractal dimensions and thermal conduction in nanofluids." Journal of Applied Physics, *108*(7), 74309. (2010). https://doi.org/10.1063/1.3481423

Goharkhah, M., Salarian, A., Ashjaee, M., & Shahabadi, M. "Convective heat transfer characteristics of magnetite nanofluid under the influence of constant and alternating magnetic field." Powder Technology, *274*, 258–267. (2015). https://doi.org/https://doi.org/10.1016/j.powtec.2015.01.031

Grossmann, S., & Lohse, D. "On geometry effects in Rayleigh-Bénard convection." Journal of Fluid Mechanics, *486*, 105–114. (2003). https://doi.org/10.1017/S0022112003004270

Grossmann, S., & Lohse, D. "Fluctuations in turbulent Rayleigh-Bénard convection: The role of plumes." Physics of Fluids, *16*(12), 4462–4472. (2004). https://doi.org/10.1063/1.1807751

Gu, H., Tang, X., Hong, R. Y., Feng, W. G., Xie, H. D., Chen, D. X., & Badami, D. "Ubbelohde viscometer measurement of water-based Fe3O4 magnetic fluid prepared by coprecipitation." Journal of Magnetism and Magnetic Materials, *348*, 88–92. (2013). https://doi.org/https://doi.org/10.1016/j.jmmm.2013.07.033

Hall, W. F., & Busenberg, S. N. "Viscosity of Magnetic Suspensions." The Journal of Chemical Physics, *51*(1), 137–144. (1969). https://doi.org/10.1063/1.1671698

Hamilton, R. L., & Crosser, O. K. "Thermal conductivity of heterogeneous two-component systems." Industrial & Engineering Chemistry Fundamentals, *1*(3), 187–191. (1962).

Hong, H., Wright, B., Wensel, J., Jin, S., Ye, X. R., & Roy, W. "Enhanced thermal conductivity by the magnetic field in heat transfer nanofluids containing carbon nanotube." Synthetic Metals, *157*(10–12), 437–440. (2007).

Hu, Y., He, Y., Qi, C., Jiang, B., & Schlaberg, H. I. "Experimental and numerical study of natural convection in a square enclosure filled with nanofluid." International Journal of Heat and Mass Transfer, *78*, 380–392. (2014).

J. J. Niemela, L. Skrbek, K. R. Sreenivasan, & R. J. Donnely. "Turbulent convection in very high {R}ayleigh numbers." Nature, *404*(April), 837. (2000).

Jafari, A., Tynjälä, T., Mousavi, S. M., & Sarkomaa, P. "Simulation of heat transfer in a ferrofluid using computational fluid dynamics technique." International Journal of Heat and Fluid Flow, *29*(4), 1197–1202. (2008).

Jana, S., Salehi-Khojin, A., & Zhong, W.-H. "Enhancement of fluid thermal conductivity by the addition of single and hybrid nano-additives." Thermochimica Acta, *462*(1), 45–55. (2007). https://doi.org/https://doi.org/10.1016/j.tca.2007.06.009

Jang, S. P., & Choi, S. U. S. "Role of Brownian motion in the enhanced thermal conductivity of nanofluids." Applied Physics Letters, *84*(21), 4316–4318. (2004). https://doi.org/10.1063/1.1756684

Jefferey, D. J. "Conduction through a random suspension of spheres." Proceedings of the Royal Society of London. A. Mathematical and Physical Sciences, *335*(1602), 355–367. (1973). https://doi.org/10.1098/rspa.1973.0130

Jin, L., & Zhang, X.-R. "Analysis of temperature-sensitive magnetic fluids in a porous square cavity depending on different porosity and Darcy number." Applied Thermal Engineering, *50*(1), 1–11. (2013).

Karimi, A., Goharkhah, M., Ashjaee, M., & Shafii, M. B. "Thermal Conductivity of Fe2O3 and Fe3O4 Magnetic Nanofluids Under the Influence of Magnetic Field." International Journal of Thermophysics, *36*(10–11), 2720–2739. (2015). https://doi.org/10.1007/s10765-015-1977-1

Karimi, A., S. Afghahi, S. S., Shariatmadar, H., & Ashjaee, M. "Experimental investigation on thermal conductivity of MFe2O4 (M=Fe and Co) magnetic nanofluids under influence of magnetic field." Thermochimica Acta, *598*, 59–67. (2014a). https://doi.org/https://doi.org/10.1016/j.tca.2014.10.022

Karimi, A., S. Afghahi, S. S., Shariatmadar, H., & Ashjaee, M. "Experimental investigation on thermal conductivity of MFe2O4 (M=Fe and Co) magnetic nanofluids under influence of magnetic field." Thermochimica Acta, *598*(10), 59–67. (2014b). https://doi.org/https://doi.org/10.1016/j.tca.2014.10.022

Katiyar, A., Dhar, P., Das, S. K., & Nandi, T. "Near-field magnetostatics and Néel-Brownian interactions mediated magneto-rheological characteristics of highly stable nano-ferrocolloids." In *Soft Matter* (Vol. 11, Issue 8). (2015). https://doi.org/10.1039/c4sm02458c

Katiyar, A., Dhar, P., Nandi, T., & Das, S. K. "Magnetic field induced augmented thermal conduction phenomenon in magneto-nanocolloids." Journal of Magnetism and Magnetic Materials, *419*, 588–599. (2016). https://doi.org/https://doi.org/10.1016/j.jmmm.2016.06.065

Khanafer, K., & Vafai, K. "A review on the applications of nanofluids in solar energy field." Renewable Energy, *123*, 398–406. (2018). https://doi.org/https://doi.org/10.1016/j.renene.2018.01.097

Khanafer, K., Vafai, K., & Lightstone, M. "Buoyancy-driven heat transfer enhancement in a two-dimensional enclosure utilizing nanofluids." International Journal of Heat and Mass Transfer, *46*(19), 3639–3653. (2003).

Khedkar, R. S., Kiran, A. S., Sonawane, S. S., & Wasewar, K. L. "Thermo-physical properties measurment of water based Fe3O4 nanofluids." Carbon – Science and Technology, *5*(1), 187–191. (2013).

Khurana, D., Choudhary, R., & Subudhi, S. "Investigation of Thermal Conductivity and Viscosity of Al 2 O 3 /Water Nanofluids Using Full Factorial Design and Utility Concept." Nano, *11*(08), 1650093. (2016). https://doi.org/10.1142/S1793292016500934

Kikura, H., Sawada, T., & Tanahashi, T. "Natural convection of a magnetic fluid in a cubic enclosure." Journal of Magnetism and Magnetic Materials, *122*(1–3), 315–318. (1993). https://doi.org/10.1016/0304-8853(93)91100-L

Kline, S. J., & McClintock, F. A. "Describing uncertainties in single-sample experiments." ASME Mech Eng, *75*, 3–8. (1952).

Koo, J., & Kleinstreuer, C. "Impact analysis of nanoparticle motion mechanisms on the thermal conductivity of nanofluids." International Communications in Heat and Mass Transfer, *32*(9), 1111–1118. (2005). https://doi.org/https://doi.org/10.1016/j.icheatmasstransfer.2005.05.014

Krakov, M. S., & Nikiforov, I. V. "Influence of a vertical uniform external magnetic

field on thermomagnetic convection in a square cavity." Magnetohydrodynamics, *37*(4), 366–372. (2001).

Kudelcik, J., Bury, P., Kopcansky, P., & Timko, M. "Dielectric breakdown in mineral oil ITO 100 based magnetic fluid." Physics Procedia, *9*, 78–81. (2010). https://doi.org/https://doi.org/10.1016/j.phpro.2010.11.019

Kumar, A., & Subudhi, S. "Preparation, characteristics, convection and applications of magnetic nanofluids: A review." Heat and Mass Transfer/Waerme- Und Stoffuebertragung, *54*(2). (2018). https://doi.org/10.1007/s00231-017-2114-4

Kumar, A., & Subudhi, S. "Preparation, characterization and heat transfer analysis of nanofluids used for engine cooling." Applied Thermal Engineering, *160*. (2019). https://doi.org/10.1016/j.applthermaleng.2019.114092

Kumar, L. G. K., Kumar, S. R., & Subudhi, S. "Experimental study of the turbulent free convection over horizontal smooth or grooved surfaces in an open cavity." Heat and Mass Transfer/Waerme- Und Stoffuebertragung, *52*(2), 245–253. (2016). https://doi.org/10.1007/s00231-015-1559-6

Kunitz, M. "AN EMPIRICAL FORMULA FOR THE RELATION BETWEEN VISCOSITY OF SOLUTION AND VOLUME OF SOLUTE ." Journal of General Physiology, *9*(6), 715–725. (1926). https://doi.org/10.1085/jgp.9.6.715

Lajvardi, M., Moghimi-Rad, J., Hadi, I., Gavili, A., Dallali Isfahani, T., Zabihi, F., & Sabbaghzadeh, J. "Experimental investigation for enhanced ferrofluid heat transfer under magnetic field effect." Journal of Magnetism and Magnetic Materials, *322*(21), 3508–3513. (2010). https://doi.org/10.1016/j.jmmm.2010.06.054

Laurent, S., Forge, D., Port, M., Roch, A., Robic, C., Vander Elst, L., & Muller, R. N. "Magnetic iron oxide nanoparticles: synthesis, stabilization, vectorization, physicochemical characterizations, and biological applications." Chemical Reviews, *108*(6), 2064–2110. (2008).

Leong, K. C., Yang, C., & Murshed, S. M. S. "A model for the thermal conductivity of nanofluids – the effect of interfacial layer." Journal of Nanoparticle Research, *8*(2), 245–254. (2006). https://doi.org/10.1007/s11051-005-9018-9

Li, Q., Lian, W., Sun, H., & Xuan, Y. "Investigation on operational characteristics of a miniature automatic cooling device." International Journal of Heat and Mass Transfer, *51*(21–22), 5033–5039. (2008). https://doi.org/10.1016/j.ijheatmasstransfer.2008.04.031

Li, Q., & Xuan, Y. "Experimental investigation on heat transfer characteristics of magnetic fluid flow around a fine wire under the influence of an external magnetic field." Experimental Thermal and Fluid Science, *33*(4), 591–596. (2009). https://doi.org/https://doi.org/10.1016/j.expthermflusci.2008.12.003

Li, Q., Xuan, Y., & Wang, J. "Experimental investigations on transport properties of magnetic fluids." Experimental Thermal and Fluid Science, *30*(2), 109–116. (2005).

Lian, W., Xuan, Y., & Li, Q. "Characterization of miniature automatic energy transport devices based on the thermomagnetic effect." Energy Conversion and

Management, *50*(1), 35–42. (2009). https://doi.org/10.1016/j.enconman.2008.09.005

Lui, S. L., & Xia, K. Q. "Spatial structure of the thermal boundary layer in turbulent convection." Physical Review E - Statistical Physics, Plasmas, Fluids, and Related Interdisciplinary Topics, *57*(5), 5494–5503. (1998). https://doi.org/10.1103/PhysRevE.57.5494

Mahian, O., Kianifar, A., Kalogirou, S. A., Pop, I., & Wongwises, S. "A review of the applications of nanofluids in solar energy." International Journal of Heat and Mass Transfer, *57*(2), 582–594. (2013). https://doi.org/https://doi.org/10.1016/j.ijheatmasstransfer.2012.10.037

Mahmoudi, A. H., Pop, I., & Shahi, M. "Effect of magnetic field on natural convection in a triangular enclosure filled with nanofluid." International Journal of Thermal Sciences, *59*, 126–140. (2012). https://doi.org/10.1016/j.ijthermalsci.2012.04.006

Mahmoudi, A., Mejri, I., Abbassi, M. A., & Omri, A. "Lattice Boltzmann simulation of MHD natural convection in a nanofluid-filled cavity with linear temperature distribution." Powder Technology, *256*, 257–271. (2014).

Mahmoudi, A., Mejri, I., & Omri, A. "Study of natural convection in a square cavity filled with nanofluid and subjected to a magnetic field." International Journal of Heat and Technology, *34*(1), 73–79. (2016). https://doi.org/10.18280/ijht.340111

Malekzadeh, A., Pouranfard, A. R., Hatami, N., Kazemnejad Banari, A., & Rahimi, M. R. "Experimental investigations on the viscosity of magnetic nanofluids under the influence of temperature, volume fractions of nanoparticles and external magnetic field." Journal of Applied Fluid Mechanics, *9*(2), 693–697. (2016). https://doi.org/10.18869/acadpub.jafm.68.225.24022

Mansour, M. A., Bakier, A. Y., & Bakeir, M. A. Y. *MHD Natural convection in the localized heat sources of an inclined trapezoidal Nanofluid-filled enclosure. 09*, 140–161. (2013).

Masoumi, N., Sohrabi, N., & Behzadmehr, A. "A new model for calculating the effective viscosity of nanofluids." Journal of Physics D: Applied Physics, *42*(5), 55501. (2009).

Masuda, H., Ebata, A., Teramae, K., Hishinuma, N., & Ebata, Y. *Alteration of thermal conductivity and viscosity of liquid by dispersing ultra-fine particles (dispersion of γ-Al2O3, SiO2 and TiO2 ultra-fine particles).* (1993).

Maxwell, J. C. *A treatise on electricity and magnetism* (Vol. 1). (1873). Clarendon press.

McTague, J. P. "Magnetoviscosity of Magnetic Colloids." The Journal of Chemical Physics, *51*(1), 133–136. (1969). https://doi.org/10.1063/1.1671697

Mejri, I., & Mahmoudi, A. "MHD natural convection in a nanofluid-filled open enclosure with a sinusoidal boundary condition." Chemical Engineering Research and Design, *98*, 1–16. (2015). https://doi.org/10.1016/j.cherd.2015.03.028

Modak, M., Chougule, S. S., & Sahu, S. K. "An experimental investigation on heat transfer characteristics of hot surface by using CuO–water nanofluids in circular jet impingement cooling." Journal of Heat Transfer, *140*(1). (2018).

Moreau, R. J. *Magnetohydrodynamics* (Vol. 3). (2013). Springer Science & Business Media.

Nabeel Rashin, M., & Hemalatha, J. "Magnetic and ultrasonic investigations on magnetite nanofluids." Ultrasonics, *52*(8), 1024–1029. (2012). https://doi.org/https://doi.org/10.1016/j.ultras.2012.08.005

Nabeel Rashin, M., & Hemalatha, J. "Magnetic and ultrasonic studies on stable cobalt ferrite magnetic nanofluid." Ultrasonics, *54*(3), 834–840. (2014). https://doi.org/https://doi.org/10.1016/j.ultras.2013.10.009

Nakatsuka, K., Jeyadevan, B., Neveu, S., & Koganezawa, H. "The magnetic fluid for heat transfer applications." Journal of Magnetism and Magnetic Materials, *252*(1-3 SPEC. ISS.), 360–362. (2002). https://doi.org/10.1016/S0304-8853(02)00683-2

Nguyen, C. T., Roy, G., Gauthier, C., & Galanis, N. "Heat transfer enhancement using Al2O3–water nanofluid for an electronic liquid cooling system." Applied Thermal Engineering, *27*(8), 1501–1506. (2007). https://doi.org/https://doi.org/10.1016/j.applthermaleng.2006.09.028

Niemela, J. J., & Sreenivasan, K. R. "Confined turbulent convection." Journal of Fluid Mechanics, *481*(481), 355–384. (2003). https://doi.org/10.1017/S0022112003004087

Nurdin, I., Yaacob, I. I., & Johan, M. R. "Enhancement of thermal conductivity and kinematic viscosity in magnetically controllable maghemite (γ-Fe2O3) nanofluids." Experimental Thermal and Fluid Science, *77*, 265–271. (2016). https://doi.org/10.1016/j.expthermflusci.2016.05.002

Obukhov, A. "Effect of Archimedean forces on the structure of the temperature field in a turbulent flow." Dokl. Akad. Nauk SSSR, *125*(6), 1246–1248. (1959).

Odenbach, S. "Magnetic fluids - Suspensions of magnetic dipoles and their magnetic control." Journal of Physics Condensed Matter, *15*(15). (2003). https://doi.org/10.1088/0953-8984/15/15/312

Parekh, K., & Lee, H. S. "Magnetic field induced enhancement in thermal conductivity of magnetite nanofluid." Journal of Applied Physics, *107*(9), 09A310. (2010).

Patel, R. "Effective viscosity of magnetic nanofluids through capillaries." Physical Review E - Statistical, Nonlinear, and Soft Matter Physics, *85*(2), 1–7. (2012). https://doi.org/10.1103/PhysRevE.85.026316

Peternele, W. S., Monge Fuentes, V., Fascineli, M. L., Rodrigues da Silva, J., Silva, R. C., Lucci, C. M., & Bentes de Azevedo, R. "Experimental Investigation of the Coprecipitation Method: An Approach to Obtain Magnetite and Maghemite Nanoparticles with Improved Properties." Journal of Nanomaterials, *2014*, 682985. (2014). https://doi.org/10.1155/2014/682985

Philip, J., & Shima, P. D. "Thermal properties of nanofluids." Advances in Colloid and Interface Science, *183–184*, 30–45. (2012). https://doi.org/https://doi.org/10.1016/j.cis.2012.08.001

Philip, J., Shima, P. D., & Raj, B. "Enhancement of thermal conductivity in magnetite based nanofluid due to chainlike structures." Applied Physics Letters, *91*(20), 203108. (2007).

Popiel, C. O., & Wojtkowiak, J. "Simple formulas for thermophysical properties of liquid water for heat transfer calculations (from 0°c to 150°c)." Heat Transfer Engineering, *19*(3), 87–101. (1998). https://doi.org/10.1080/01457639808939929

Puliti, G., Paolucci, S., & Sen, M. "Nanofluids and their properties." Applied Mechanics Reviews, *64*(3). (2011).

Putra, N., Roetzel, W., & Das, S. K. "Natural convection of nano-fluids." Heat and Mass Transfer, *39*(8–9), 775–784. (2003).

Putra, N., Yanuar, & Iskandar, F. N. "Application of nanofluids to a heat pipe liquid-block and the thermoelectric cooling of electronic equipment." Experimental Thermal and Fluid Science, *35*(7), 1274–1281. (2011). https://doi.org/https://doi.org/10.1016/j.expthermflusci.2011.04.015

Raj, K., & Moskowitz, R. "Commercial applications of ferrofluids." Journal of Magnetism and Magnetic Materials, *85*(1–3), 233–245. (1990).

Reddy, K. S., Kamnapure, N. R., & Srivastava, S. "Nanofluid and nanocomposite applications in solar energy conversion systems for performance enhancement: a review." International Journal of Low-Carbon Technologies, *12*(1), 1–23. (2017).

Robinson, J. V. "The Viscosity of Suspensions of Spheres." The Journal of Physical and Colloid Chemistry, *53*(7), 1042–1056. (1949). https://doi.org/10.1021/j150472a007

Rosensweig, R. E. "Viscosity of Magnetic Fluid in a Magnetic Field." Journal of Colloid and Interface Science, *20*(4), 680–687. (1969).

Roszko, A., & Fornalik-Wajs, E. "Extend of magnetic field interference in the natural convection of diamagnetic nanofluid." Heat and Mass Transfer/Waerme- Und Stoffuebertragung, *54*(8), 2243–2254. (2018). https://doi.org/10.1007/s00231-017-2172-7

Roszko, A., Fornalik-wajs, E., Donizak, J., Wajs, J., Kraszewska, A., Pleskacz, L., & Kenjeres, S. "Magneto-thermal convection of low concentration nanofluids." MATEC Web of Conferences, *18*(June), 1–8. (2014). https://doi.org/10.1051/matecconf/20141803006

Saidur, R., Leong, K. Y., & Mohammed, H. A. "A review on applications and challenges of nanofluids." Renewable and Sustainable Energy Reviews, *15*(3), 1646–1668. (2011). https://doi.org/https://doi.org/10.1016/j.rser.2010.11.035

Saien, J., Bamdadi, H., & Daliri, S. "Liquid–liquid extraction intensification with magnetite nanofluid single drops under oscillating magnetic field." Journal of Industrial and Engineering Chemistry, *21*, 1152–1159. (2015).

Sano, M., Wu, X. Z., & Libchaber, A. "Turbulence in helium-gas free convection." Physical Review A, *40*(11), 6421–6430. (1989). https://doi.org/10.1103/PhysRevA.40.6421

Sawada, T., Kikura, H., Saito, A., & Tanahashi, T. "Natural convection of a magnetic fluid in concentric horizontal annuli under nonuniform magnetic fields." Experimental Thermal and Fluid Science, *7*(3), 212–220. (1993). https://doi.org/10.1016/0894-1777(93)90004-3

Scherer, C., & Neto, A. M. F. *Ferrofluids : Properties and Applications*. *35*(3), 718–727. (2005).

Sengers, J. V., & Watson, J. T. R. "Improved International Formulations for the Viscosity and Thermal Conductivity of Water Substance." Journal of Physical and Chemical Reference Data, *15*(4), 1291–1314. (1986). https://doi.org/10.1063/1.555763

Shahsavar, A., Salimpour, M. R., Saghafian, M., & Shafii, M. B. "Effect of magnetic field on thermal conductivity and viscosity of a magnetic nanofluid loaded with carbon nanotubes." Journal of Mechanical Science and Technology, *30*(2), 809–815. (2016). https://doi.org/10.1007/s12206-016-0135-4

Shang, X. D., Tong, P., & Xia, K. Q. "Scaling of the local convective heat flux in turbulent rayleigh- bénard convection." Physical Review Letters, *100*(24), 1–4. (2008). https://doi.org/10.1103/PhysRevLett.100.244503

Shete, P. B., Patil, R. M., Tiwale, B. M., & Pawar, S. H. "Water dispersible oleic acid-coated Fe3O4 nanoparticles for biomedical applications." Journal of Magnetism and Magnetic Materials, *377*, 406–410. (2015). https://doi.org/https://doi.org/10.1016/j.jmmm.2014.10.137

Shima, P. D., & Philip, J. "Tuning of Thermal Conductivity and Rheology of Nanofluids Using an External Stimulus." The Journal of Physical Chemistry C, *115*(41), 20097–20104. (2011). https://doi.org/10.1021/jp204827q

Shima, P. D., Philip, J., & Raj, B. "Magnetically controllable nanofluid with tunable thermal conductivity and viscosity." Applied Physics Letters, *95*(13), 9–12. (2009). https://doi.org/10.1063/1.3238551

Shima, P. D., Raj, B., & Philip, J. "Thermal properties of magnetic nanofluids." Nanofluids: Synthesis, Properties and Applications, 77–108. (2014).

Shliomis, M. "Effective Viscosity Of Magnetic Suspensions." Sov. Phys. JETP, *34*, 1291–1294. (1972).

Shliomis, M. I., & Morozov, K. I. "Negative viscosity of ferrofluid under alternating magnetic field." Physics of Fluids, *6*(8), 2855–2861. (1994). https://doi.org/10.1063/1.868108

Singh, D. K., Pandey, D. K., & Yadav, R. R. "An ultrasonic characterization of ferrofluid." Ultrasonics, *49*(8), 634–637. (2009).

Snyder, S. M., Cader, T., & Finlayson, B. A. "Finite element model of magnetoconvection of a ferrofluid." Journal of Magnetism and Magnetic Materials, *262*(2), 269–279. (2003). https://doi.org/10.1016/S0304-8853(02)01502-0

Sourtiji, E., & Hosseinizadeh, S. F. "Heat transfer augmentation of magnetohydrodynamics natural convection in L-shaped cavities utilizing nanofluids." Thermal Science, *16*(2), 489–501. (2012).

Stoian, F. D., & Holotescu, S. "Experimental study of cooling enhancement using a Fe3O4 magnetic nanofluid, in an applied magnetic field." Journal of Physics: Conference Series, *547*(1). (2014). https://doi.org/10.1088/1742-6596/547/1/012044

Sun, C., & Xia, K.-Q. "Multi-point local temperature measurements inside the conducting plates in turbulent thermal convection." Journal of Fluid Mechanics, *570*, 479–489. (2007). https://doi.org/10.1017/S0022112006003181

Sundar, L. S., Ramana, E. V., Singh, M. K., & Sousa, A. C. M. "Magnetic Field Induced Enhancement in Thermal Conductivity and Viscosity of Stabilized Vacuum Pump Oil (VPO)—Fe3O4 Magnetic Nanofluids." Journal of Nanofluids, *4*(1), 7–15. (2015). https://doi.org/10.1166/jon.2015.1124

Sundar, L. S., Singh, M. K., Ramana, E. V., Singh, B., Grácio, J., & Sousa, A. C. M. "Enhanced Thermal Conductivity and Viscosity of Nanodiamond-Nickel Nanocomposite Nanofluids." Scientific Reports, *4*(1), 4039. (2014). https://doi.org/10.1038/srep04039

Sundar, L. S., Singh, M. K., & Sousa, A. C. M. "Investigation of thermal conductivity and viscosity of Fe3O4 nanofluid for heat transfer applications." International Communications in Heat and Mass Transfer, *44*, 7–14. (2013). https://doi.org/10.1016/j.icheatmasstransfer.2013.02.014

Syam Sundar, L., Ravi Kumar, N. T., Naik, M. T., & Sharma, K. V. "Effect of full length twisted tape inserts on heat transfer and friction factor enhancement with Fe3O4 magnetic nanofluid inside a plain tube: An experimental study." International Journal of Heat and Mass Transfer, *55*(11), 2761–2768. (2012). https://doi.org/https://doi.org/10.1016/j.ijheatmasstransfer.2012.02.040

Syam Sundar, L., Venkata Ramana, E., Singh, M. K., & De Sousa, A. C. M. "Viscosity of low volume concentrations of magnetic Fe3O4nanoparticles dispersed in ethylene glycol and water mixture." Chemical Physics Letters, *554*, 236–242. (2012). https://doi.org/10.1016/j.cplett.2012.10.042

Taylor, R., Coulombe, S., Otanicar, T., Phelan, P., Gunawan, A., Lv, W., Rosengarten, G., Prasher, R., & Tyagi, H. "Small particles, big impacts: A review of the diverse applications of nanofluids." Journal of Applied Physics, *113*(1), 11301. (2013). https://doi.org/10.1063/1.4754271

Theerthan, S. A., & Arakeri, J. H. "Planform structure and heat transfer in turbulent free convection over horizontal surfaces." Physics of Fluids, *12*(4), 884–894. (2000). https://doi.org/10.1063/1.870343

Vand, V. "Viscosity of Solutions and Suspensions. II. Experimental Determination of the Viscosity–Concentration Function of Spherical Suspensions." The Journal of Physical and Colloid Chemistry, *52*(2), 300–314. (1948). https://doi.org/10.1021/j150458a002

Veera Raghavalu, K., & Govindha Rasu, N. "Review on Applications of NanoFluids used in Vapour Compression Refrigeration System for Cop Enhancement." IOP Conference Series: Materials Science and Engineering, *330*, 12112. (2018). https://doi.org/10.1088/1757-899x/330/1/012112

Vishnu, V. T., De, A. K., & Mishra, P. K. "Dynamics and statistics of reorientations of large-scale circulation in turbulent rotating Rayleigh-Bénard convection." Physics of Fluids, *31*(5). (2019). https://doi.org/10.1063/1.5093948

Völker, T., Blums, E., & Odenbach, S. "Heat and mass transfer phenomena in magnetic fluids." GAMM-Mitteilungen, *30*(1), 185–194. (2007).

Vouros, A., & Panidis, T. "Statistical analysis of turbulent thermal free convection over a horizontal heated plate in an open top cavity." Experimental Thermal and Fluid Science, *36*, 44–55. (2012). https://doi.org/10.1016/j.expthermflusci.2011.08.002

Wagh, D. K., & Avashia, A. "On the viscosity of a magnetic fluid." Journal of Magnetism and Magnetic Materials, *153*(3), 359–365. (1996). https://doi.org/10.1016/0304-8853(95)00541-2

Wang, J., & Xia, K. Q. "Spatial variations of the mean and statistical quantities in the thermal boundary layers of turbulent convection." European Physical Journal B, *32*(1), 127–136. (2003). https://doi.org/10.1140/epjb/e2003-00081-y

Wang, L., Wang, Y., Yan, X., Wang, X., & Feng, B. "Investigation on viscosity of Fe3O4 nanofluid under magnetic field." International Communications in Heat and Mass Transfer, *72*, 23–28. (2016). https://doi.org/10.1016/j.icheatmasstransfer.2016.01.013

Wang, Y., He, X., & Tong, P. "Turbulent temperature fluctuations in a closed Rayleigh-Bénard convection cell." Journal of Fluid Mechanics, *874*, 263–284. (2019). https://doi.org/10.1017/jfm.2019.405

Wen, C. Y., Chen, C. Y., & Yang, S. F. "Flow visualization of natural convection of magnetic fluid in a rectangular Hele-Shaw cell." Journal of Magnetism and Magnetic Materials, *252*(1-3 SPEC. ISS.), 206–208. (2002). https://doi.org/10.1016/S0304-8853(02)00671-6

Wu, X.-Z., Kadanoff, L., Libchaber, A., & Sano, M. "Frequency power spectrum of temperature fluctuations in free convection." Physical Review Letters, *64*(18), 2140–2143. (1990). https://doi.org/10.1103/PhysRevLett.64.2140

Xi, H.-D., Zhou, S.-Q., Zhou, Q., Chan, T.-S., & Xia, K.-Q. "Origin of the Temperature Oscillation in Turbulent Thermal Convection." Physical Review Letters, *102*(4), 044503. (2009). https://doi.org/10.1103/PhysRevLett.102.044503

Xu, A., Shi, L., & Xi, H. D. "Statistics of temperature and thermal energy dissipation rate in low-Prandtl number turbulent thermal convection." Physics of Fluids, *31*(12). (2019). https://doi.org/10.1063/1.5129818

Xuan, Y., & Lian, W. "Electronic cooling using an automatic energy transport device based on thermomagnetic effect." Applied Thermal Engineering, *31*(8–9), 1487–1494. (2011). https://doi.org/10.1016/j.applthermaleng.2011.01.033

Xuan, Y., & Roetzel, W. "Conceptions for heat transfer correlation of nanofluids." International Journal of Heat and Mass Transfer, *43*(19), 3701–3707. (2000). https://doi.org/https://doi.org/10.1016/S0017-9310(99)00369-5

Xue, Q., & Xu, W.-M. "A model of thermal conductivity of nanofluids with interfacial shells." Materials Chemistry and Physics, *90*(2), 298–301. (2005). https://doi.org/https://doi.org/10.1016/j.matchemphys.2004.05.029

Yamaguchi, H., Sumiji, A., Shuchi, S., & Yonemura, T. "Characteristics of thermo-magnetic driven motor using magnetic fluid." Journal of Magnetism and Magnetic Materials, *272*(III), 2362–2364. (2004). https://doi.org/10.1016/j.jmmm.2003.12.970

Yamaguchi, H., Zhang, Z., Shuchi, S., & Shimada, K. "Heat transfer characteristics of

magnetic fluid in a partitioned rectangular box." Journal of Magnetism and Magnetic Materials, *252*(1-3 SPEC. ISS.), 203–205. (2002). https://doi.org/10.1016/S0304-8853(02)00731-X

Yamaguchi, H, Kobori, I., Uehata, Y., & Shimada, K. *Natural convection of magnetic # uid in a rectangular box. 201*, 930–933. (1999).

Yamaguchi, Hiroshi, Zhang, X. R., Niu, X. D., & Yoshikawa, K. "Thermomagnetic natural convection of thermo-sensitive magnetic fluids in cubic cavity with heat generating object inside." Journal of Magnetism and Magnetic Materials, *322*(6), 698–704. (2010). https://doi.org/10.1016/j.jmmm.2009.10.044

Yang, C., Bian, X., Guo, T., Zhang, K., & Liu, Y. "Investigation of Fe3O4 aqueous ferrofluids before and after freezing." Soft Materials, *12*(3), 346–351. (2014). https://doi.org/10.1080/1539445X.2014.896823

Yang, L., & Du, K. "A comprehensive review on heat transfer characteristics of TiO2 nanofluids." International Journal of Heat and Mass Transfer, *108*, 11–31. (2017).

Yu, W, & Choi, S. U. S. "The Role of Interfacial Layers in the Enhanced Thermal Conductivity of Nanofluids: A Renovated Maxwell Model." Journal of Nanoparticle Research, *5*(1), 167–171. (2003). https://doi.org/10.1023/A:1024438603801

Yu, Wei, Xie, H., Chen, L., & Li, Y. "Enhancement of thermal conductivity of kerosene-based Fe3O4nanofluids prepared via phase-transfer method." Colloids and Surfaces A: Physicochemical and Engineering Aspects, *355*(1–3), 109–113. (2010). https://doi.org/10.1016/j.colsurfa.2009.11.044

Zablotsky, D., Mezulis, A., & Blums, E. "Surface cooling based on the thermomagnetic convection: Numerical simulation and experiment." International Journal of Heat and Mass Transfer, *52*(23–24), 5302–5308. (2009). https://doi.org/10.1016/j.ijheatmasstransfer.2009.08.001

Zhang, X., Yu, J., Su, G., Yao, Z., Hao, P., & He, F. "Statistical analysis of turbulent thermal free convection over a small heat source in a large enclosed cavity." Applied Thermal Engineering, *93*, 446–455. (2016). https://doi.org/10.1016/j.applthermaleng.2015.10.011

Zhou, Q., Sugiyama, K., Stevens, R. J. A. M., Grossmann, S., Lohse, D., & Xia, K. Q. "Horizontal structures of velocity and temperature boundary layers in two-dimensional numerical turbulent Rayleigh-Bénard convection." Physics of Fluids, *23*(12). (2011). https://doi.org/10.1063/1.3662445

Zhou, Q., Sun, C., & Xia, K. Q. "Morphological evolution of thermal plumes in turbulent rayleigh- bénard convection." Physical Review Letters, *98*(7), 1–4. (2007). https://doi.org/10.1103/PhysRevLett.98.074501

Zhou, Q., & Xia, K. Q. "Thermal boundary layer structure in turbulent Rayleigh-Bénard convection in a rectangular cell." Journal of Fluid Mechanics, *721*, 199–224. (2013). https://doi.org/10.1017/jfm.2013.73

Zhou, S. Q., & Xia, K. Q. "Plume Statistics in Thermal Turbulence: Mixing of an Active Scalar." Physical Review Letters, *89*(18), 8–11. (2002). https://doi.org/10.1103/PhysRevLett.89.184502

Zhu, H., Zhang, C., Liu, S., Tang, Y., & Yin, Y. *Effects of nanoparticle clustering and alignment on thermal conductivities of Fe3O4 aqueous nanofluids Effects of nanoparticle clustering and alignment on thermal conductivities of Fe 3 O 4 aqueous nanofluids. 023123*, 4–7. (2006). https://doi.org/10.1063/1.2221905